NASA/TM—2002-211693

International Space Station Increment-3 Microgravity Environment Summary Report

Kenol Jules
Glenn Research Center, Cleveland, Ohio

Kenneth Hrovat and Eric Kelly
ZIN Technologies, Inc., Brook Park, Ohio

Kevin McPherson
Glenn Research Center, Cleveland, Ohio

Timothy Reckart and Carlos Grodsinksy
ZIN Technologies, Inc., Brook Park, Ohio

June 2002

The NASA STI Program Office . . . in Profile

Since its founding, NASA has been dedicated to the advancement of aeronautics and space science. The NASA Scientific and Technical Information (STI) Program Office plays a key part in helping NASA maintain this important role.

The NASA STI Program Office is operated by Langley Research Center, the Lead Center for NASA's scientific and technical information. The NASA STI Program Office provides access to the NASA STI Database, the largest collection of aeronautical and space science STI in the world. The Program Office is also NASA's institutional mechanism for disseminating the results of its research and development activities. These results are published by NASA in the NASA STI Report Series, which includes the following report types:

- TECHNICAL PUBLICATION. Reports of completed research or a major significant phase of research that present the results of NASA programs and include extensive data or theoretical analysis. Includes compilations of significant scientific and technical data and information deemed to be of continuing reference value. NASA's counterpart of peer-reviewed formal professional papers but has less stringent limitations on manuscript length and extent of graphic presentations.

- TECHNICAL MEMORANDUM. Scientific and technical findings that are preliminary or of specialized interest, e.g., quick release reports, working papers, and bibliographies that contain minimal annotation. Does not contain extensive analysis.

- CONTRACTOR REPORT. Scientific and technical findings by NASA-sponsored contractors and grantees.

- CONFERENCE PUBLICATION. Collected papers from scientific and technical conferences, symposia, seminars, or other meetings sponsored or cosponsored by NASA.

- SPECIAL PUBLICATION. Scientific, technical, or historical information from NASA programs, projects, and missions, often concerned with subjects having substantial public interest.

- TECHNICAL TRANSLATION. English-language translations of foreign scientific and technical material pertinent to NASA's mission.

Specialized services that complement the STI Program Office's diverse offerings include creating custom thesauri, building customized data bases, organizing and publishing research results . . . even providing videos.

For more information about the NASA STI Program Office, see the following:

- Access the NASA STI Program Home Page at ***http://www.sti.nasa.gov***

- E-mail your question via the Internet to help@sti.nasa.gov

- Fax your question to the NASA Access Help Desk at 301–621–0134

- Telephone the NASA Access Help Desk at 301–621–0390

- Write to:
  NASA Access Help Desk
  NASA Center for AeroSpace Information
  7121 Standard Drive
  Hanover, MD 21076

NASA/TM—2002-211693

International Space Station Increment-3 Microgravity Environment Summary Report

Kenol Jules
Glenn Research Center, Cleveland, Ohio

Kenneth Hrovat and Eric Kelly
ZIN Technologies, Inc., Brook Park, Ohio

Kevin McPherson
Glenn Research Center, Cleveland, Ohio

Timothy Reckart and Carlos Grodsinksy
ZIN Technologies, Inc., Brook Park, Ohio

National Aeronautics and
Space Administration

Glenn Research Center

June 2002

Acknowledgments

The authors would like to acknowledge a number of people who contributed significantly to this report. Without their contribution this report would have not been possible. Nissim Lugasy, Ted Wright, and Gene Liberman made significant contributions in the area of software development. The software enabled PIMS to process, analyze, troubleshoot, and display both MAMS and SAMS acceleration data acquired aboard the ISS. We would like also to acknowledge the development efforts of the SAMS-II team and the MAMS project team/Canopus, Inc.

Mike Myszka, Payload Rack Officer (PRO) (MSFC) provided command timeline for ER2 that helped with deactivation identification for EXPPCS and ARIS-ICE.

Bill Telesco, Payload Rack Officer (PRO) (Teledyne Brown Engineering) provided command timeline for ER2 AAA fan (de)activations during ARIS-ICE testing.

David Thompson (University of Akron) provided technical assistance that has proved to be of much value for acceleration data archiving.

Robert Janney (JSC) provided some background exercise information.

James Allen (Boeing) provided timeline and operational information with regards to the ARIS-ICE.

Karen Bush, Attitude Determination and Control Officer (ADCO) (JSC) provided information and explanations for various attitude maneuvers and events.

Available from

NASA Center for Aerospace Information
7121 Standard Drive
Hanover, MD 21076

National Technical Information Service
5285 Port Royal Road
Springfield, VA 22100

Available electronically at http://gltrs.grc.nasa.gov/GLTRS

Table of Contents

Table of Contents ii
List of Tables iii
List of Figures iv
1 Introduction 1
2 International Space Station 2
2.1 Configuration at Assembly Complete 2
2.2 ISS Coordinate Systems 3
2.3 ISS Flight Attitude at Assembly Complete 4
3 ISS Increment-3 8
3.1 Increment-3 Configuration 8
3.2 Increment-3 Coordinate Systems 9
3.3 Increment-3 Overall Attitude 9
3.4 Increment-3 Crew Members 9
4 Acceleration Measurement System Descriptions: Increment-3 13
4.1 Microgravity Acceleration Measurement System (MAMS) 13
4.2 MAMS Coordinate Systems 13
4.3 Space Acceleration Measurement System (SAMS) 13
4.4 SAMS Coordinate Systems 14
5 Specific Facilities and Experiments Supported by PIMS: Increment-3 15
5.1 Increment-3 Facilities 15
5.2 Increment-3 Experiments 15
6 ISS Increment-3 Reduced Gravity Environment Description 19
6.1 Quasi-steady Microgravity Environment 19
6.2 Vibratory Microgravity Environment 50
7 Principal Component Spectral Analysis 108
8 Vehicle Dynamics 115
9 Summary of Increment-3 Analysis 122
9.1 Quasi-steady Environment 122
9.2 Vibratory Environment 123
10 References 125
Appendix A. On-line Access to PIMS Acceleration Data Archive 127
Appendix B. Some Useful Acceleration Data and Microgravity Related URLs 129
Appendix C. Acronym List and Definition 131
Appendix D. SAMS and MAMS Data Flow Descriptions 133
Appendix E. Data Analysis Techniques and Processing 135
E.1. Acceleration Data Coordinate Conversion 135
E.2. Quasi-steady Regime 137
E.3. Vibratory Regime 142

List of Tables

Table 2-1 ISS Specification at Assembly Complete 2
Table 3-1 Increment-3 Missions 8
Table 4-1 MAMS Sensor Coordinate System 13
Table 4-2 SAMS SE Coordinate Systems 14
Table 5-1 Increment-3 Payloads 16
Table 6-1 Quasi-steady Vector for TEA and XPOP Attitudes 20
Table 6-2 Excerpt of Increment-3 As-Flown Timeline for EVA-5 23
Table 6-3 Excerpt of Increment-3 As-Flown Attitude Timeline 51
Table 6-4 Progress Thruster Peak Acceleration, GMT 27-August-2001, 239/01:mm:ss 52
Table 6-5 Progress 4P Undocking Peak Acceleration Vector Magnitudes 52
Table 6-6 AAA Fan (De)activations During ARIS-ICE Testing 54
Table 6-7 Structural Mode Regime Before STS-108 Undocked ("Joint Ops") 56
Table 6-8 Structural Mode Regime After STS-108 Undocked ("Unmated") 57
Table 6-9 Simple ARIS Comparison GMT 11-September-2001, 254/08:09:19 60
Table 6-10 RMS Acceleration for EXPPCS Activation 61
Table 6-11 PRO Command Timeline for ER2 on GMT 7-September-11, 250/hh:mm:ss 61
Table 6-12 Joint Ops Shuttle Ergometer Exercise Test Sequence (DTO 262) 63
Table 7-1 MAMS HiRAP (100 Hz) PCSA Parameters 108
Table 7-2 SAMS 121f06 (25 Hz) PCSA Parameters 108
Table 7-3 SAMS 121f05 (25 Hz) PCSA Parameters 108
Table 7-4 SAMS 121f04 (25 Hz) PCSA Parameters 108
Table 7-5 SAMS 121f03 (25 Hz) PCSA Parameters 109
Table 9-1 Summary of Findings for Increment-3 Quasi-steady Analysis 122
Table 9-2 Summary of Findings for Increment-3 Vibratory Analysis 124
Table D - 1 SAMS Data Flow Rates 133

List of Figures

Figure 2-1 International Space Station at Assembly Complete 5
Figure 2-2 Space Station Analysis Coordinate System 6
Figure 2-3 Integrated Truss Segment S0 Coordinate System 6
Figure 2-4 United States Laboratory Module (Destiny) Coordinate System 7
Figure 2-5 ISS XVV Flight Attitude 7
Figure 3-1 ISS Increment-3 Configuration 10
Figure 3-2 Increment-3 Coordinate Systems 11
Figure 3-3 ISS in the XPOP Inertial Flight Attitude 12
Figure 5-1 EXPRESS Racks 1 & 2, 7A On-Orbit Configuration 17
Figure 5-2 EXPRESS Rack 4 & 5, 7A On-Orbit Configuration 17
Figure 5-3 US Lab Rack Locations. 18
Figure 6-1 Time Series of Quasi-steady Vector During TEA (OSS) 25
Figure 6-2 Acceleration Magnitude of Quasi-steady Vector During TEA (OSS) 26
Figure 6-3 Time Series of Quasi-steady Vector During XPOP (OSS) 27
Figure 6-4 Acceleration Magnitude of Quasi-steady Vector During XPOP (OSS) 28
Figure 6-5 Time Series of CMG 2 Restoration to Steering Law (OSS) 29
Figure 6-6 Time Series of ISS Attitude Data During CMG 2 Restoration (OSS) 30
Figure 6-7 Time Series of ISS Angular Rates During CMG 2 Restoration (OSS) 31
Figure 6-8 QTH of Time Period Following CMG 2 Restoration (OSS) 32
Figure 6-9 QTH of Torque Equilibrium Attitude (OSS) 33
Figure 6-10 Time Series of Progress 4P Undocking (OSS) 34
Figure 6-11 Time Series of DC-1 Docking Test Maneuvers (OSS) 35
Figure 6-12 Time Series of DC-1 Docking Maneuvers (OSS) 36
Figure 6-13 Time Series of Soyuz-2 Relocation (OSS) 37
Figure 6-14 Time Series of RS-EVA-2 SSRMS Maneuver and DC-1 Depressurization (OSS) 38
Figure 6-15 Acceleration Magnitude of RS-EVA-2 SSRMS Maneuver and DC-1 Depressurization (OSS) 39
Figure 6-16 Time Series of RS-EVA-2 (OSS) 40
Figure 6-17 Time Series for Russian EVA (OSS) 41
Figure 6-18 Time Series of DC-1 Depressurization (OSS) 42
Figure 6-19 Time Series of Recovery From SM Thrusters Inhibited (OSS) 43
Figure 6-20 Time Series of ISS Angular Rates for Recovery From SM Thrusters Inhibited (OSS) 44
Figure 6-21 Time Series of Progress 5P Propellant Line Purge Activities (OSS) 45
Figure 6-22 Time Series of Progress 5P Fuel Purge (OSS) 46
Figure 6-23 Acceleration Magnitude of Progress 5P Fuel Purge (OSS) 47
Figure 6-24 Time Series of 5P Oxygen Purge and Momentum Management 48
Figure 6-25 Acceleration Magnitude of 5P Oxygen Purge and Momentum Management 49
Figure 6-26 PAD Profile for August of 2001 65
Figure 6-27 PAD Profile for September of 2001 66
Figure 6-28 PAD Profile for October of 2001 67
Figure 6-29 PAD Profile for November of 2001 68
Figure 6-30 PAD Profile for December of 2001 69

Figure 6-31 Spectrogram of Progress Thruster Tests (121f05) 70
Figure 6-32 Acceleration Magnitude of Progress Thruster Manifold 1 Tests (HiRAP)..... 71
Figure 6-33 Acceleration Magnitude of Progress Thruster Manifold 1 Tests (121f05,121f06)..... 72
Figure 6-34 Time Series of Progress 4P Undocking (121f02) 73
Figure 6-35 Time Series of Progress 4P Undocking (121f03) 74
Figure 6-36 Time Series of Progress 4P Undocking (121f04) 75
Figure 6-37 Time Series of Progress 4P Undocking (121f05) 76
Figure 6-38 Time Series of Progress 4P Undocking (121f06) 77
Figure 6-39 Acceleration Magnitude of Progress 5P Vehicle Docking (HiRAP)..... 78
Figure 6-40 Time Series of Progress 5P Vehicle Docking (HiRAP)..... 79
Figure 6-41 Spectrogram of AAA Fan (De)activations (121f03)..... 80
Figure 6-42 Spectrogram of AAA Fan (De)activations (121f06)..... 81
Figure 6-43 Spectrogram of AAA Fan (De)activations Zoom Around 181 Hz(121f06) 82
Figure 6-44 Spectrogram of AAA Fan (De)activations Zoom Around 362 Hz (121f06)(121f06)..... 83
Figure 6-45 Spectrogram of STS-108 Undock (121f03) 84
Figure 6-46 Spectrogram of STS-108 Undock (121f04) 85
Figure 6-47 Spectrogram of STS-108 Undock 3-Hour Zoom Below 5 Hz (121f03)..... 86
Figure 6-48 Spectrogram of STS-108 Undock 3-Hour Zoom Below 5 Hz (121f04)..... 87
Figure 6-49 PSDs of Before STS-108 Undock Below 10 Hz (121f03,121f04) 88
Figure 6-50 PSDs of After STS-108 Undock Below 10 Hz (121f03,121f04)..... 89
Figure 6-51 PSDs of Before vs. After STS-108 Undock Below 10 Hz (121f03,121f04) 90
Figure 6-52 Spectrogram of ARIS Transition to Active Mode (121f06) 91
Figure 6-53 Spectrogram of ARIS in Active Mode (121f06)..... 92
Figure 6-54 Spectrogram of ARIS Transition to Active Mode (121f05) 93
Figure 6-55 Spectrogram of ARIS in Active Mode (121f05)..... 94
Figure 6-56 Spectrogram of ARIS Transition to Active Mode Zoom (121f06)..... 95
Figure 6-57 Spectrogram of ARIS Transition to Active Mode Zoom (121f05)..... 96
Figure 6-58 Time Series of ARIS in Active Mode Comparison (121f05,121f06)..... 97
Figure 6-59 OTO of ARIS in Active Mode Comparison (121f05,121f06) 98
Figure 6-60 OTO of ARIS in Active Mode Offboard Sensors (121f02,121f03,121f04) 99
Figure 6-61 Spectrogram of EXPPCS Activation (121f03) 100
Figure 6-62 Interval RMS of EXPPCS Activation (121f03)..... 101
Figure 6-63 Spectrogram of EXPPCS and ARIS-ICE POP Deactivation (121f06)..... 102
Figure 6-64 Spectrogram of [Not Apparent] APCF Deactivation/Activation (HiRAP)..... 103
Figure 6-65 Spectrogram of STS-108 Shuttle Ergometer Exercise (121f03)..... 104
Figure 6-66 Cumulative RMS of STS-108 Shuttle Ergometer Exercise (121f03)..... 105
Figure 6-67 Cumulative RMS of Various Shuttle and Mir Exercise Periods (SAMS)..... 106
Figure 6-68 PSDs of STS-108 Shuttle Ergometer Exercise (121f03) 107
Figure 7-1 PCSA for MAMS HiRAP (HiRAP)..... 110
Figure 7-2 PCSA for SAMS 121f06 (121f06)..... 111
Figure 7-3 PCSA for SAMS 121f05 (121f05)..... 112
Figure 7-4 PCSA for SAMS 121f04 (121f04)..... 113
Figure 7-5 PCSA for SAMS 121f03 (121f03)..... 114
Figure 8-1 Y-Axis autospectra PSD Pre-Endeavor undocking..... 116

Figure 8-2 Y-Axis autospectra PSD post-Endeavor undocking 117
Figure 8-3 Y-Axis PSD ratio of SE 121F03 to 121F04 response for Pre-Endeavor undocking 118
Figure 8-4 Y-Axis PSD ratio of SE 121F03 to 121F04 response for Post-Endeavor undocking 119
Figure 8-5 X-Axis PSD ratio of SE 121F03 to 121F04 response for Pre-Endeavor undocking 120
Figure 8-6 X-Axis PSD ratio of SE 121F03 to 121F04 response for Post-Endeavor undocking 121
Figure A - 1 On-Line Data Access Flow Chart 127
Figure A - 2 Screenshot of Sample PAD File Listing 128
Figure E - 1 Trimmed Mean Filter Process 146

1 Introduction

The NASA Office of Biological and Physical Research sponsors science experiments on various reduced-gravity carriers/platforms and facilities such as the Space Transportation System (STS), parabolic flight-path aircraft, sounding rockets, drop towers and the International Space Station (ISS). To provide support for the science experiments, which require acceleration data measurement on the ISS, the Physical Science Division sponsors two microgravity accelerometer systems, the Space Acceleration Measurement System (SAMS) and the Microgravity Acceleration Measurement System (MAMS). SAMS measures vibratory acceleration data in the range of 0.01 to 400 Hz for payloads requiring such measurement. MAMS consists of two sensors, the Orbital Acceleration Research Experiment (OARE) Sensor Subsystem (OSS) and the High Resolution Accelerometer Package (HiRAP). The OSS is a low frequency range sensor (up to 1 Hz) used to characterize the quasi-steady environment for payloads and the ISS vehicle. The HiRAP is used to characterize the ISS vibratory environment from 0.01 Hz to 100 Hz. Both MAMS and SAMS were flown to the ISS on STS-100, which was launched April 19, 2001 from the Kennedy Space Center (KSC).

The residual acceleration environment of an orbiting spacecraft in a low earth orbit is a complex phenomenon [1]. Many factors, such as experiment operation, life-support systems, crew activities, aerodynamic drag, gravity gradient, rotational effects and the vehicle structural resonance frequencies (structural modes) contribute to form the overall reduced gravity environment. Weightlessness is an ideal state, which cannot be achieved in practice because of the various sources of acceleration present in an orbiting spacecraft. As a result, the environment in which experiments are conducted is *not zero* gravity, and most experiments can be affected by the residual acceleration because of their dependency on acceleration magnitude, frequency, orientation and duration. Therefore, experimenters must know what the environment was when their experiments were performed in order to analyze and correctly interpret the result of their experimental data. In a terrestrial laboratory, researchers are expected to know and record certain parameters such as pressure, temperature, and humidity level in their laboratory prior to and possibly throughout their experiment. The same holds true in space, except that acceleration effects emerge as an important consideration.

The NASA Glenn Research Center (GRC) Principal Investigator Microgravity Services (PIMS) project has the responsibility for processing and archiving acceleration measurements, analyzing these measurements, characterizing the reduced gravity environment in which the measurements were taken, and providing expertise in reduced gravity environment assessment for a variety of carriers/platforms and facilities, such as the Space Shuttle, parabolic flight-path aircraft, sounding rockets, drop towers and the ISS in support of the NASA's Physical Science Division Principal Investigators (PIs). The PIMS project supports PIs from the microgravity science disciplines of biotechnology, combustion science, fluid physics, material science and fundamental physics. The PIMS project is funded by the NASA Headquarters and is part of the NASA GRC's Microgravity Environment Program (MEP), which integrates the analysis and interpretation component of PIMS with the various NASA sponsored acceleration measurement systems. For the ISS,

these acceleration measurement systems include SAMS and MAMS. The PIMS project is responsible for receiving, processing, analyzing, displaying, distributing, and archiving the acceleration data for SAMS and MAMS during ISS operations. This report presents to the microgravity scientific community the results of some of the analyses performed by PIMS using the acceleration data measured by the two-accelerometer systems during the period of August to December 2001 aboard the ISS.

2 International Space Station

2.1 Configuration at Assembly Complete

The ISS represents a global partnership of many nations. This project is an engineering, scientific and technological marvel ushering in a new era of human space exploration. Assembly of the ISS began in late 1998 [2] and will continue until completion sometime around the year 2004. During its assembly and over its nominal 10-year lifetime, the ISS will serve as an orbital platform for the United States and its International Partners to make advances in microgravity, space, life, and earth sciences, as well as in engineering research and technology development. The completed space station will have six fully equipped laboratories, nearly 40 payload racks [3] or experiment storage facilities, and more than 15 external payload locations for conducting experiments in the vacuum of space. The six main laboratories, which will house research facilities, are: Destiny (US), the Centrifuge Accommodations Module (CAM-US), Columbus (European Space Agency (ESA)), Kibo (National Space Development Agency of Japan (NASDA)) and two Russian Research Modules (yet to be named). The pressurized living and working space aboard the completed ISS will be approximately 43,000 ft^3 [4] (Table 2-1). Its giant solar arrays will generate the electricity needed. An initial crew of three, increasing to seven when assembly is complete (Figure 2-1), is living aboard the ISS. The space station represents a quantum leap in our ability to conduct research on orbit and explore basic questions in a variety of disciplines [4] such as biomedical, fundamental biology, biotechnology, fluid physics, advanced human support technology, material science, combustion science, fundamental physics, earth science and space science.

TABLE 2-1 ISS SPECIFICATION AT ASSEMBLY COMPLETE

Wingspan Width	356 feet (108.5 m)
Length	290 feet (88.4 m)
Mass (weight)	About 1 million pounds (453,592 kg)
Operating Altitude	220 nautical miles average (407 km)
Inclination	51.6 degrees to the Equator
Atmosphere inside	14.7 psi (101.36 kilopascals)
Pressurized Volume	43,000 ft^3 (1,218 m^3) in 6 laboratories
Crew Size	3, increasing to 7

2.2 ISS Coordinate Systems

For ISS operations, PIMS reports acceleration data to the microgravity scientific community using the ISS analysis coordinate system or in a specific sensor's local coordinate system.

2.2.1 Space Station Analysis Coordinate System

The ISS analysis system [5] is derived using the Local Vertical Local Horizontal (LVLH) flight orientation. When defining the relationship between this coordinate system and another, the Euler angle sequence to be used is a yaw, pitch, roll sequence around the Z_A, Y_A, and X_A axes, respectively (Figure 2-2). The ISS Analysis frame is aligned with the Starboard Truss Segment 0 (S0) Coordinate frame, and the origin (Figure 2-3) is located at the geometric center of the Integrated Truss Segment (ITS) S0. The X_A axis is parallel to the longitudinal axis of the module cluster. The positive X_A axis is in the forward (flight) direction. The Y_A axis is identical to the S0 axis. The nominal alpha solar array joint rotational axis is parallel with the Y_A axis. The positive Y_A axis is in the starboard direction. The positive Z_A axis is in the direction of Nadir (toward earth) and completes the right-handed Cartesian system (RHCS). This analysis coordinate system is used by PIMS in its analysis and reporting of the acceleration data measured on ISS unless a sensor coordinate system is specified. A more detailed description of the ISS coordinate systems can be found in [5].

2.2.2 Integrated Truss Segment S0 Coordinate System

This coordinate system defines the origin, orientation, and sense of the ISS analysis coordinate system. The YZ plane nominally contains the centerline of all four trunnion pins. The origin is defined as the intersection of two diagonal lines connecting the centers of the bases of opposite trunnion pins, running T1 to T3 and from T2 to T4 (Figure 2-3). The X-axis (X_{S0}) is parallel to the vector cross product of the Y-axis with the line from the center of the base trunnion pin T2 to the center of the base trunnion pin T3, and is positive forward. The Y-axis (Y_{S0}) is parallel with the line from the center of the base of trunnion pin T2 to the center of the base of trunnion pin T1. The positive Y-axis is toward starboard. The Z-axis (Z_{S0}) completes the RHCS.

2.2.3 United States Laboratory Module (Destiny) Coordinate System

The US Laboratory module makes use of a RHCS [5], body-fixed to the pressurized module. The origin is located forward of the pressurized module such that the center of the bases of the aft trunnions have X_{LAB} components nominally equal to 1000 inches. The X_{LAB} -axis is perpendicular to the nominal aft Common Berthing Mechanism (CBM) interface plane and pierces the geometric center of the array of mating bolts at the aft end of the pressurized module. The positive X_{LAB} -axis is toward the pressurized module from the origin. The Y_{LAB} -axis completes the RHCS. The Z_{LAB} -axis is parallel to the perpendicular line from the

X_{LAB} -axis to the center base of the keel pin base, and positive in the opposite direction as shown in Figure 2-4.

2.3 ISS Flight Attitude at Assembly Complete

The basic flight attitude [6] for ISS is called X body axis toward the Velocity Vector (XVV) Z Nadir Torque Equilibrium Attitude (TEA), or XVV TEA for short. XVV Z Nadir (XVV for short) stands for X body axis toward the velocity vector, Z body axis toward Nadir (earth), and TEA is for torque equilibrium attitude. The ISS vehicle design is optimized for the XVV attitude (Figure 2-5). The XVV attitude places the most modules in the microgravity volume; supports altitude reboosts, services vehicle dockings, and minimizes aerodynamic drag. The ISS is designed to tolerate deviations from perfect XVV Z Nadir of +/- 15 degrees in each axis. This envelope was expanded to -20 degrees in pitch.

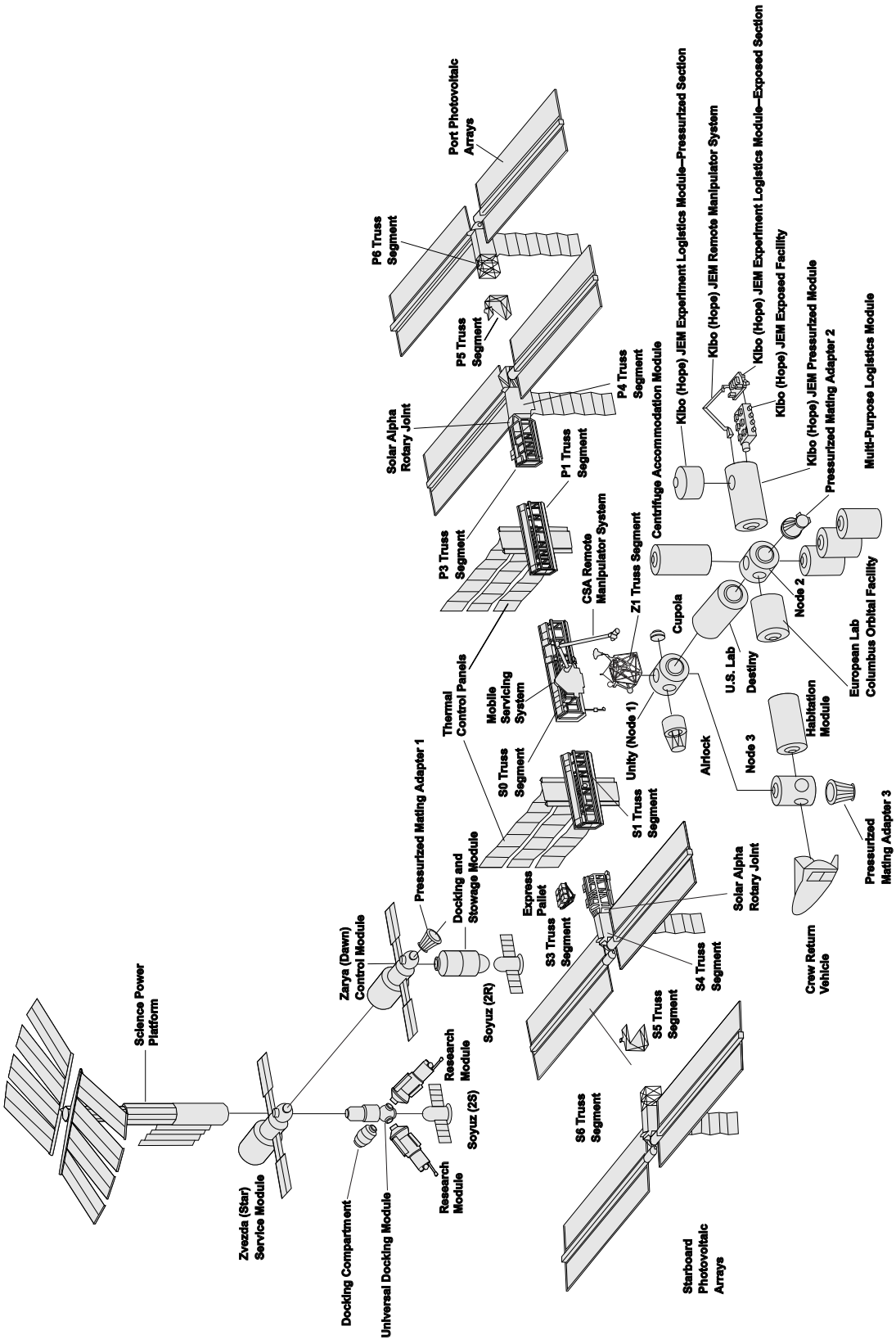

Figure 2-1 International Space Station at Assembly Complete

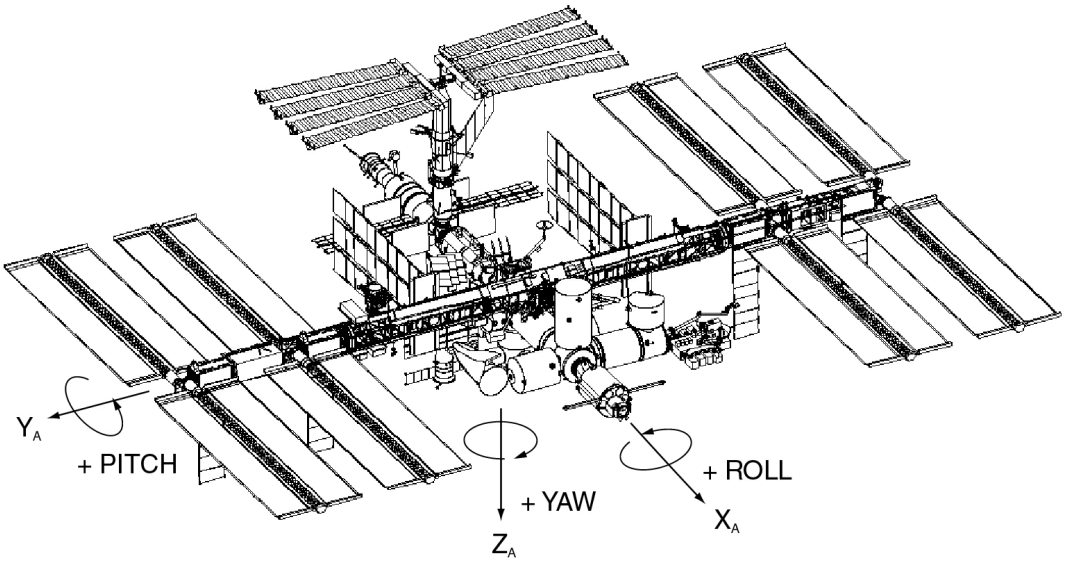

Figure 2-2 Space Station Analysis Coordinate System

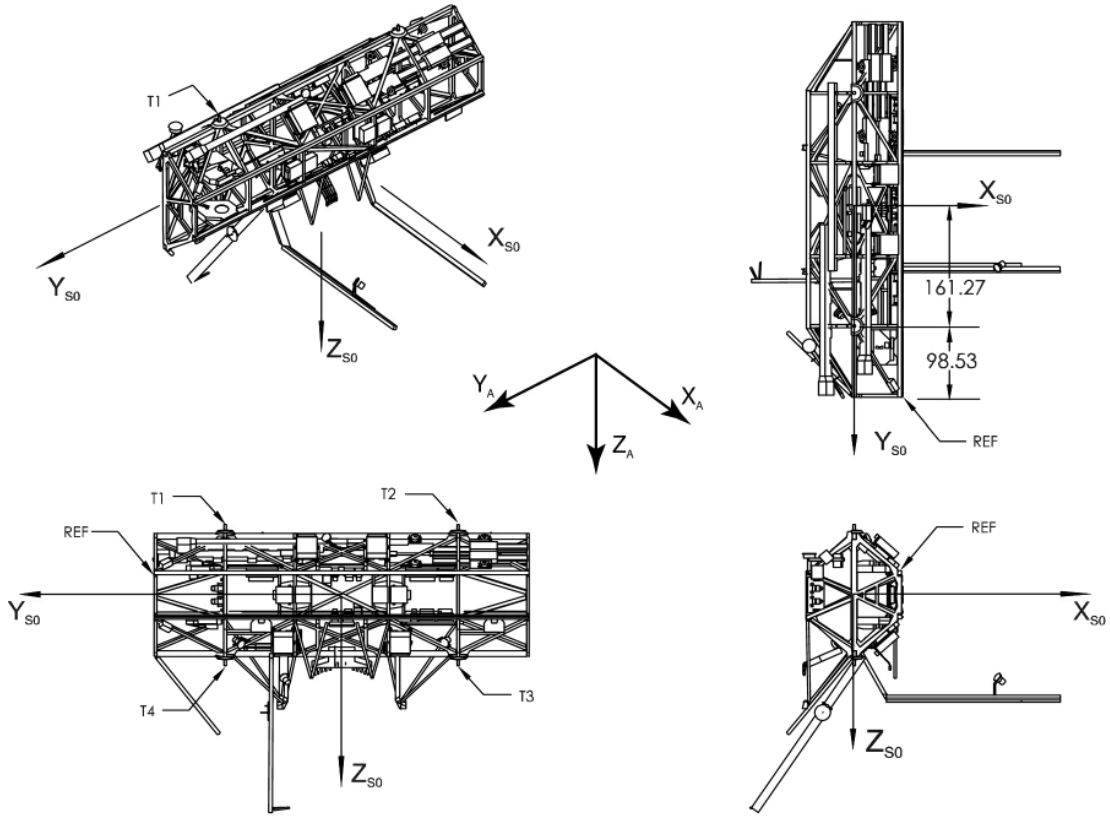

Figure 2-3 Integrated Truss Segment S0 Coordinate System

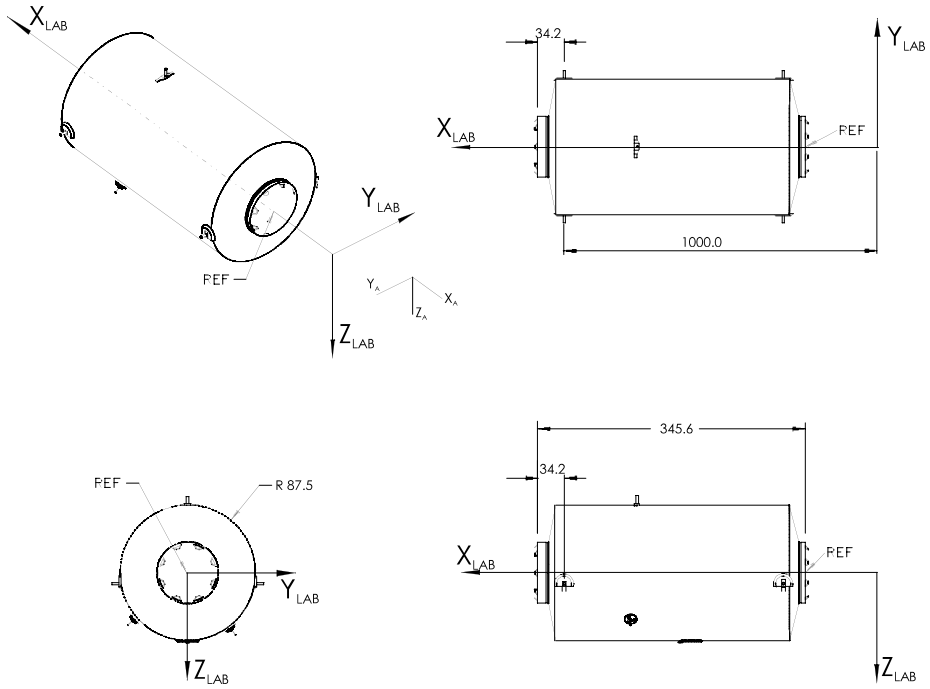

Figure 2-4 United States Laboratory Module (Destiny) Coordinate System

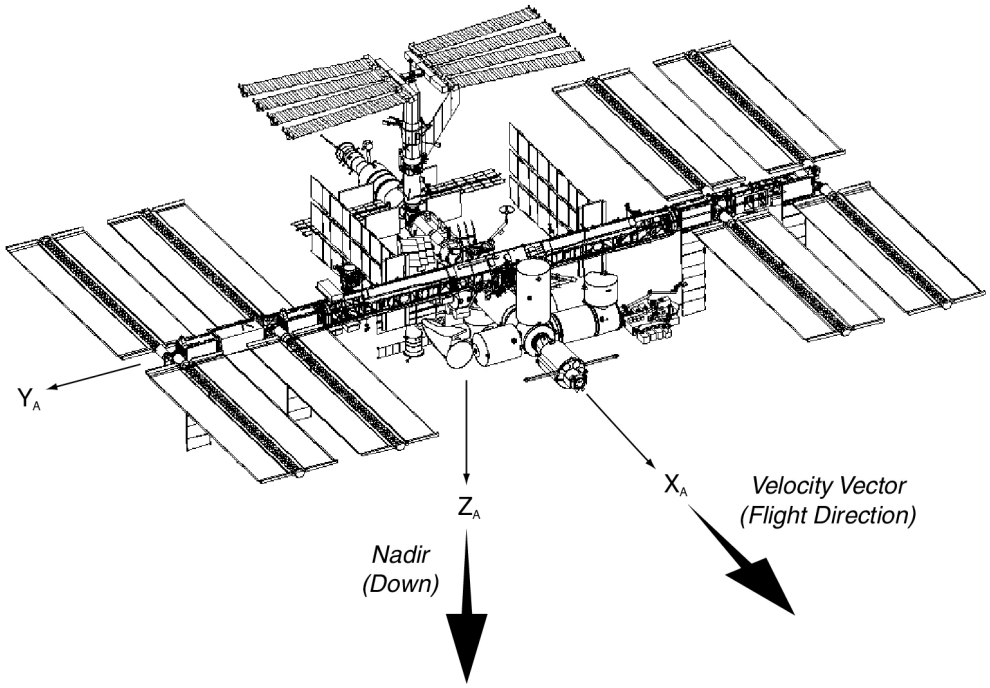

Figure 2-5 ISS XVV Flight Attitude

3 ISS Increment-3

3.1 Increment-3 Configuration

An increment should average about 4 months and is determined by crew rotations and flights to/from ISS. Each increment has a theme that focuses on the primary science or activities to be performed. This Increment is called Increment-3 or Expedition Three and its theme is: Bone and muscle research [7]. The 3-member crew for Increment-3 mission was launched to ISS on August 12, 2001 on STS-105 from KSC and returned to earth on STS-108 on December 17, 2001 after a 129 days stay in space. During the Increment-3 segment, ISS was expanded from four to five modules with the addition of the Russian Docking Compartment (DC-1). The following modules are now on-orbit [8] Unity (Node), Zarya (Functional Cargo Block), Zvezda (Service Module), Destiny, and the Russian DC-1 (Figure 3-1).

During the Expedition Three crew's four-month stay aboard the station, the Russian DC-1 module (Pirs) was added to ISS. DC-1 was launched on a Soyuz rocket from the Baikonur Cosmodrome in Kazakhstan for an automated linkup to the nadir (earthward facing) docking port on the Zvezda Service Module. The new module serves as an additional docking port for visiting Soyuz and Progress craft, and as an airlock from which Russian segment spacewalks can be conducted [3]. DC-1 has a total mass (with support equipment) of 8,090 lbs., maximal length of 14.6 ft (16.1 ft with docking assembly probe extended), maximum diameter of 8.3 ft, and a pressurized compartment volume of 459 ft^3 [3].

Table 3-1 is a list of missions to the ISS during Increment-3 four-month stay aboard the station [9]:

TABLE 3-1 INCREMENT-3 MISSIONS

Mission	Date	Mission Objective
7A.1 – STS-105	August 12-20, 2001	Arrival of Expedition Three crew
4P – Progress 4	August 22, 2001	Undock of Progress 4 supply craft
5P – Progress 5	August 23, 2001	Dock of Progress 5 supply craft to Zvezda aft port
4R – DC-1	September 17, 2001	Russian Docking Compartment (DC-1) docked to Zvezda nadir port
M1	September 26, 2001	DC-1 Engine Undock
2S – Soyuz 2	October 18, 2001	"Old" Soyuz taxi vehicle at ISS relocated from Zarya nadir port to DC-1
3S – Soyuz 3	October 22, 2001	New Soyuz taxi vehicle arrived at ISS and docked to Zarya nadir port
2S – Soyuz 2	October 31, 2001	"Old" Soyuz taxi vehicle undocked
5P – Progress 5	November 22, 2001	Progress 5 supply craft undocked
6P – Progress 6	November 28, 2001	Progress 6 supply craft docked to Zvezda aft port
UF-1 – STS-108	December 7-15, 2001	Arrival of Expedition Four crew

3.2 Increment-3 Coordinate Systems

The coordinate systems [10] shown in Figure 3-2 were used in performing the data analysis presented in this report. Figure 3-2 shows MAMS OSS and MAMS HiRAP positive acceleration axes alignment relative to the ISS analysis coordinate system (for SAMS, see section 4.4). However, the origin of the coordinate systems shown is not exactly at the location shown (except for the ISS analysis coordinate system). They are shown here for relative alignment only, not their origin. For their location relative to the ISS analysis coordinate system, the reader should refer to section 4.2. In Figure 3-2, XYZ_A refers to the ISS analysis coordinate system, XYZ_H refers to the MAMS HiRAP coordinate system, XYZ_{OSS} refers to the MAMS OSS coordinate system. Figure 3-2 is provided only to illustrate the coordinate system relationships during Increment-3.

3.3 Increment-3 Overall Attitude

During the assembly stages (stages 2A through 12A.1), the ISS will not be capable of generating enough power to sustain the required electrical loads in the XVV flight attitude at mid-to-high solar beta angles because these vehicle configurations have only a single solar array gimbal axis, which is aligned so that it only perfectly tracks the Sun when the solar beta angle is near zero. Therefore, the ISS is designed to accommodate a second basic flight orientation for these increments. This attitude is referred to as X Principal Axis Perpendicular to the Orbit Plane (XPOP) (see Figure 3-3), which stands for X principal axis perpendicular to the orbit plane, Z Nadir at orbital noon. The XPOP flight attitude [6] sets up geometry between the ISS and the Sun so that the Sun aligns with the ISS/XZ body axis plane. This allows all the solar arrays to track the Sun regardless of the solar beta angle. XPOP also places the dominant inertia axis in the local horizontal to minimize gravity gradient torques and allow Control Moment Gyro (CMG) non-propulsive attitude control.

3.4 Increment-3 Crew Members

During Increment-3 (Expedition Three), the crew worked with several experiments. The Increment-3 primary focused was the effects of space flight on bone and muscle mass during extended stays in space and how such phenomena may relate to similar conditions on earth. Additional experiments during Expedition Three were intended to lead to new insights in the fields of human life sciences, biotechnology, education, and video technology [3]. Increment-3 had one astronaut and two cosmonauts. The commander was astronaut Frank L. Culbertson; Soyuz vehicle commander was cosmonaut Vladimir Dezhurov and flight engineer was cosmonaut Mikhail Tyurin. The crew was launched to the ISS on August 10, 2001 aboard the Space Shuttle Discovery STS-105 and returned to KSC on December 17, 2001 aboard STS-108.

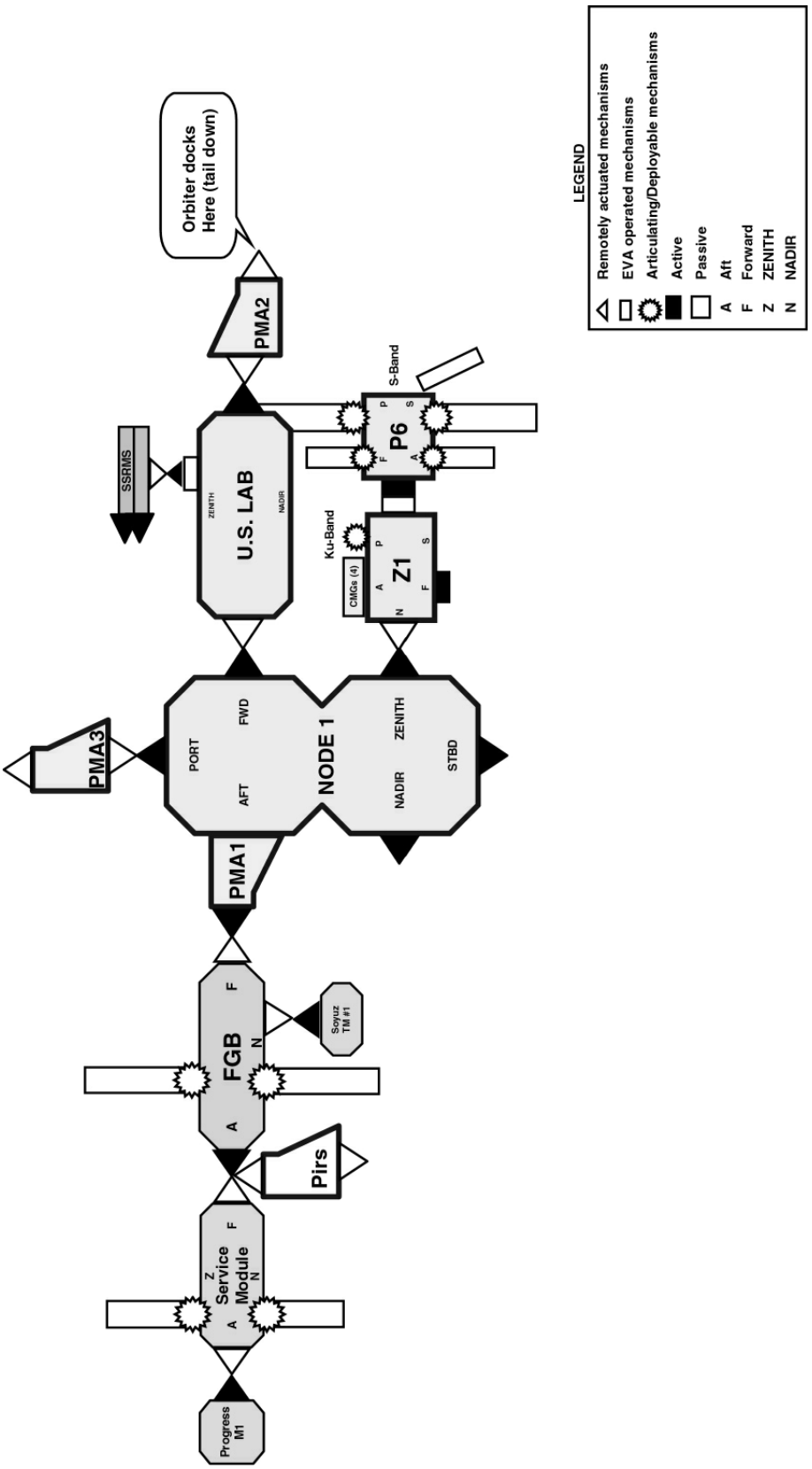

Figure 3-1 ISS Increment-3 Configuration

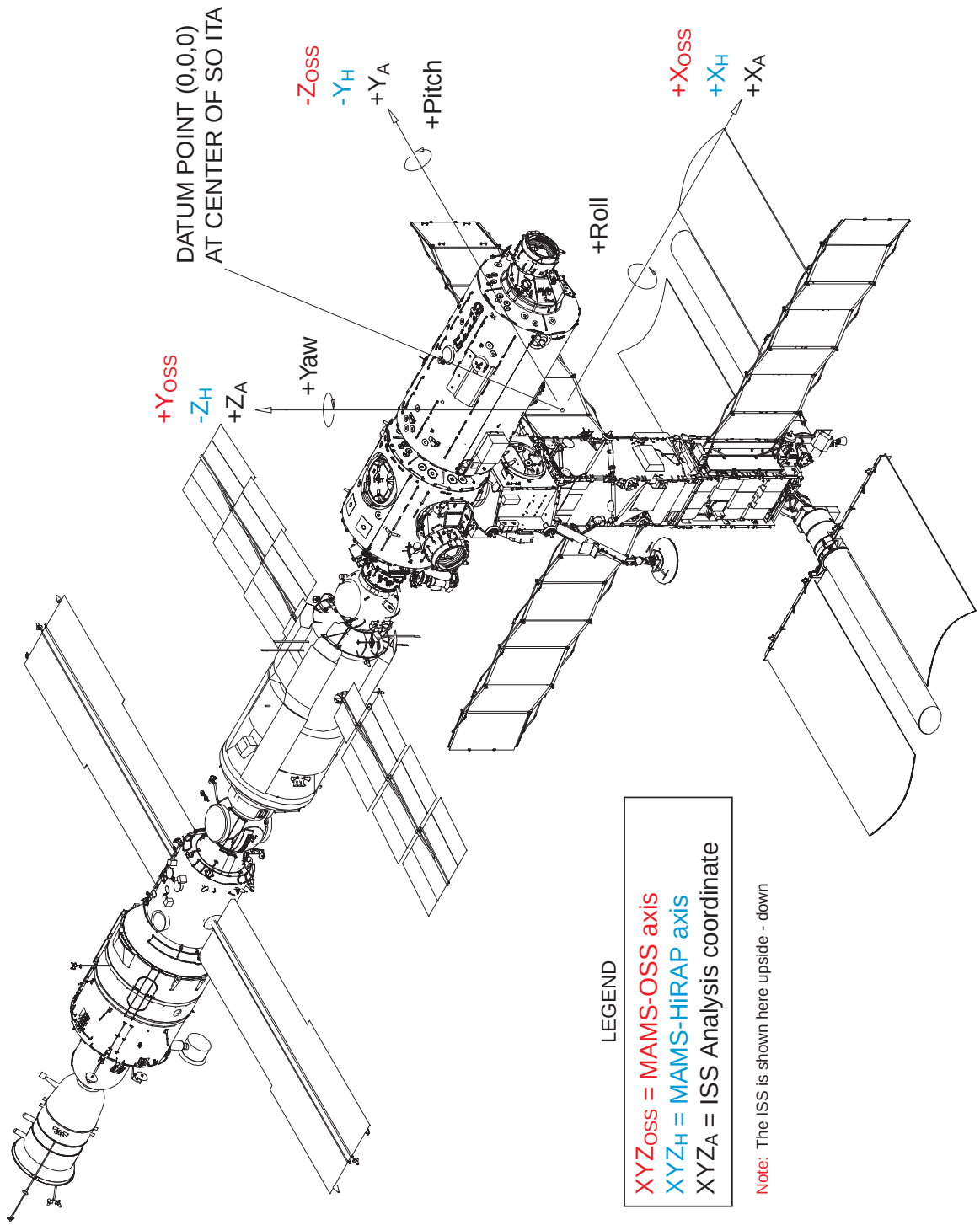

Figure 3-2 Increment-3 Coordinate Systems

Figure 3-3 ISS in the XPOP Inertial Flight Attitude

4 Acceleration Measurement System Descriptions: Increment-3

One of the major goals of ISS is to provide a quiescent reduced gravity environment to perform fundamental scientific research. However, small disturbances aboard the Space Station impact the overall environment in which experiments are being performed. Such small disturbances need to be measured in order to assess their potential impact on the experiments. Two accelerometer systems developed by NASA's GRC in Cleveland, Ohio, are being used aboard the station to acquire such measurements. These two systems were flown to the ISS on April 19, 2001 aboard the space shuttle flight STS-100.

4.1 Microgravity Acceleration Measurement System (MAMS)

MAMS measures acceleration caused by aerodynamic drag, vehicle rotations, and vents of air and water. MAMS consists of two sensors. MAMS OSS, a low frequency sensor (up to 1 Hz), is used to characterize the quasi-steady environment for payloads and the vehicle. MAMS HiRAP [11] is used to characterize the ISS vibratory environment up to 100 Hz. For Increment-3, MAMS was located in a double middeck locker, in the US Laboratory Module (Destiny) in the EXpedite the PRocessing of Experiments to the Space Station (EXPRESS) Rack 1.

4.2 MAMS Coordinate Systems

MAMS was located in middeck lockers 3 and 4 of EXPRESS Rack 1, in overhead bay 2 of the US Laboratory Module (LAB1O2). The origin of the OSS coordinate system is located at the center of gravity of the OSS proof mass. Table 4-1 gives the orientation and location of the OSS and HiRAP coordinate systems with respect to Space Station Analysis coordinate system.

TABLE 4-1 MAMS SENSOR COORDINATE SYSTEM

MAMS Sensor	Location (inches)			Orientation (degrees)			Unit Vector in Analysis Coordinates			
	X_A	Y_A	Z_A	Roll	Pitch	Yaw	Axes	X_A	Y_A	Z_A
OSS	135.28	-10.68	132.12	90	0	0	X_{OSS}	1	0	0
							Y_{OSS}	0	0	1
							Z_{OSS}	0	-1	0
HiRAP	138.68	-16.18	142.35	180	0	0	X_H	1	0	0
							Y_H	0	-1	0
							Z_H	0	0	-1

4.3 Space Acceleration Measurement System (SAMS)

SAMS measures accelerations caused by vehicle, crew, and experiment disturbances. SAMS measures the vibratory/transient accelerations, which occur in the frequency range of 0.01 to 400 Hz. For Increment-3, there were five SAMS sensor heads located in the EXPRESS

Racks 1 and 2. The sensors measure the accelerations electronically and transmit the data to the Interim Control Unit (ICU) located in the EXPRESS Rack drawer. Data is collected from all the sensors and downlinked to the Telescience Support Center (TSC) at GRC. The PIMS project processes, and displays the data on the PIMS Web site for easy access by the microgravity scientific community at:

http://pims.grc.nasa.gov.

4.4 SAMS Coordinate Systems

During Increment-3, five SAMS Sensor Enclosure (SE) heads were active: 121f02 through121f06. Each sensor head has a defined coordinate system whose location and orientation is with respect to the Space Station Analysis Coordinate System. The origin is defined as the triaxial center point of the three accelerometers that comprise the head.

SAMS SE 121f02 was mounted in the SAMS ISIS drawer 1 in EXPRESS Rack 1. SAMS SE heads 121f03, 121f04 and 121f05 were installed in support of Active Ract Isolation System ISS Characterization Experiment (ARIS-ICE) activities. Head 121f03 was mounted on the lower Z Panel assembly below EXPRESS Rack 2, head 121f04 was mounted on the lower Z Panel assembly below EXPRESS Rack 1, and head 121f05 was mounted on a bracket around the upper Z Panel light assembly of EXPRESS Rack 2. SAMS SE 121f06 was mounted on the front panel of the EXPeriment of Physics of Colloids in Space (EXPPCS) test section on EXPRESS Rack 2. Table 4-2 summarizes the SAMS SE coordinate systems.

TABLE 4-2 SAMS SE COORDINATE SYSTEMS

Sensor	Location (inches)			Orientation (degrees)			Unit Vector in Analysis Coordinates			
	X_A	Y_A	Z_A	Roll	Pitch	Yaw	Axes	X_A	Y_A	Z_A
121f02	128.73	-23.53	144.15	-90	0	-90	X_{F02}	0	-1	0
							Y_{F02}	0	0	-1
							Z_{F02}	1	0	0
121f03	191.54	-40.54	135.25	0	30	-90	X_{F03}	0	-.866	-.500
							Y_{F03}	1	0	0
							Z_{F03}	0	-.5	.866
121f04	149.54	-40.54	135.25	0	30	-90	X_{F04}	0	-.866	-.500
							Y_{F04}	1	0	0
							Z_{F04}	0	-.5	.866
121f05	185.17	38.55	149.93	90	0	90	X_{F05}	0	1	0
							Y_{F05}	0	0	1
							Z_{F05}	1	0	0
121f06	179.90	-6.44	145.55	180	90	0	X_{F06}	0	0	-1
							Y_{F06}	0	-1	0
							Z_{F06}	-1	0	0

5 Specific Facilities and Experiments Supported by PIMS: Increment-3

5.1 Increment-3 Facilities

Research facilities that were launched to the station during Increment-3 include EXPRESS Racks 4 and 5, and the Cellular Biotechnology Operations Support System (CBOSS). EXPRESS Racks 1 and 2 as well as the Human Research Facility continue to support existing and new experiments. Utilities provided to experiments by the four racks currently on the ISS include power, fluids, gasses, cooling, and data management support. Over the life of the Space Station, these facilities will support a wide range of experiments [12]. During Increment-3, the PIMS project supported EXPRESS Racks 1 and 2.

The EXPRESS Rack [13] is a standardized payload rack system that transports, stores and supports experiments aboard the International Space Station. The EXPRESS Rack system supports science payloads in several disciplines, including biology, chemistry, physics, ecology and medicine. The EXPRESS Rack with its standardized interfaces enables quick, simple integration of multiple payloads aboard the station. Each EXPRESS Rack is housed in an International Standard Payload Rack – a refrigerator-size container that acts as the EXPRESS Rack's exterior shell-- and can be divided into segments. The EXPRESS Racks [14] have eight middeck locker locations and two drawer locations each (Figure 5-1, Figure 5-2). Figure 5-3 illustrates the relative locations of each EXPRESS rack within the US laboratory volume.

5.2 Increment-3 Experiments

During this increment, the PIMS project supported the following experiments, which require acceleration data measurements to assess the impact of the ISS reduced gravity environment on the science: Active Rack Isolation System ISS Characterization Experiment (ARIS-ICE) and Experiment of Physics of Colloids in Space (EXPPCS). Table 5-1 [15] shows the experiments that were performed by the Increment-3 crew.

TABLE 5-1 INCREMENT-3 PAYLOADS

Facility/Experiment	Mission information	Duration	Location on ISS	Research Area
Active Rack Isolation System	Mission 6A STS-100	15 years	Express Rack 2 Destiny module	
Express Racks 1, 2, 4, 5	Mission 6A STS-100/7A.1 STS-105	15 years	Destiny module	Multidisciplinary
Human Research Facility	Mission 5A.1 STS-102	15 years	Destiny module	Human Life sciences
Payload Equipment Restraint System	Mission 5A.1 STS-102	15 years	Destiny module	
Bonner Ball Neutron Detector Radiation	Mission 5A.1 STS-102	8 months	Destiny module	Human Life Sciences -- Radiation
Crew Earth Observation	Mission 4A STS-97	15 years	Destiny and Zvezda modules	Space Flight Utilization Earth observation
Earth Knowledge Acquired by Middle Schools (EarthKAM)	Mission 5A STS-98	15 years	Russian Service Module window	Space Flight Utilization—Earth observation and outreach
Hoffman-Reflex	Mission 5A.1 STS-102	Approx. 1 year (Expeditions 2-4)	Human Research Facility Rack Destiny module	Human Life Sciences---Neurovestibular
Crew Interactions	Mission 7A.1 STS-105	28 months (Expeditions 2-6)	Human Research Facility Rack Destiny module	Human Life Sciences--Psychosocial
ARIS-ISS Characterization	Mission 6A STS-100	Approx. 10 months	Active Rack Isolation	Space Flight Utilization
Microgravity Acceleration Measurement System (MAMS)	Mission 6A STS-100	15 years	Express Rack 1 Destiny module	Physical Sciences--Environmental
Physics of Colloids in Space (EXPPCS)	Mission 6A STS-100	1 year (return on mission UF2 STS-111)	Express Rack 2 Destiny module	Physical Sciences—Fluids science
Space Acceleration Measurement System II (SAMS-II)	Mission 6A STS-100	15 years	Destiny module	Physical Sciences--Environmental
Sub-regional Assessment of Bone Loss in Axial Skeleton (Sub-regional Bone	Mission 5A.1 STS-102	2 years, 4 months (assigned to Exp. 2-6)	N/A—Preflight and post-flight data collection only	Human Life Sciences—Bone and muscle
Cellular Biotechnology Operations Support System	Mission 7A.1 STS-105	4 months (returns on STS-108, UF-1)	Mid-deck locker in EXPRESS Rack 4	Cell & tissue growth, cellular biotech research
Dynamically Controlled Protein Crystal Growth	Mission 7A.1 STS-105	4 months (return on STS-108, UF-1)	EXPRESS Rack 1 Destiny module	Physical Sciences—Protein crystallization
Renal Stone Investigation	Mission 7A.1 STS-105	40 months (Expeditions 3-12)	N/A—pre and post mission only	Human Life Sciences
Advanced Protein Crystallization Facility	Mission 7A.1 STS-105	4 months (Return on STS-108, UF-1)	EXPRESS Rack 1, Locker 5	Physical Sciences—Protein crystallization
Dreamtime	Mission 7A.1 STS-105	4 months (return on STS-108, UF-1)	Destiny module	Commercialization—HDTV technology
Materials International Space Station Experiment	Mission 7A.1 STS-105	Approx. 1 year	Outside airlock between PMA1 and Destiny	Physical Sciences
Xenon 1	Mission 7A.1 STS-105	Approx. 16 months (Expeditions 3-6)	N/A pre-and post-flight	Human Life Sciences
Pulmonary Function in Flight	Mission 7A.1 STS-105	Approx. 1 year (Expeditions 3-6)	Human Rack Facility, Destiny module	Human Life Sciences

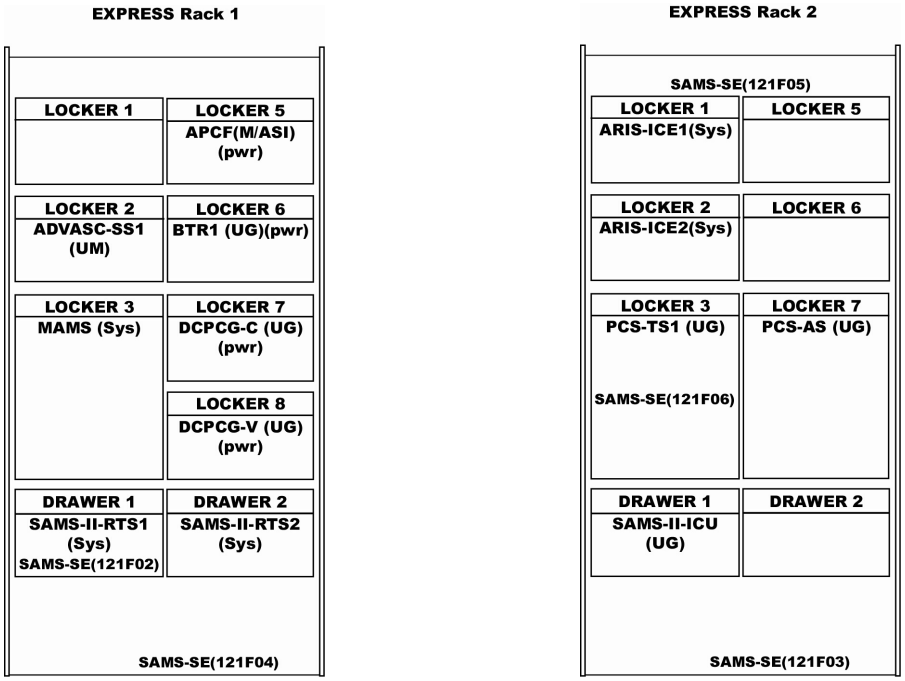

Figure 5-1 EXPRESS Racks 1 & 2, 7A On-Orbit Configuration

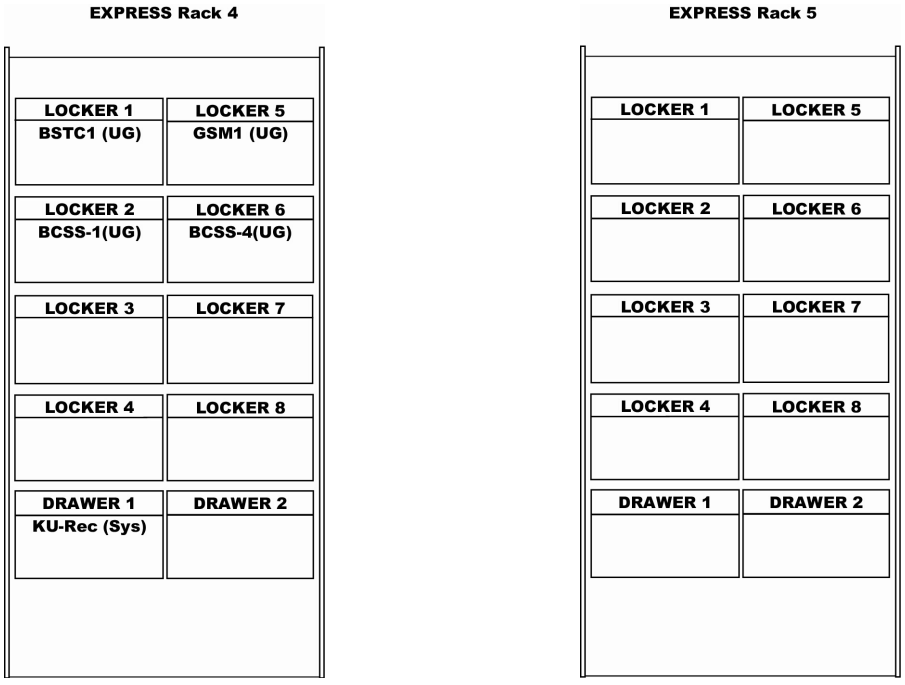

Figure 5-2 EXPRESS Rack 4 & 5, 7A On-Orbit Configuration

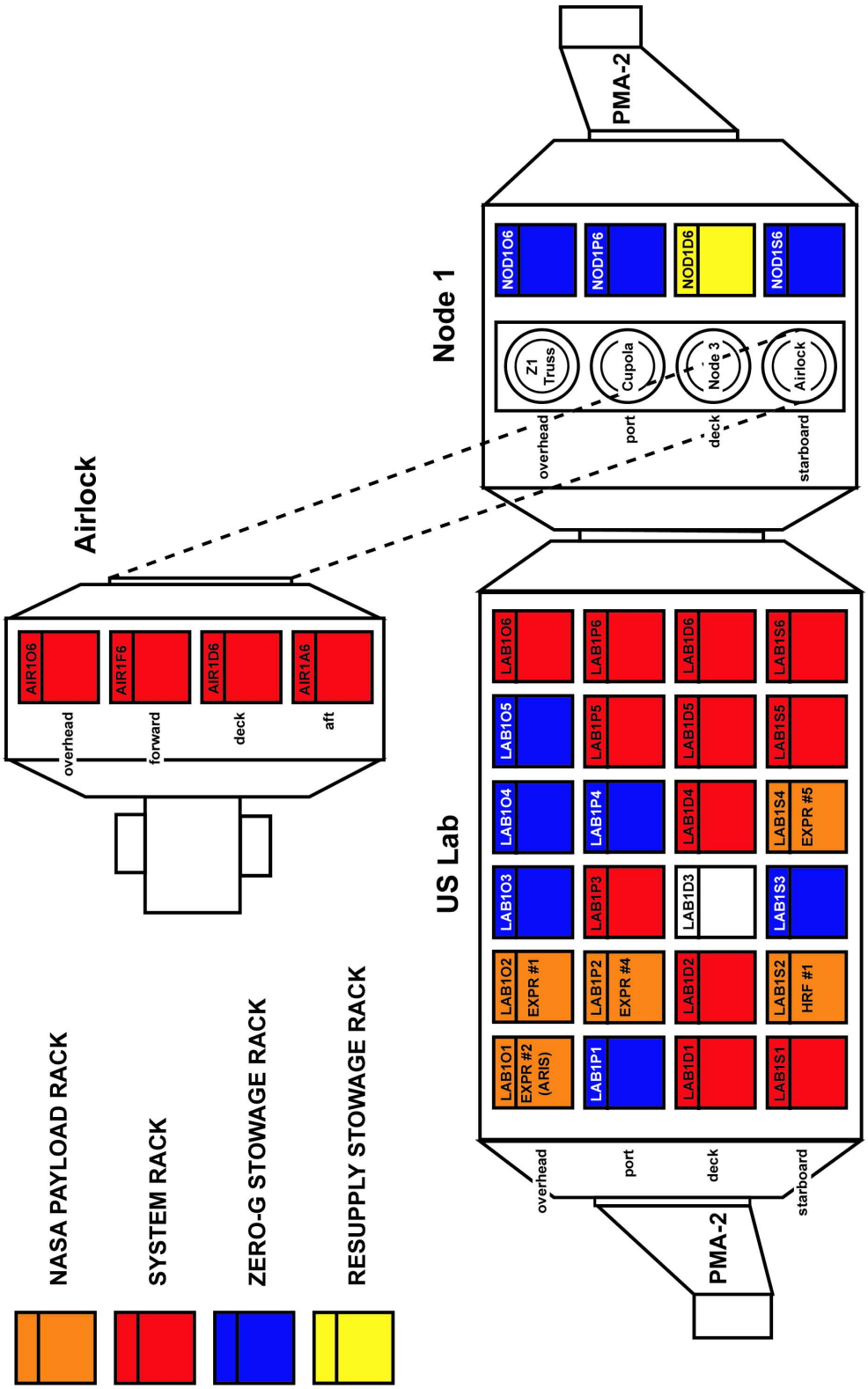

Figure 5.3 US Lab Rack Locations.

6 ISS Increment-3 Reduced Gravity Environment Description

6.1 Quasi-steady Microgravity Environment

The quasi-steady regime is comprised of accelerations with frequency content below 0.01 Hz and magnitudes expected to be on the order of 2 μg or less. These low-frequency accelerations are associated with phenomena related to the orbital rate, primarily aerodynamic drag. However, gravity gradient and rotational effects may dominate in this regime, depending on various conditions and an experiment's location relative to the vehicle's center of mass (CM). A final source of acceleration to consider in this regime is venting of air or water from the spacecraft. This action results in a nearly constant, low-level propulsive force. The different quasi-steady environment characteristics seen on the ISS for Increment-3 are primarily related to altitude and attitude of the station. Variation in atmospheric density with time and altitude contribute to the differences in the aerodynamic drag component. Different attitudes will affect the drag component due to the variation of the frontal cross-sectional area of the station with respect to the velocity vector.

6.1.1 ISS Attitudes

6.1.1.1 +ZLV +XVV Torque Equilibrium Attitude (TEA)

Torque Equilibrium Attitude (TEA) is an attitude that balances the vehicle's gravity gradient and aerodynamic drag torques. This is the attitude that will be flown during microgravity mode to support research. However, TEA will vary with station configuration because of change in mass and aerodynamic properties.

Figure 6-1 is a plot of MAMS OSS data measured during crew sleep, while the ISS was in TEA. For the time span in Figure 6-1, the TEA attitude was nominally YPR = (350.0, 350.7, 0.0) relative to the LVLH coordinate system. The black line in the plot represents the quasi-steady vector as measured by MAMS at the OSS location. The red line is an estimate of the quasi-steady vector at the CM and was calculated using telemetry data available through the Operational Data Request Center (ODRC) and the methods described in Appendix E.2.2. For this time period, the OSS sensor was located [16.10, -0.44, 0.25] meters from the ISS CM in the Space Station Analysis (SSA) coordinate system. Gaps appearing in the red line that are not in the black line are a result of S-Band Loss of Signal (LOS) periods for which data dumps of telemetry data are not received. Those gaps that appear at the same location in time in both lines (red and black) are the result of OSS bias periods or data loss. As expected, the difference between the two locations in the X_A axis is small, due to the cancellation of gravity gradient and rotational components at the OSS location when the vehicle maintains an LVLH attitude [16]. The largest difference in the means (0.91 μg) is seen in the Z_A axis, primarily due to the rotation about the Y_A axis at the orbital rate.

The quasi-steady vector at the CM can also be considered an estimate of the drag because the gravity gradient or rotational component contributions are both zero at the CM. The means of the components are as expected, a negative value in the X_A axis indicates the drag is in the direction opposite of flight and a positive value in Z_A axis indicates the loss of altitude. The

Y_A axis, which is perpendicular to the flight direction, has a component whose value is near zero (<0.01 μg). The red trace in Figure 6-2 shows the magnitude of the quasi-steady vectors at the CM for the same time span shown in Figure 6-1. The CM is the only location not subjected to gravity gradient or rotational accelerations. Therefore, the difference between the black and red traces is the residual acceleration contribution from gravity gradient and rotational accelerations at the OSS location, which on average for this period was 0.67 μg.

6.1.1.2 X-Axis Perpendicular to Orbital Plane (XPOP) Inertial Flight Attitude

XPOP is a sun-tracking, quasi-inertial flight attitude used for power generation. In this attitude, the vehicle's X_A axis is maintained perpendicular to the direction of flight. The time series plot for crew sleep during XPOP attitude at the OSS location in Figure 6-3 shows a fairly constant X_A axis acceleration component of 1.89 μg. The rotational components are very small for this attitude because it is maintained relative to inertial space. Because of this and the large moment arm in the X_A direction, the X_A component is nearly entirely due to gravity gradient effects. The OSS location was [-15.84 0.45 -0.42] meters distant from the CM for this time period. The in-plane axes, Y_A and Z_A, show more pronounced cyclical drag profiles as they are alternately subjected to the drag and gravity gradient vectors as the vehicle completes an orbit.

The magnitudes of the quasi-steady vector during XPOP can be seen for the OSS location and the CM location in Figure 6-4. The mean magnitude for the OSS location during XPOP attitude reflects the larger gravity gradient component relative to those during TEA. Table 6-1 summarizes the quasi-steady vector information for the two attitudes.

TABLE 6-1 QUASI-STEADY VECTOR FOR TEA AND XPOP ATTITUDES

Attitude/Location	Mean X_A (μg)	Mean Y_A (μg)	Mean Z_A (μg)	Mean Magnitude (μg)
TEA at OSS	-0.22	-0.40	-0.80	0.94
TEA at CM	-0.16	0.01	0.11	0.27
XPOP at OSS	1.89	0.00	-0.30	2.05
XPOP at CM	-0.13	-0.01	-0.01	0.50

6.1.1.3 CMG 2 Outer Gimbal Test

During Increment-3, the Outer Gimbal of the Control Moment Gyroscope #2 (CMG 2) began to exhibit an angular measurement bias. At GMT 09-October-2001, 281/19:51 a test began as attempt to measure this bias. The test involved removing CMG 2 from the steering law, moving it to a specific position and then alternating between some attitude modes. These attitude maneuvers, while still disturbances in the quasi-steady environment, were small compared to attitude changes for docking events or between XPOP and LVLH. After the test was complete, at GMT 11-October-2001, 283/04:50, CMG 2 was restored to the steering law and a different profile for the quasi-steady vector was seen due to a larger variance (magnitude and frequency) in the attitude and angular rates of the ISS. Figure 6-5 shows this transition marked by the red dotted line. Figure 6-6 and Figure 6-7 show the attitude relative to LVLH and angular rate data obtained from ODRC for the same time period.

Based on the MAMS OSS measurements, this state of large variance lasted until approximately GMT 13-October-2001, 286/08:00. Figure 6-8 is a QTH plot of the time period from GMT 11-October-2001, 283/04:50 to GMT 13-October-2001, 286/08:00, minus an interval encompassing at GMT 11-October-2001, 284/06:00 - 22:00 to avoid the effects of a re-boost. The quasi-steady vector direction was much less stable than that of a normal TEA period (compare with Figure 6-9). From Figure 6-5 it can be determined that the amplitude (AC component) for the quasi-steady vector increased from $X_A = \pm 0.20$ μg, $Y_A = \pm 0.07$ μg, $Z_A = \pm 0.22$ μg to $\pm X_A = \pm 0.48$ μg, $Y_A = \pm 0.45$ μg, $Z_A = \pm 0.74$ μg, whereas the mean values remained approximately the same.

6.1.2 Docking and Undocking Events

6.1.2.1 Progress 4P Undocking

The Progress undocking scheduled to be at GMT 22-August-2001, 234/06:05 was preceded by an attitude change from +ZLV +XVV TEA (nominal YPR = [350.0,352.5,0]) to +ZLV -XVV (nominal YPR = [180.0,0,0]) at approximately GMT 03:58. The Progress 4P undocked from the Service Module aft position. After the undocking at GMT 06:07, the ISS began a maneuver to return to +ZLV +XVV TEA. Both of these maneuvers are prominent in the $-X_A$ direction in Figure 6-10 as 10-20 μg disturbances lasting for approximately 20 minutes each. The actual undocking event is not apparent in the data due to the nature of the TMF applied. The disturbances in the Y_A and Z_A axes are significantly smaller due to the shorter distance to the CM in these directions and thus relatively smaller angular acceleration components.

6.1.2.2 DC-1 Docking and Docking Test

The new Pirs docking compartment, also called DC-1, docked automatically to the nadir port on the Service Module at GMT 17-September-2001, 260/01:05. Preparation for this event included attitude changes for both the docking, and also for docking tests, which occurred at GMT 14-September-2001, 257/00:12. In both cases, the ISS attitude was changed from +ZLV +XVV TEA (nominal YPR = [359.2, 355.8, 0] relative to LVLH) to -YPH -ZNN (nominal YPR = [135.7, 317.0, 238.2] relative to J2000). The time series plots for the test and the actual docking are shown in Figure 6-11 and Figure 6-12 respectively. The effects are seen in the X_A-axis, a -10 μg step for the change to docking attitude and a –25 μg step for the return to TEA. Note that OSS data for the change to docking attitude for the actual docking event was not recorded due to a MAMS OSS bias period. This appears as a gap approximately 2 hours into the plot in Figure 6-12.

6.1.2.3 Relocation of Soyuz-2

On GMT 292 (19-October-2001), the Soyuz-2 vehicle was moved from its position at Functional Cargo Block (FGB) nadir to DC-1 nadir in preparation for the Soyuz-3 docking. Figure 6-13 is a time series plot of MAMS OSS data measured during the relocation event. After free drift for FGB "hooks open" at 07:58 (about the 1 hour mark in the figure), the ISS was commanded to the inertial undocking attitude (nominal YPR = [164.0, 338.9, 237.5] relative to J2000). This event is barley noticeable in relation to the rest of events in the plot.

It appears as a 1μg, -3 μg and -4 μg disturbance in the X_A, Y_A, and Z_A axes respectively. The ISS was in free drift at the spring-propelled physical separation of the spacecraft. The undocking at 10:48 (just before the 4 hour mark) is not evident in the figure. The ISS was again maneuvered to docking attitude, which is evident as spikes in all three axes on the order of 10 μg. Re-docking of the Soyuz-2 was confirmed at 11:04, during an extended free drift period of approximately 22 minutes. The ISS was maneuvered to +ZLV +XVV duty attitude (nominal YPR = [350.0, 350.4, 0] relative to LVLH) in the time span from GMT 292/11:28 to 292/11:48.

6.1.3 Extravehicular Activities (EVA)

During the construction of the ISS, a frequent source of disturbances to the microgravity environment will be EVAs. The disturbances these events will cause, of course, depend on the activity, the type of equipment used, and attitude adjustments to accommodate these events. During Increment-3, MAMS was able to capture a few of these events and a variety of effects.

6.1.3.1 Space Station Remote Manipulator System (SSRMS) Maneuvers

On GMT 08-October-2001, 281/14:23, cosmonauts Vladimir Dezhurov and Mikhail Tyurin performed the first excursion from the new Pirs DC-1 module, to install new handrails and a ladder to help in future EVAs. The first disturbances in the quasi-steady environment that can be attributed to the EVA was a SSRMS/Canadarm maneuver to prepare to get into position to record the EVA on video. This event is seen in Figure 6-14 as a -13.2 μg in the Z_A direction and -7.2 μg in the X_A direction at approximately the 58 minute mark. Figure 6-15 is an acceleration magnitude plot showing the event as a triplet of large spikes, the largest being 13.2 μg.

Figure 6-16 is a time series of MAMS OSS data measured encompassing the EVA period with the red dotted lines marking the official time of the EVA defined by DC-1 egress and ingress. It is clear that the overall quasi-steady environment is significantly noisier in the Y_A and Z_A axes, with numerous peaks in the -12 to -18 μg range. This condition is repeated for the 5 hour EVA starting at GMT 12-November-2001, 316/21:41, seen in Figure 6-17.

6.1.3.2 DC-1 Depressurization

The depressurization of the DC-1/PkhO volume began at GMT 08-October-2001, 281/13:46 (106 minutes in Figure 6-14). It is primarily a -3 μg step in the X_A-axis. Spikes on the order of 6-8 μg can be seen in the Y_A and Z_A axes. Figure 6-15 shows peak magnitudes for this event of 9.1 μg, and tailing off down to the baseline near 1 μg after approximately 15 minutes. Similar effect can be seen in Figure 6-18 for the DC-1 depressurization for the EVA at GMT 12-November-2001, 316/19:35. The red dotted box highlights the depressurization with steps of -4 μg, -3 μg and 2 μg in the X_A, Y_A and Z_A axes respectively.

6.1.3.3 SM Thrusters Inhibited

EVA-5 was performed at GMT 03-December-2001, 337/13:20 to remove a rubber seal that was obstructing the hard mating of Progress. During the EVA, ISS flight attitude was under control of the CMG momentum management and the SM control thrusters were inhibited because the location of the obstruction was in close proximity to the Zvezda thrusters. Without these thrusters, de-saturation of the CMGs is not possible and the ISS was in free drift. The 2 hour 46 minute EVA was completed at 16:06 and thruster control was restored at 17:45. The table below is an excerpt from the as-flown Attitude Timeline (ATL) showing the details of this event.

TABLE 6-2 EXCERPT OF INCREMENT-3 AS-FLOWN TIMELINE FOR EVA-5

#	Maneuver Start-Stop GMT	Attitude Name	Ref Frame	YPR	Event	Remarks
227	337/14:00	+ZLV +XVV	LVLH	350.0 352.4 0.0	Thrusters Inhibited	For EVA
228	337/14:30	Free Drift			Free Drift (reserve)	For Probe Extension
229	337/17:45	Free Drift			Attitude Handover: US to RS (reserve)	Prepare for Thrusters control
230	337/17:55 18:25	+ZLV +XVV	LVLH	350.0 352.4 0.0	LVLH TEA (reserve)	Return to TEA after EVA
231	337/18:30	+ZLV +XVV	LVLH	350.0 352.4 0.0	Attitude Handover: RS to US (reserve)	CCDB 03002
232	337/18:40	+ZLV +XVV	LVLH	350.0 352.4 0.0	Momentum Management (reserve)	CCDB 10503
233	337/19:00	+ZLV +XVV	LVLH	350.0 352.4 0.0	Thrusters Enabled	
234	337/21:15	+ZLV +XVV	LVLH	350.0 352.4 0.0	Thrusters Inhibited	For Clamp Install
235	337/23:42	+ZLV +XVV	LVLH	350.0 352.4 0.0	Thrusters Enabled	

Figure 6-19 is a time series of the "recovery" period as the station returned to TEA. The X_A component gradually changes and reaches -20 μg just before the 4 hour mark. At 3 hour 40 minutes into the plot the X_A component stays under -10 μg for 20 minutes. This event corresponds closely to the ISS angular rates as seen in Figure 6-20. The angular rate about the Y_A-axis is accelerated to as much as -0.19 degrees/sec.

6.1.4 Progress 5P Propellant Line Purge

The propellant lines of Progress 5P were used to transfer propellant from the SM to the FGB and had to be purged of the fuel, unsymmetrical dimethyl hydrazine (ZUG), prior to undocking. The purge consists of two steps that would be expected to have an effect in the quasi-steady environment, a fuel purge and an oxygen purge. The event began with the ISS being commanded to an attitude hold state at GMT 20-November-2001, 324/19:10.

According to the 7A.1 As Flown Motion Control System Operations Timeline, the fuel purge was scheduled to start within the period from 19:38 to 19:45 and was scheduled to last for 800 seconds. Figure 6-21 shows a timeline of events in respect to the quasi-steady environment. In Figure 6-22, the effects of the fuel purge can be seen as a 3.4 μg peak in the Y_A and a -5.1 μg peak in the Z_A axis. Looking at Figure 6-23, the peak magnitude for the fuel purge is 5.2 μg, and the total effect only lasted approximately 392 seconds.

The oxygen purge was slated to begin within the window between 21:18 to 21:38 and was also scheduled to last for 800 seconds. The red dotted lines in Figure 6-24 highlight an estimate on the start and stop time for the oxygen purge, which is approximately 708 seconds in length. The disturbance looks like a step function with a maximum disturbance of -5.7 μg occurring in the Z_A axis, 27 minutes into the plot. Figure 6-25 is an acceleration magnitude plot for the oxygen purge, which shows peak acceleration magnitude during the purge of 6 μg.

Also evident in Figure 6-24 and Figure 6-25 is a disturbance at 21:45 (45 minute mark in the plot), which is suspected to be the manual de-saturation of the CMG by thruster firing as part of the transition to momentum management. Since MAMS OSS is designed to measure quasi-steady accelerations, disturbances caused by thruster firings are better quantified from SAMS or MAMS HiRAP data.

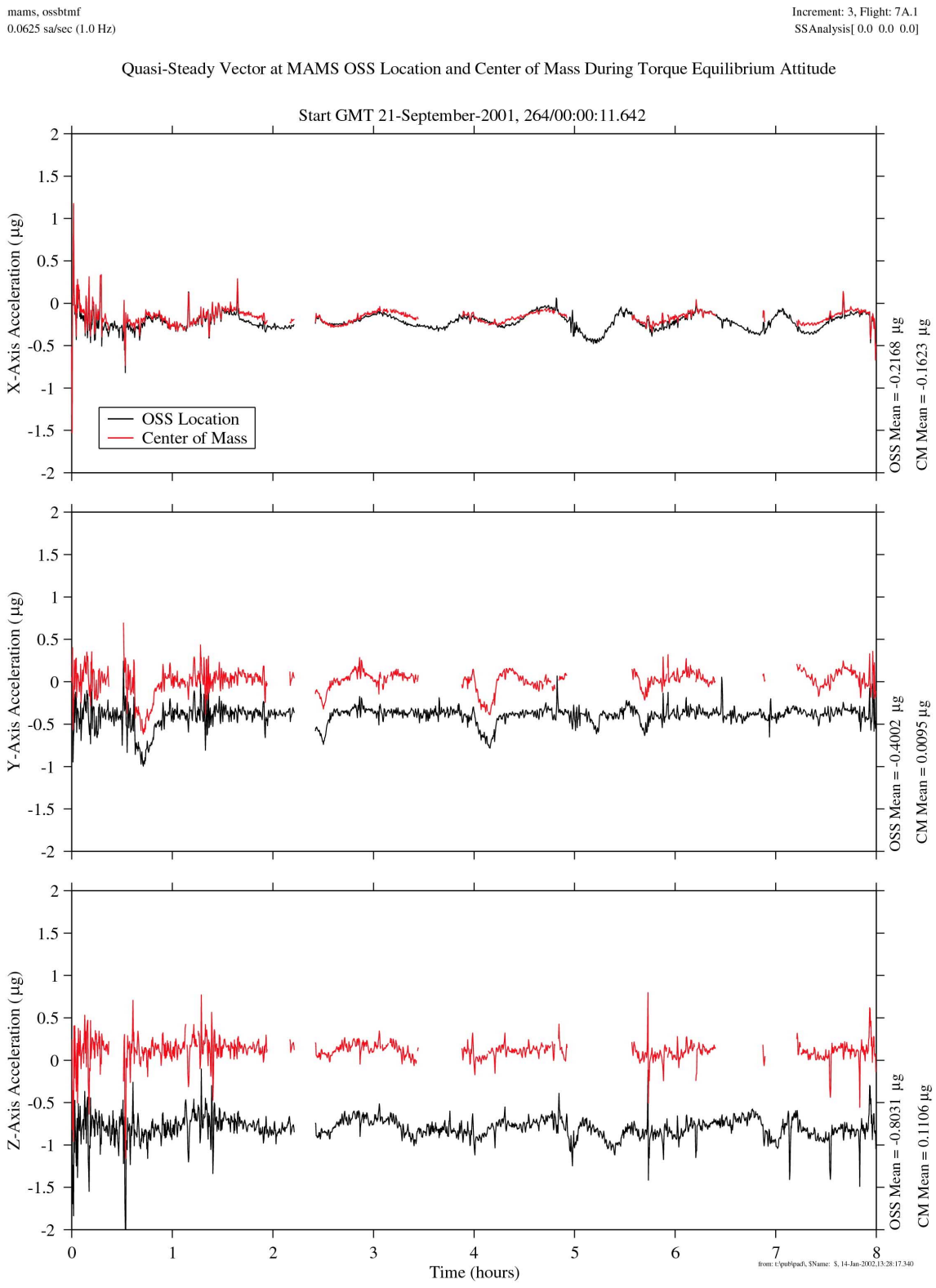

Figure 6-1 Time Series of Quasi-steady Vector During TEA (OSS)

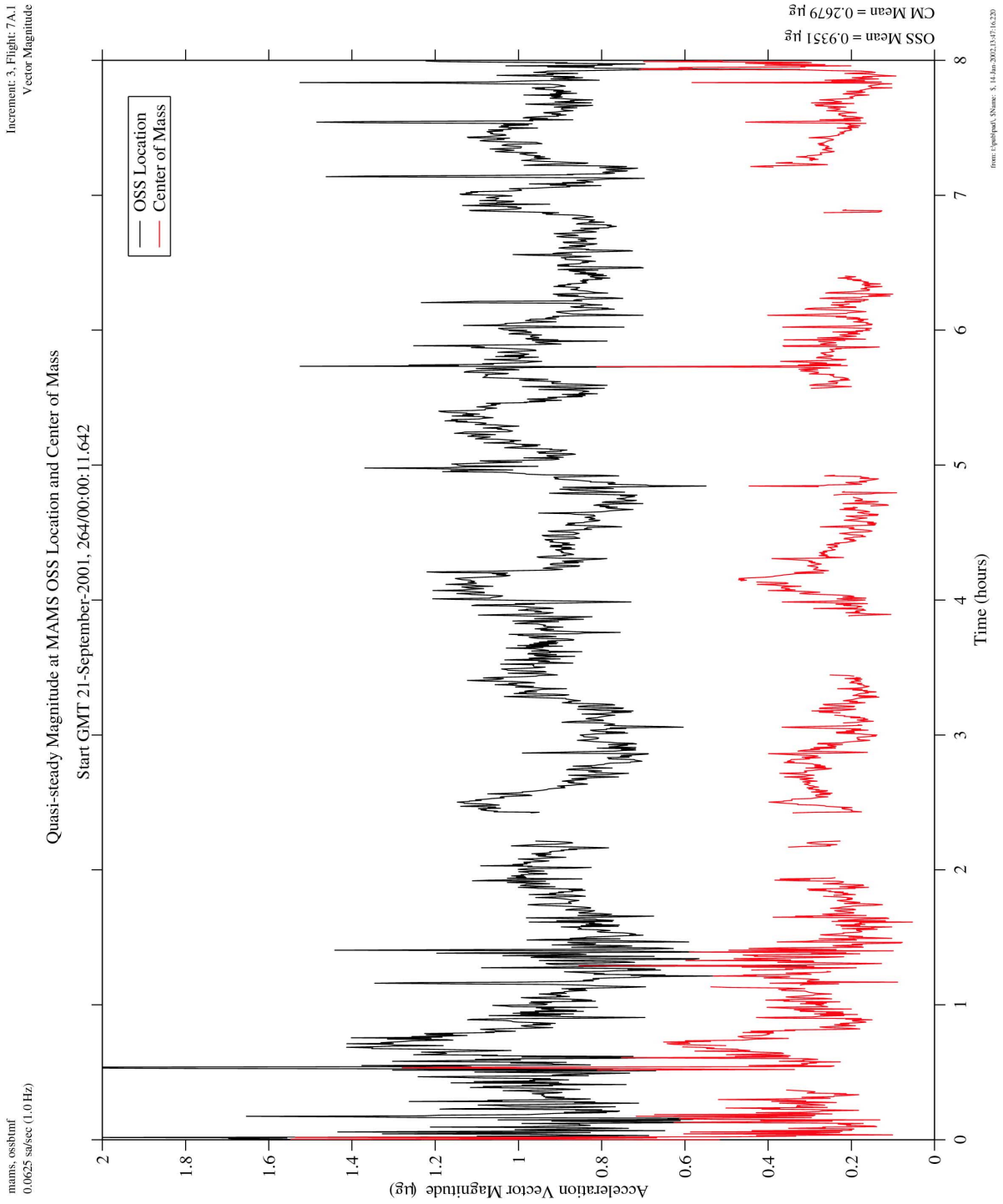

Figure 6-2 Acceleration Magnitude of Quasi-steady Vector During TEA (OSS)

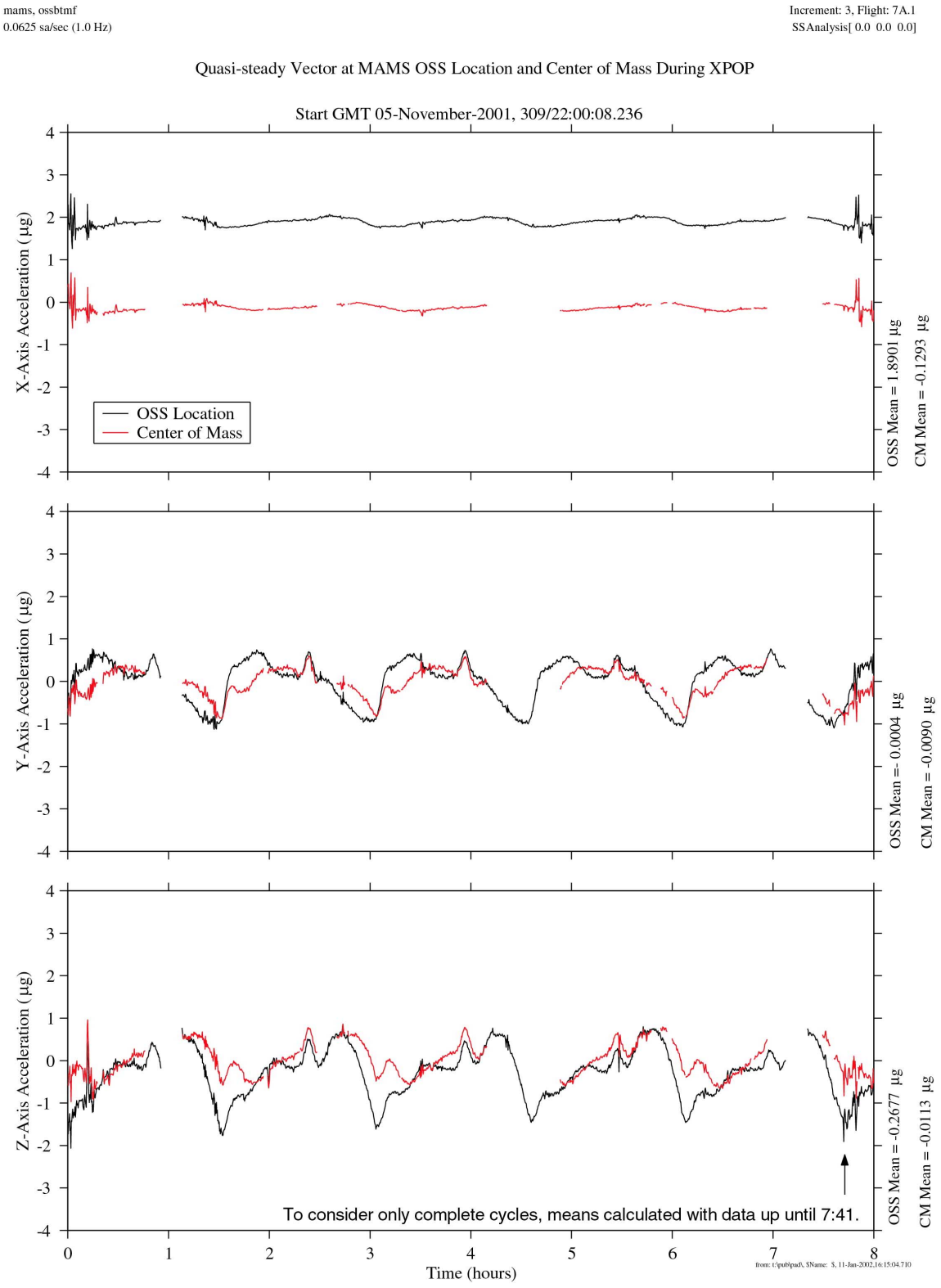

Figure 6-3 Time Series of Quasi-steady Vector During XPOP (OSS)

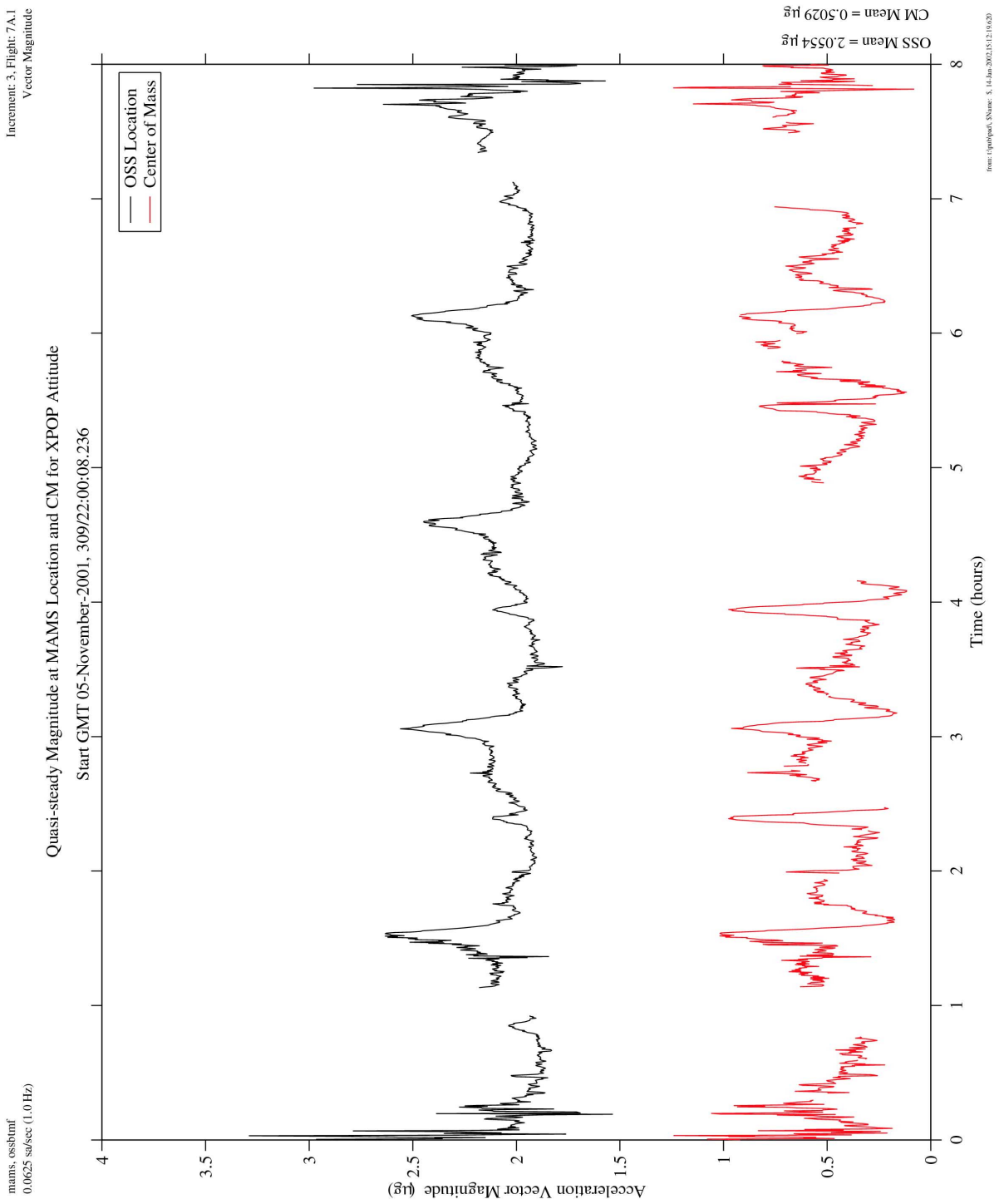

Figure 6-4 Acceleration Magnitude of Quasi-steady Vector During XPOP (OSS)

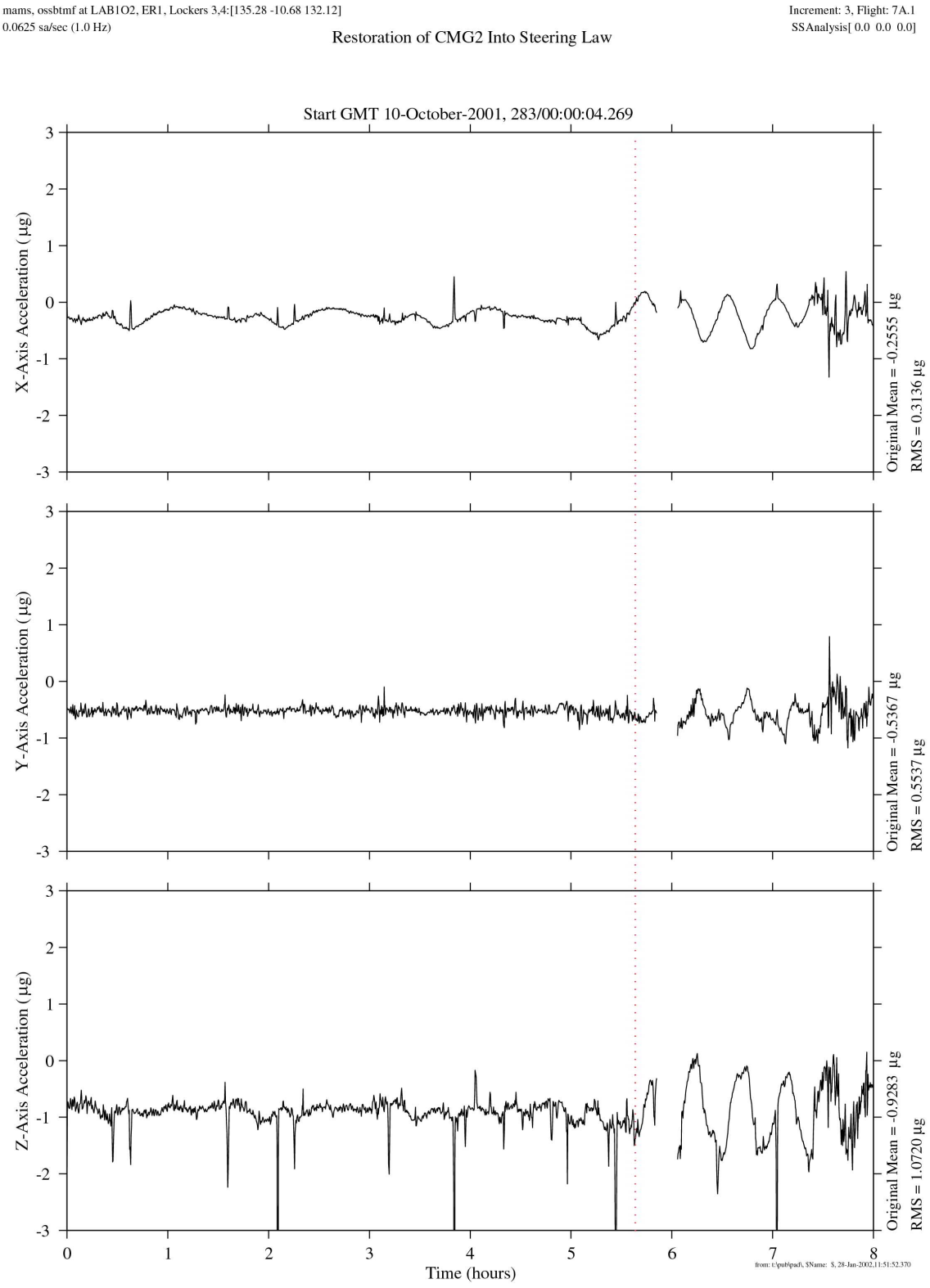

Figure 6-5 Time Series of CMG 2 Restoration to Steering Law (OSS)

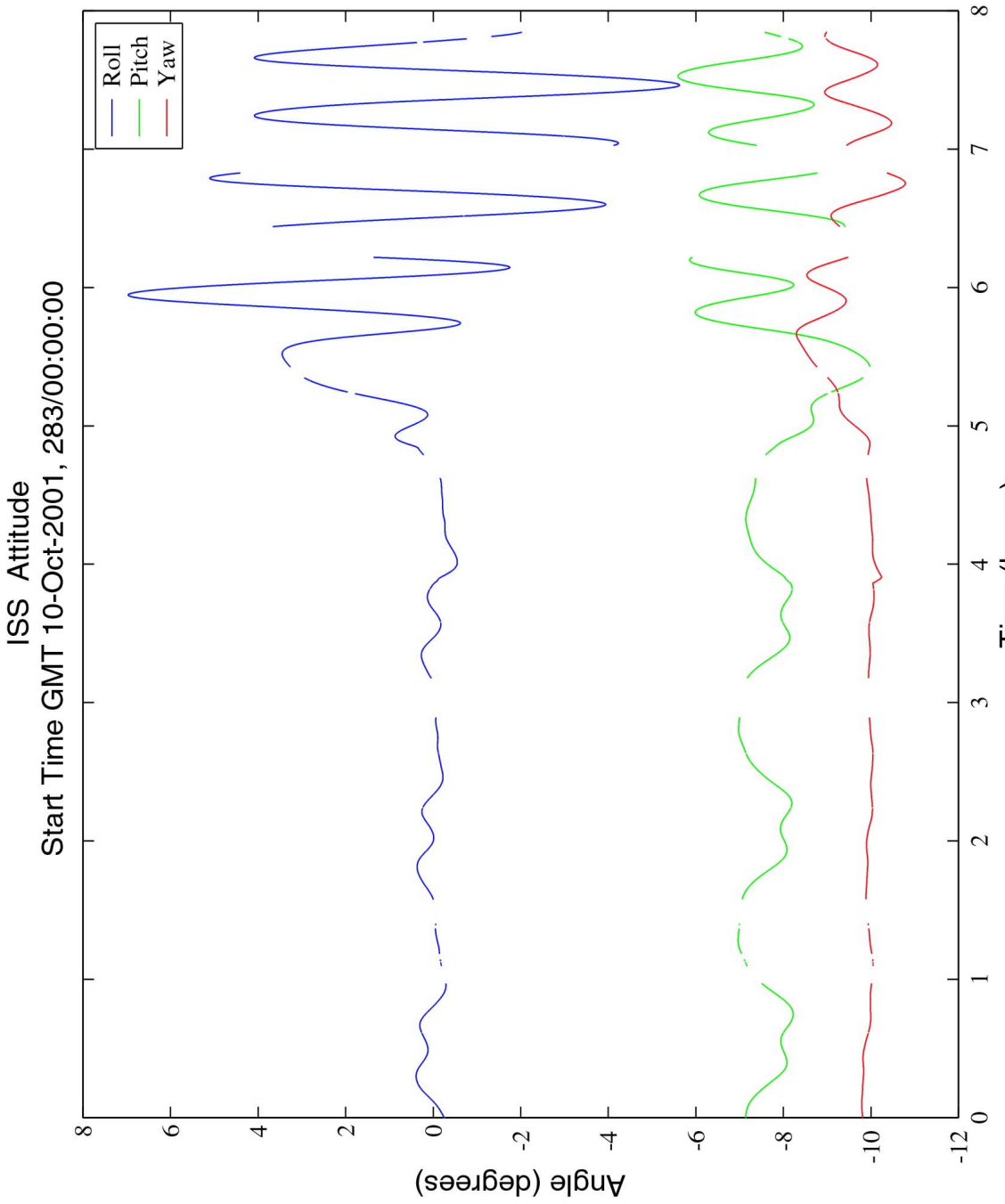

Figure 6-6 Time Series of ISS Attitude Data During CMG 2 Restoration (OSS)

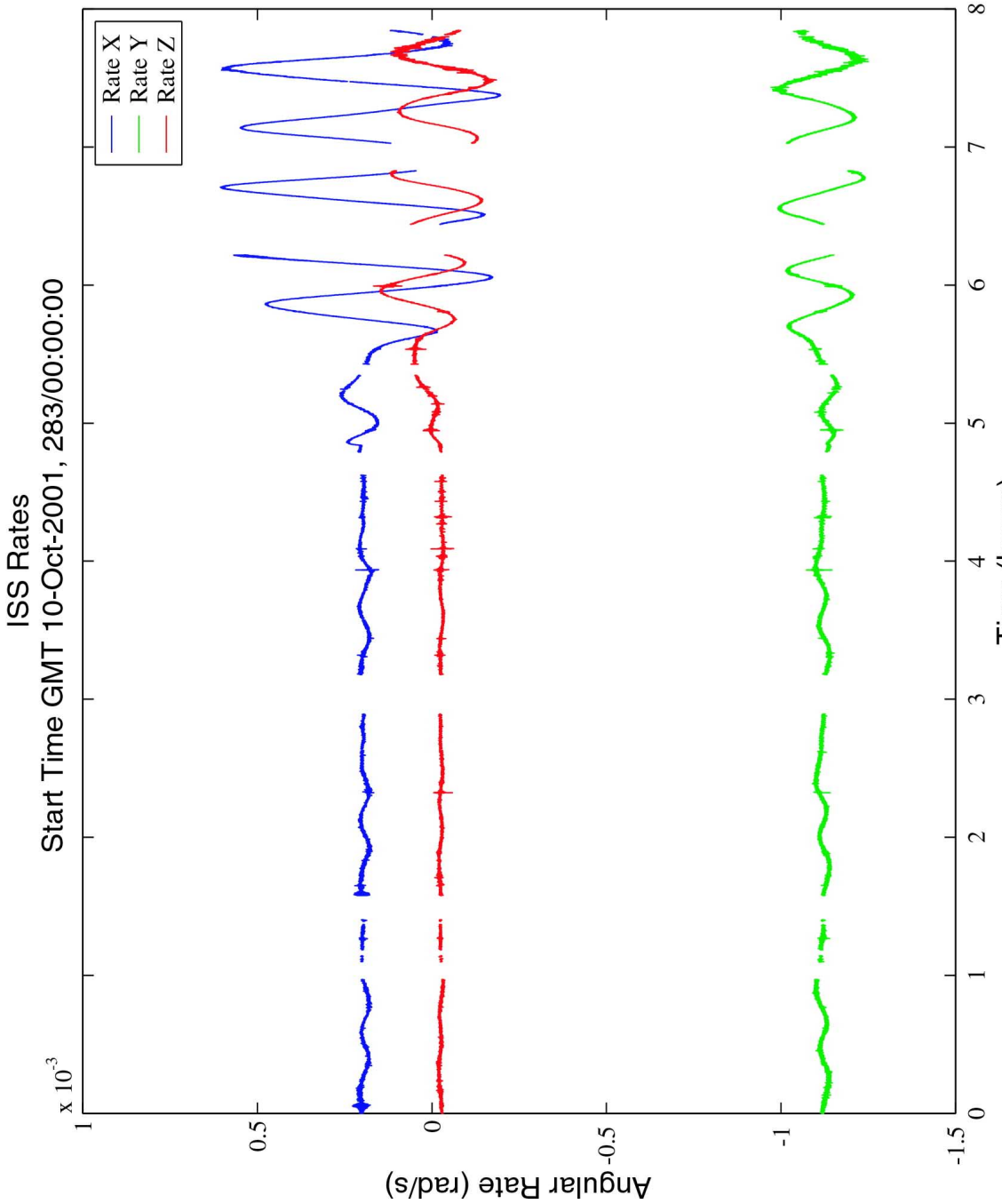

Figure 6-7 Time Series of ISS Angular Rates During CMG 2 Restoration (OSS)

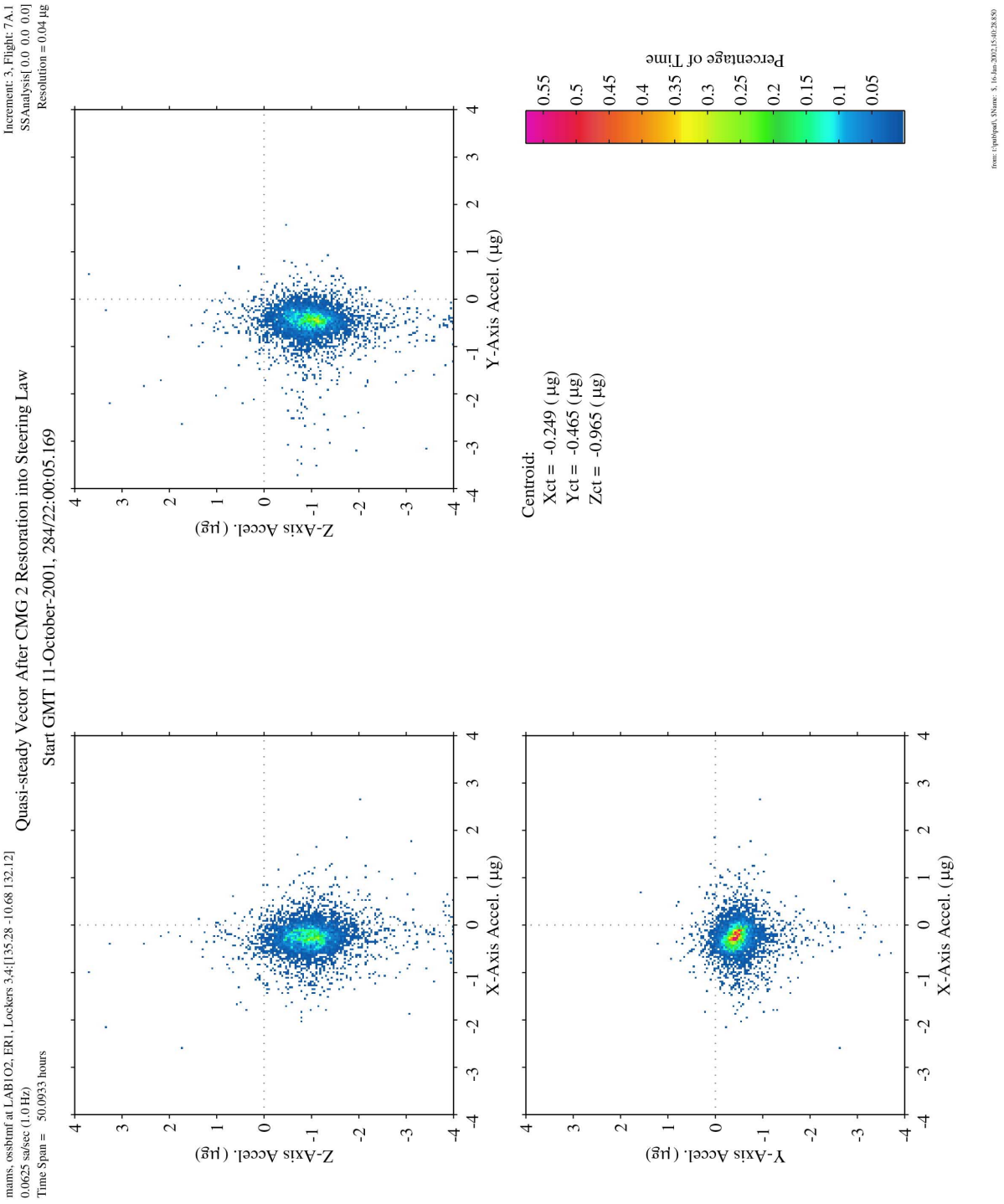

Figure 6-8 QTH of Time Period Following CMG 2 Restoration (OSS)

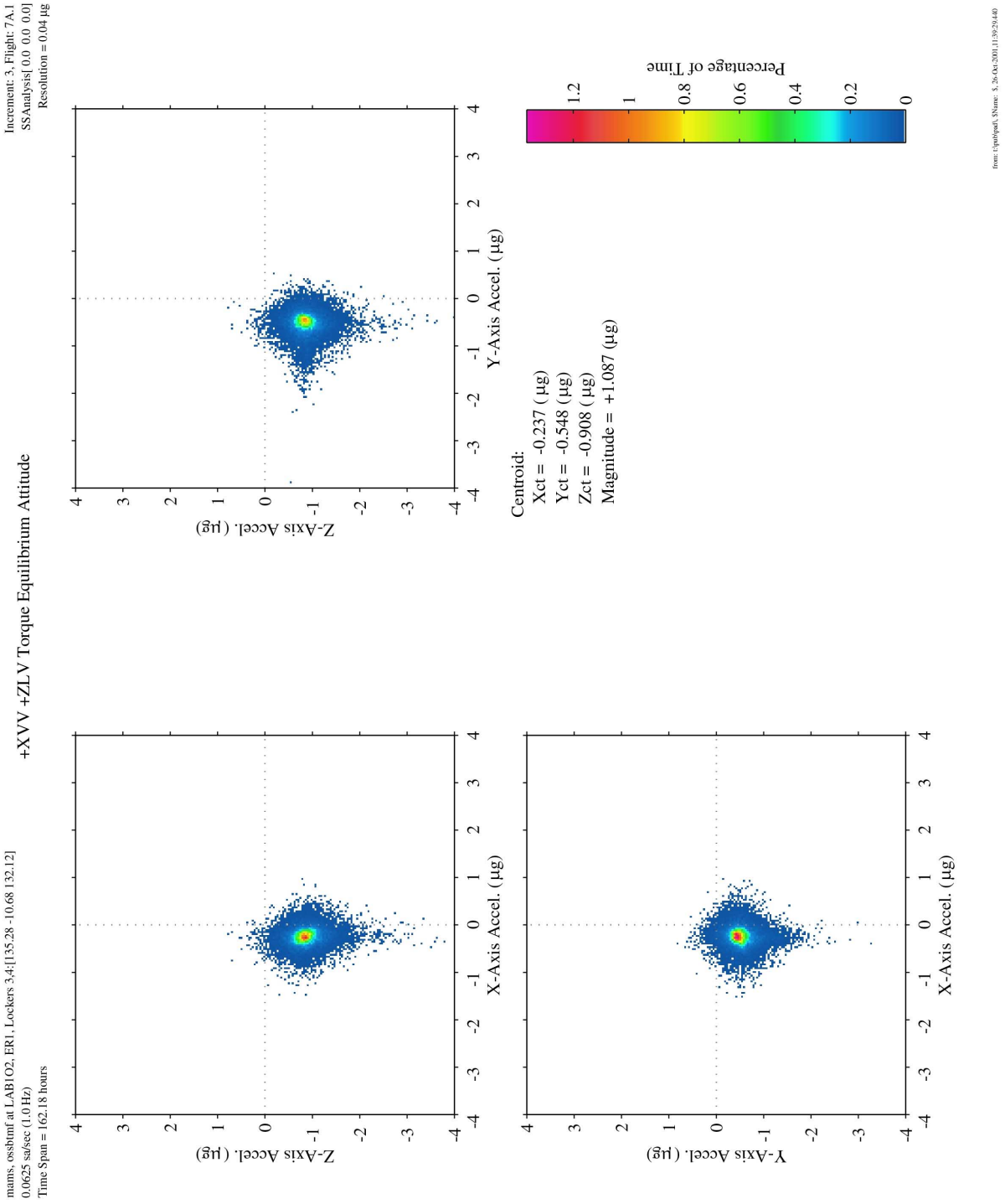

Figure 6-9 QTH of Torque Equilibrium Attitude (OSS)

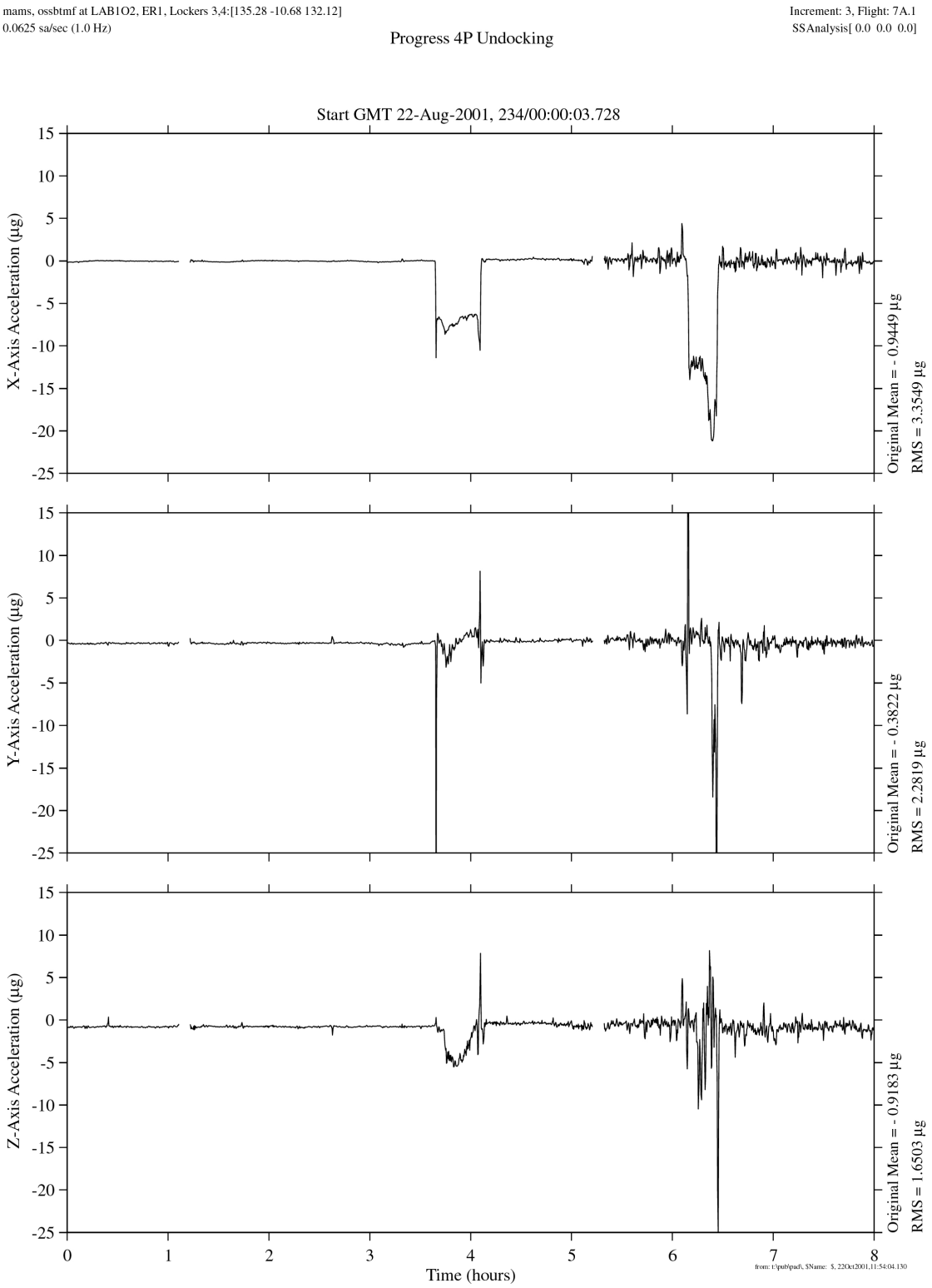

Figure 6-10 Time Series of Progress 4P Undocking (OSS)

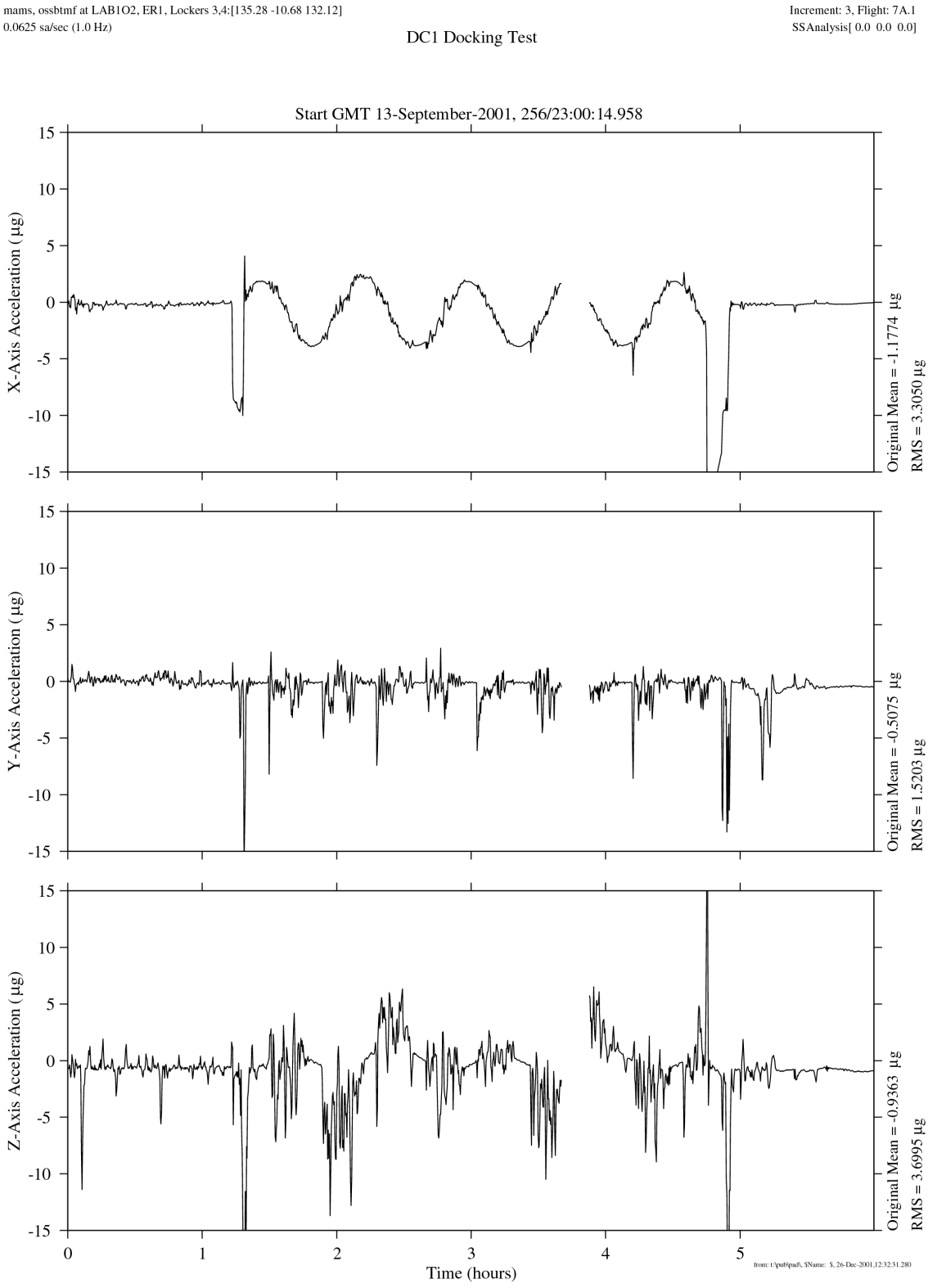

Figure 6-11 Time Series of DC-1 Docking Test Maneuvers (OSS)

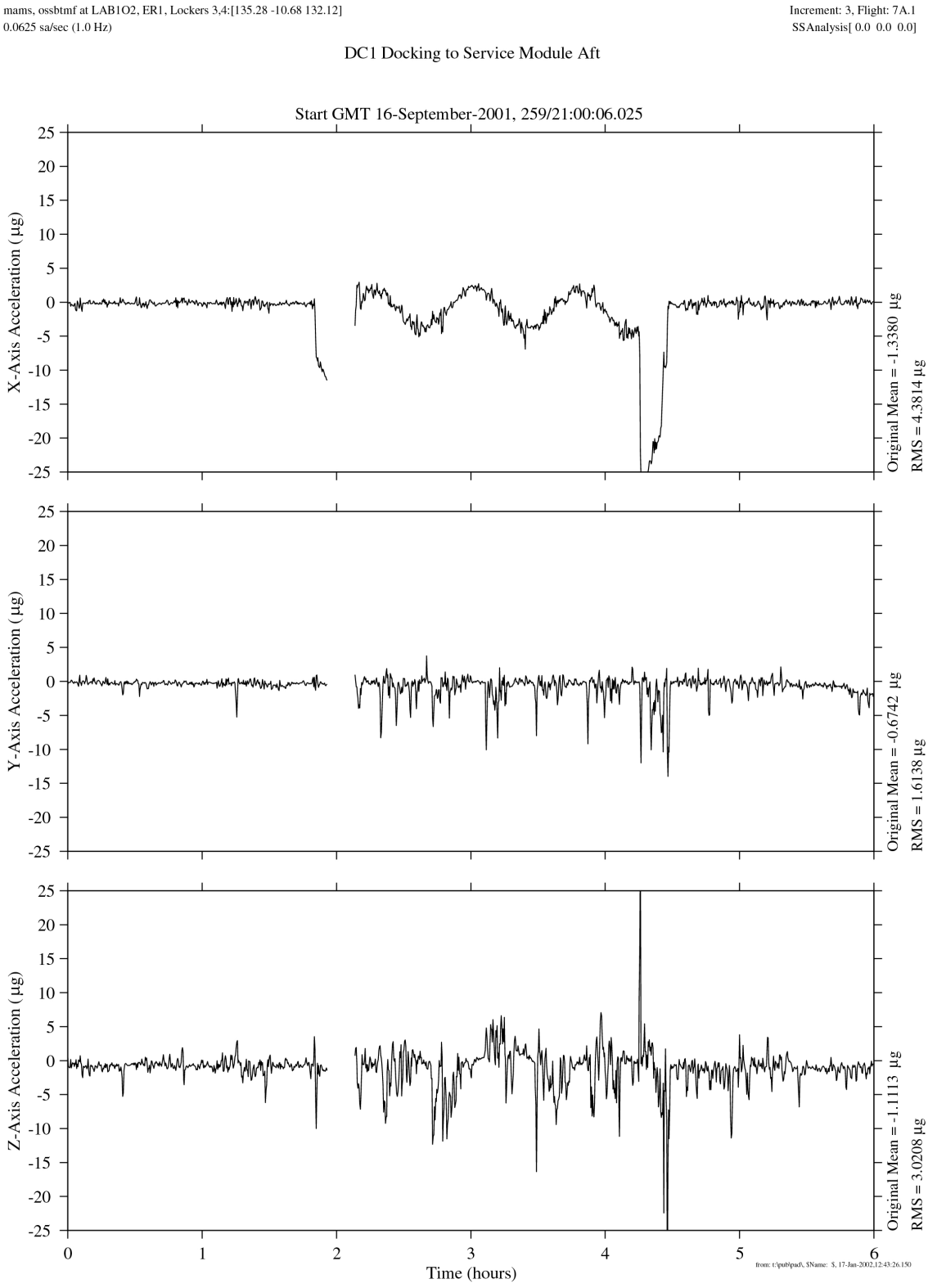

Figure 6-12 Time Series of DC-1 Docking Maneuvers (OSS)

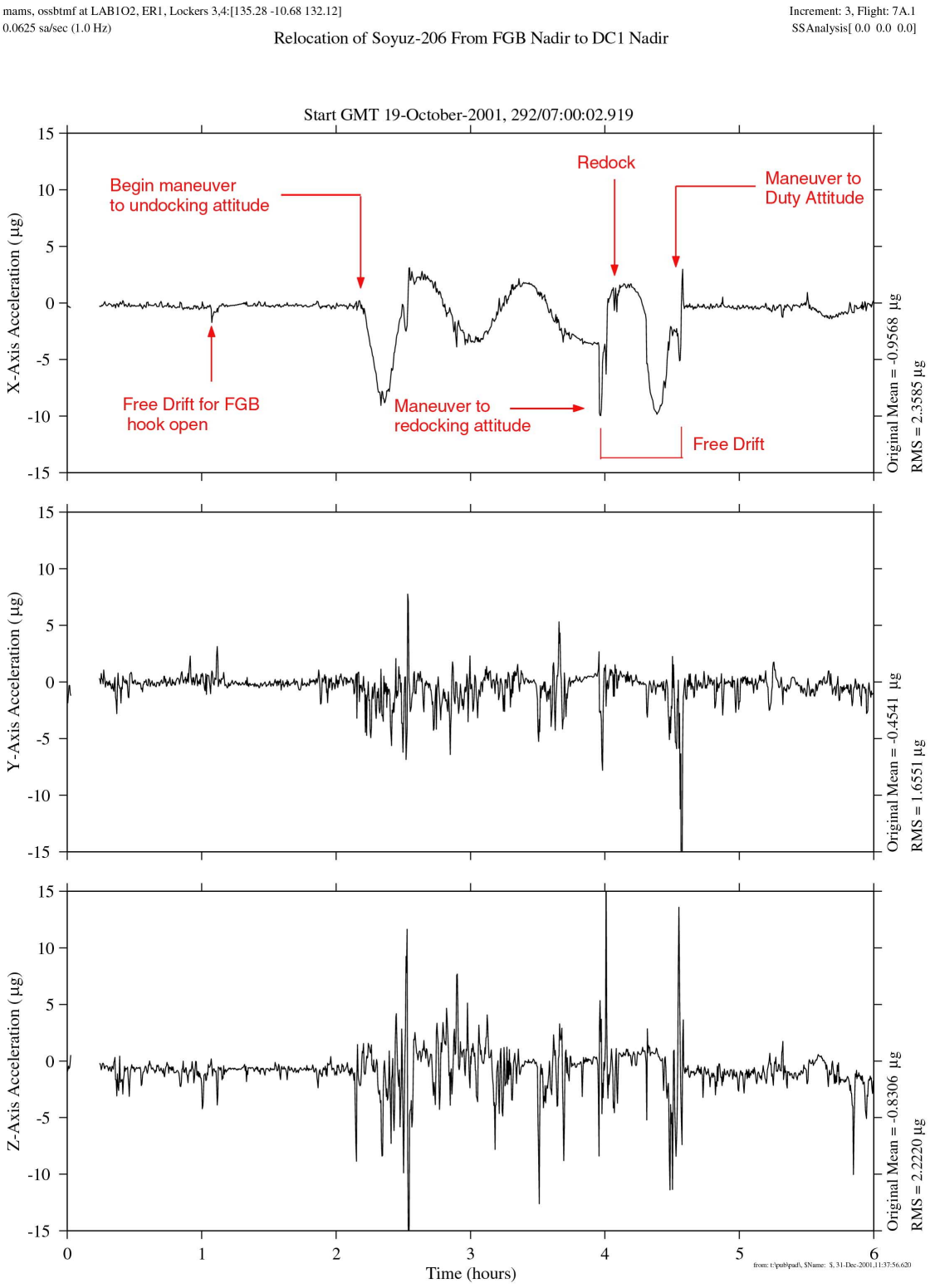

Figure 6-13 Time Series of Soyuz-2 Relocation (OSS)

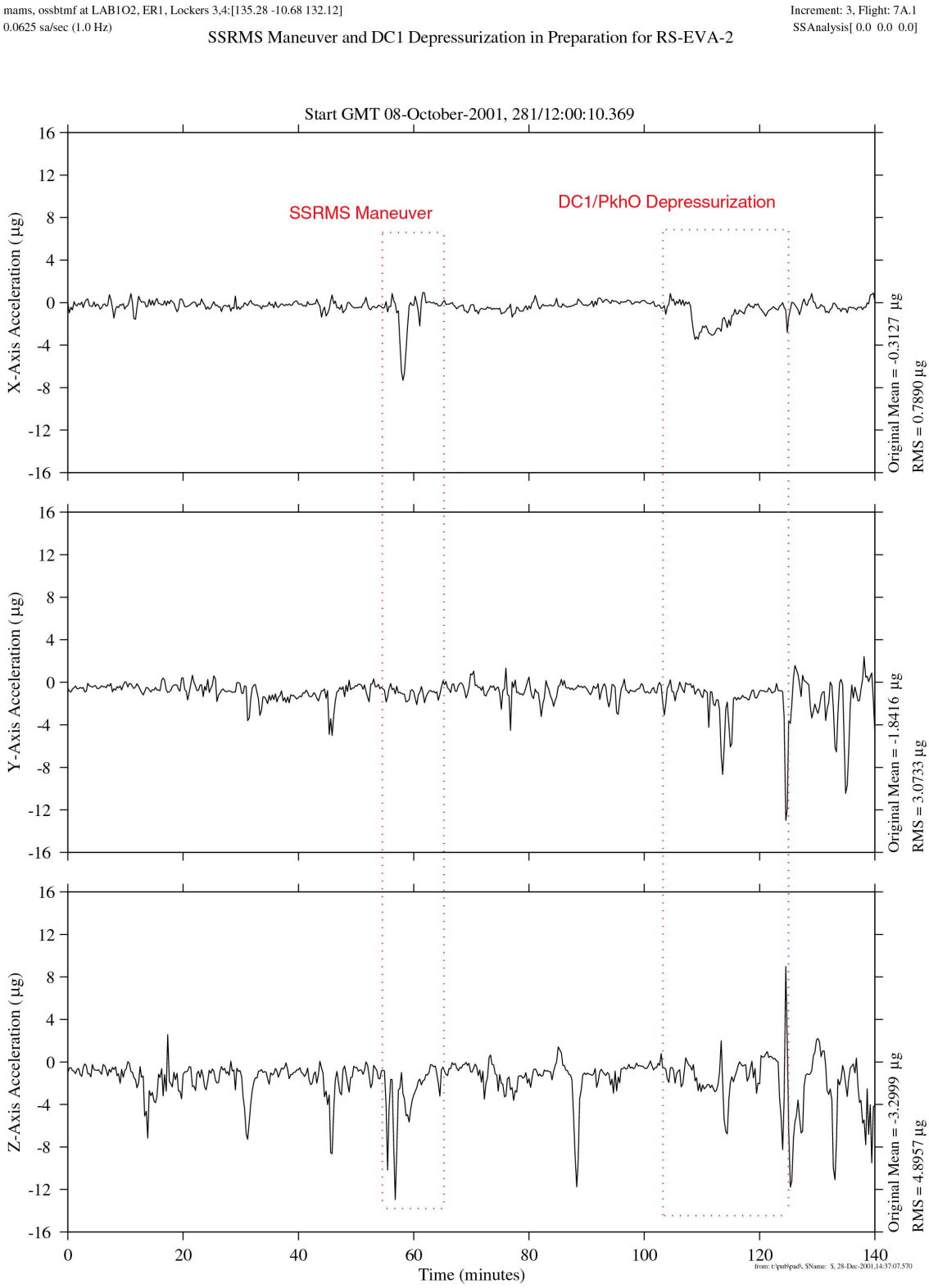

Figure 6-14 Time Series of RS-EVA-2 SSRMS Maneuver and DC-1 Depressurization (OSS)

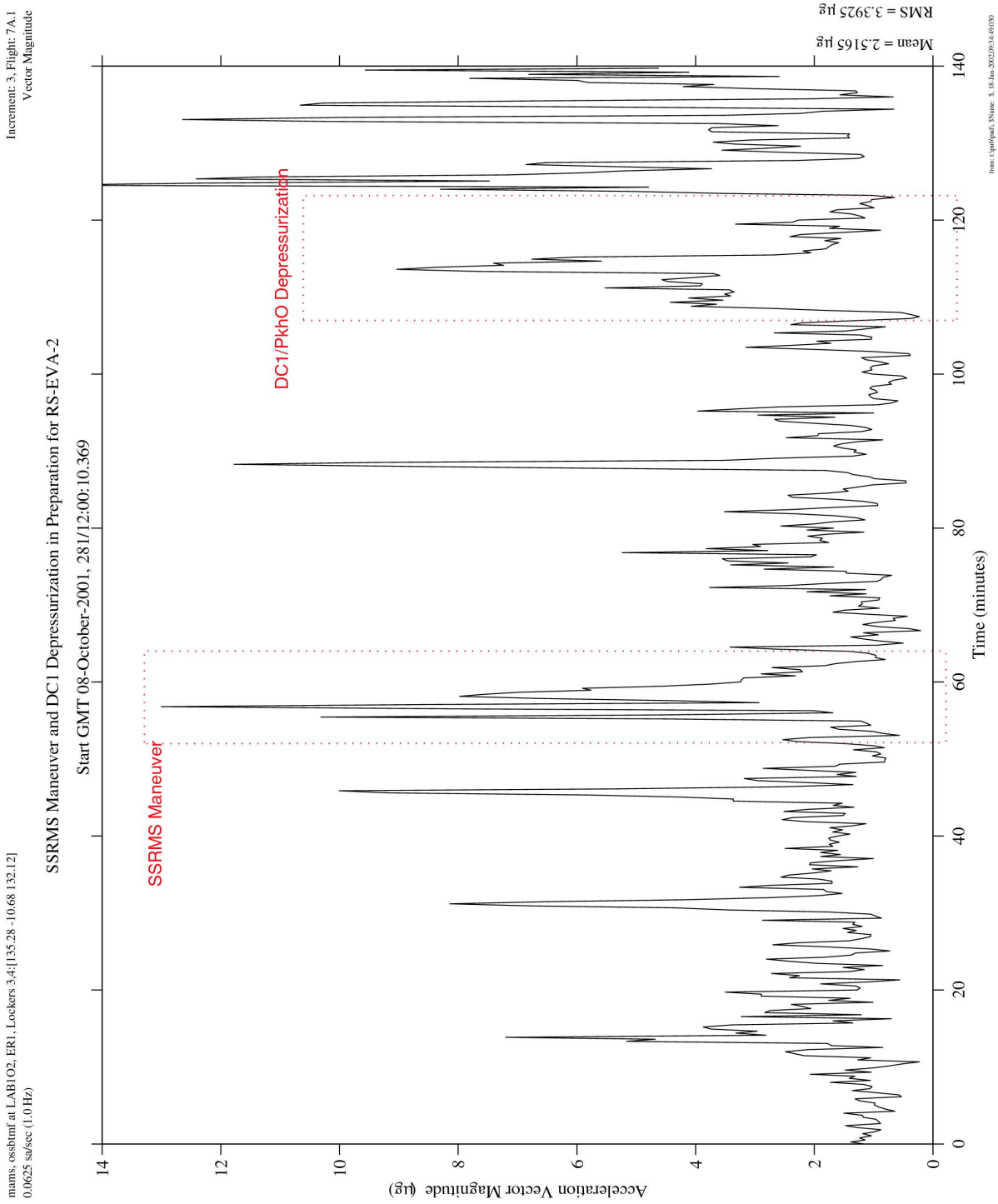

Figure 6-15 Acceleration Magnitude of RS-EVA-2 SSRMS Maneuver and DC-1 Depressurization (OSS)

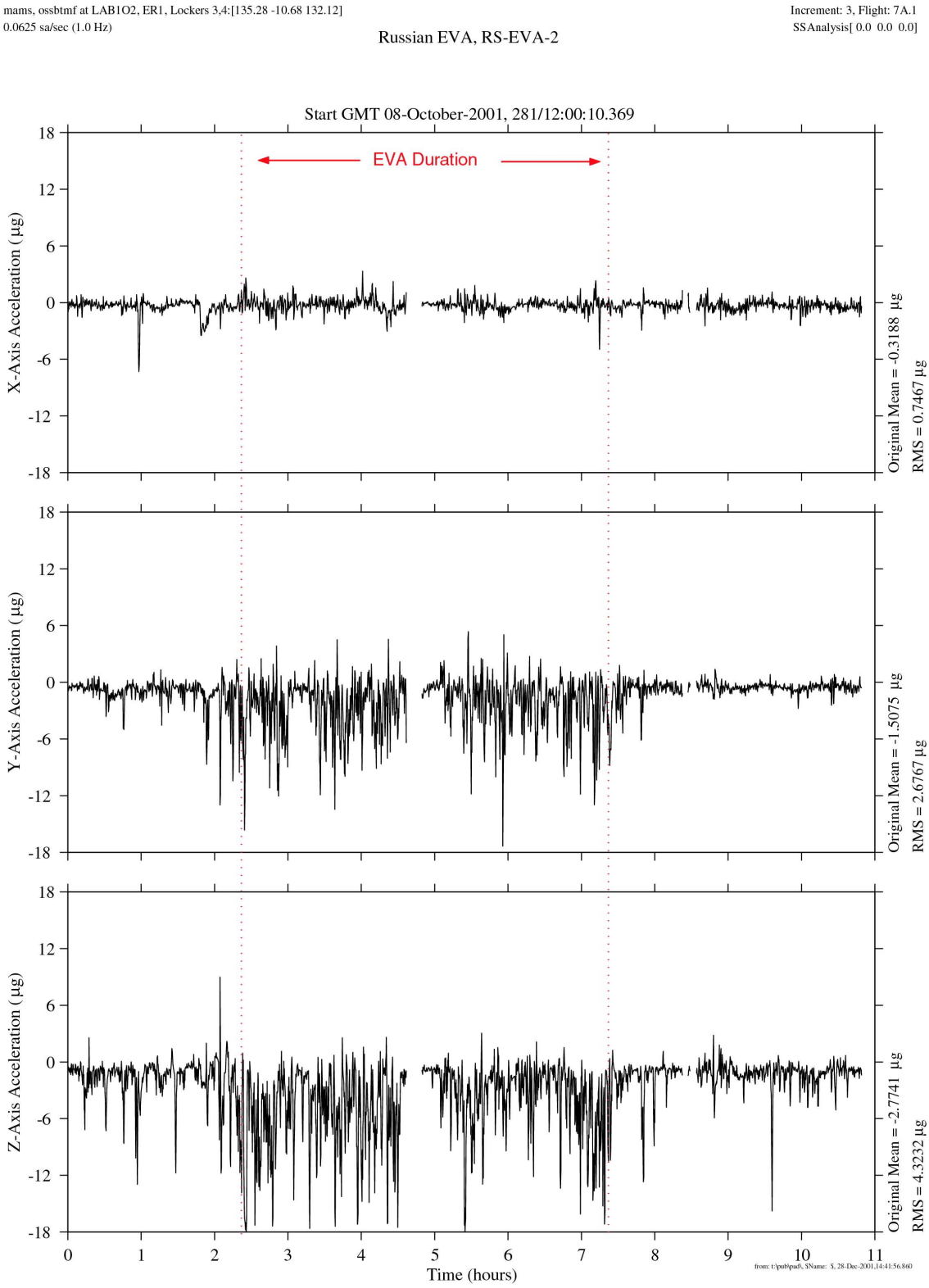

Figure 6-16 Time Series of RS-EVA-2 (OSS)

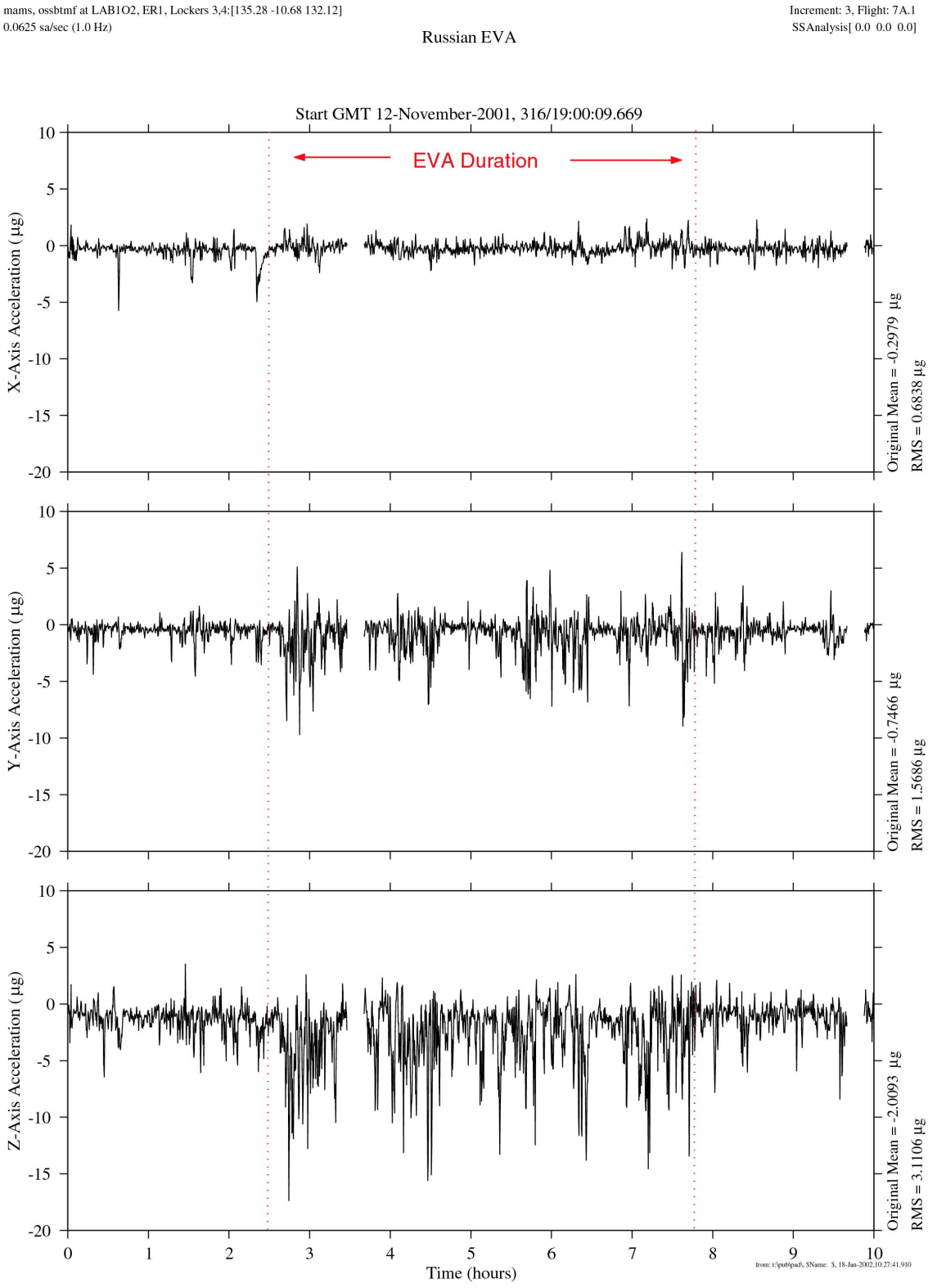

Figure 6-17 Time Series for Russian EVA (OSS)

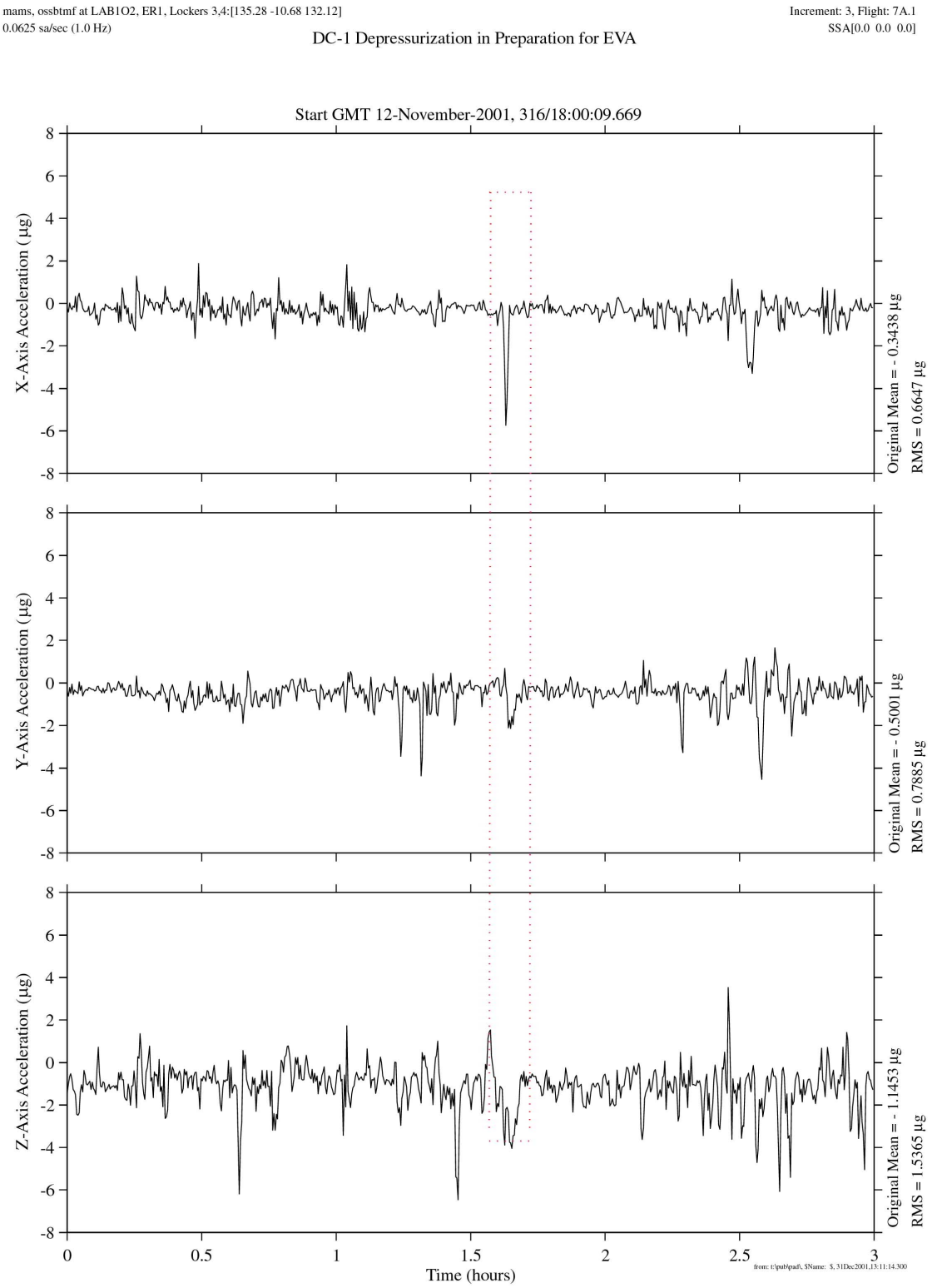

Figure 6-18 Time Series of DC-1 Depressurization (OSS)

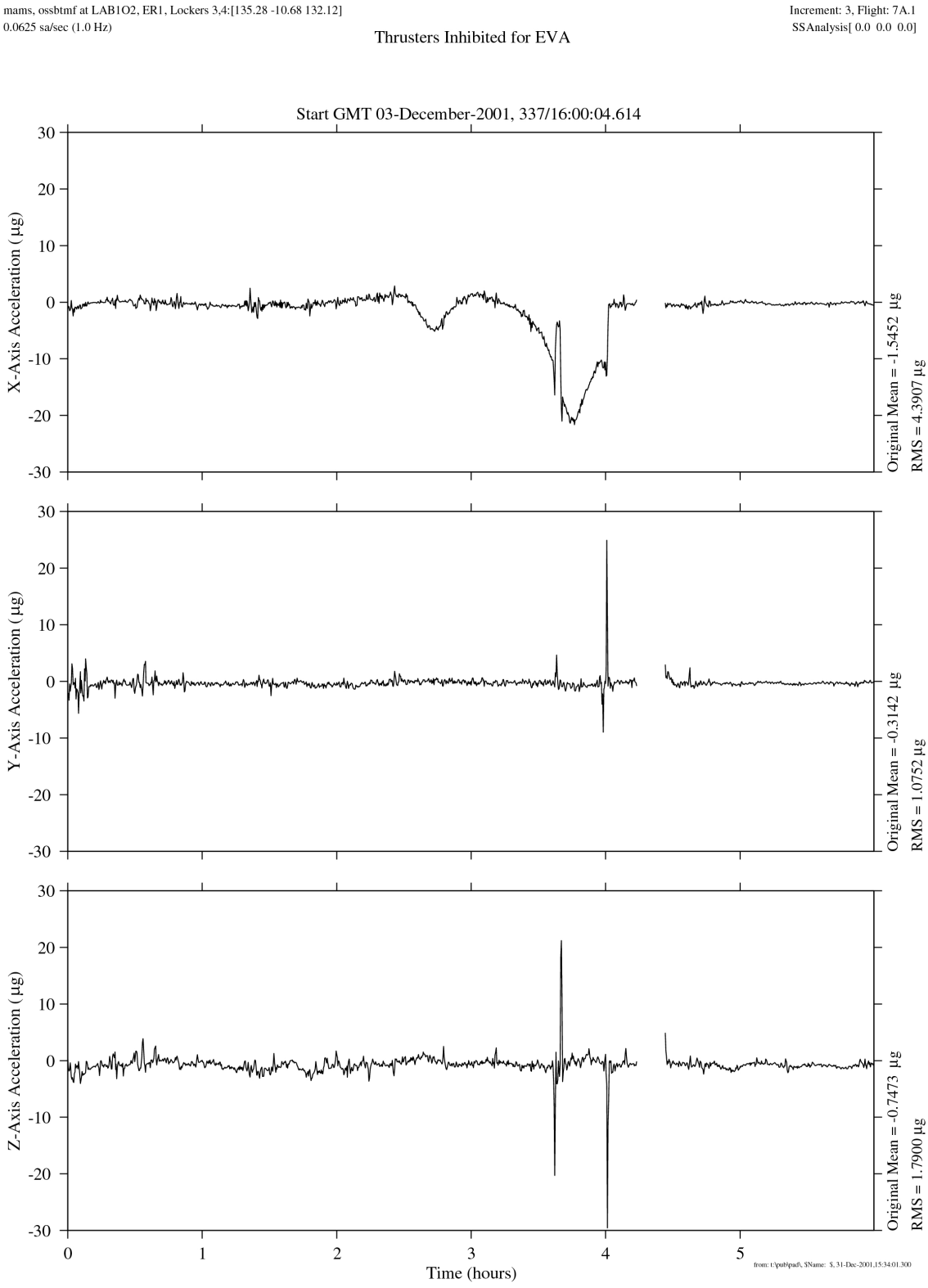

Figure 6-19 Time Series of Recovery From SM Thrusters Inhibited (OSS)

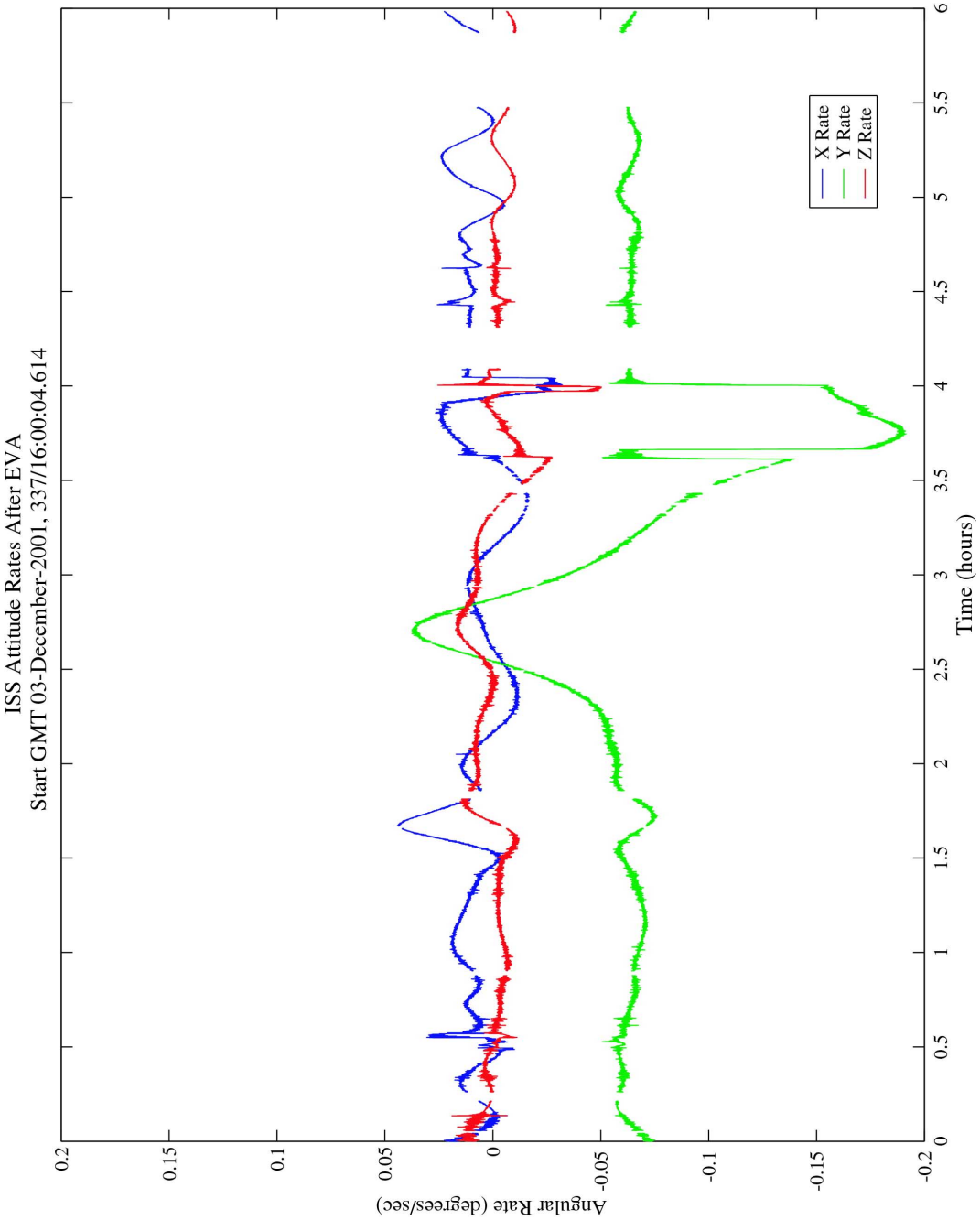

Figure 6-20 Time Series of ISS Angular Rates for Recovery From SM Thrusters Inhibited (OSS)

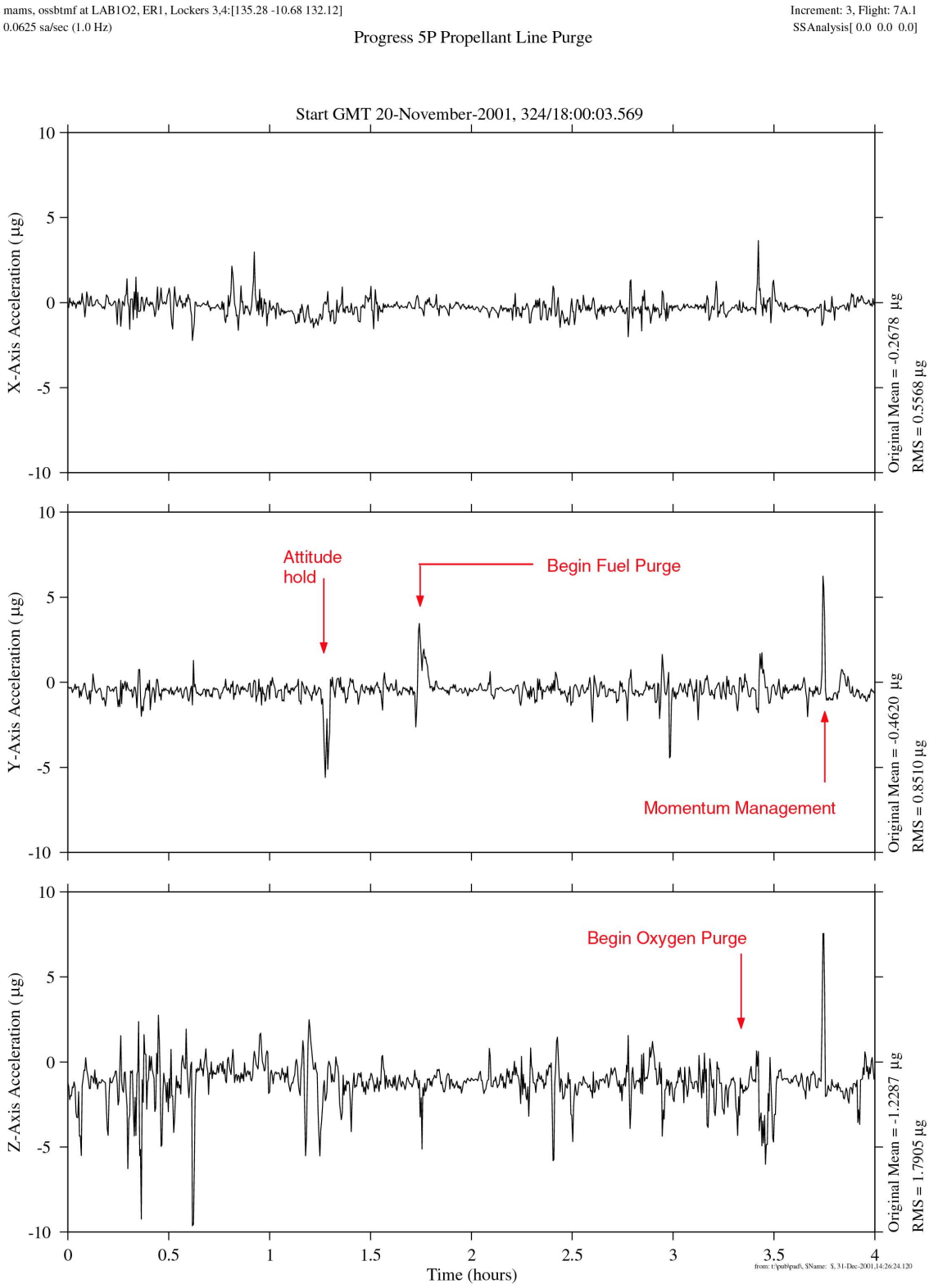

Figure 6-21 Time Series of Progress 5P Propellant Line Purge Activities (OSS)

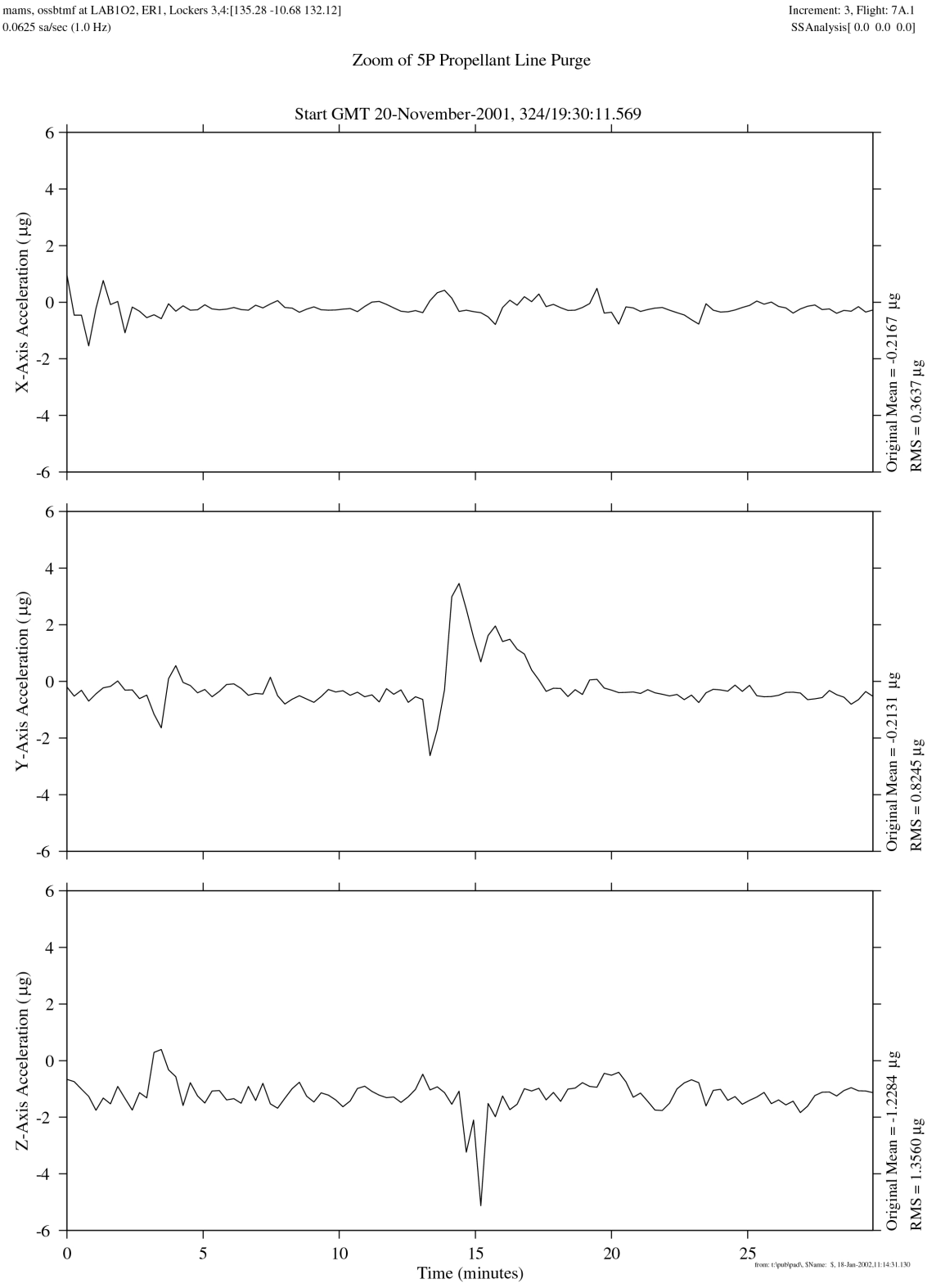

Figure 6-22 Time Series of Progress 5P Fuel Purge (OSS)

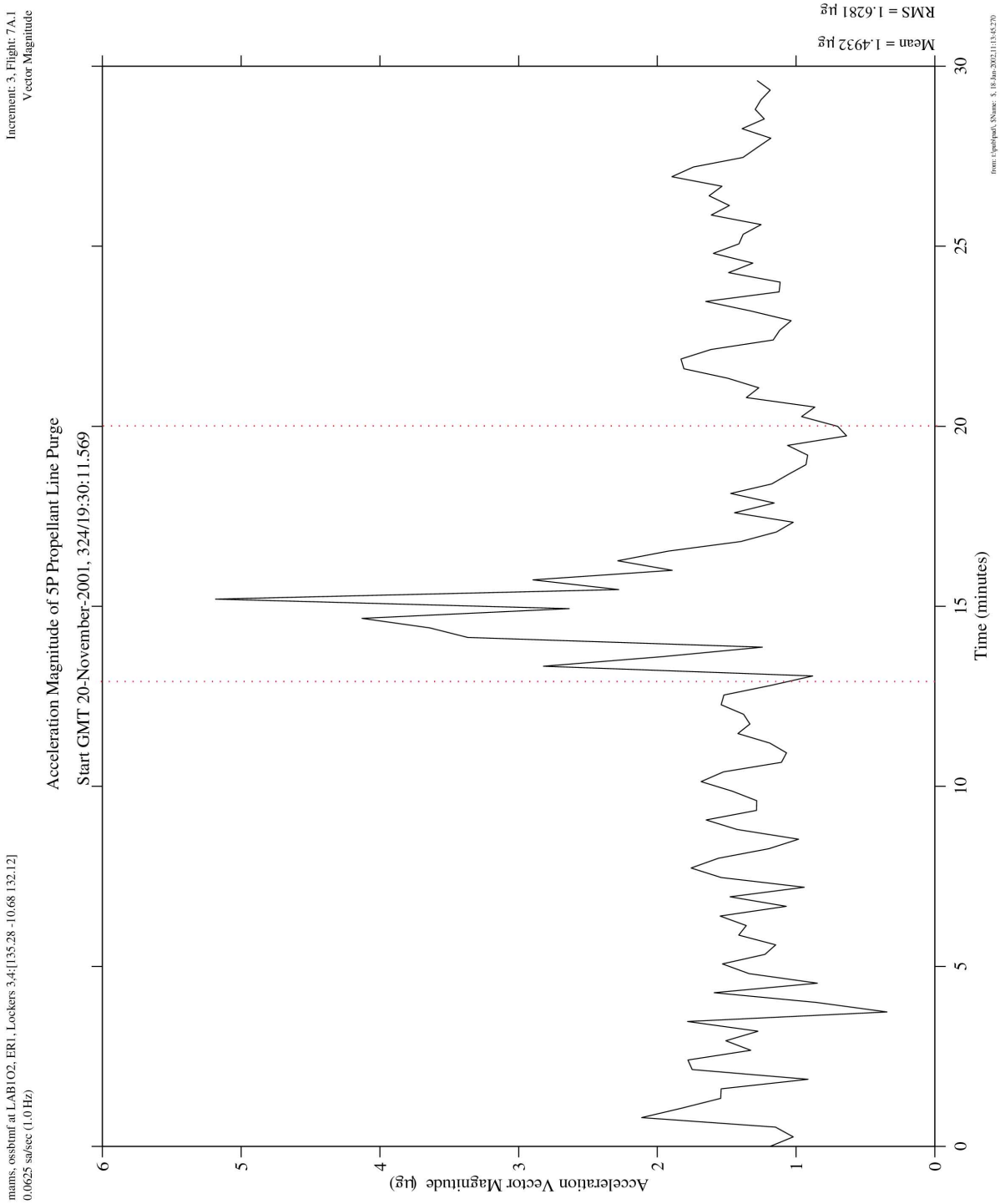

Figure 6-23 Acceleration Magnitude of Progress 5P Fuel Purge (OSS)

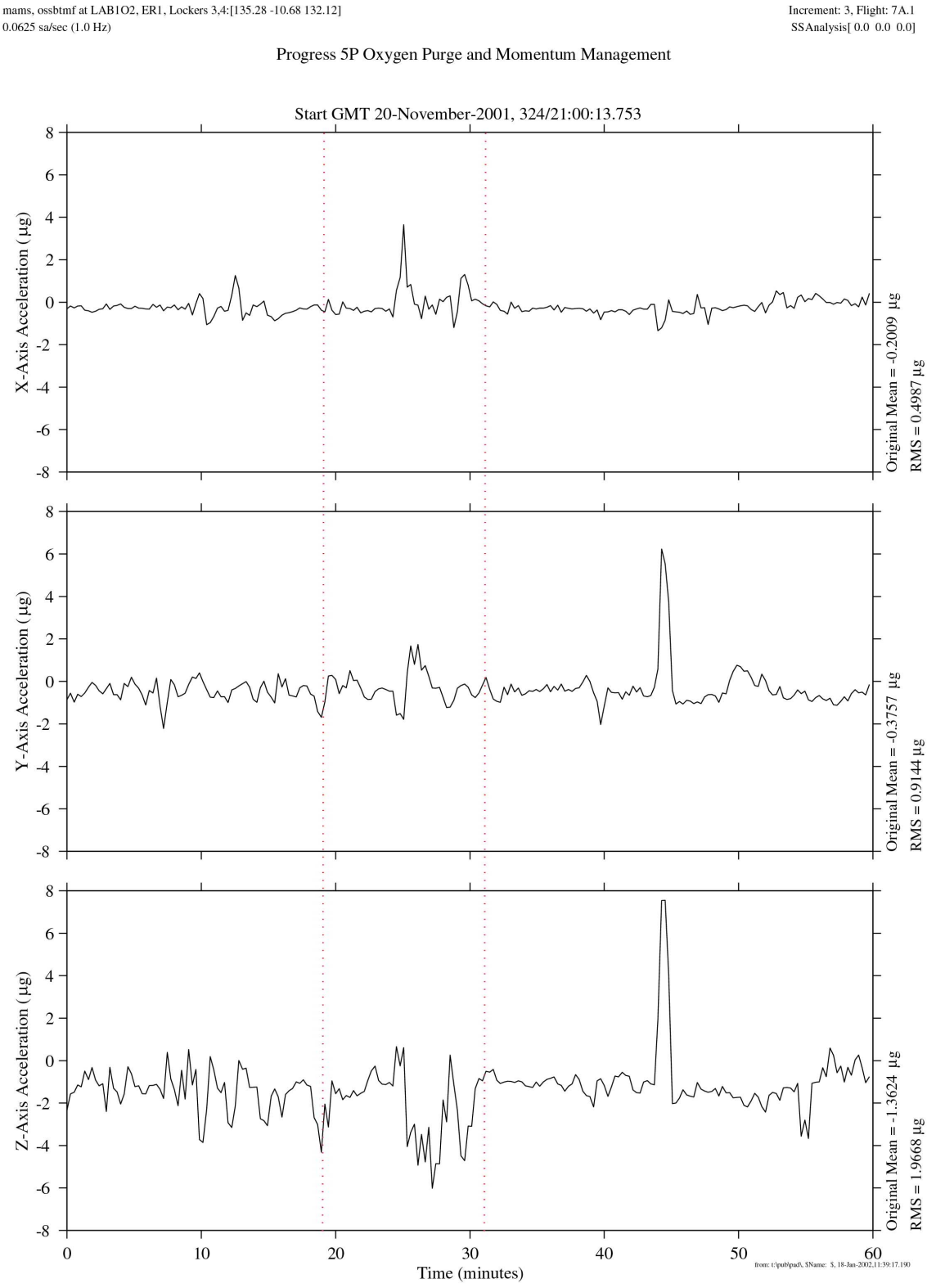

Figure 6-24 Time Series of 5P Oxygen Purge and Momentum Management

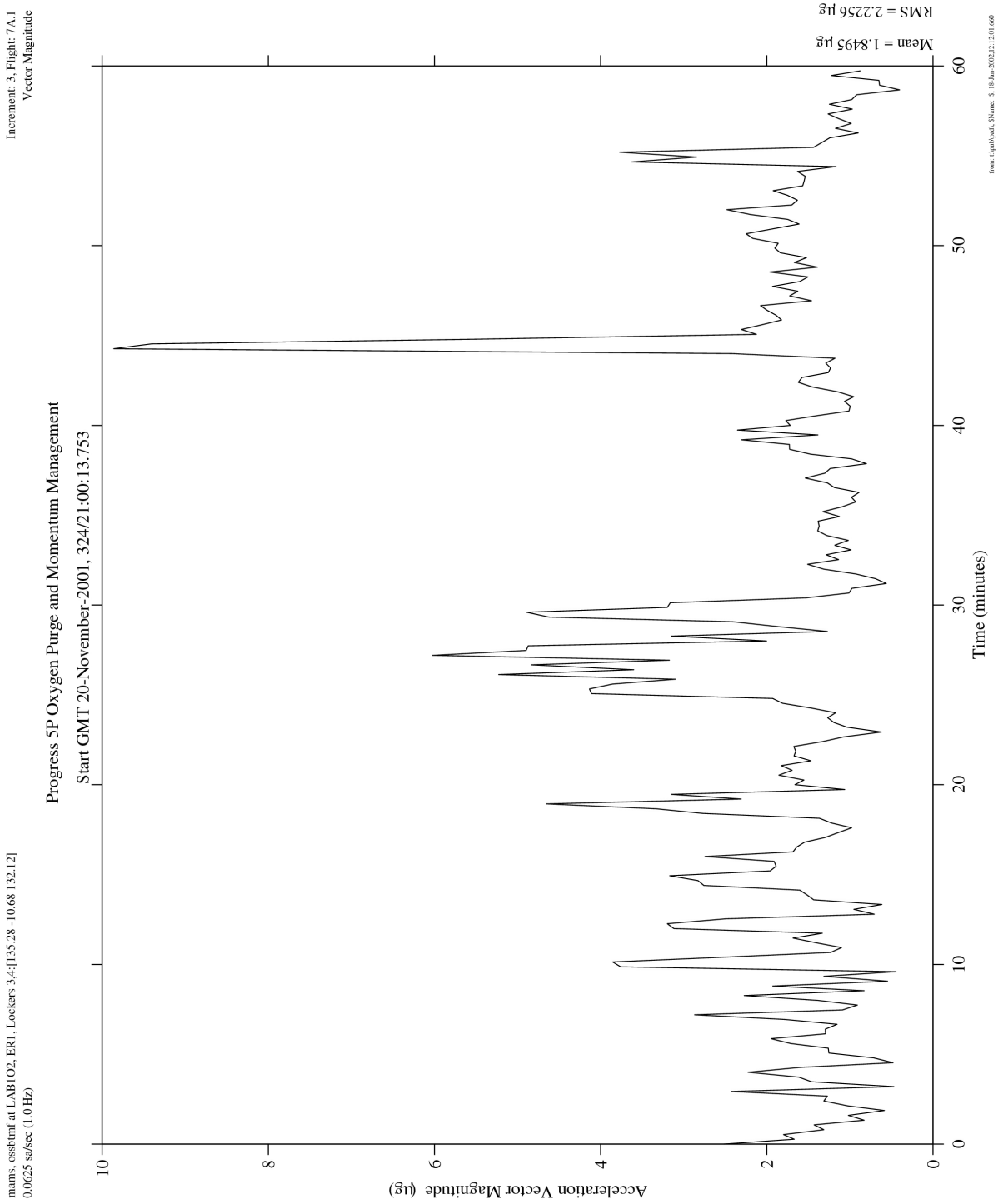

Figure 6-25 Acceleration Magnitude of 5P Oxygen Purge and Momentum Management

6.2 Vibratory Microgravity Environment

The vibratory acceleration regime consists of the acceleration spectrum from 0.01 to 400 Hz, with magnitudes expected to vary greatly depending on the nature of the disturbance and on the transmissibility from the source to locations of interest. The relatively high frequency accelerations that shape the vibratory environment of the ISS are usually associated with vehicle operations, vehicle systems, experiment-related equipment, and crew activity.

This section examines the effects of some of these vibratory disturbances as measured by SAMS or MAMS HiRAP sensors. Section 6.2.1 discusses the impact of vehicle operations such as Progress thruster tests and vehicle dockings. In Section 6.2.2, vehicle subsystems including Avionics Air Assembly (AAA) equipment, vehicle structural modes, and the ARIS are considered. Experiment equipment related to EXPPCS and Advanced Protein Crystallisation Facility (APCF) are the focus of Section 6.2.3. The last category of vibratory disturbance analyzed for this report is crew activity. A special case of ergometer exercise is the subject of Section 6.2.4. Section 9.1 serves to summarize the vibratory analysis results for this report. Figure 6-26 through Figure 6-30 show the available acceleration data for the five SAMS SEs and MAMS HiRAP for the Increment-3 time span analyzed in this report.

6.2.1 Vehicle Operations

This section includes vibratory acceleration events related to Progress thruster tests conducted on GMT 239 (27-August-2001), the Progress 4P undocking on GMT 234 (22-August-2001), and the Progress 5P docking on GMT 235 (23-August-2001).

6.2.1.1 Progress Thruster Tests

Over the span of about 4 hours starting on GMT 238 (26-August-2001), a series of tests were conducted using the Progress 5P vehicle's thrusters. The ISS as-flown timeline calls out some details as the excerpt of Table 6-3 shows.

TABLE 6-3 EXCERPT OF INCREMENT-3 AS-FLOWN ATTITUDE TIMELINE

#	Maneuver Start-Stop (GMT)	Attitude Name	YPR	Event	Remarks
47	238/23:20	+ZLV +XVV TEA	350.0 352.5 0.0	Handover US to RS	Handover for Progress thrusters test
48	238/23:55	+ZLV +XVV	359.2 355.8 1.4	Duty Attitude	
49	239/01:29	+ZLV +XVV	354.2 355.9 1.8	Negative Yaw Maneuver	Progress Thruster Test (manifold 1)
50	239/01:30	+ZLV +XVV	359.2 355.8 1.4	Positive Yaw Maneuver	Progress Thruster Test (manifold 1)
51	239/01:33	+ZLV +XVV	359.1 350.8 1.5	Negative Pitch Maneuver	Progress Thruster Test (manifold 1)
52	239/01:33	+ZLV +XVV	359.2 355.8 1.4	Positive Pitch Maneuver, then SM control	Progress Thruster Test (manifold 1)
53	239/03:04	+ZLV +XVV	354.2 355.9 1.8	Negative Yaw Maneuver	Progress Thruster Test (manifold 2)
54	239/03:05	+ZLV +XVV	359.2 355.8 1.4	Positive Yaw Maneuver	Progress Thruster Test (manifold 2)
55	239/03:08	+ZLV +XVV	359.1 350.8 1.5	Negative Pitch Maneuver	Progress Thruster Test (manifold 2)
56	239/03:08	+ZLV +XVV	359.2 355.8 1.4	Positive Pitch Maneuver	Progress Thruster Test (manifold 2)
57	239/03:20	+ZLV +XVV	359.2 355.8 1.4	Handover RS to US	Handover after thrusters test

There was a series of "manifold 1" yaw, then pitch maneuvers around GMT 27-August-2001, 239/01:30:00, and a series of "manifold 2" yaw, then pitch maneuvers not long after GMT 27-August-2001, 239/03:00:00. These two series of firings are shown at around 01:30 and 03:00 in the color spectrogram of Figure 6-31, respectively.

The "manifold 1" thruster firing that produced the largest peak acceleration as measured by SAMS and MAMS HiRAP was studied. For direct comparison, the HiRAP data were first low pass filtered at 25 Hz to produce the acceleration magnitude plot of Figure 6-32. That plot shows largest peak of 1.93 mg at about the 9.6-minute mark as indicated by the black dashed vertical line below the time axis. Similar plots for SAMS 121f05 and 121f06 are shown in Figure 6-33. These results are summarized in Table 6-4.

TABLE 6-4 PROGRESS THRUSTER PEAK ACCELERATION, GMT 27-AUGUST-2001, 239/01:MM:SS

mm:ss	Sensor	Location	Peak Acceleration (mg)
34:36	HiRAP	LAB1O2, ER1, Lockers 3,4	1.93
34:00	121f05	LAB1O1, ER2, Upper Light Tray	3.03
34:00	121f06	LAB1O1, ER2, EXPPCS	2.78

Note that the HiRAP data set appears to lag the SAMS data sets by about 36 seconds around the time of the "manifold 1" test sequence. The "manifold 2" thruster firing sequence was analyzed in similar fashion to further check timing about one orbital period later. The results show a distinctive thruster firing in the "manifold 2" sequence occurred at GMT 27-August-2001, 239/03:05:46 in the SAMS 121f05 data and one second later in the SAMS 121f06 data set. The HiRAP data set recorded this event at GMT 27-August-2001, 239/03:06:29, which lags the SAMS data by about 43 seconds. The time difference between SAMS data and HiRAP data is under investigation.

One last note on these Progress thruster tests. Within the frequency resolution shown at the top of Figure 6-31, these impulsive thruster firing events briefly excited apparent structural modes at 0.4, 0.5, 0.9, 1.4, 1.8, and 2.7 Hz. See Section 6.2.2.2 for a more detailed accounting on this subject.

6.2.1.2 Progress Flight 4P Undocking

The Progress 4P vehicle was scheduled to undock from the ISS complex at GMT 22-August-2001, 234/06:05:00 and sent on a course to burn up in Earth's atmosphere a few hours later. This was done to clear the way for the Progress 5P vehicle docking with the station as discussed in Section 6.2.1.3. As seen in Figure 6-34 through Figure 6-38, for the five SAMS sensor heads operating at the time, the Progress 4P cargo vehicle was undocked from the aft end of the Zvezda Service Module at about GMT 22-August-2001, 234/06:07:13. Note that the acceleration histories plotted in those figures are relative to the SSA coordinate system. The vehicle pushed away from the station and was expected to produce transient accelerations primarily aligned with the $+X_A$-axis. Those figures do show an initial spike in that direction, but also show large $-Y_A$-axis and large bipolar Z_A-axis accelerations. The peak acceleration vector magnitudes registered by the SAMS sensor heads around the undocking time are shown in Table 6-5.

TABLE 6-5 PROGRESS 4P UNDOCKING PEAK ACCELERATION VECTOR MAGNITUDES

Sensor	Location	Time (seconds) After GMT 22-August-2001, 234/06:07:00	Peak Acceleration (mg)
121f02	LAB1O2, ER1, Drawer 1	13.6	1.02
121f03	LAB1O1, ER2, Lower Z Panel	13.3	1.55
121f04	LAB1O2, ER1, Lower Z Panel	13.3	1.55
121f05	LAB1O1, ER2, Upper Light Tray	13.3	1.35
121f06	LAB1O1, ER2, EXPPCS	16.4	1.50

Note from the ancillary text in the upper left margin of Figure 6-35 through Figure 6-37 that those data were low pass filtered with a cutoff frequency of 25 Hz for direct comparison to the other SAMS sensor head data. Also, the 121f06 sensor was located on the EXPPCS test section of ER2, an ARIS-equipped rack. See Section 6.2.2.3 for more on ARIS.

6.2.1.3 Progress Flight 5P Docking

The Progress 5P vehicle initiated docking contact with aft end of the Zvezda Service Module of the ISS at about GMT 23-August-2001, 235/09:52:16 according to the MAMS HiRAP record. A peak acceleration magnitude of 18.72 mg occurred a few seconds later as seen at the 11-second mark of Figure 6-39. Temporal comparison of the vector magnitude plot of Figure 6-39 to the 3 orthogonal component acceleration histories of Figure 6-40 shows that the nearly 20 mg peak occurred at the time just before the large $+X_H$-axis ($+X_A$-axis) excursion. This is the expected directionality given the Progress vehicle impacted at the aft end of the Service Module while traveling in the $+X_A$-direction. Also, the middle plot of Figure 6-40 shows that a structural mode at about 1 Hz, primarily aligned with the Y_H-axis (Y_A-axis), appears to have been excited around the docking time (more on this subject in Section 6.2.2.2).

6.2.2 Vehicle Systems

This section includes analysis of vibratory disturbances attributable to operation of AAA equipment, vehicle structural modes, and examines the vibratory environment on the ARIS-equipped ER2.

6.2.2.1 AAA Fans

ISS payload racks include an AAA to provide forced-air cooling. This assembly has limited capability and is shared by all payloads within a specific rack volume to cool and circulate air within the rack. Some payload developers may augment airflow rate for their specific payloads with an internal fan or some equivalent. Furthermore, use of cabin-air cooling is restricted for ER payloads due to fire detection and suppression concerns and restricted heat dissipation allocation for racks in the ISS [17].

Figure 6-41 and Figure 6-42 are spectrograms computed from acceleration measurements made on ER2 by the SAMS 121f03 and 121f06 sensors, respectively. These 3-hour plots include 2 thick, white traces overlaid on the acceleration data. The upper trace shows AAA fan speed (in counts) for ER2 retrieved from the ODRC at JSC via the Mission Evaluation Workstation System (MEWS). The precise nomenclature for the parameter queried in the ODRC database was:

MSID	Description
LAEP02FA0001R	AA LAC1 [ER2] HW ISPR Fan Speed L2

The lower trace shows the off/on state of the fan as covered by most of the span shown in the shaded rows of Table 6-6. The information for this table were conveyed via e-mail by Payload Rack Office (PRO) Bill Telesco (Teledyne Brown Engineering). The acceleration spectrum near 181 Hz along with harmonics near 362 Hz in Figure 6-42 strongly suggests a correlation between the acceleration measurements and the AAA fan on/off times with one

notable exception. According to Table 6-6, the ER2 AAA fan turned on at GMT 20-October-2001, 293/00:36:24, while the spectrogram shows it turned on at GMT 20-October-2001, 293/00:32:16, about 4 minutes earlier than the e-mail from the PRO. The ODRC fan speed data, however, is in agreement with the acceleration measurements. Therefore we conclude that there was a typographical error in the e-mail used to build Table 6-6.

TABLE 6-6 AAA FAN (DE)ACTIVATIONS DURING ARIS-ICE TESTING

GMT Day	OFF	ON
	hh:mm:ss	hh:mm:ss
19-October-2001, 292	23:26:36	23:36:24
20-October-2001, 293	00:22:05	00:36:24[1]
20-October-2001, 293	01:02:06	01:12:03
20-October-2001, 293	02:02:04	02:12:04
20-October-2001, 293	02:42:04	02:52:03
20-October-2001, 293	04:20:30	04:30:38
26-October-2001, 299	15:08:03	15:13:58

Further examination of Figure 6-42 with the time scale zoomed from the 5- to 95-minute marks are shown in Figure 6-43 and Figure 6-44. The former shows the spectra from 161 to 201 Hz, while the latter spans from 342 to 382 Hz. In addition, the topmost (strongest) value in the colormap of these 2 zoomed spectrograms was changed to black for emphasis, especially around 181 Hz. Figure 6-43 shows that the primary impact of this AAA fan in the vicinity of SAMS 121f06 was centered around 181 Hz.

6.2.2.2 Structural Modes

The Shuttle Endeavour docked with the ISS at about GMT 07-December-2001, 341/20:03:00 and maintained joint operations during flight UF-1 until it undocked at about GMT 15-December-2001, 349/17:28:00. This section focuses on the structural mode regime transition that took place when Endeavour undocked. The undock time is indicated by the dashed vertical line on the time axis of the color spectrograms shown in Figure 6-45 and Figure 6-46. These spectrograms were computed from SAMS 121f03 ER2 and 121f04 ER1 measurements, respectively[2]. These 2 sensor heads were located on the lower Z panel of adjacent racks in the US Lab, and consequently show similar vibratory environments below about 13 Hz. The 121f03 environment did, however, exhibit heightened broadband with frequency approaching 15 Hz. This disturbance was primarily imparted on the Y_AZ_A-plane at the 121f03 sensor location. When the spectrograms below 5 Hz were examined with a 3-hour span around the Shuttle undock time, the results are shown in the spectrogram zooms of Figure 6-47 and Figure 6-48. The horizontal dashed line on the Y_A-axis (middle) subplot of Figure 6-47 at approximately 0.32 Hz shows the only significant difference between these locations. This 0.32 Hz disturbance was measurable at the 121f03 sensor location on the Y_A-axis while the Shuttle was docked to the ISS, but was not discernible in the 121f04 sensor data.

[1] this time does not correlate with acceleration measurements or ODRC database [suspect e-mail typo]

[2] parameters used to compute spectrogram were not typical, but were adjusted to improve frequency resolution and as noted on the figures for Section 6.2.2.2, the SAMS data were transformed to the SSA coordinate system

Further quantitative insight below 10 Hz comes from Figure 6-49 for the vibratory environment before the Shuttle undocked. In this figure, the spectral average of several PSDs for both 121f03 (green trace) and 121f04 (red trace) are shown. The 3 subplots from top to bottom show the X_A, Y_A, and Z_A-axes spectra, respectively. Comparison of these "joint ops" data sets for these 2 prime structure sensor locations shows negligible difference with the following notable exceptions:

- 121f03 was mounted forward of 121f04 by 42 inches (in the $+X_A$-direction)
- 121f03 location (green trace) was subject to the following distinct spectral peaks not appreciably measured at the 121f04 location:
  - $\Rightarrow$ 0.32 Hz on the Y_A-axis
  - $\Rightarrow$ 5.22 Hz and 5.26 Hz on all 3 axes
  - $\Rightarrow$ 7.84 Hz and 7.90 Hz primarily on the X_A-axis
  - $\Rightarrow$ 9.19 Hz primarily on the X_AY_A-plane
- 121f04 location was subject to a broadband disturbance around 8 Hz primarily on the Y_AZ_A-plane

A similar comparison of "unmated" data sets follows from Figure 6-50. This figure is analogous to Figure 6-49 except that the time frame is 2 hours later, or about 1 hour after the Shuttle undocked. These "unmated" data sets for the 2 sensor locations match closely with the exception that the 121f04 (red trace) location exhibited heightened broadband excitation on the Y_AZ_A-plane above about 7 Hz. One additional observation regarding this figure is that the 2 closely-spaced peaks at 5.22 Hz and 5.26 Hz observed only at the 121f03 location in the "joint ops" data sets appear at both sensor locations in these "unmated" data sets.

Since the 2 sensor locations showed similar spectra before and similar spectra after the Shuttle undocked, comparison of the 121f04 "joint ops" to the 121f03 "unmated" spectra is shown in Figure 6-51. This figure expectedly shows much contrast between the vibratory environments of the 2 distinct vehicles: (1) "joint ops" with the massive Shuttle mated to the ISS, and (2) "unmated". The "joint ops" Z_A-axis (black trace, bottom subplot) shows broadband excitation centered on a couple of familiar Shuttle structural modes at about 3.5 Hz and 4.8 Hz. Also, but not seen in the figure, the Shuttle's Ku band antenna dither disturbance once again was measured on the ISS in the "joint ops" data as shown in Table 6-7. This table serves to quantify and summarize comparison of the structural mode regime while the Shuttle was mated to the ISS. Table 6-8 serves likewise for the unmated configuration. Of particular note below 20 Hz in the unmated configuration, the difference between 121f03 X_A-axis and 121f04 X_A-axis spectra is negligible. Likewise below about 7 Hz for the Y_AZ_A-plane.

TABLE 6-7 STRUCTURAL MODE REGIME BEFORE STS-108 UNDOCKED ("JOINT OPS")

SSA Axis	Frequency (Hz)				ug_{RMS}		Comment
	f_1	f_2	peak				
			121f03	121f04	121f03	121f04	
X	0.12	0.20	0.15	0.15	12.4	13.0	XZ
X	0.27	0.35	0.32	0.32	3.8	3.8	
X	0.35	0.43	0.38	0.38	4.3	4.3	
X	0.63	0.72	0.66	0.66	6.4	5.6	
X	0.72	0.79	0.75	0.75	2.6	2.6	
X	1.11	1.21	1.16	1.17	2.3	2.2	XZ
X	1.73	1.83	1.77	1.77	3.2	3.3	XZ
X	2.38	2.47	2.43	2.43	2.1	2.1	
X	2.47	2.58	2.50	2.50	2.3	2.3	
X	3.17	3.22	3.20	3.22	1.6	1.5	
X	3.22	3.40	3.30	3.31	3.3	3.0	
X	3.40	4.00	3.95	3.95	3.4	3.1	likely Shuttle born
X	4.40	5.00	4.67	4.64	5.2	5.1	likely Shuttle born
X	5.16	5.25	5.23	5.20	3.4	1.1	mainly 121f03
X	5.25	5.33	5.28	5.31	3.3	0.9	mainly 121f03
X	5.81	6.39	6.16	6.16	3.6	3.5	
X	6.74	7.40	7.23	7.13	3.8	2.7	mainly 121f03
X	7.78	7.89	7.86	7.84	20.1	1.1	mainly 121f03
X	7.89	7.95	7.90	7.90	4.3	0.8	mainly 121f03
X	9.12	9.26	9.19	9.17	2.7	1.5	mainly 121f03, XY
X	11.58	11.68	11.64	11.64	34.7	36.1	not a mode; on/off[3]
X	16.93	17.13	17.03	17.03	9.1	8.8	Shuttle born Ku antenna dither[4]
Y	0.29	0.40	0.32	0.31	3.5	1.7	mainly 121f03
Y	0.40	0.53	0.44	0.44	8.9	9.4	
Y	0.69	0.89	0.76	0.76	12.7	11.9	Y
Y	2.37	2.49	2.43	2.43	3.3	3.5	
Y	3.40	4.00	3.94	4.00	12.0	8.7	likely Shuttle born
Y	4.40	5.00	4.84	4.84	6.3	9.0	likely Shuttle born
Y	5.16	5.25	5.22	5.25	8.5	2.3	mainly 121f03
Y	5.25	5.33	5.26	5.29	7.7	2.1	mainly 121f03, XYZ
Y	7.80	7.87	7.84	7.86	7.3	1.6	mainly 121f03
Y	7.87	8.68	7.90	8.18	4.7	7.7	mainly 121f04
Y	9.12	9.26	9.19	9.16	3.9	2.0	mainly 121f03, XY
Y	11.58	11.68	11.64	11.64	23.6	25.6	not a mode; on/off[3]
Y	16.93	17.13	17.03	17.03	25.2	17.9	Shuttle born Ku antenna dither[4]
Z	0.12	0.20	0.15	0.15	10.0	10.5	XZ
Z	0.35	0.43	0.38	0.41	2.4	1.9	mainly 121f03
Z	0.58	0.70	0.66	0.66	2.2	3.0	
Z	0.99	1.11	1.05	1.05	4.1	5.8	
Z	1.13	1.21	1.17	1.17	2.2	2.3	XZ
Z	1.73	1.83	1.77	1.77	2.0	2.4	XZ
Z	2.35	2.62	2.50	2.50	8.7	9.7	
Z	3.40	4.00	3.52	3.56	14.2	14.3	likely Shuttle born
Z	4.40	5.00	4.67	4.62	13.6	13.3	likely Shuttle born
Z	5.16	5.25	5.22	5.23	4.5	1.5	mainly 121f03
Z	5.25	5.33	5.26	5.31	4.4	1.6	mainly 121f03
Z	6.50	6.59	6.53	6.52	4.5	3.2	mainly 121f03
Z	7.77	7.89	7.86	7.80	5.9	2.6	mainly 121f03
Z	7.89	8.85	7.90	8.18	3.2	7.3	mainly 121f04
Z	11.58	11.68	11.64	11.64	19.4	34.3	not a mode; on/off[3]
Z	16.93	17.13	17.03	17.03	7.2	10.6	Shuttle born Ku antenna dither[4]

[3] see turn off at about GMT 15-December, 349/19:45 of Figure 6-45 or Figure 6-46
[4] not a structural mode, but included for comparison with corresponding entry in Table 6-6

TABLE 6-8 STRUCTURAL MODE REGIME AFTER STS-108 UNDOCKED ("UNMATED")

SSA Axis	Frequency (Hz)				ug_{RMS}		Comment
	f_1	f_2	peak				
			121f03	121f04	121f03	121f04	
X	0.02	0.09	0.06	0.06	1.8	1.7	X
X	0.09	0.20	0.14	0.14	2.0	1.9	
X	0.20	0.24	0.23	0.23	0.9	0.9	
X	0.24	0.32	0.27	0.27	1.5	1.5	
X	0.32	0.44	0.40	0.40	2.5	2.5	
X	0.44	0.50	0.47	0.47	1.5	1.5	
X	0.50	0.63	0.55	0.55	3.8	3.9	XY
X	0.79	0.99	0.90	0.90	6.6	6.3	XZ
X	1.16	1.22	1.21	1.21	1.9	1.8	
X	1.22	1.27	1.25	1.25	3.1	3.0	
X	1.27	1.34	1.31	1.31	6.2	6.1	XYZ
X	1.71	1.88	1.79	1.79	4.0	3.8	
X	2.59	2.70	2.64	2.64	2.2	2.2	
X	3.40	4.00	3.74	3.74	2.5	2.4	
X	4.00	4.09	4.04	4.04	0.8	0.8	
X	5.16	5.25	5.25	5.25	3.4	3.3	
X	5.25	5.33	5.28	5.28	2.7	2.6	
X	6.41	6.77	6.53	6.53	10.0	9.8	
X	6.84	6.93	6.87	6.87	4.6	4.6	
X	7.77	8.03	7.86	7.86	32.6	33.7	XYZ
X	9.11	9.22	9.19	9.19	3.3	3.2	
X	11.58	11.68	11.64	11.64	25.9	28.1	not a mode; on/off (see spectrogram)
X	16.93	17.13	17.06	17.06	3.5	3.3	No Shuttle, compare to Table 6-7 entry
Y	0.43	0.66	0.55	0.55	22.6	20.4	XY
Y	1.22	1.27	1.25	1.25	4.0	3.0	
Y	1.27	1.36	1.30	1.30	6.2	5.4	XYZ
Y	2.37	2.53	2.44	2.44	2.4	1.9	
Y	2.53	3.19	2.64	2.64	4.9	3.7	
Y	4.46	5.16	5.00	5.00	3.9	5.2	
Y	5.16	5.25	5.23	5.23	5.8	5.8	
Y	5.25	5.33	5.26	5.26	4.9	4.5	
Y	6.41	6.77	6.58	6.58	13.2	16.1	
Y	6.77	7.77	6.79	7.75	5.4	14.1	
Y	7.77	8.03	7.86	7.86	14.7	24.5	XYZ
Y	8.03	9.08	9.03	8.12	6.5	14.8	
Y	9.08	9.26	9.19	9.19	5.1	6.3	
Y	9.26	10.36	9.46	9.46	5.7	9.4	
Y	11.58	11.68	11.64	11.64	11.3	16.0	not a mode; on/off (see spectrogram)
Y	16.93	17.13	17.06	17.06	3.4	4.7	No Shuttle, compare to Table 6-7 entry
Z	0.35	0.47	0.40	0.40	11.3	9.5	
Z	0.73	0.99	0.90	0.90	21.0	18.0	XZ
Z	1.16	1.22	1.19	1.19	8.0	6.5	
Z	1.22	1.27	1.25	1.25	14.5	11.6	
Z	1.27	1.34	1.31	1.31	24.2	20.0	XYZ
Z	1.74	1.82	1.79	1.79	4.2	3.4	
Z	2.52	2.58	2.55	2.55	2.5	2.0	
Z	2.58	2.70	2.61	2.61	3.4	2.6	
Z	5.16	5.25	5.25	5.23	2.9	3.4	
Z	5.25	5.33	5.28	5.26	2.1	2.8	
Z	6.41	6.77	6.59	6.59	11.2	14.4	
Z	6.77	7.77	7.46	7.77	8.4	17.6	
Z	7.77	8.03	7.87	7.86	9.0	26.2	XYZ
Z	8.03	9.34	8.04	8.12	5.7	16.4	
Z	9.34	9.54	9.48	9.37	2.4	3.4	
Z	9.54	10.39	9.84	9.84	3.7	6.5	
Z	11.58	11.68	11.64	11.64	11.3	25.7	not a mode; on/off (see spectrogram)
Z	16.93	17.13	17.01	17.06	3.1	3.8	No Shuttle, compare to Table 6-7 entry

The material presented in this section was not intended to be a comprehensive analysis of the structural dynamics of the ISS. There are other members in the microgravity community who have the models, tools, and engineering know-how to better present those results. The ISS is being assembled, and as its configuration evolves so will its structural mode regime. At assembly complete and beyond, a general characterization and tracking of these vehicle modes will be undertaken and results tailored for presentation to investigators for their consideration. Precise comparison of the results here to existing model predictions is complicated by, for example, non-stationarity that leads to practical frequency resolution limitations for the acceleration measurements.

6.2.2.3 ARIS Environment

During the span covered by this report, the ARIS was installed on ER2. The ARIS acts to isolate experiments located in its rack, in this case EXPPCS, from disturbances that would otherwise propagate from various external disturbance sources through ISS structure to the sensitive experiment location. The ARIS uses a sophisticated control system of sensors to measure external disturbances, a control law to compute appropriate and timely forces, and 8 pushrod actuators to apply these reactive forces between the rack and the US Lab structure. In this way, the ARIS serves to attenuate the vibrations transmitted to the payload. Active isolation is configuration dependent and generally takes place between 0.01 and 1 to 2 Hz. Besides the active mode described above, ARIS has these other modes of operation:

IDLE: ARIS does not attempt to control position or acceleration of the rack

HOLD: ARIS centers the rack and holds its position relative to the ISS without attempting to reduce vibrations (also referred to as STANDBY)

NOGO: ARIS is in an idle-like state and does not attempt to control position or acceleration; ARIS enters this state upon any error, or failure of the active built-in test that is part of the initialization sequence

For the purpose of this report, an active mode time frame was sought to compare the vibratory environment provided by the ARIS to a nearby, non-isolated location. The intention here is to convey a useful comparison and is not intended to characterize performance of the ARIS. Those interested in information of that nature are referred to the ARIS-ICE team, namely James Allen, at the Boeing Company. An excerpt of an e-mail correspondence from James Allen on 17-September-2001 did provide ARIS mode timeline information as follows:

"... here are some times for ARIS mode transitions and shaker tests over the last week. All times listed are GMT. Some of the times are inferred since the transitions occurred during LOS periods or during times when we had no telemetry due to a rack lockup. These times, which may be off by several minutes, are marked by an asterisk. Also, all times listed may be off by a minute or two because of variations between the POP time and the actual GMT time and the fact that the POP does not put a timestamp on every single command ...

GMT	Transition to:
8-September-2001, 251/06:46	NOGO (ARIS had been in STANDBY since late the previous night)
9-September-2001, 252/07:11	STANDBY
9-September-2001, 252/16:49	NOGO
10-September-2001, 253/08:30	IDLE
10-September-2001, 253/08:31	STANDBY
10-September-2001, 253/09:46	ACTIVE
10-September-2001, 253/15:40	IDLE*
11-September-2001, 254/07:42	STANDBY
11-September-2001, 254/07:43	ACTIVE
11-September-2001, 254/14:10	IDLE*
13-September-2001, 256/04:00	POP shutdown to support ER2 software load (ARIS should be in IDLE or NOGO)"

The transition to active mode at GMT 11-September-2001, 254/07:43 cited above is clearly visible in the SAMS 121f06 data measured during this time frame. It appears as the yellow vertical streak at this time in Figure 6-52. Figure 6-53 shows continued operation in this mode until about 10:45, at which time there is a gap in the SAMS acceleration record. Note that the start of the gap may not be immediately obvious owing to the quiet environment at the 121f06 location below the cutoff frequency for this sensor. Gaps in color spectrograms for this report appear as solid, dark blue vertical bands. This is the bottom most color for the PSD magnitude colorbar scale. To clearly see where the SAMS gap starts and for general comparison to similar spectrograms computed for 121f05 (mounted on the light tray "on top" of ER2) see Figure 6-54 and Figure 6-55. The four aforementioned 8-hour color spectrograms all are colorbar scaled from 10^{-12} g^2/Hz to 10^{-6} g^2/Hz. These settings are typical and appropriate for the 121f05 data, but do not serve well for the much quieter 121f06 data. Therefore, Figure 6-56 and Figure 6-57 show spectrograms recomputed with colorbar scales adjusted to range from 10^{-14} g^2/Hz to 10^{-8} g^2/Hz for a better look at the 121f06 data. On these plots, the span was shortened to 4 hours and the start time set to occur about 1 hour before the transition to active mode. The 121f05 spectrogram expectedly shifts toward the red for these "quiet" colorbar settings. For relative comparisons and qualitative looks at the vibratory environment, these spectrograms may suffice. However, for precise quantitative comparison, other means are in order.

A simple means of quantitative comparison between the isolated environment at the 121f06 location and the non-isolated 121f05 location can be made from Figure 6-58. The black traces show 121f05 data aligned to the SSA coordinate system, while the yellow traces show 121f06 data. Table 6-9 quantitatively summarizes the 101-second span of Figure 6-58. For this period, the maximum acceleration vector magnitude was over 315 μg for 121f05, whereas the maximum for 121f06 was below 25 μg. This is over an order of magnitude smaller on ARIS for these accelerations measured below 25 Hz.

TABLE 6-9 SIMPLE ARIS COMPARISON GMT 11-SEPTEMBER-2001, 254/08:09:19

Sensor	Location	SSA Axis	Acceleration (µg)		
			MIN	MAX	RMS
121f05	Light Tray, Top of ER2	X	-156.8	145.6	39.2
		Y	-252.4	233.6	46.3
		Z	-281.9	286.6	57.3
121f06	EXPPCS Test Section (on ARIS)	X	-16.7	17.0	4.7
		Y	-23.6	20.5	6.3
		Z	-12.3	10.9	2.9

A somewhat more detailed quantitative comparison for the same time span as shown in Figure 6-58 and Table 6-9 can be made from a frequency domain perspective. Figure 6-59 shows RMS accelerations computed from measurements made by 121f05 (red trace) and 121f06 (green trace). These measurements are overlaid against the vibratory acceleration limits in specified One-Third Octave (OTO) frequency bands [18][4]. Notice in this figure that below 25 Hz, with particular attention below 1 Hz, the ARIS environment has RMS levels well below the non-ARIS location. Finally, Figure 6-60 is a similar OTO band plot of the RMS accelerations for 3 other non-ARIS locations: 121f02 (orange trace), 121f03 (blue trace), and 121f04 (magenta trace). The RMS levels shown here show the same trend as the 121f05 data from the previous figure. That is, below about 1 Hz, they breach the limits curve in most of the OTO bands. Above 1 Hz, they are below the limits curve for the most part.

6.2.3 Experiment Equipment

Experiment equipment related to EXPPCS and APCF are the focus of this section.

6.2.3.1 EXPPCS

Monitoring of PIMS real-time displays on August 21, 2001 helped identify an EXPPCS activation time. The color spectrogram of Figure 6-61 was computed from SAMS 121f03 measurements and shows the start of a distinct 119.6 Hz spectral peak at GMT 21-Aug-2001 233/16:11:46. Past experience with flight hardware suggests this may be the onset of a computer hard drive.

Parseval's theorem applied to a 2-minute span centered on EXPPCS activation produced Figure 6-62, which is a 2-second interval RMS plot for the frequency range from 119.55 to 119.71 Hz. Similar plots (not shown here) were analyzed for the other frequency ranges shown in Table 6-10.

[4] those induced by the mechanisms (fans, pumps, exercise equipment, latches, hinges, vents, etc.) of the ISS and the combined payload complement [18]

TABLE 6-10 RMS ACCELERATION FOR EXPPCS ACTIVATION

Frequency Range (Hz)	RMS Acceleration (mg_{RMS})	
	Before Activation	After Activation
0.25 - 119.55	0.80	0.80
119.55 - 119.71	0.02	0.14
119.71 - 200	1.00	1.00
0.25 - 200	1.28	1.29

Note that the frequency range in the last row of Table 6-10 spans the previous 3 rows in that table, yet the RMS values in the last row are not simply the sum of the RMS values from the rows above. This comes mathematically from Parseval's theorem, such that Parseval

$$\mathrm{RMS}_{14} = \sqrt{(\mathrm{RMS}_{12})^2 + (\mathrm{RMS}_{23})^2 + (\mathrm{RMS}_{34})^2}$$

where RMS_{12} is the RMS value for the frequency range from f_1=0.25 Hz to f_2=119.55 Hz, RMS_{23} for the range from f_2 to f_3=119.71 Hz, and RMS_{34} for the range from f_3 to f_4=200 Hz. This calculation shows that this disturbance source [computer hard drive] contributes about 0.01 mg_{RMS} in the frequency range from f_1=0.25 Hz to f_4=200 Hz, the overall RMS acceleration level in the passband of the demeaned SAMS 121f03 data.

6.2.3.1.1 EXPPCS AND ARIS-ICE POP DEACTIVATION ON 07-SEPTEMBER-2001

TABLE 6-11 PRO COMMAND TIMELINE FOR ER2 ON GMT 7-SEPTEMBER-11, 250/HH:MM:SS

hh:mm:ss	PRO Note
05:48:42	Disabled power to EXPPCS T2 (Locker 4)
05:48:46	Disabled power to EXPPCS T1 (Locker 4)
05:49:17	Disabled communications to EXPPCS DN (Locker 8)
05:50:10	Disabled power and communications to ARIS ICE; single command for both (Locker 1)
06:13:08	Disabled power and communications to SAMS ICU; single command for both (Drawer 1)

Within the temporal resolution of the spectrogram plot, a close inspection of Figure 6-63 showed that the first set of seven disturbances at 56.5, 57.3, 58.5, 59.5, 101.3, 105.2, 119.6 Hz turned off at GMT 07-September-2001, 250/05:48:38 and the second at 90 Hz turned off at 07-September-2001, 250/05:50:37. Comparing the PRO command timeline of Table 6-11 to these times, we associate the first set of disturbance sources with EXPPCS and the one that turned off later with ARIS-ICE.

6.2.3.2 APCF

An excerpt of an ISS on-orbit status report stated that: "APCF was powered down at GMT 235[23-Aug-2001]/18:14:50 to change its SSPCM power channel from a 10amp threshold to 15amps. It was then powered back on at 235[23-Aug-2001]/18:16:27. This change was made in response to APCF's two over current conditions with the channel set at 10amps." The color spectrogram of Figure 6-64 shows no discernible effects at the HiRAP ER1 location at these activation/deactivation times. The HiRAP was located in the same rack as the APCF.

6.2.4 Crew Activity

Experimental setups, equipment transfer or stowage, exercise, and locomotion all contribute to a category of disturbance called crew activity. These actions give rise to reactive forces, which are manifested as acceleration disturbances transferred through the vehicle's structure. Future in-depth analyses will seek to correlate acceleration effects with all of the various crew activities, but for this report only a special case of crew ergometer exercise was examined.

6.2.4.1 Exercise

While there is an abundance of acceleration data for and characterization of exercise during several past Shuttle microgravity missions, the available ISS record has been devoid of ancillary information to document times and other aspects of crew exercise that enables complete analysis. Correspondence in the form of e-mail from Robert Janney (JSC) on 4-December-2001, stated that there are currently 4 exercise devices aboard the ISS:

1) Russian velo ergometer (in the Service Module)
2) US Treadmill with Vibration Isolation System, TVIS (in the Service Module)
3) US Cycle Ergometer with Vibration Isolation System, CEVIS (in the US Lab)
4) US Resistive Exercise Device, RED (in Node 1)

During STS-108 joint operations, a Shuttle ergometer pedaling frequency test (Detailed Test Objectiver (DTO) 262) was conducted as detailed in [19]. Excerpts are noted here:

Equipment Preparation:

- Ergometer in on-orbit configuration.
- Verify with Mission Control Center–Houston (MCC-H) attitude control system jets are inhibited or ISS CMGs are active (momentum management mode is acceptable).
- Verify with MCC–H/MSFC payload ops that SAMS is actively transmitting acceleration data.

Test Notes:

- Test must be performed while docked to ISS.
- ISS exercise during this test is undesirable.
- Any planned ergometer exercise session will suffice for this test.
- Request crewmember strapped in ergometer, if practical.

- Any ergometer hard mount attachment location is acceptable.
- Any crewmember is acceptable for the test.

The sequence for desired pedaling frequency is shown in Table 6-12.

TABLE 6-12 JOINT OPS SHUTTLE ERGOMETER EXERCISE TEST SEQUENCE (DTO 262)

Test #	Pedal Frequency (RPM)		Time
	From	To	
1	50	55	1 min 40 sec
2	55	60	1 min 35 sec
3	60	65	1 min 30 sec
4	65	70	1 min 25 sec
5	70	75	1 min 20 sec
6	75	80	1 min 10 sec
7	80	85	1 min 5 sec
8	85	90	1 min
9	90	95	55 sec
10	95	100	50 sec
11	100	105	40 sec
12	105	110	35 sec
13	110	115	30 sec
14	115	120	25 sec
15	120	125	20 sec

The ergometer exercise equipment for this test was located in the Shuttle middeck and the exercise protocol was of special design for this test. Therefore, the results for this section are not presented as typical or representative of nominal ISS ergometer exercise. The closest SAMS sensor to the exercise location in the Shuttle during joint operations was 121f03 and Figure 6-65 shows its vibratory environment below 25 Hz during this period. As indicated by the red vertical dashed lines on that figure, the exercise started at GMT 15-December-2001, 349/11:36:03 and lasted approximately 17 minutes. This is about 2 minutes more than the total for the protocol shown in Table 6-12. Based on acceleration measurements made during numerous Shuttle ergometer exercise periods, the expected acceleration signature is a pair of spectral peaks at the shoulder-sway and pedaling frequencies. These typically occur around 1.25 and 2.5 Hz, respectively, and are usually accompanied by heightened structural excitation below about 10 Hz. Considering a two per revolution factor for ergometer pedaling, Figure 6-65 indicates that the crewmember started pedaling at about 54 RPM (1.8 Hz peak at first red dashed vertical line) and finished at about 120 RPM (4 Hz peak at second red dashed vertical line) over the span of 17 minutes. The shoulder sway disturbance is also discernible, but much less pronounced at half the pedaling frequencies. Spectral analysis to quantify the impact of this disturbance is complicated by non-stationarity. That is, a steady state is necessary to apportion RMS acceleration levels to pedaling and shoulder sway motion. In this case (as called for by the special protocol), the exerciser did not dwell at any one rate for an appreciable amount of time. As a result, 2 minutes near the beginning of the exercise period were selected for detailed quantification. The cumulative RMS acceleration as a function of frequency for this period is shown in Figure 6-66. The RMS scale was not

optimized for this figure to stand alone, but instead was set for direct comparison to some historical Shuttle and Mir data. These are shown in Figure 6-67. Comparing these 2 figures, it is noted that the recent STS-108 exercise is quantitatively on par with USMP-2 ergometer hardmount exercise below about 3 Hz. Above 3 Hz, the black trace of Figure 6-66 would fall among, or slightly above, the weaker traces in Figure 6-67. The difference primarily stems from a strong Shuttle structural mode at about 4.8 Hz that is less distinct in the joint ops data. When aggregated with the background vibratory environment below 10 Hz, this Shuttle-born ergometer exercise imparted about 150 μg_{RMS} at the 121f03 location. One final note for this comparison is that while most traces in Figure 6-67 show the steep slope of a step at the shoulder sway frequency (about 1.25 Hz), the seemingly analogous step in Figure 6-66 is instead a structural mode aligned primarily with the X_A-axis at about 0.7 Hz. This structural mode peak far outweighs the direct effect of shoulder sway. A priori knowledge regarding ergometer exercise and its effects on the microgravity environment suggested checking for a shoulder sway spectral peak closer to 0.9 Hz. This was undertaken and the PSDs of Figure 6-68 indeed show what is presumed to be the shoulder sway peak at the red vertical indicator lines along with the pedal peak at the blue vertical indicator lines. The intent of this special exercise was to sweep through the structural mode regime and the pedal peak clearly was doing that here (see Table 6-7).

To date, ready access to timeline information that would assist in isolating an exercise period for a particular piece of equipment on the ISS along with other pertinent information like which piece of equipment, what exercise protocol, and the like has proved elusive. However, characterization of ISS exercise disturbances is important for various members of the microgravity community and will be an ongoing effort for PIMS and other concerned parties such as those studying loads and dynamics of the vehicle. Several SDTOs have been planned to capture exercise information of this sort in a coordinated effort among loads/dynamics, payloads, medical operations, and mission evaluation teams. There are currently plans to capture TVIS exercise in February 2002.

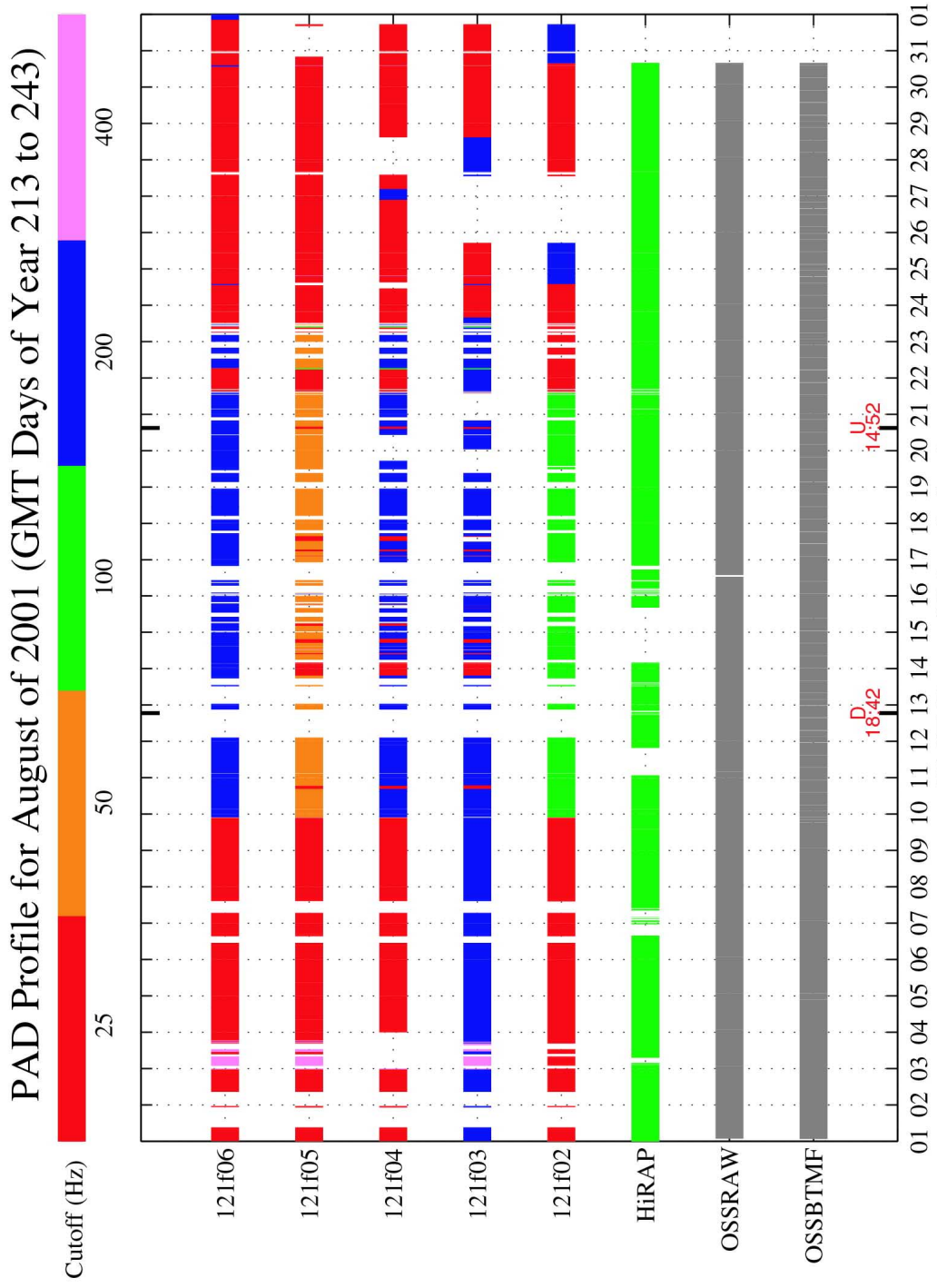

Figure 6-26 PAD Profile for August of 2001

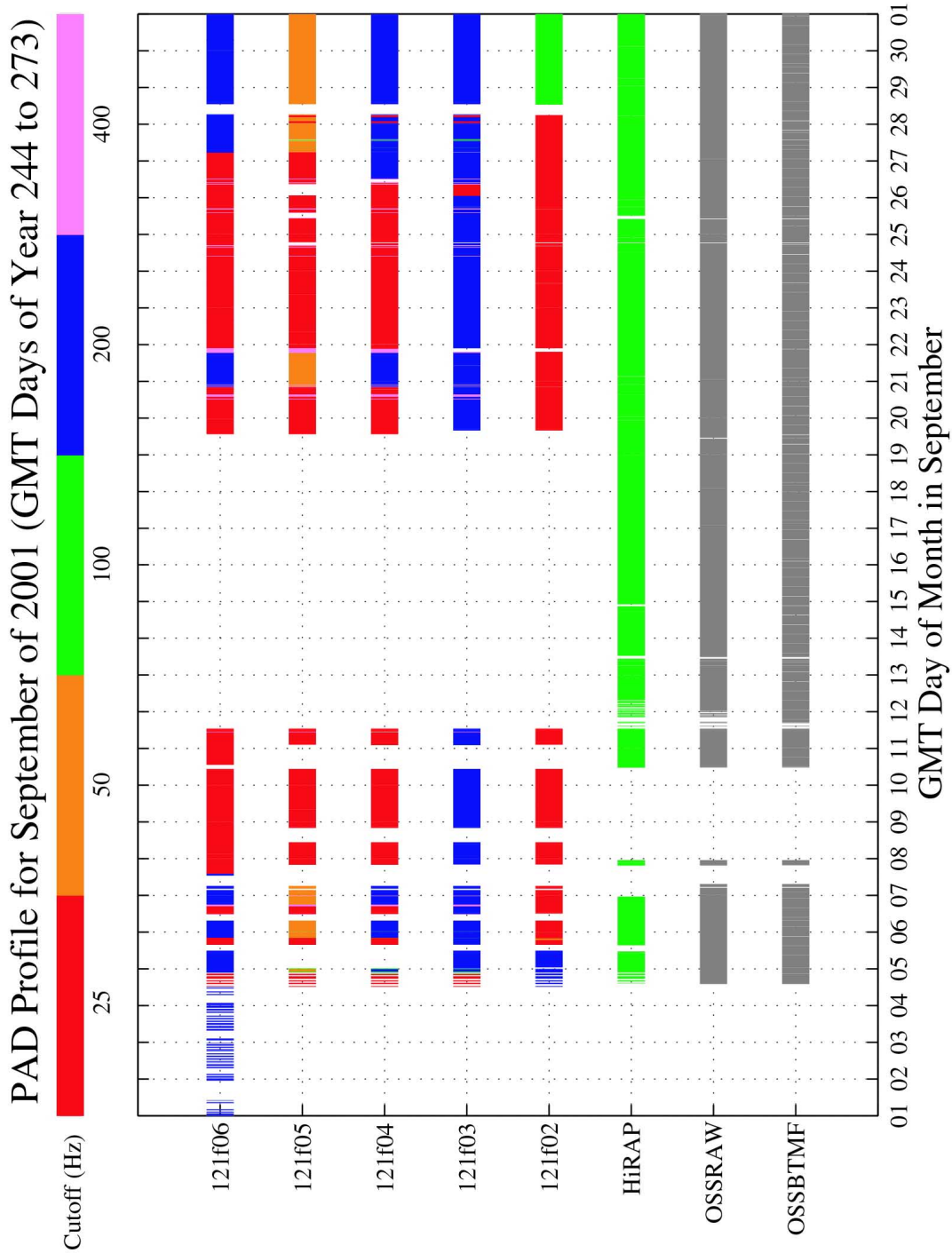

Figure 6-27 PAD Profile for September of 2001

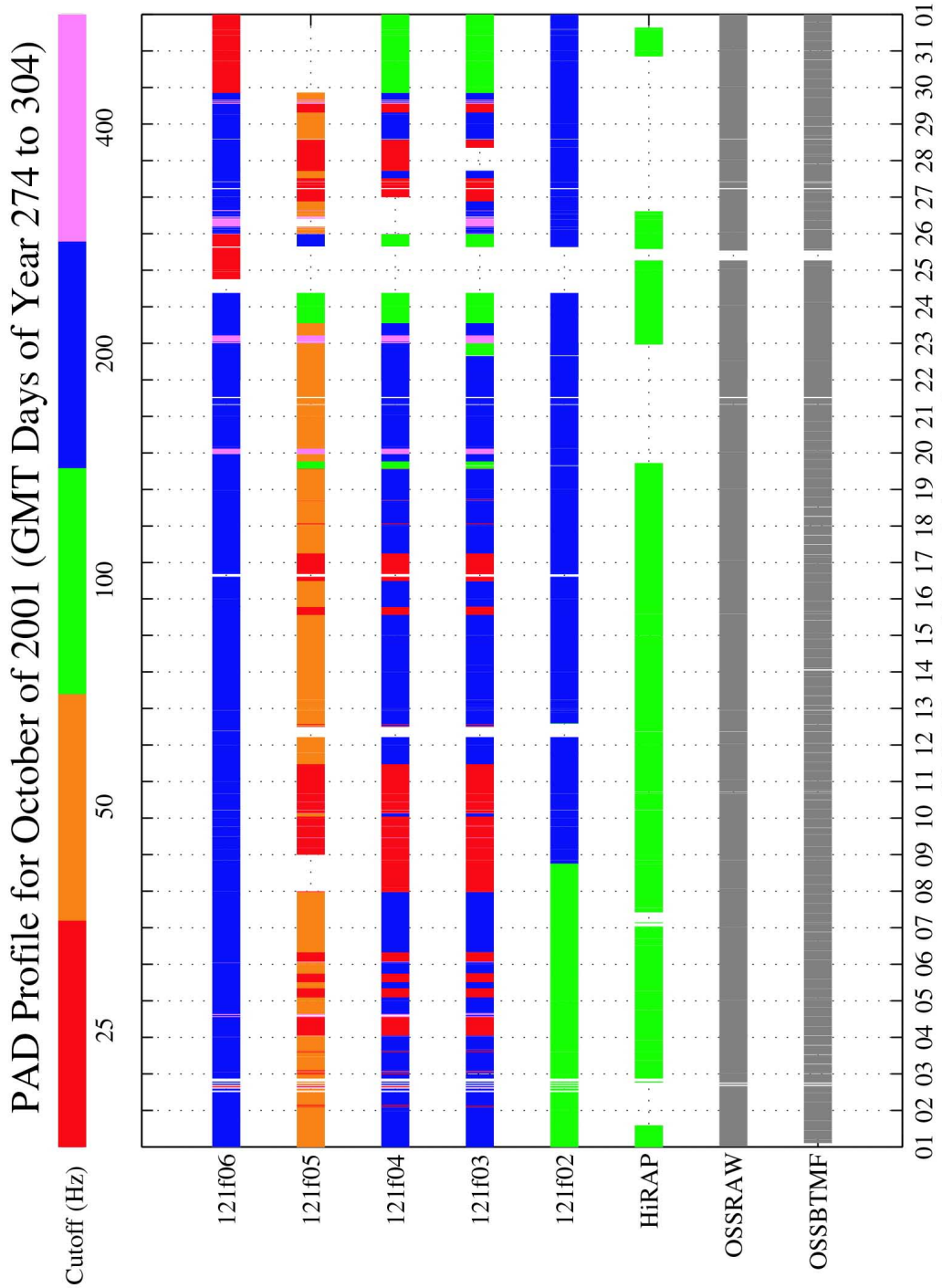

Figure 6-28 PAD Profile for October of 2001

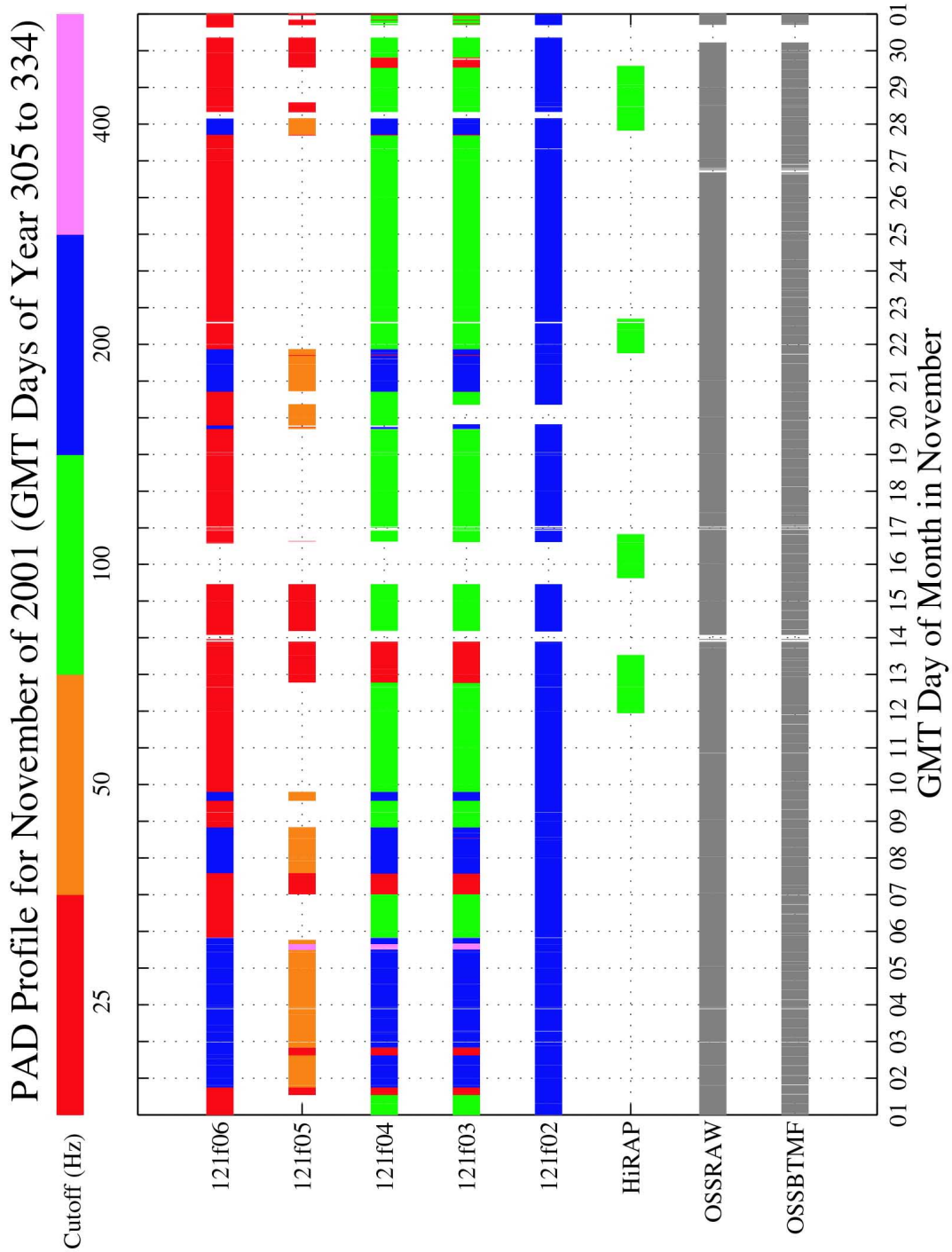

Figure 6-29 PAD Profile for November of 2001

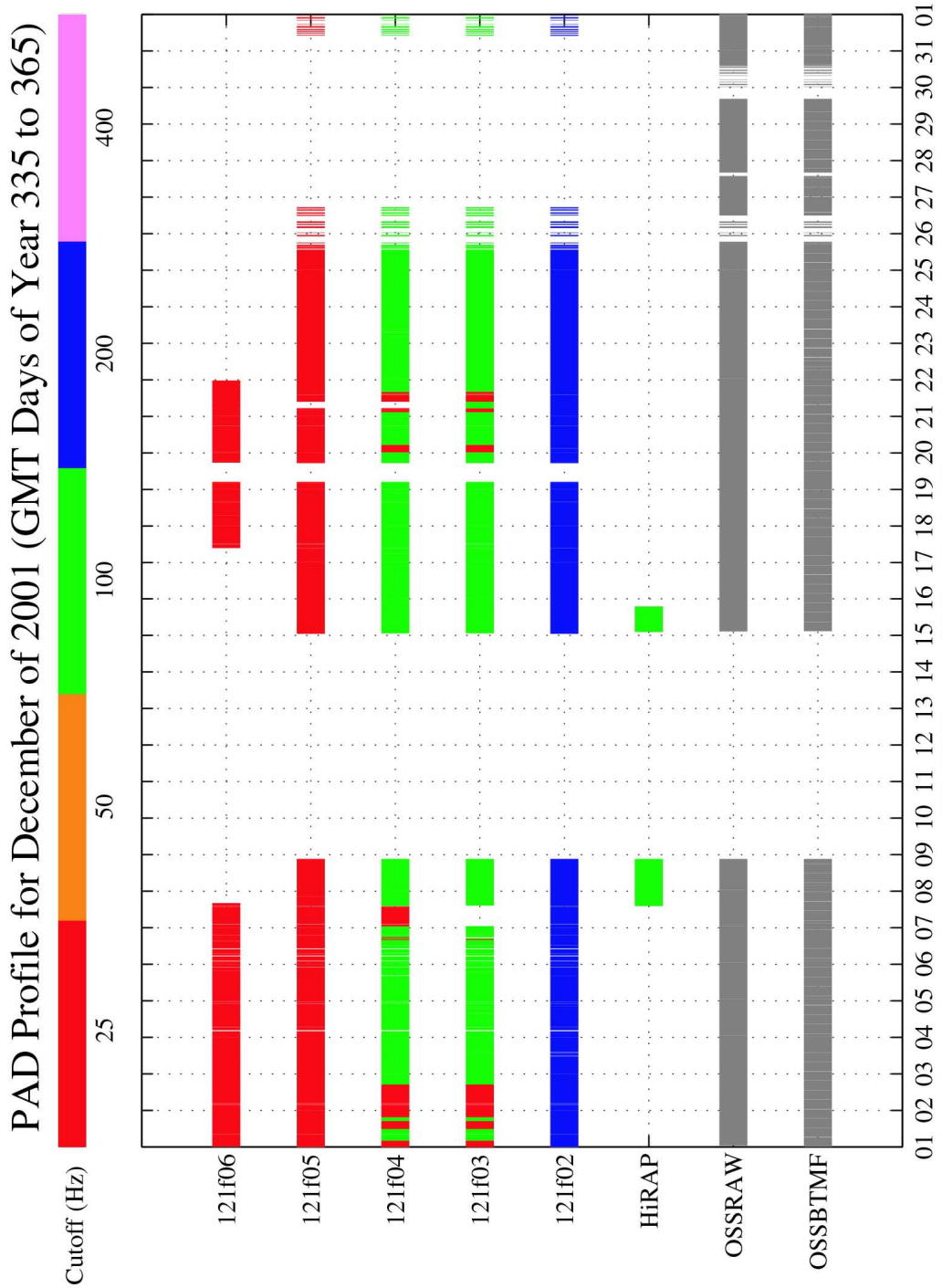

Figure 6-30 PAD Profile for December of 2001

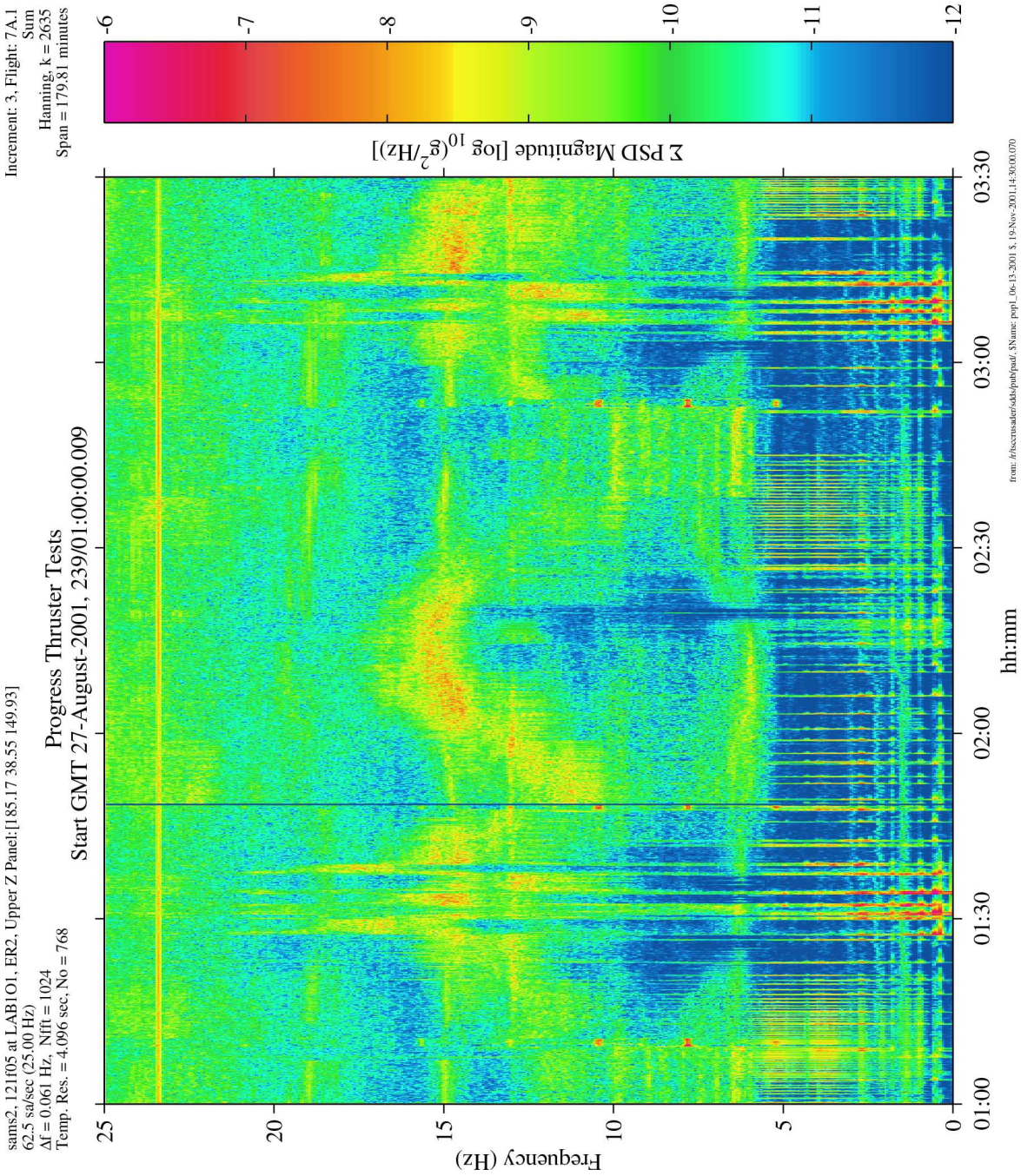

Figure 6-31 Spectrogram of Progress Thruster Tests (121f05)

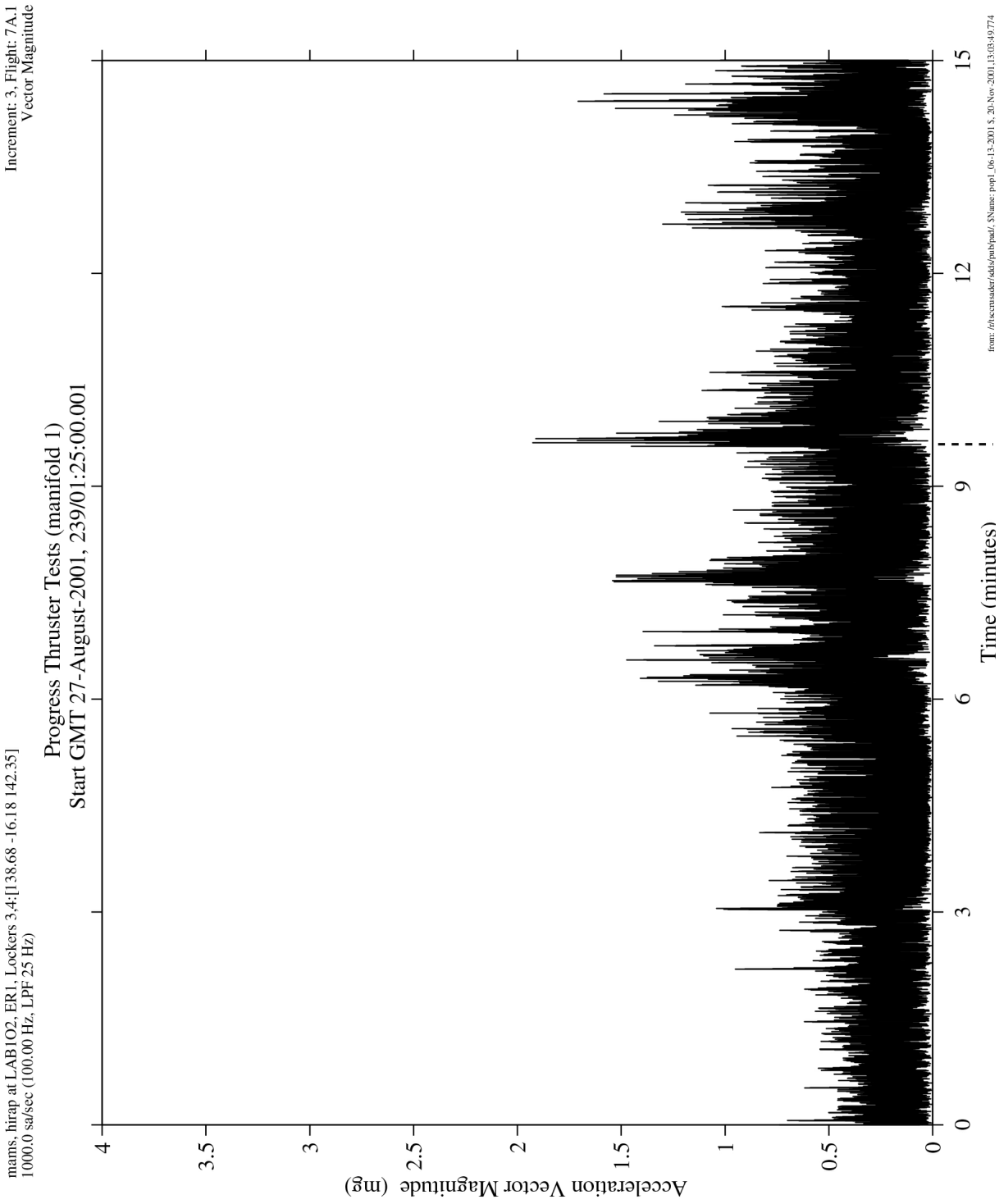

Figure 6-32 Acceleration Magnitude of Progress Thruster Manifold 1 Tests (HiRAP)

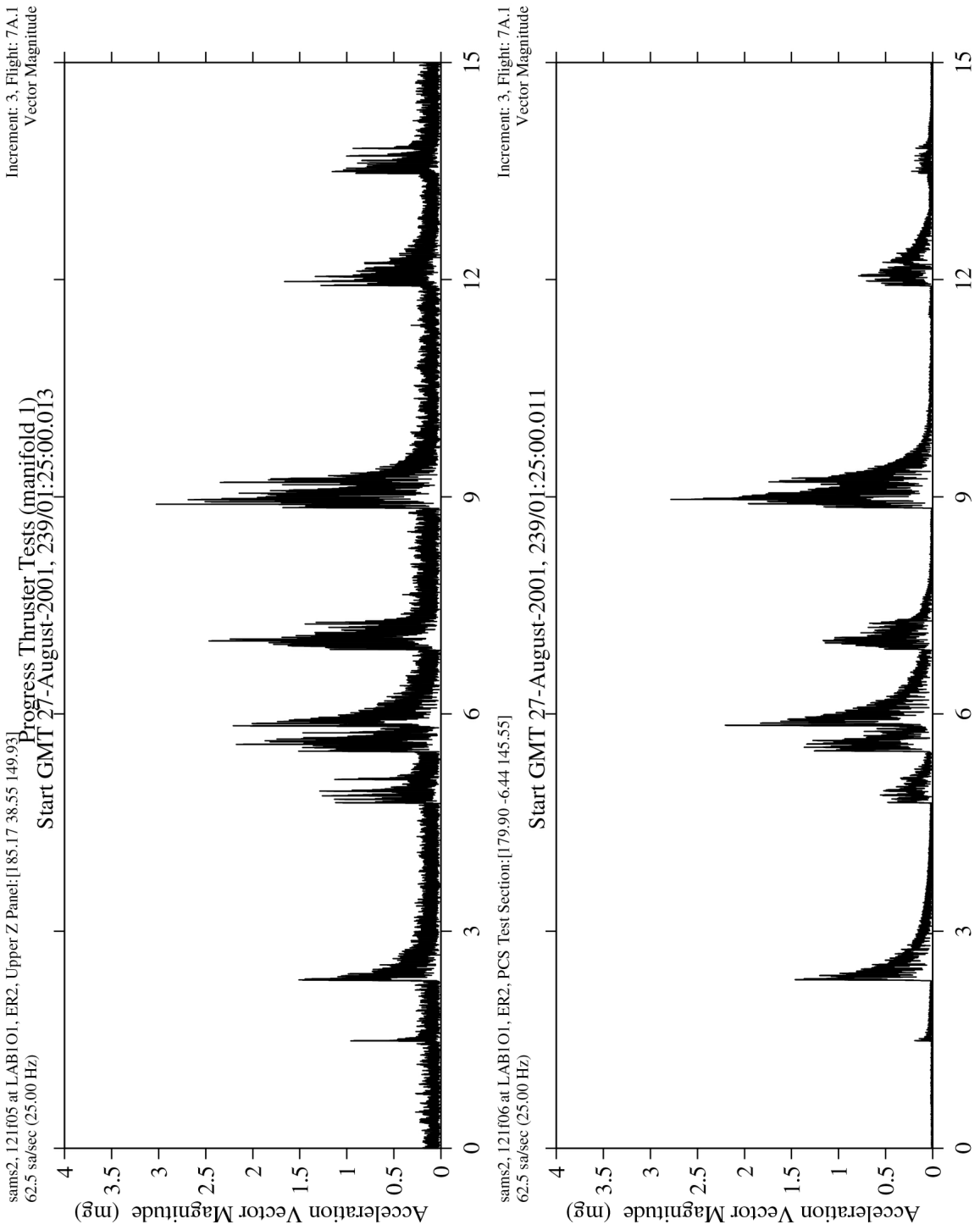

Figure 6-33 Acceleration Magnitude of Progress Thruster Manifold 1 Tests (121f05,121f06)

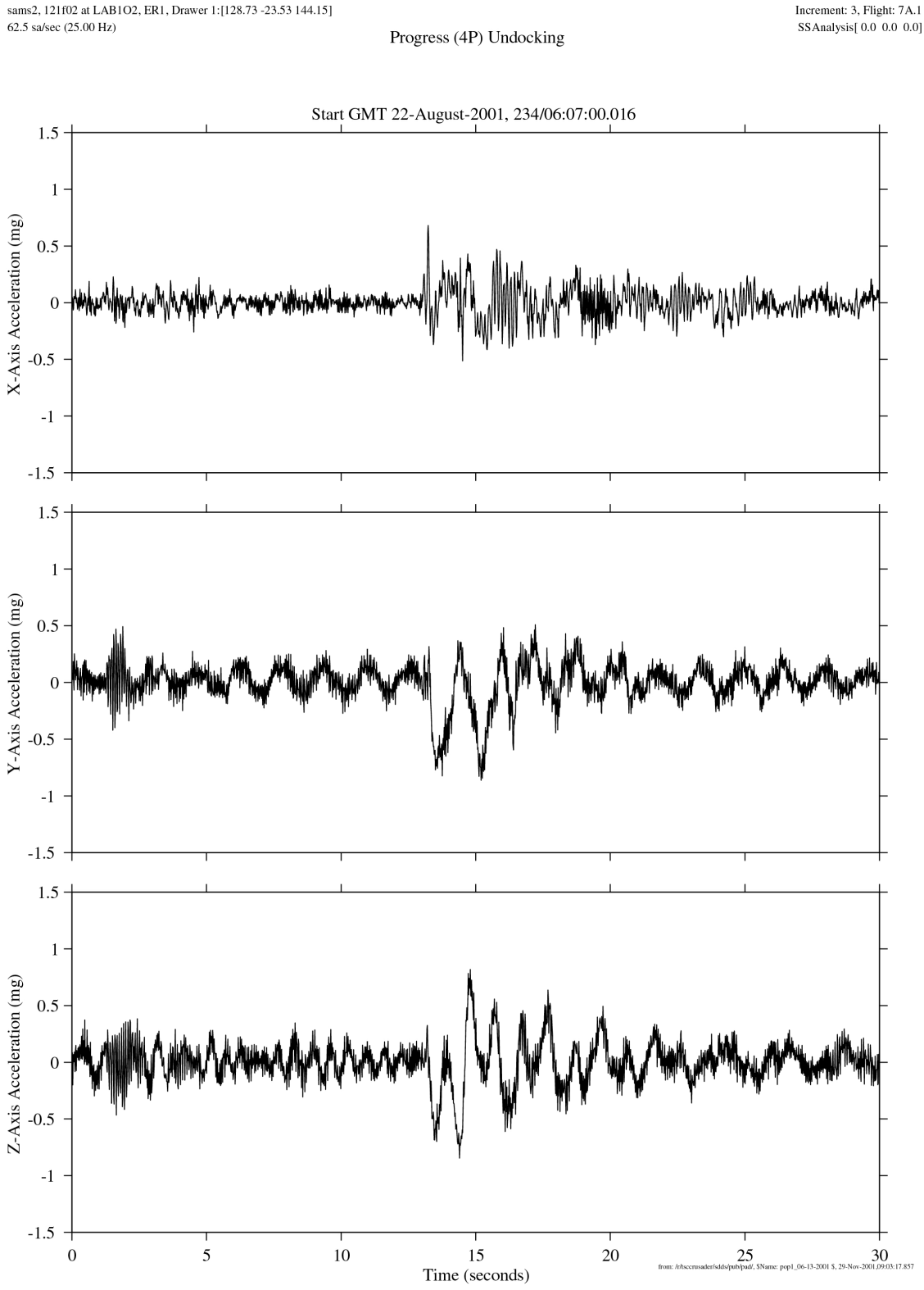

Figure 6-34 Time Series of Progress 4P Undocking (121f02)

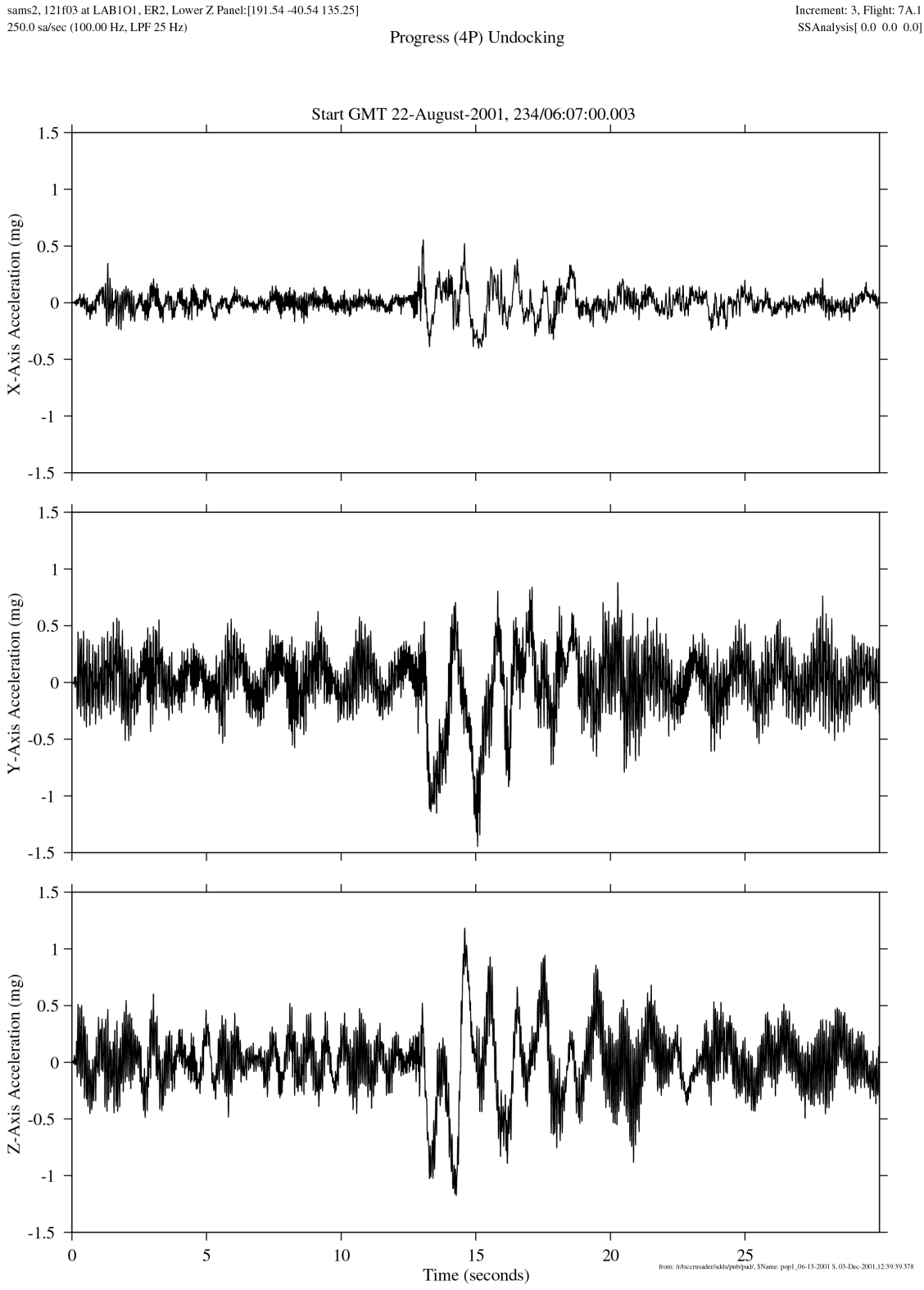

Figure 6-35 Time Series of Progress 4P Undocking (121f03)

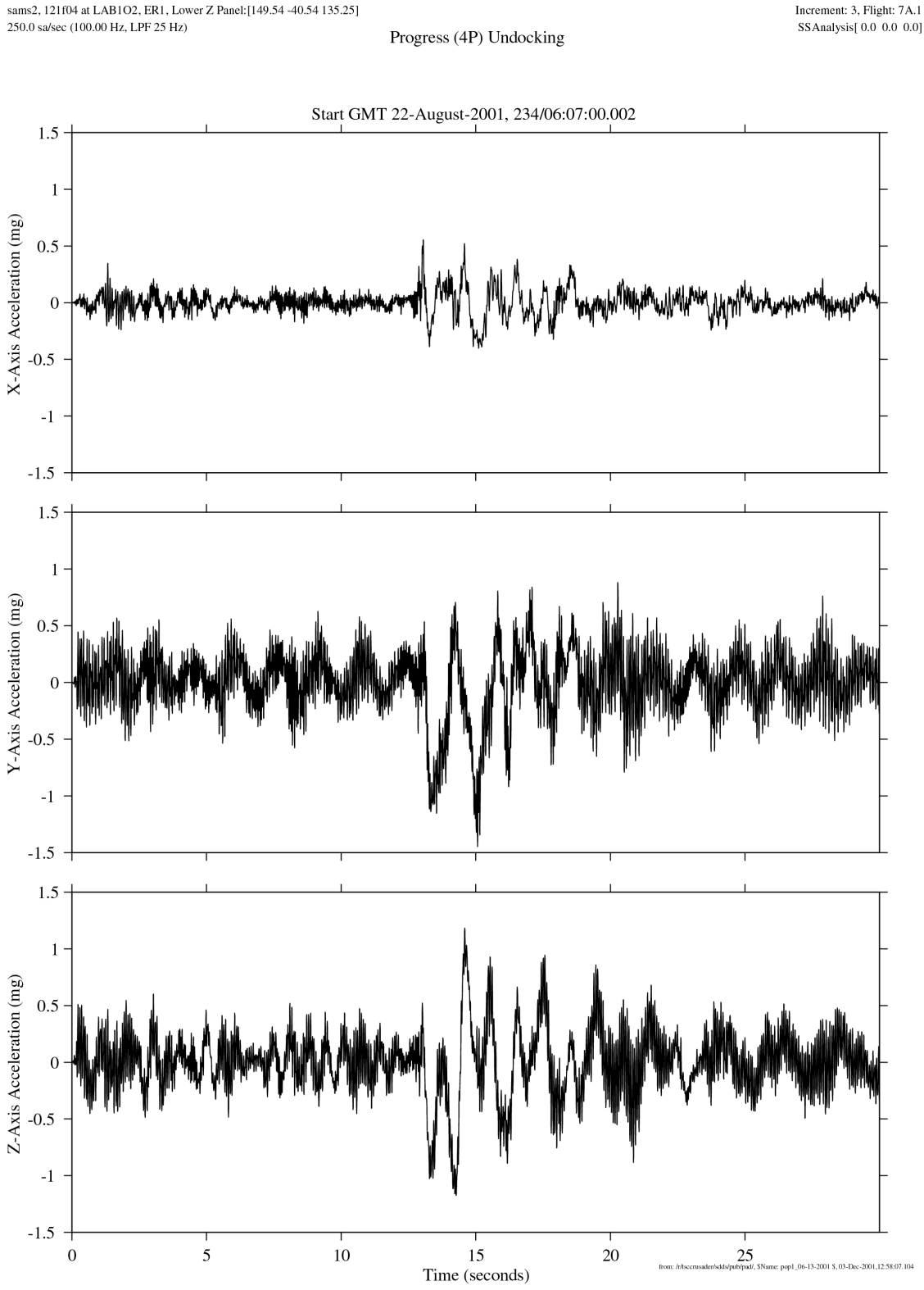

Figure 6-36 Time Series of Progress 4P Undocking (121f04)

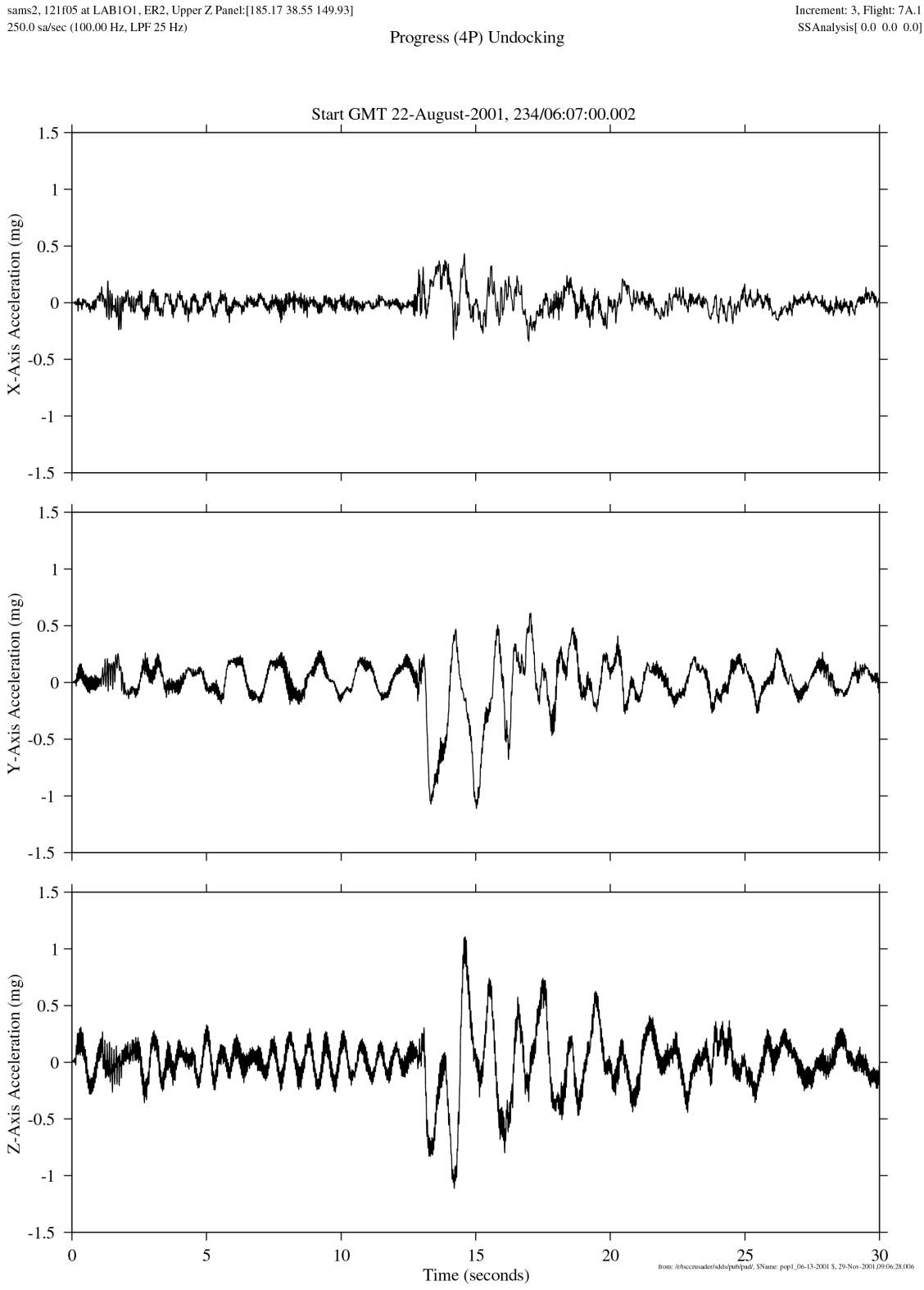

Figure 6-37 Time Series of Progress 4P Undocking (121f05)

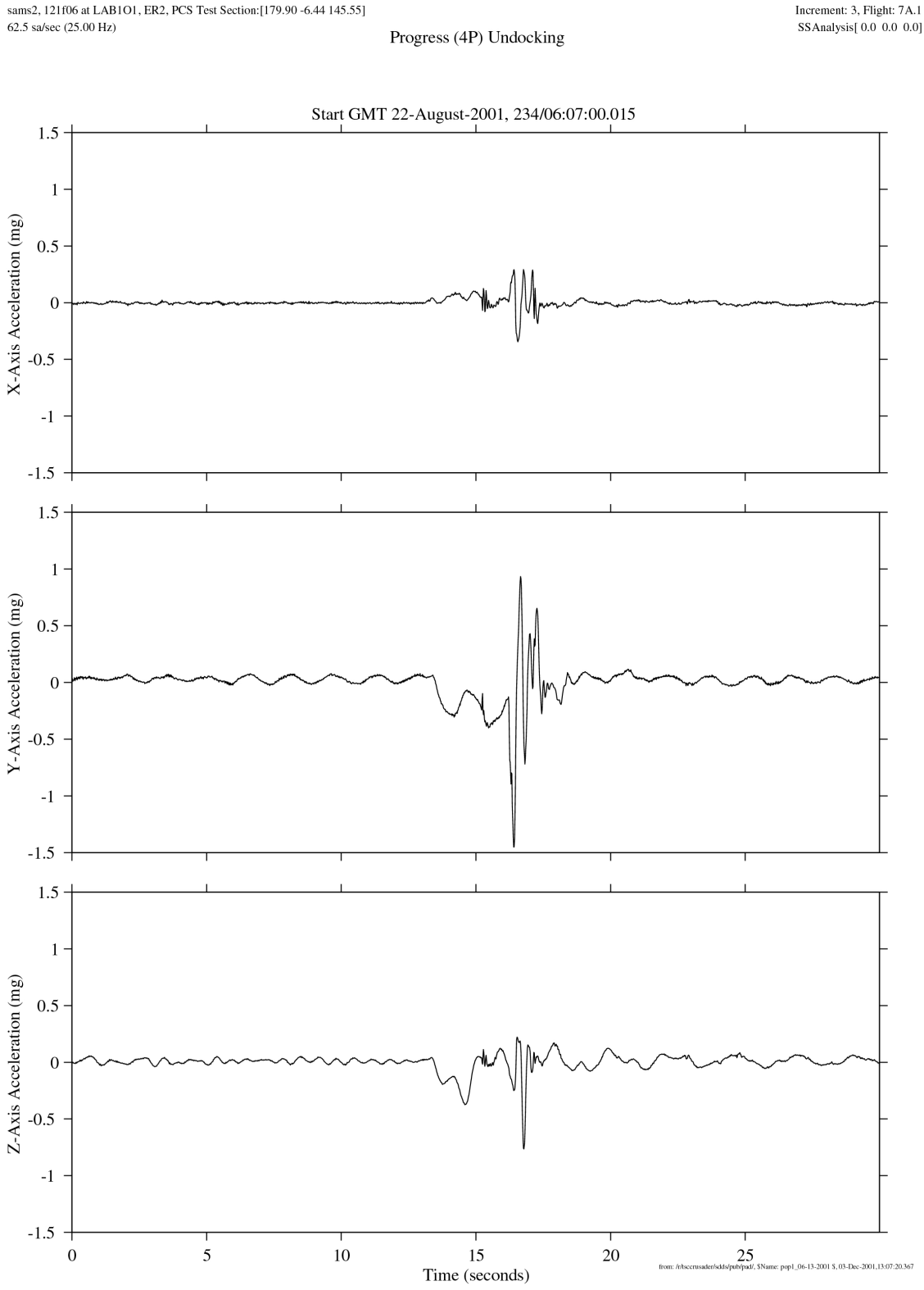

Figure 6-38 Time Series of Progress 4P Undocking (121f06)

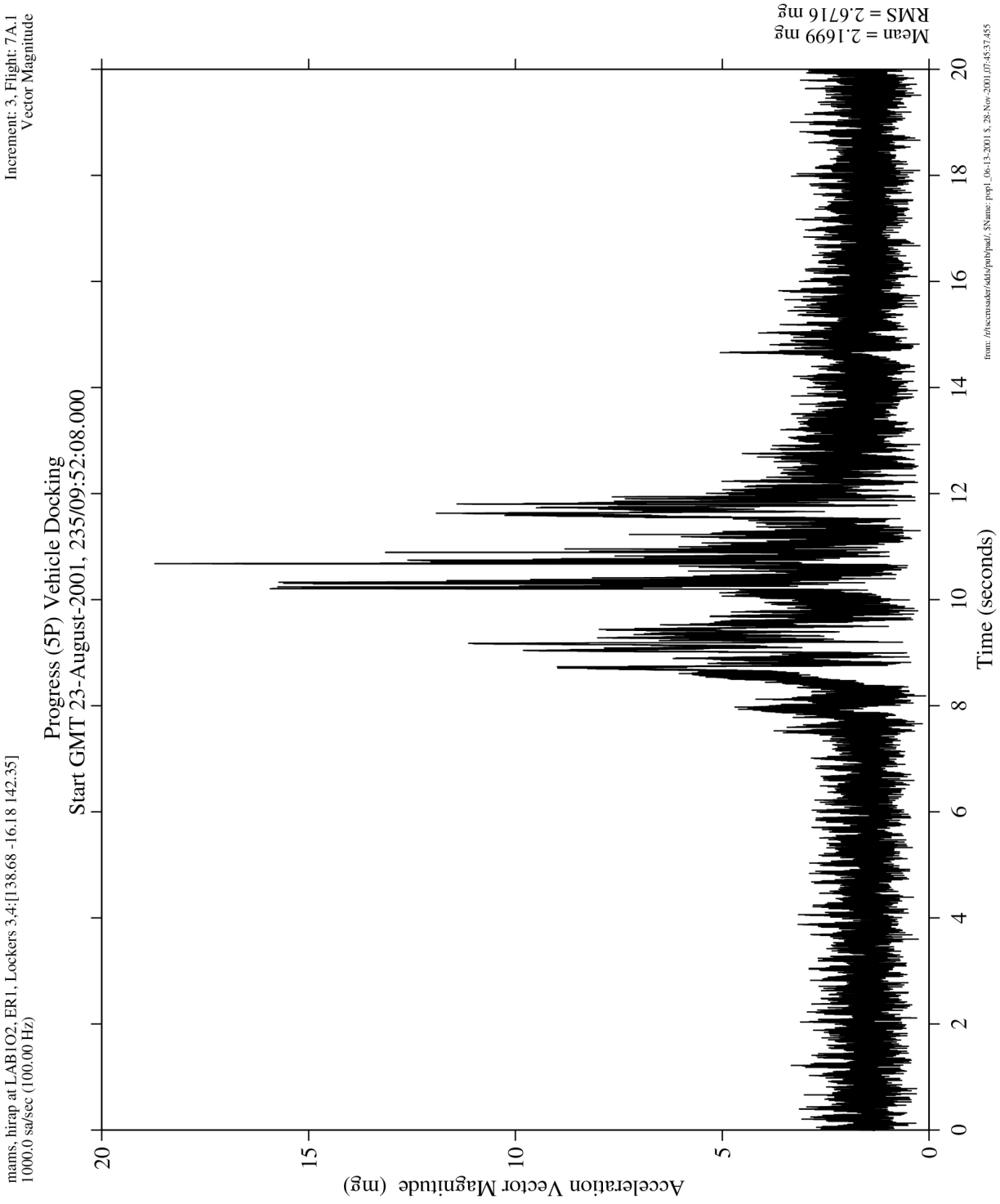

Figure 6-39 Acceleration Magnitude of Progress 5P Vehicle Docking (HiRAP)

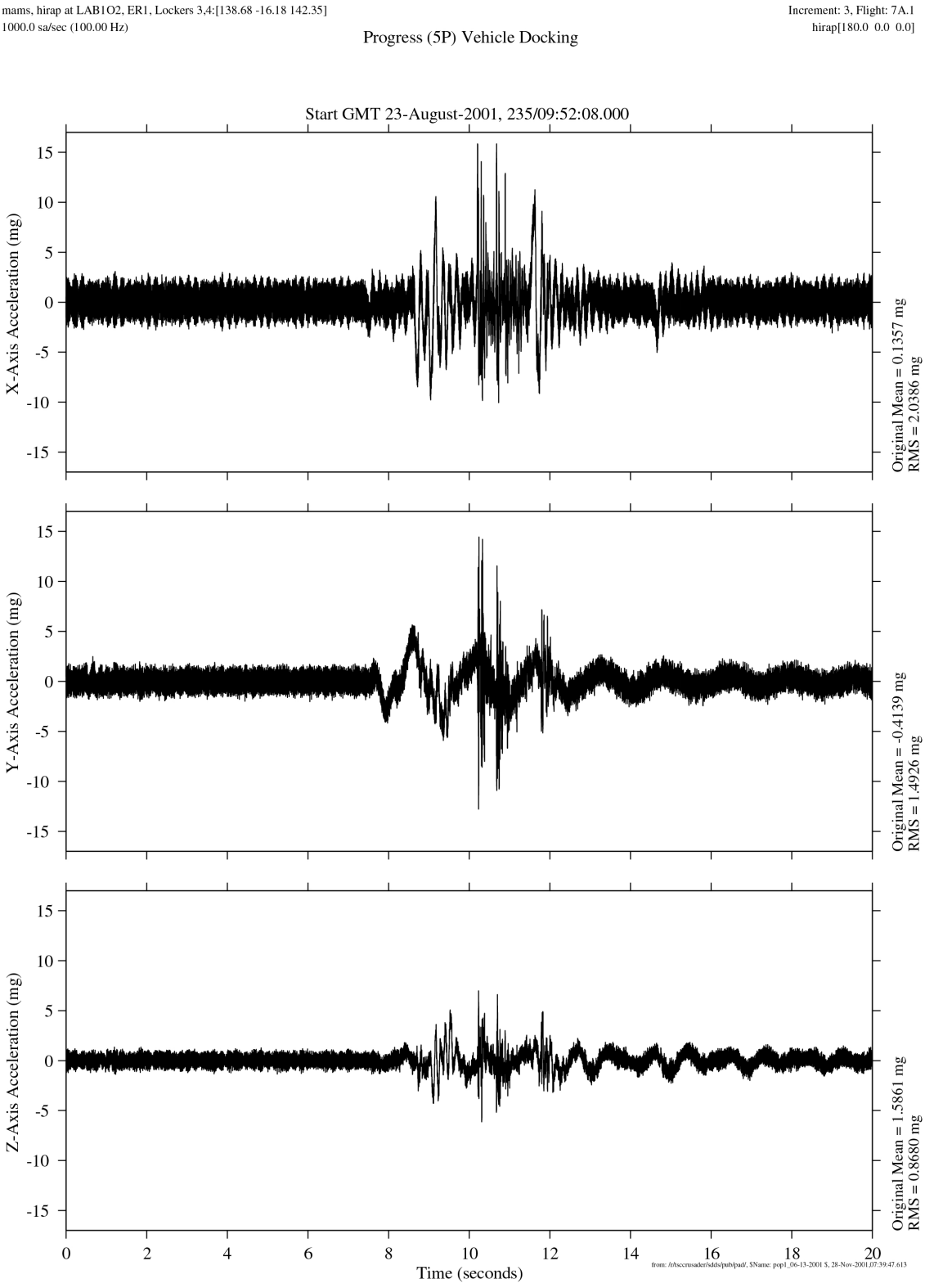

Figure 6-40 Time Series of Progress 5P Vehicle Docking (HiRAP)

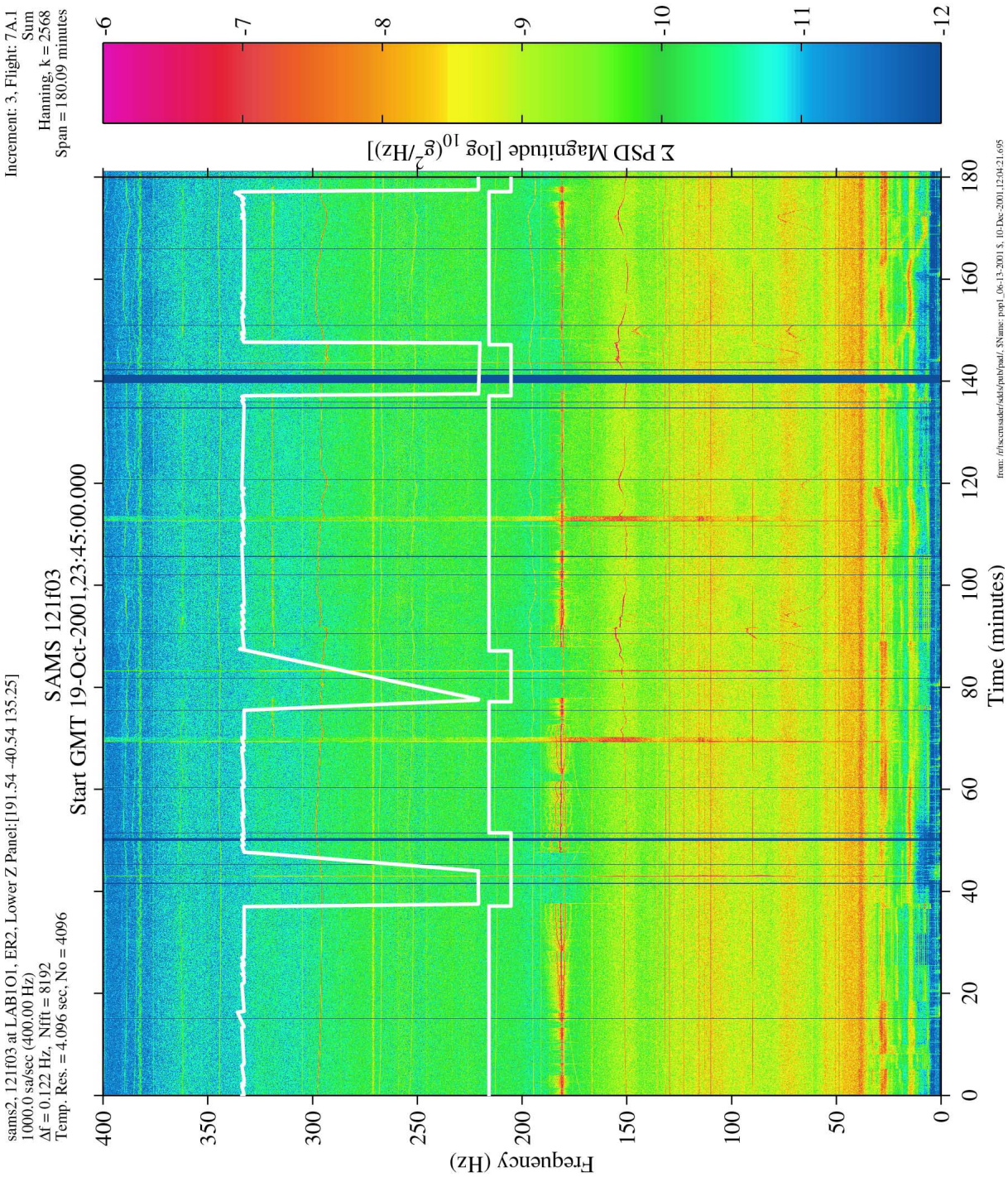

Figure 6-41 Spectrogram of AAA Fan (De)activations (121f03)

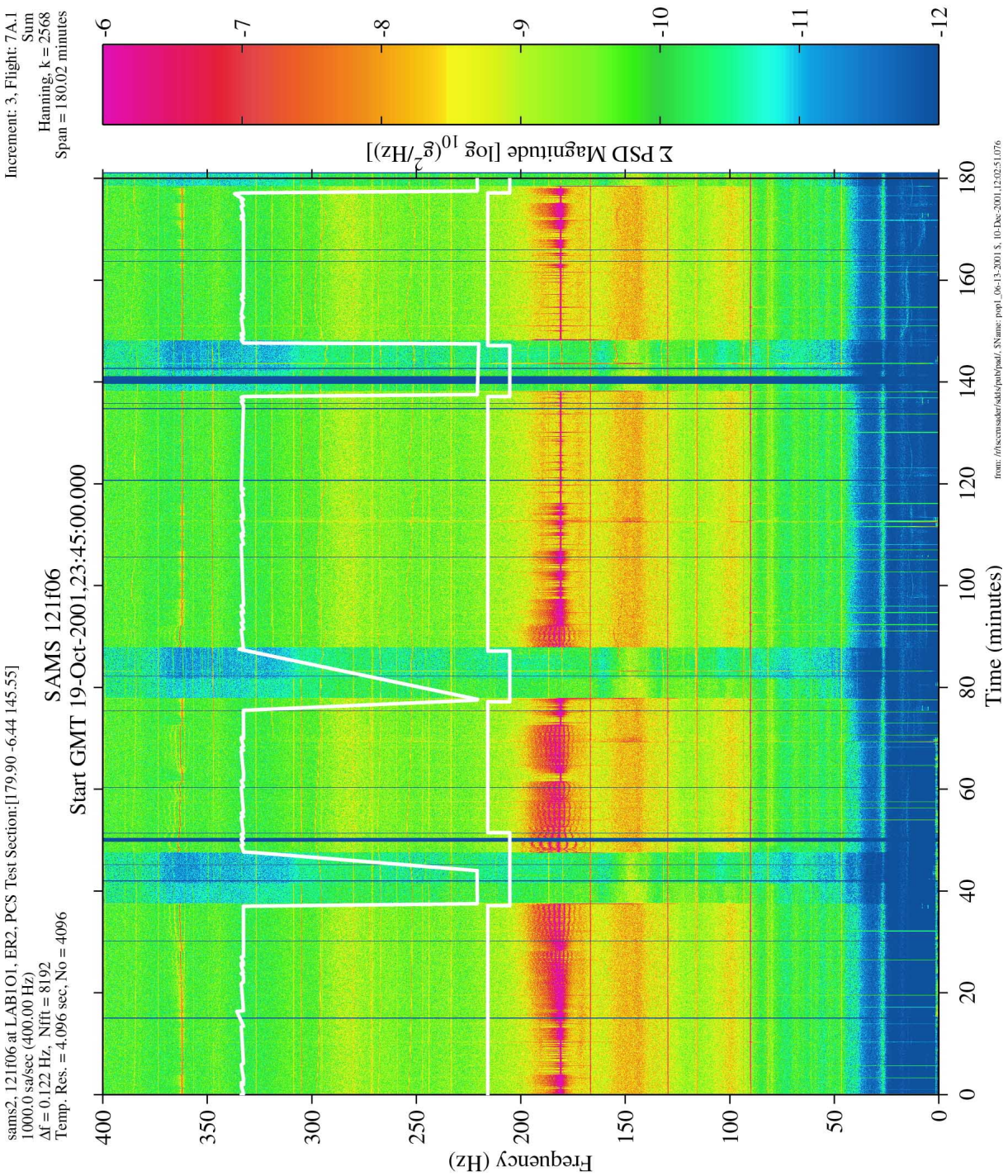

Figure 6-42 Spectrogram of AAA Fan (De)activations (121f06)

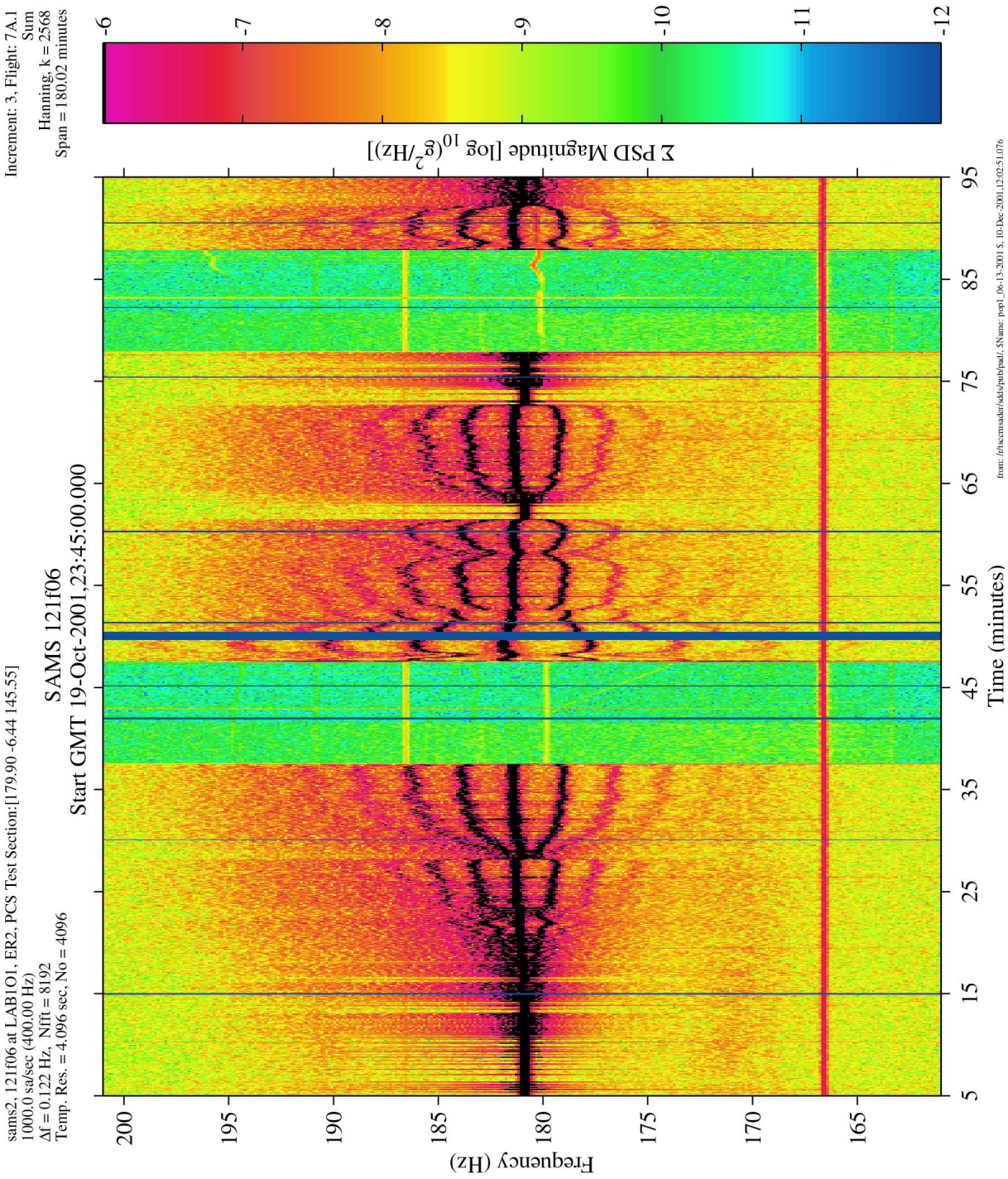

Figure 6-43 Spectrogram of AAA Fan (De)activations Zoom Around 181 Hz (121f06)

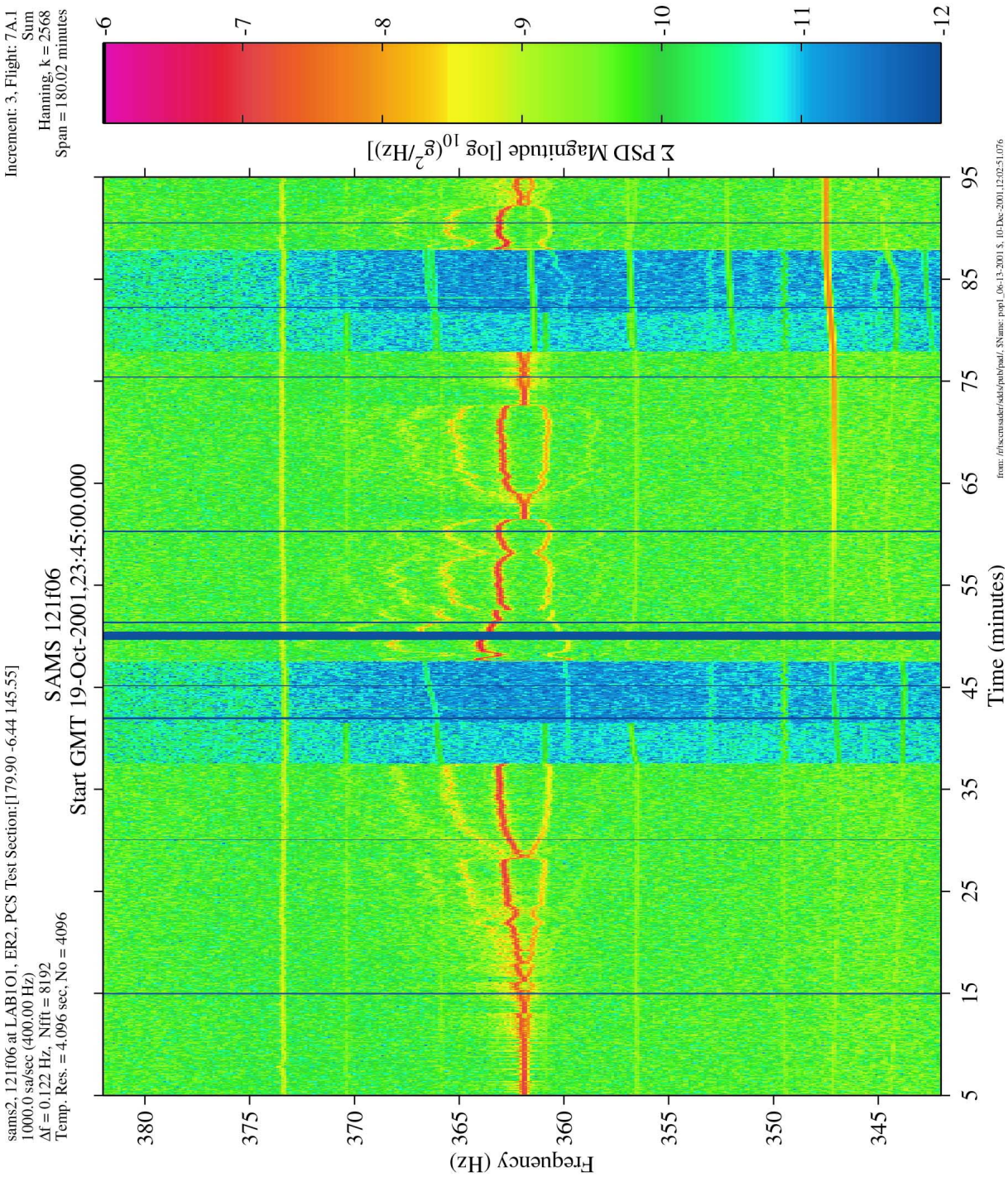

Figure 6-44 Spectrogram of AAA Fan (De)activations Zoom Around 362 Hz (121f06)

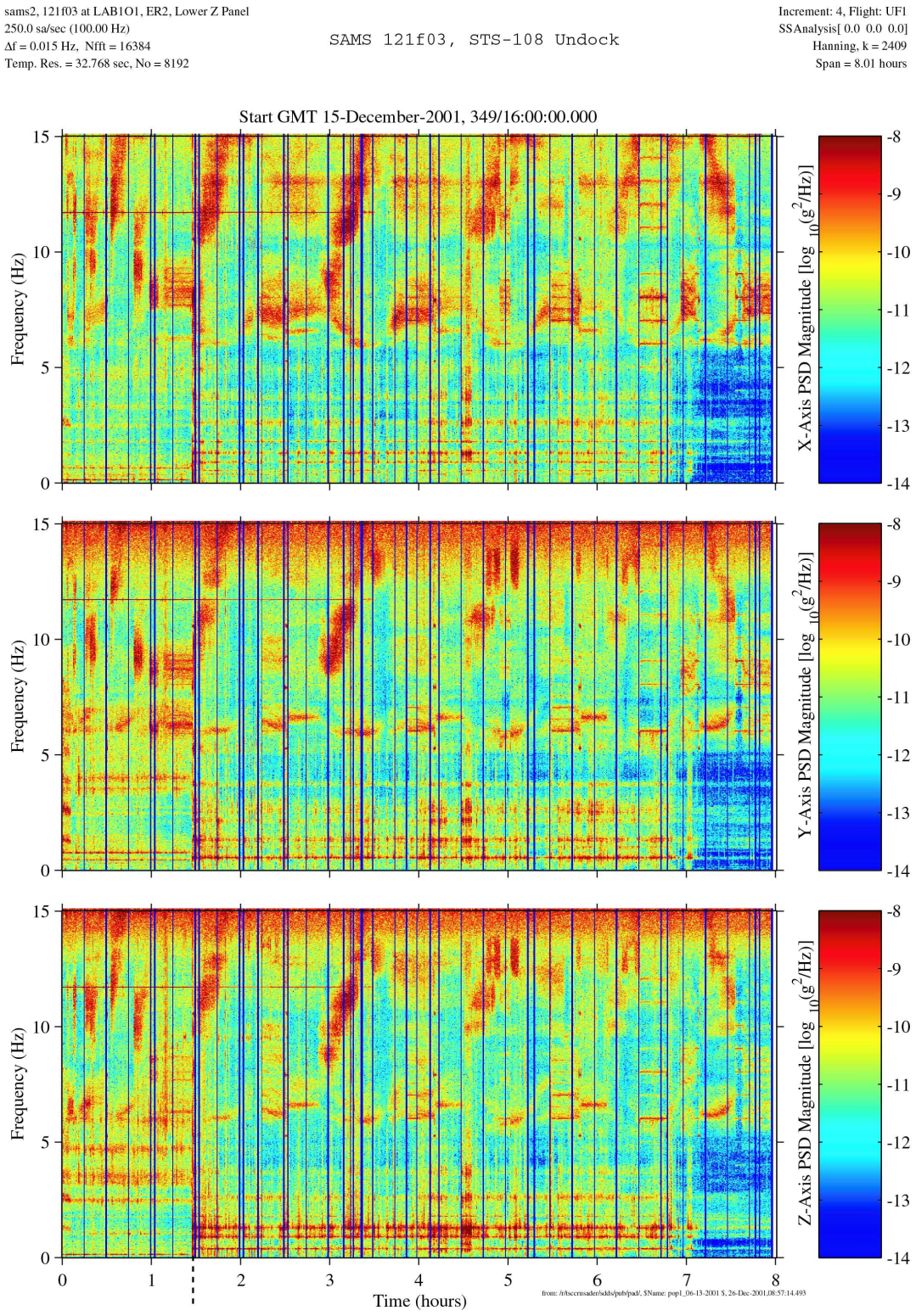

Figure 6-45 Spectrogram of STS-108 Undock (121f03)

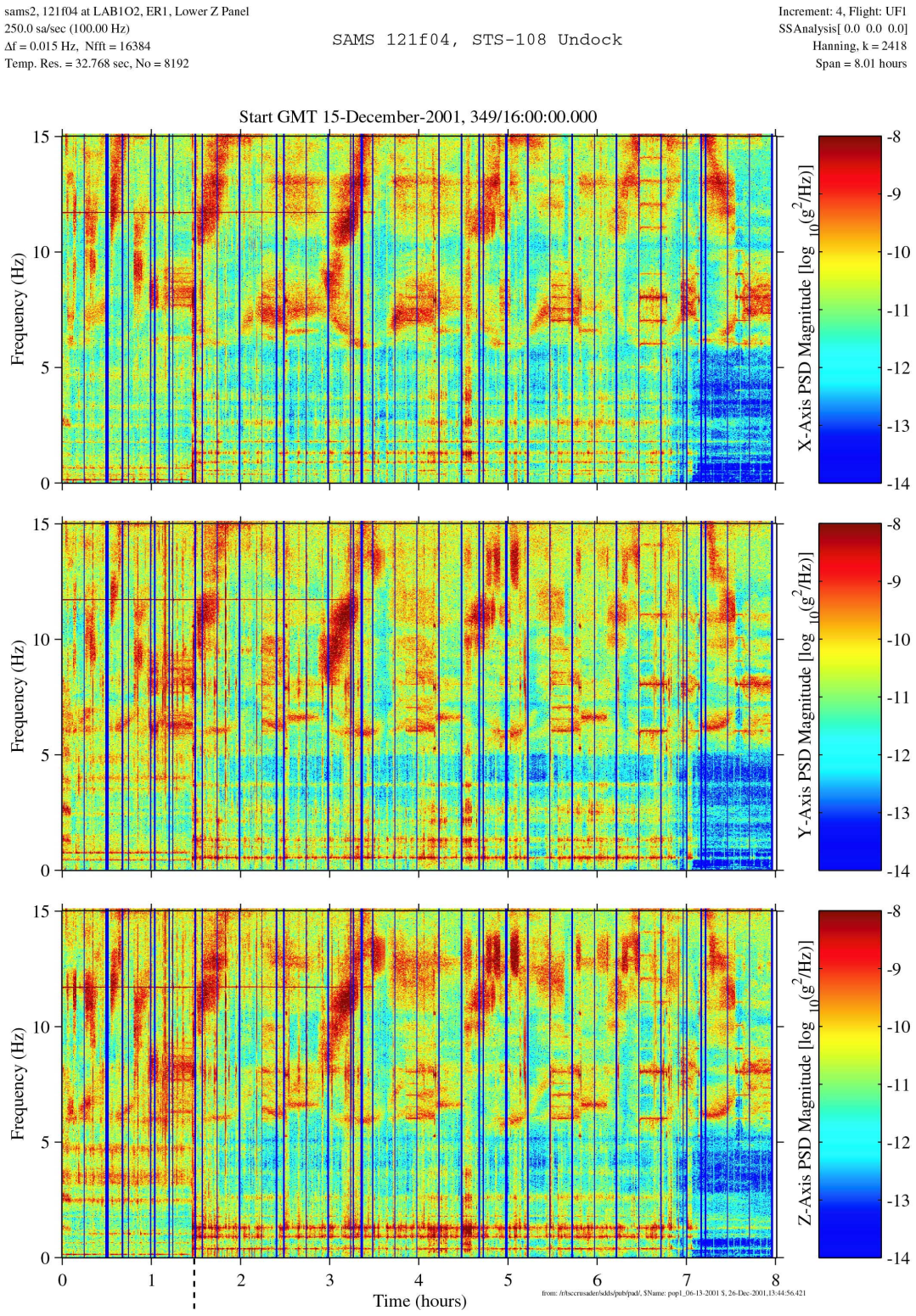

Figure 6-46 Spectrogram of STS-108 Undock (121f04)

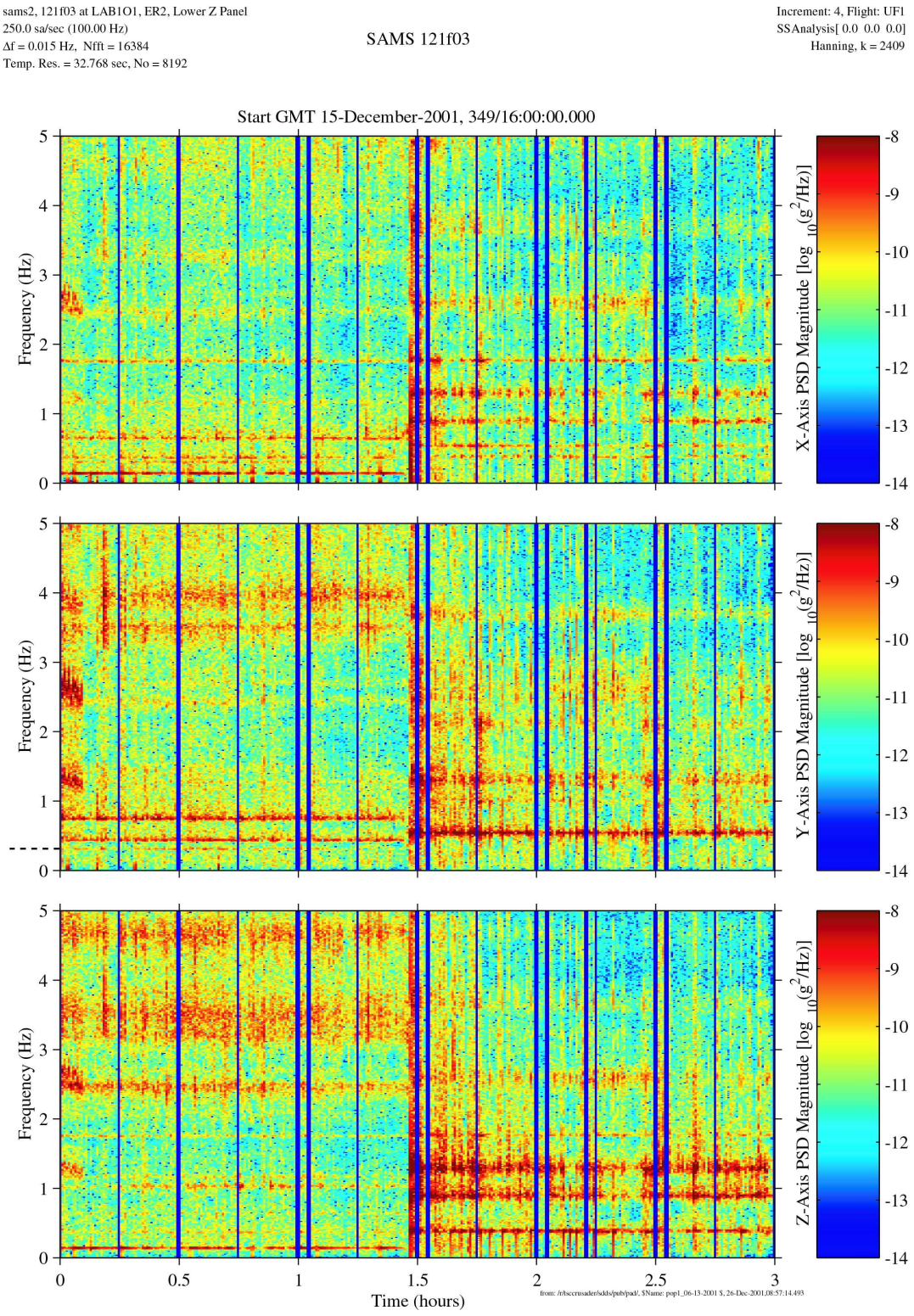

Figure 6-47 Spectrogram of STS-108 Undock 3-Hour Zoom Below 5 Hz (121f03)

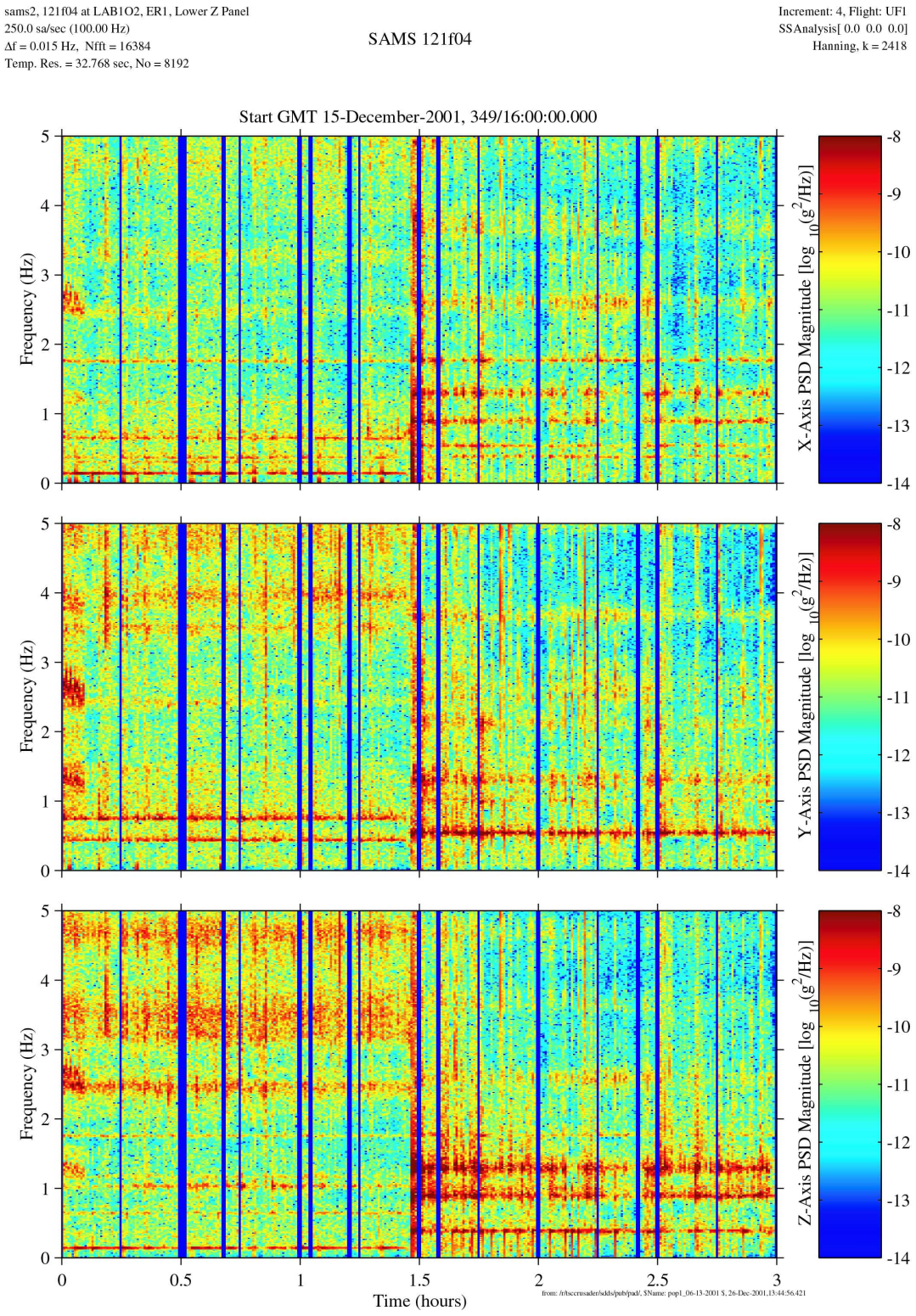

Figure 6-48 Spectrogram of STS-108 Undock 3-Hour Zoom Below 5 Hz (121f04)

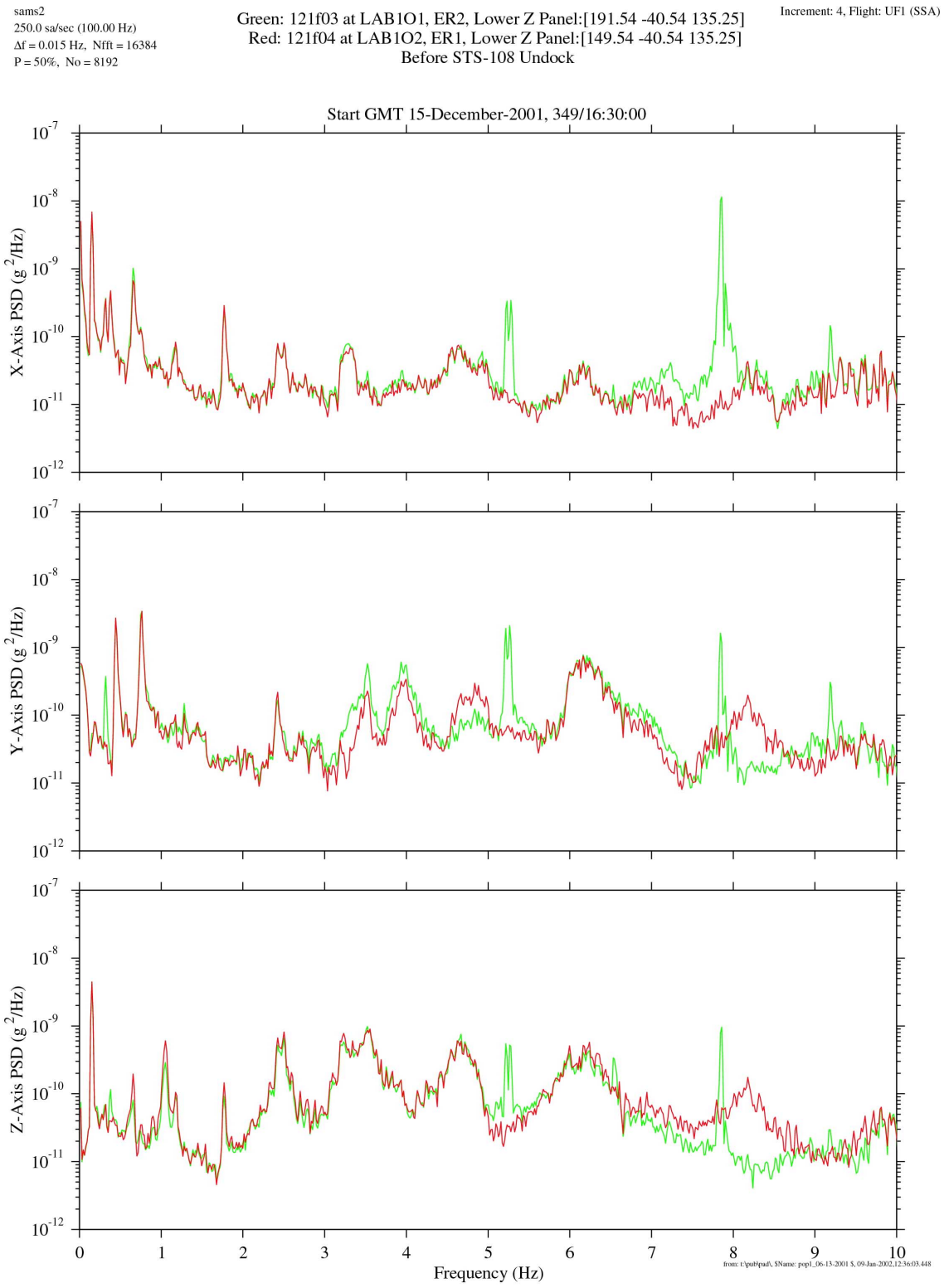

Figure 6-49 PSDs of Before STS-108 Undock Below 10 Hz (121f03,121f04)

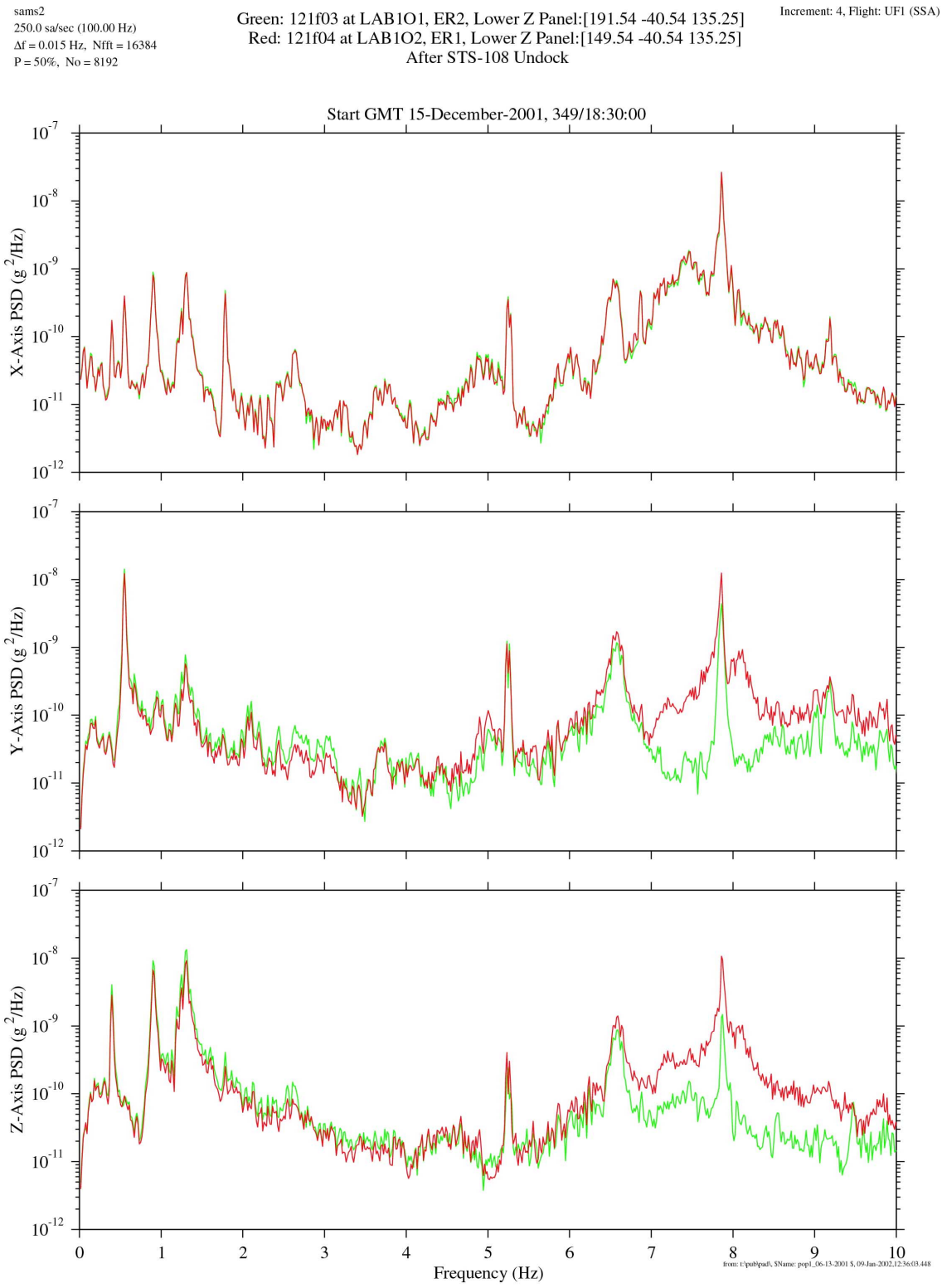

Figure 6-50 PSDs of After STS-108 Undock Below 10 Hz (121f03,121f04)

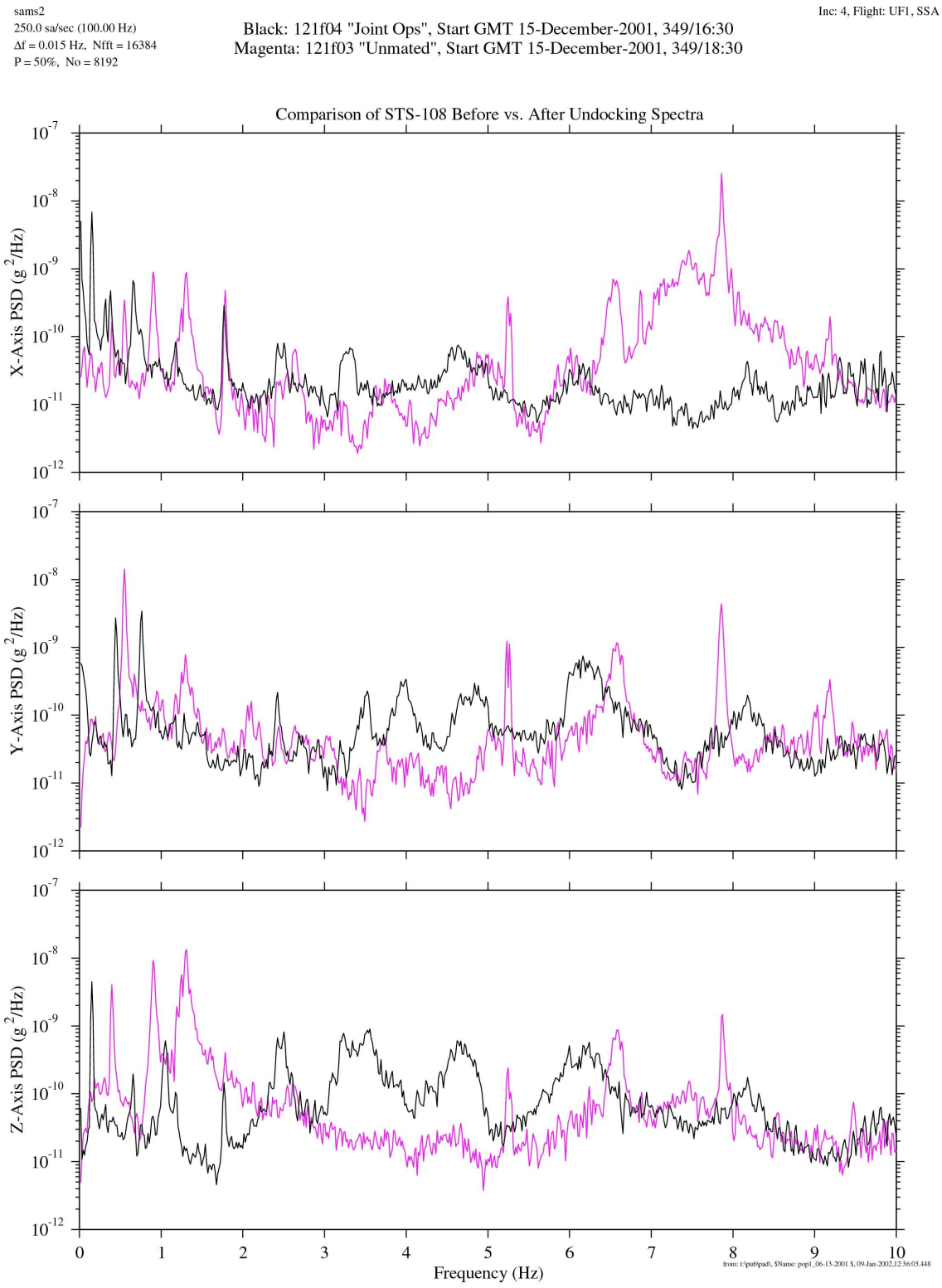

Figure 6-51 PSDs of Before vs. After STS-108 Undock Below 10 Hz (121f03,121f04)

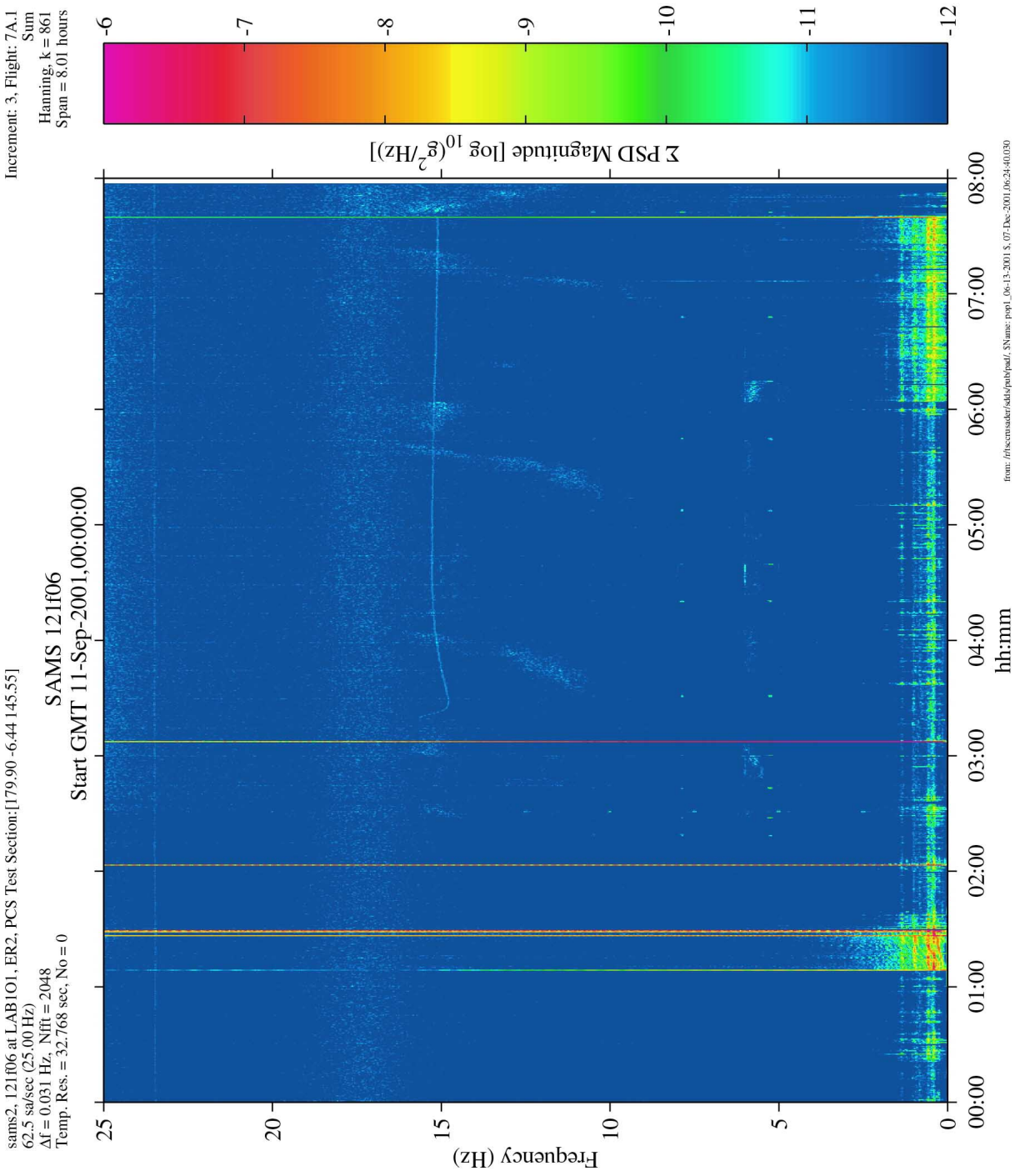

Figure 6-52 Spectrogram of ARIS Transition to Active Mode (121f06)

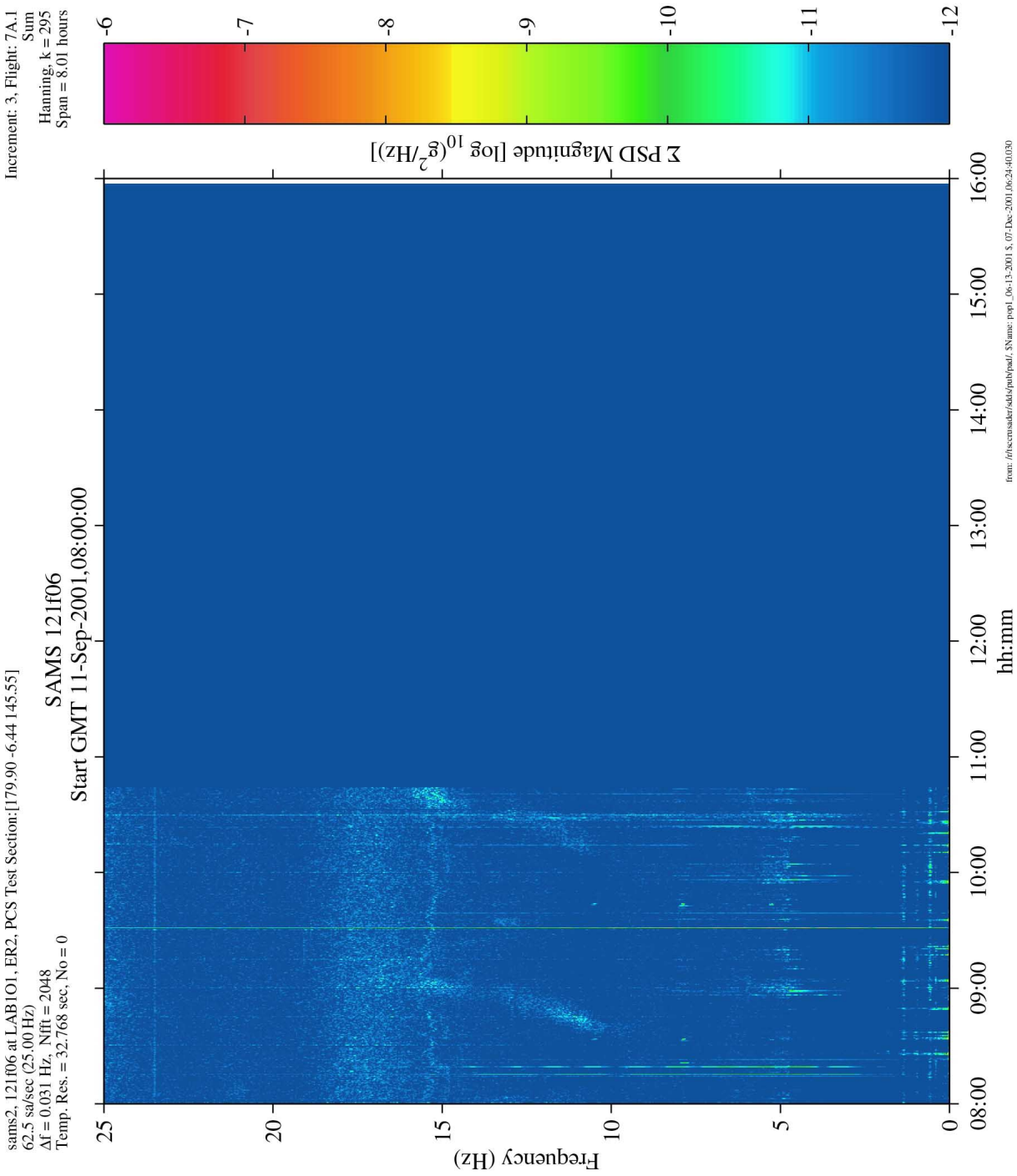

Figure 6-53 Spectrogram of ARIS in Active Mode (121f06)

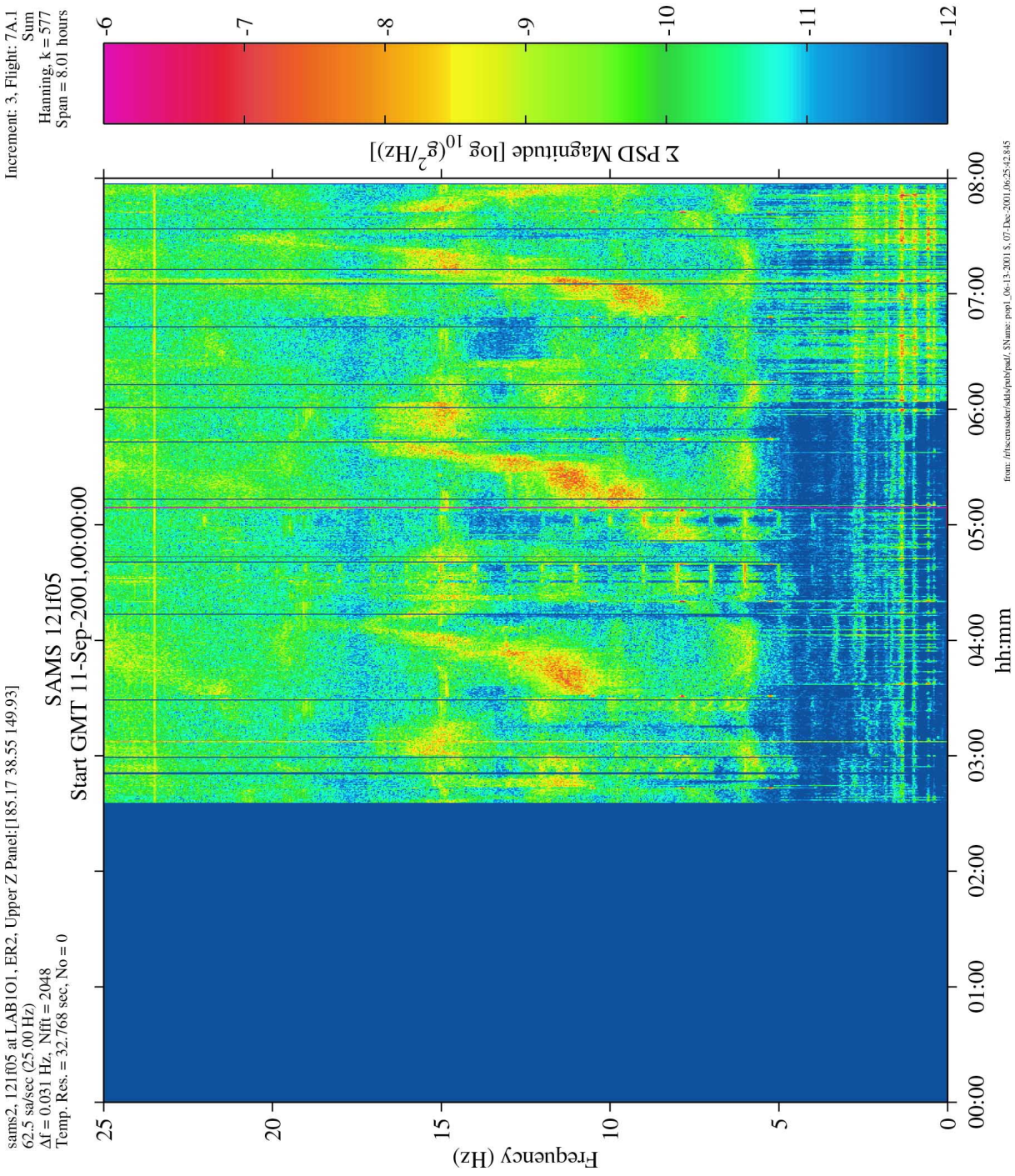

Figure 6-54 Spectrogram of ARIS Transition to Active Mode (121f05)

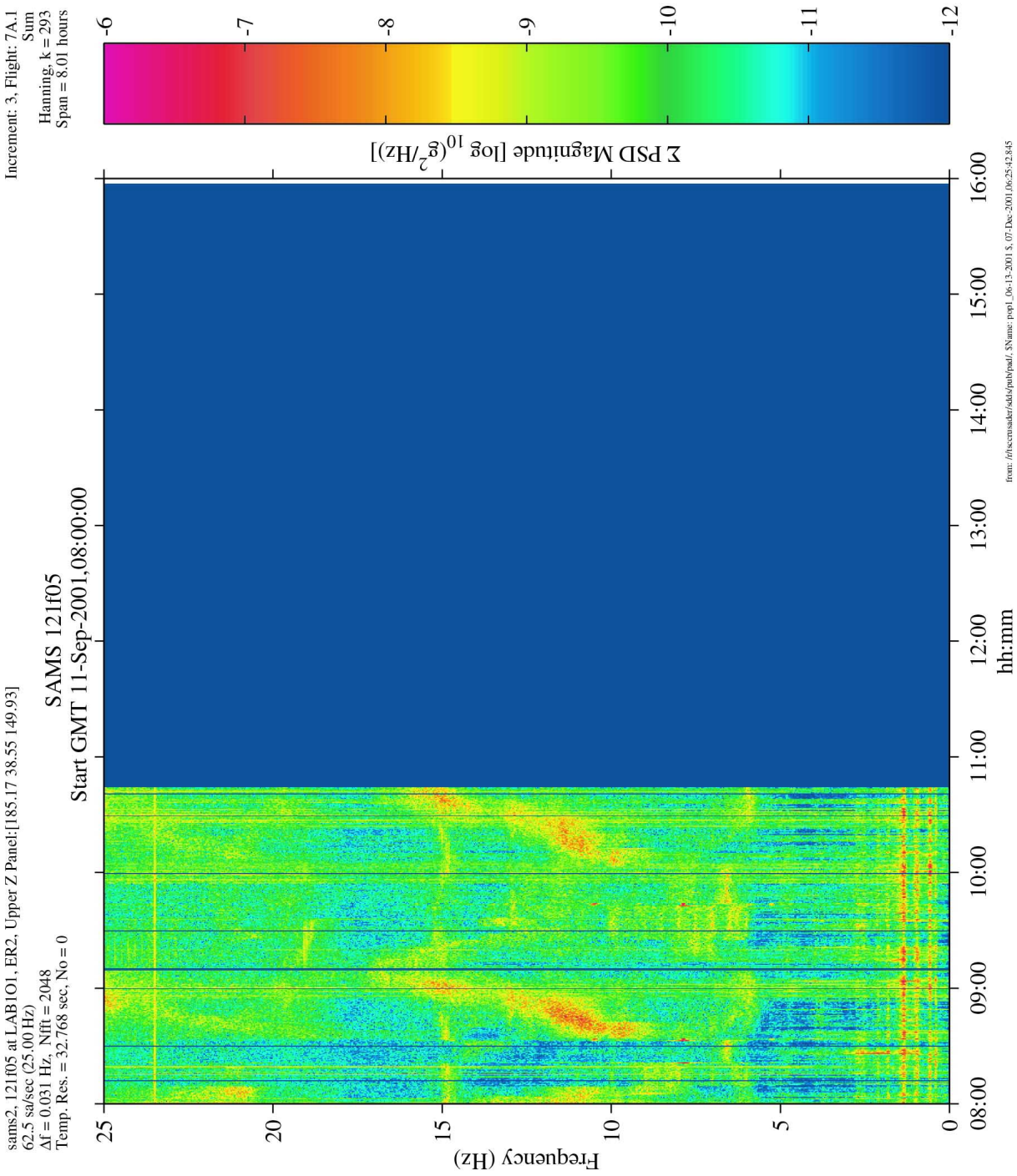

Figure 6-55 Spectrogram of ARIS in Active Mode (121f05)

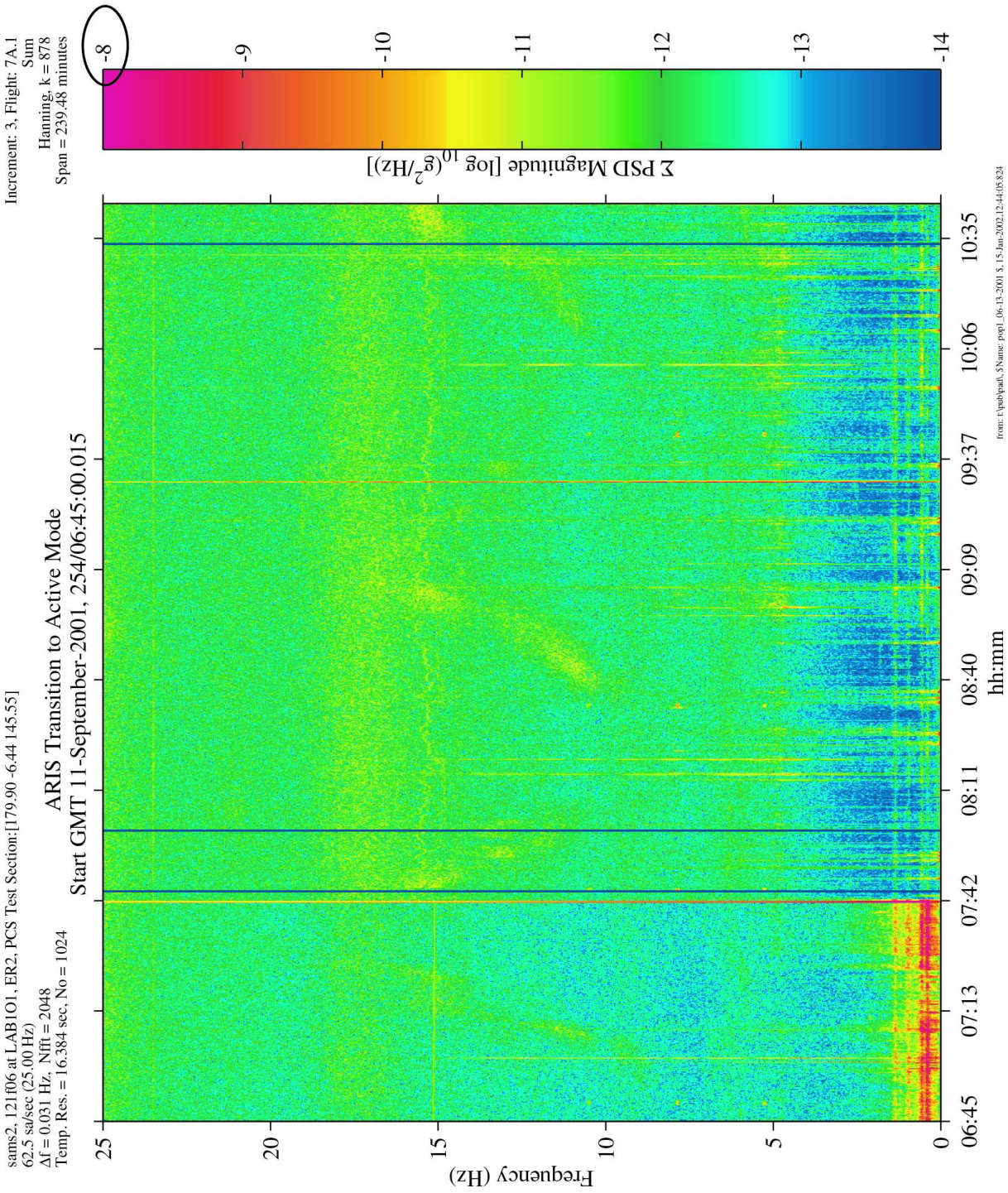

Figure 6-56 Spectrogram of ARIS Transition to Active Mode Zoom (121f06)

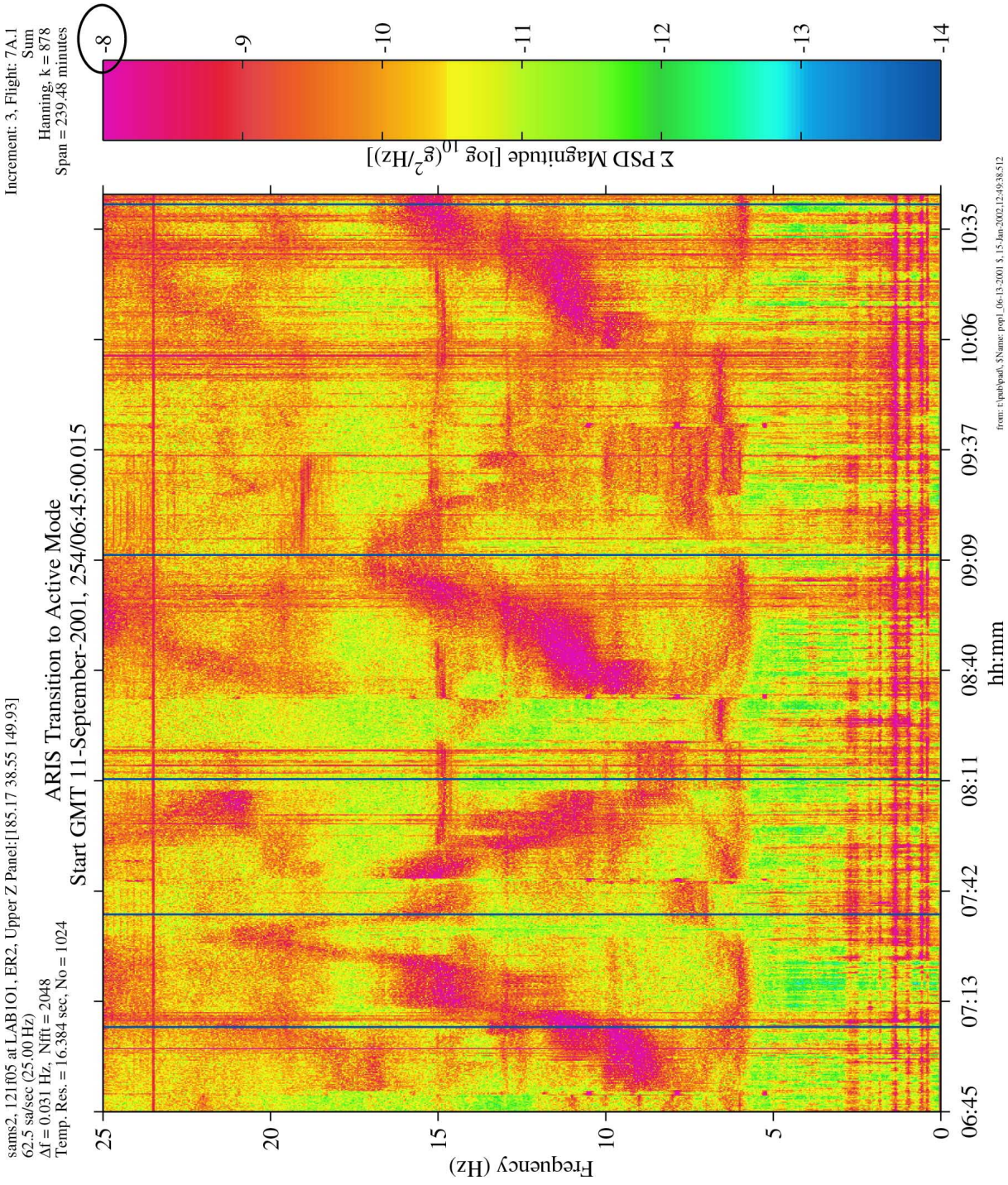

Figure 6-57 Spectrogram of ARIS Transition to Active Mode Zoom (121f05)

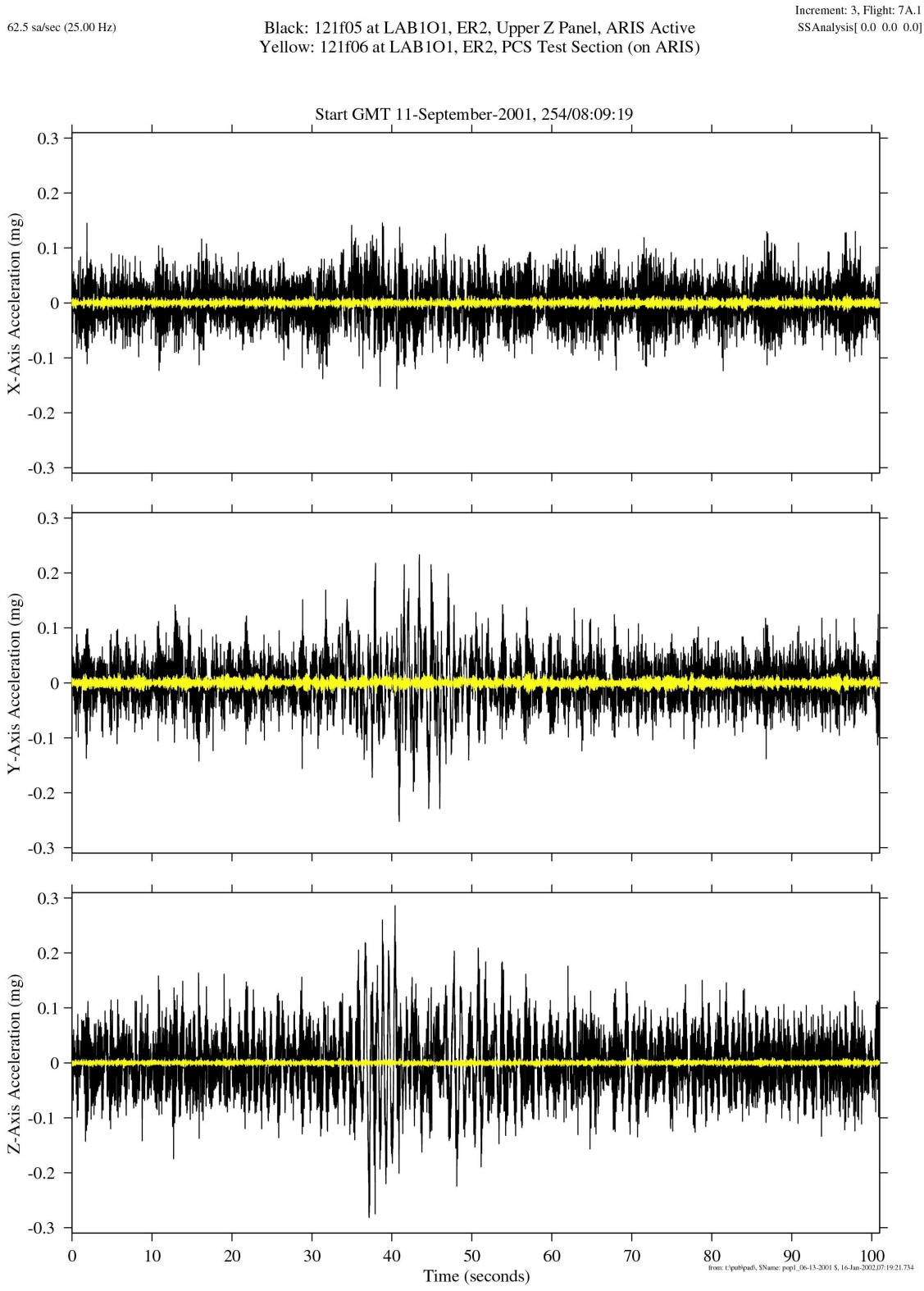

Figure 6-58 Time Series of ARIS in Active Mode Comparison (121f05,121f06)

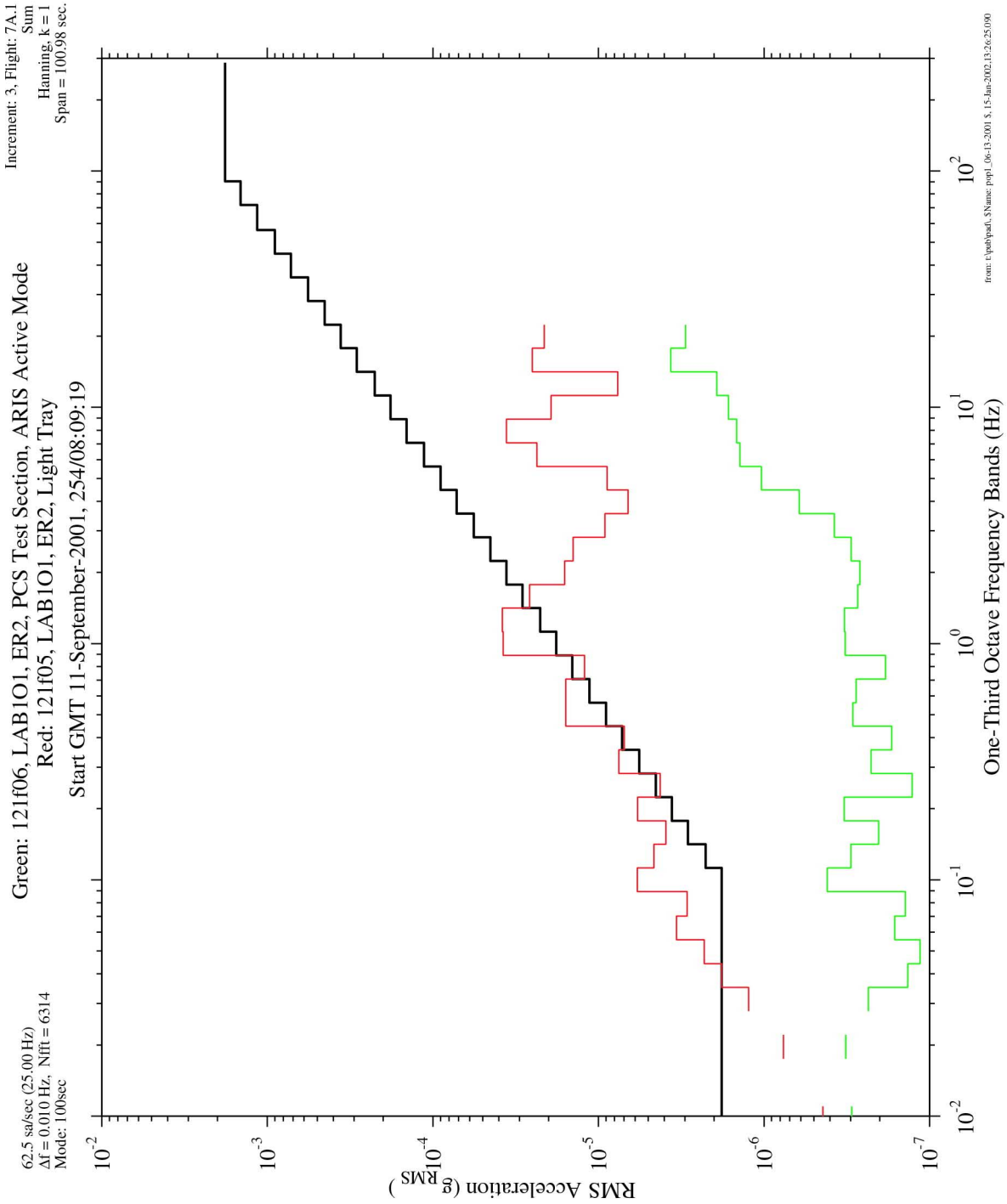

Figure 6-59 OTO of ARIS in Active Mode Comparison (121f05,121f06)

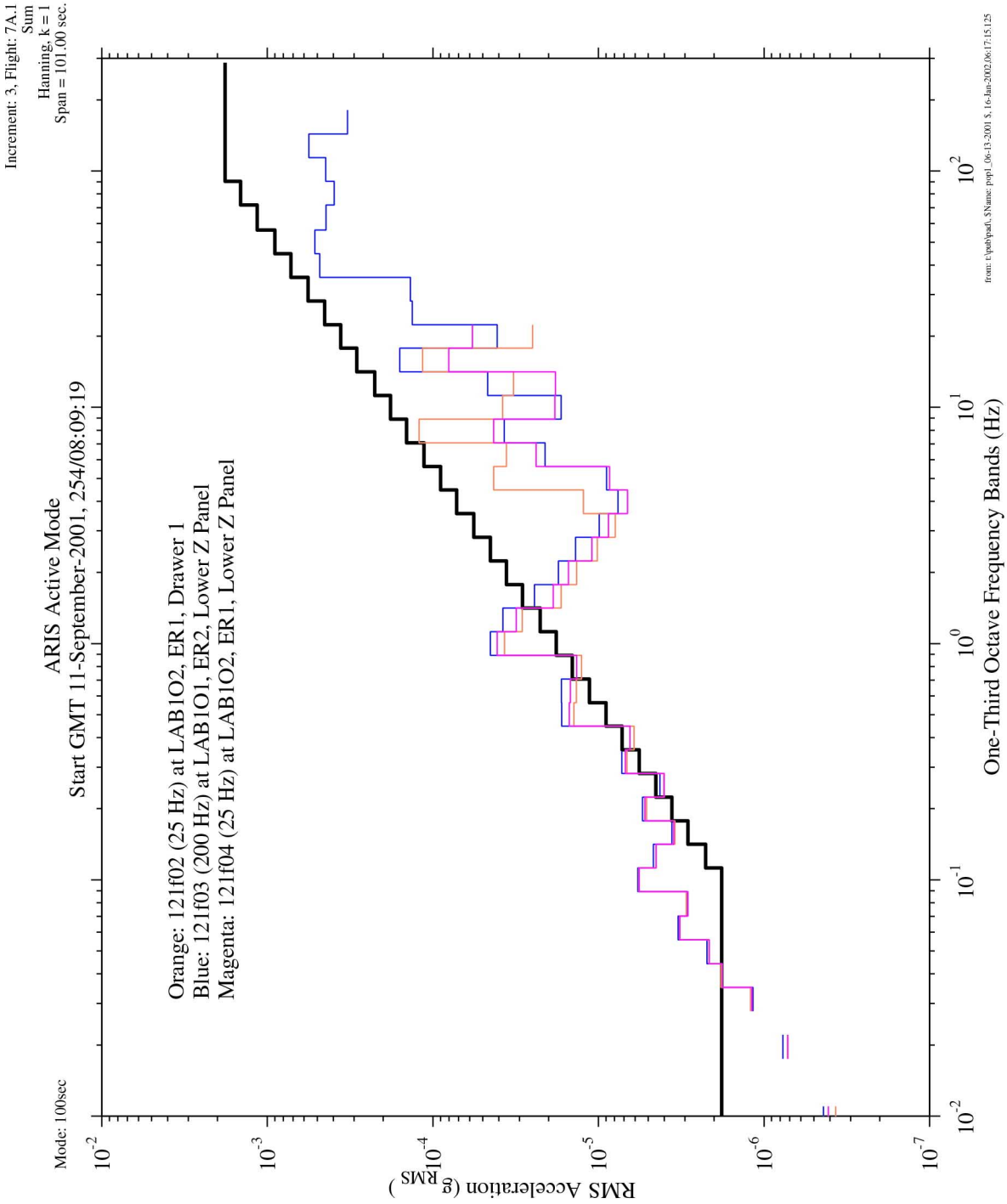

Figure 6-60 OTO of ARIS in Active Mode Offboard Sensors (121f02,121f03,121f04)

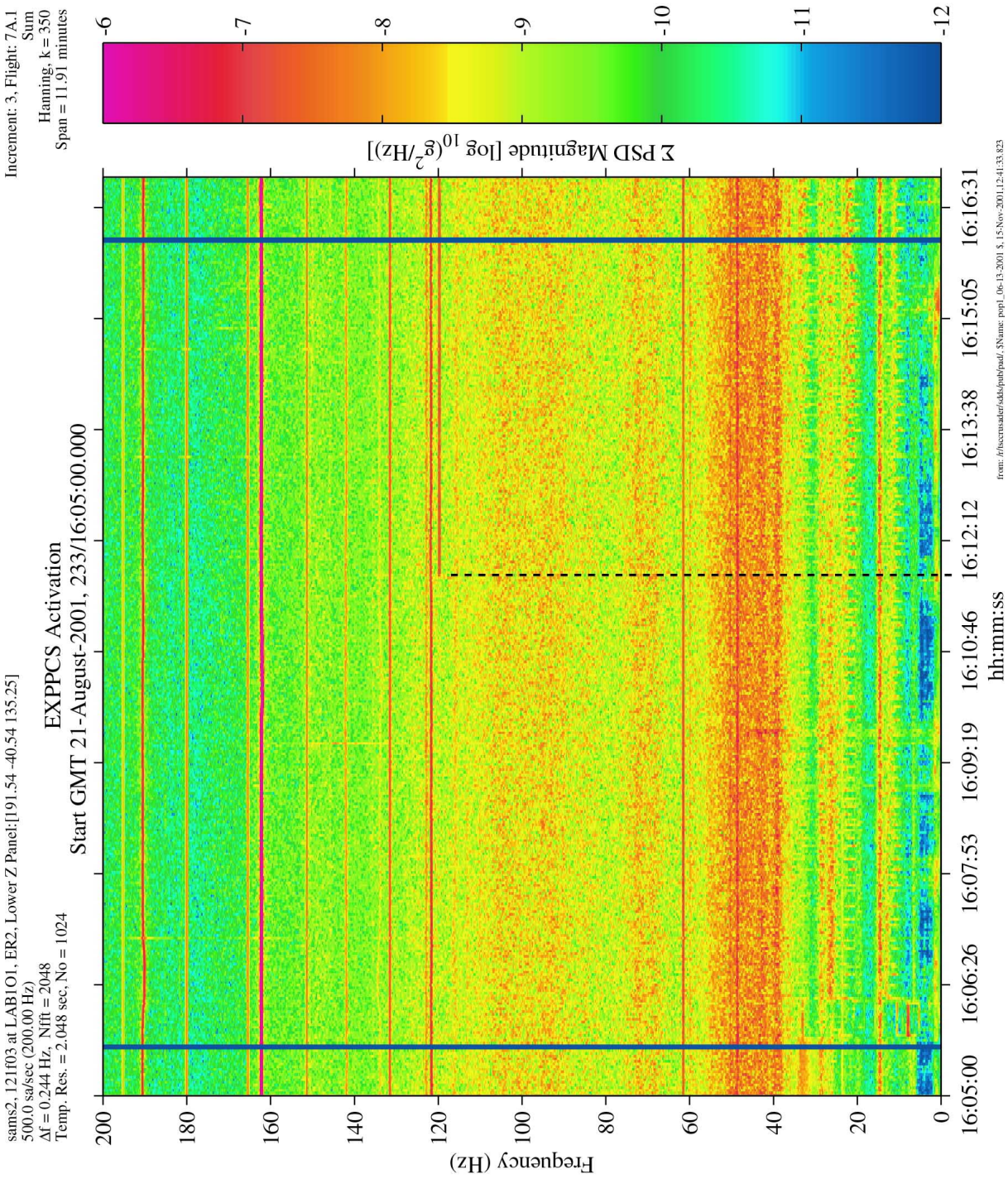

Figure 6-61 Spectrogram of EXPPCS Activation (121f03)

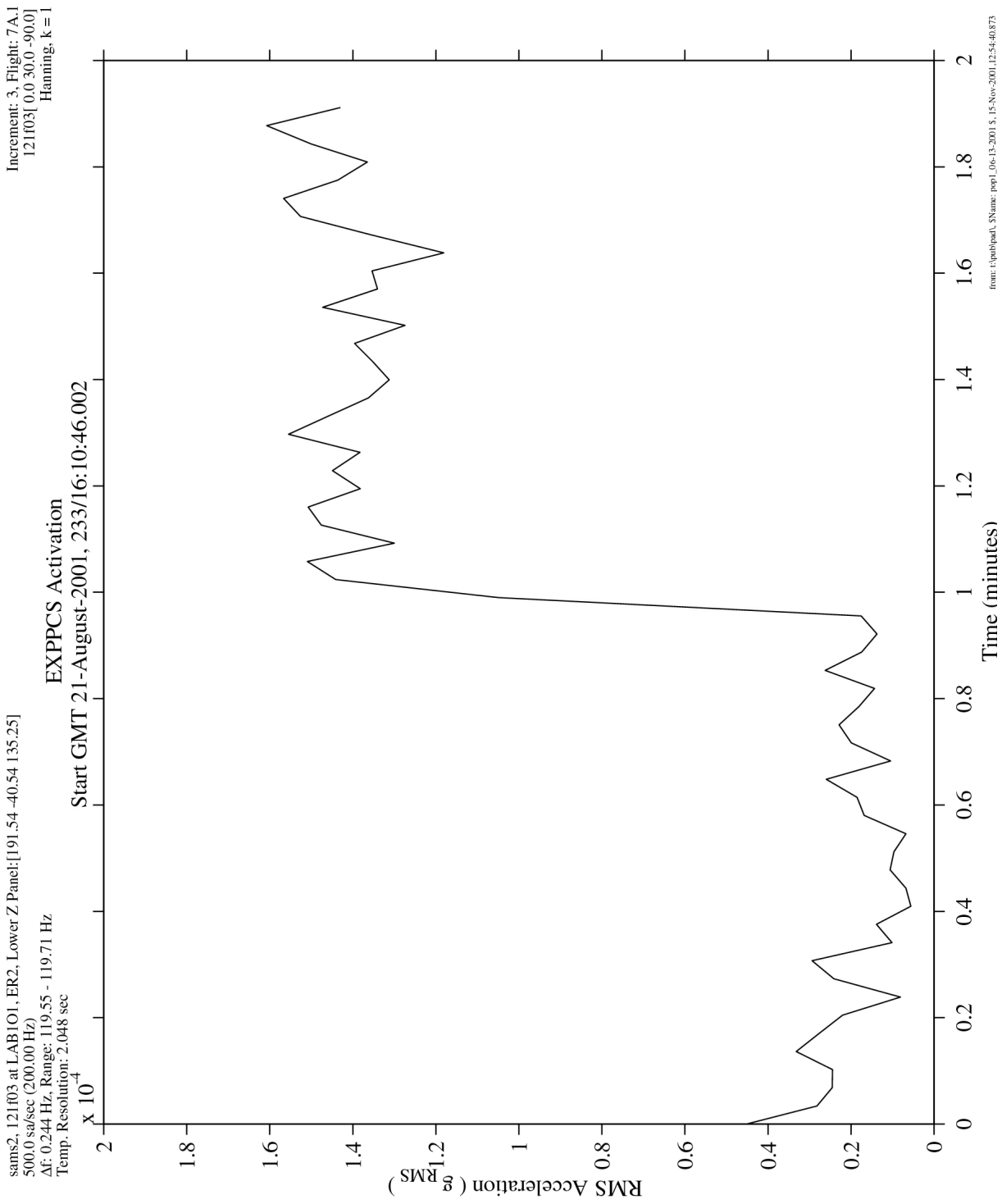

Figure 6-62 Interval RMS of EXPPCS Activation (121f03)

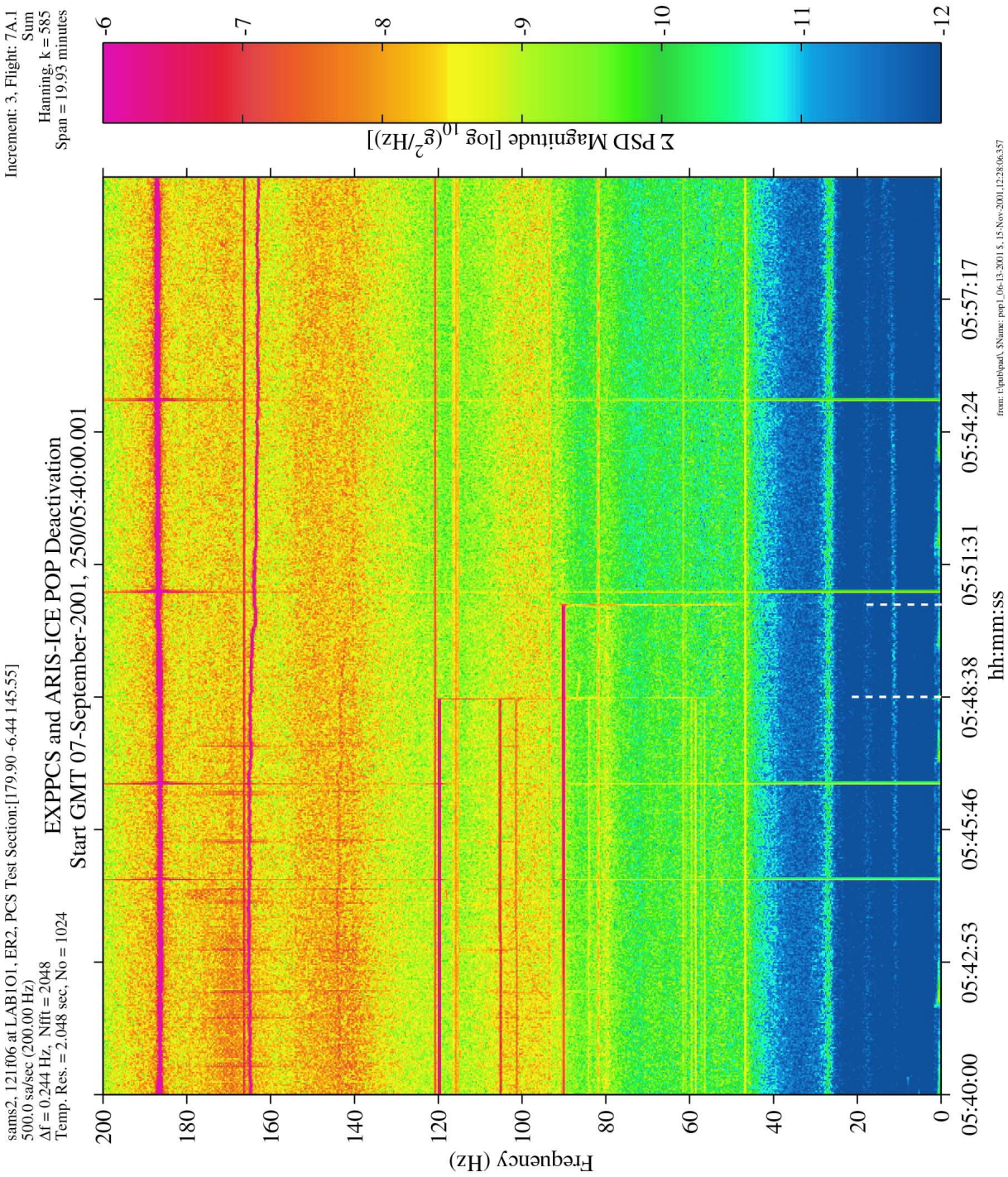

Figure 6-63 Spectrogram of EXPPCS and ARIS-ICE POP Deactivation (121f06)

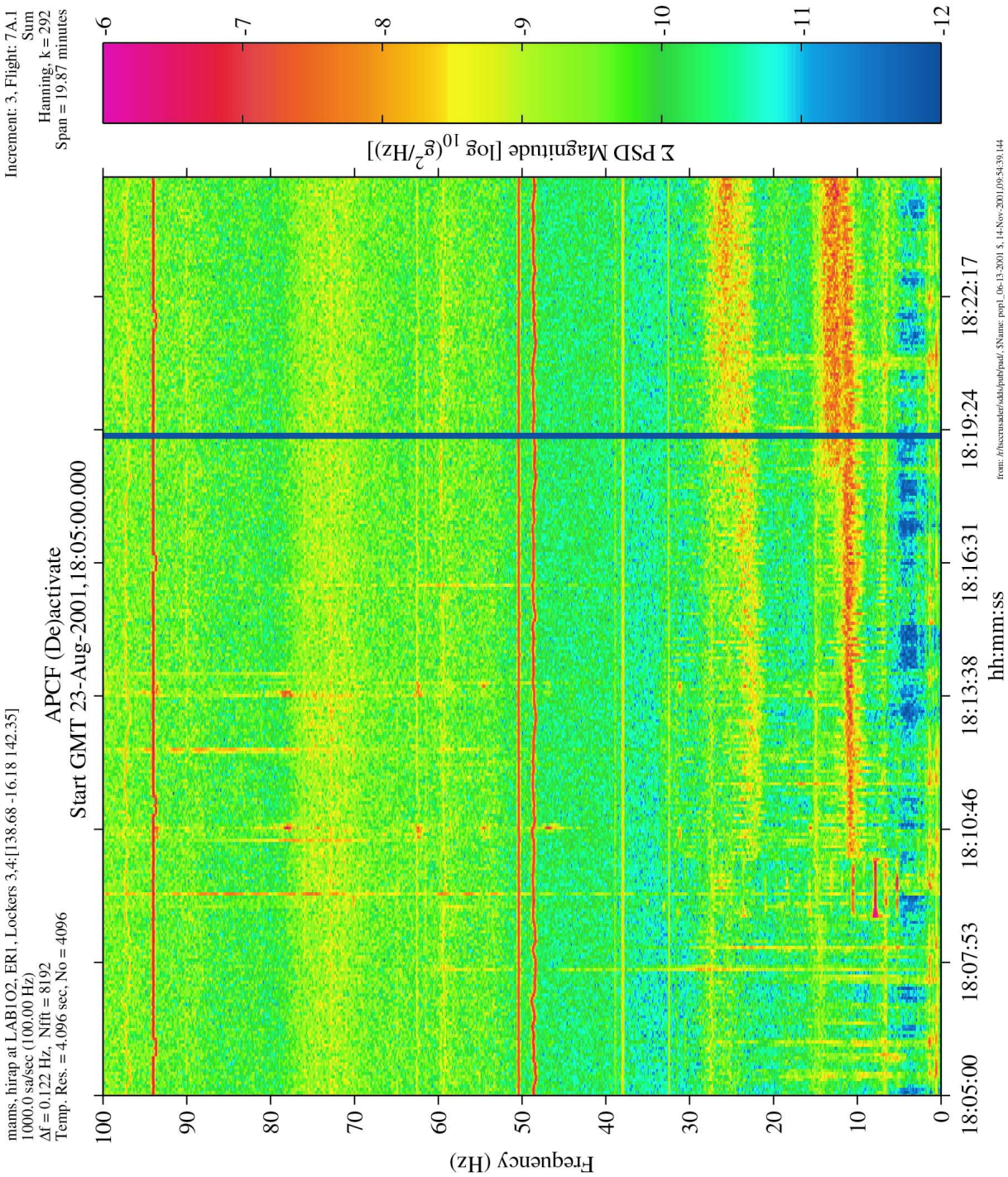

Figure 6-64 Spectrogram of [Not Apparent] APCF Deactivation/Activation (HiRAP)

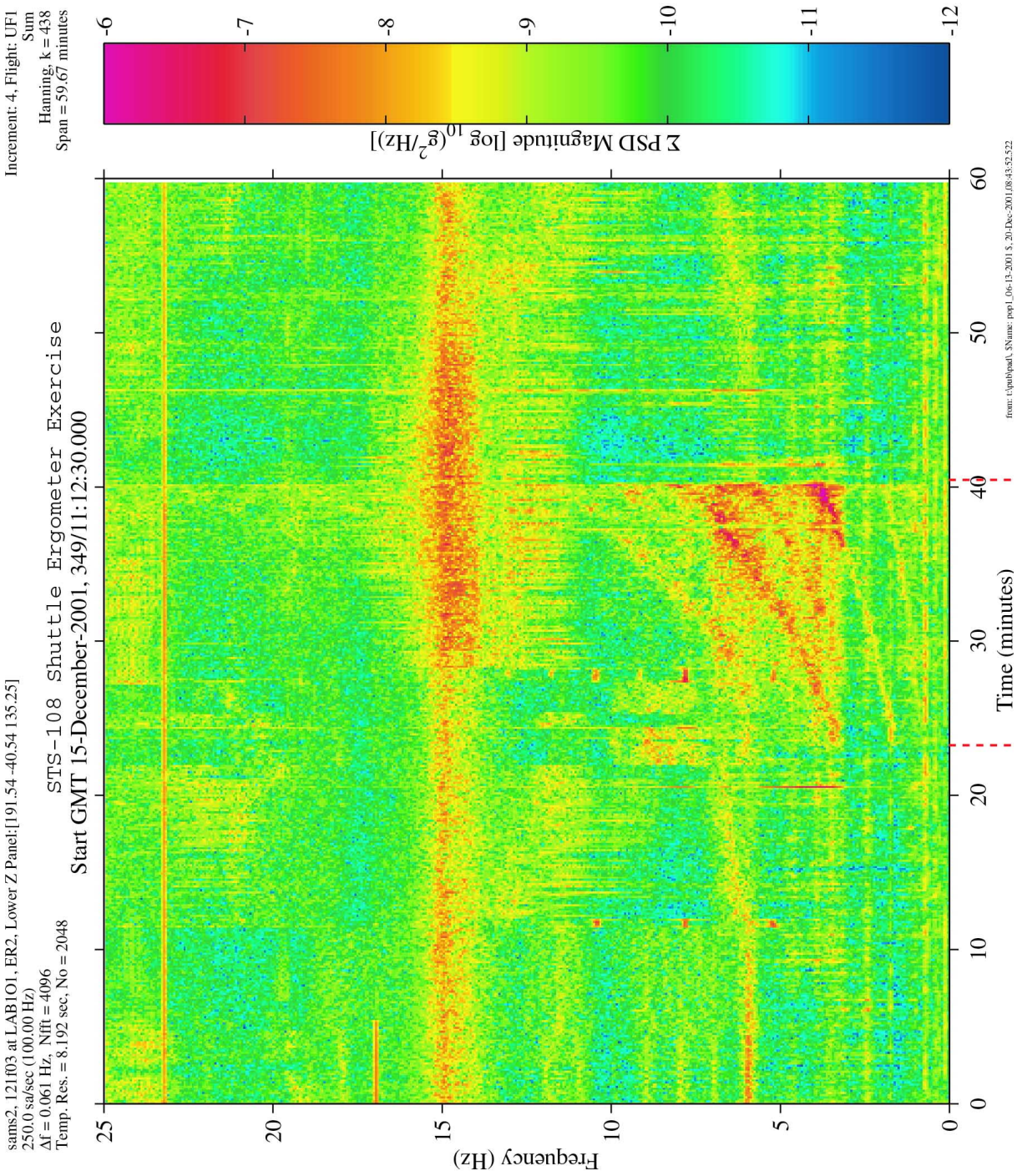

Figure 6-65 Spectrogram of STS-108 Shuttle Ergometer Exercise (121f03)

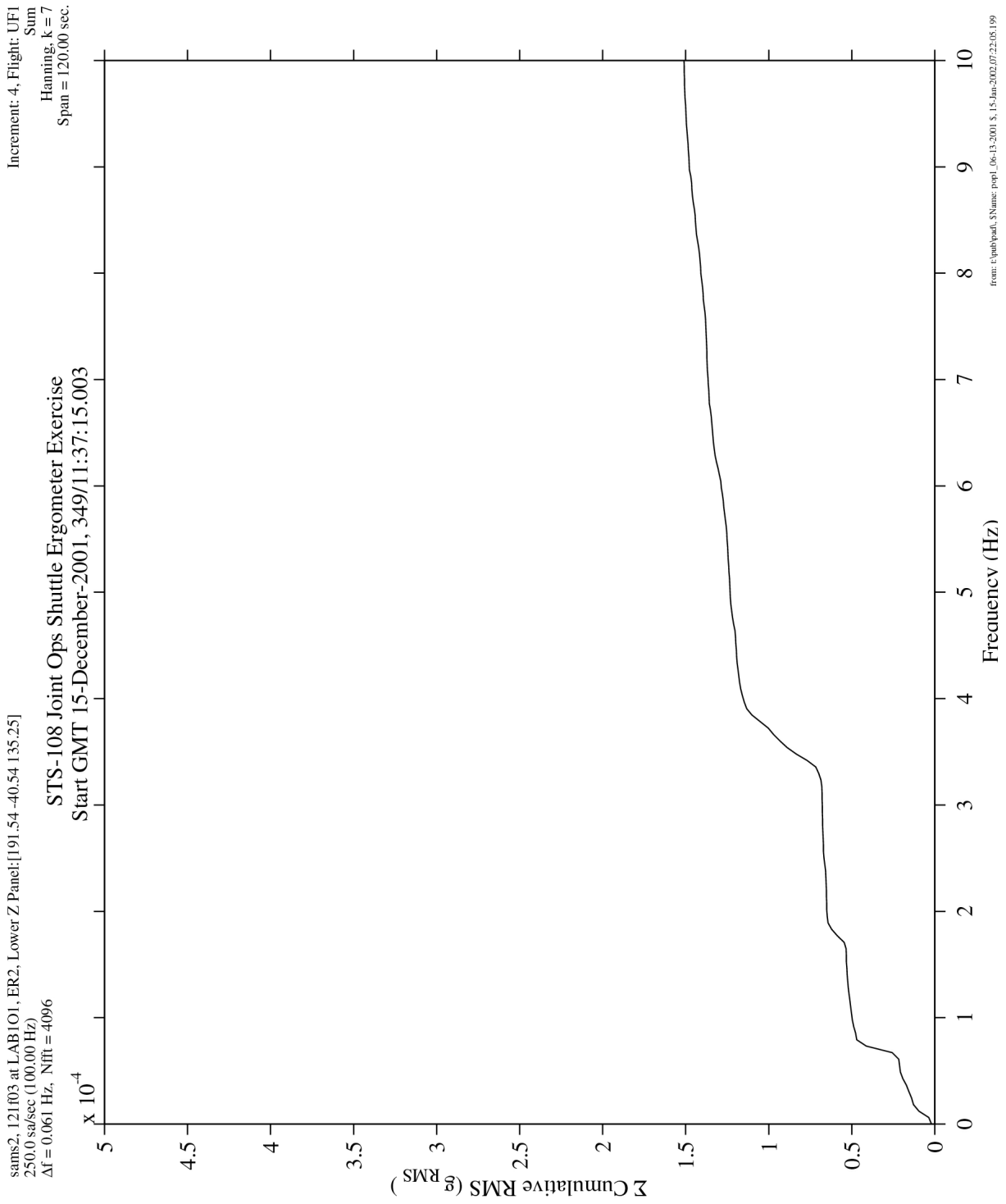

Figure 6-66 Cumulative RMS of STS-108 Shuttle Ergometer Exercise (121f03)

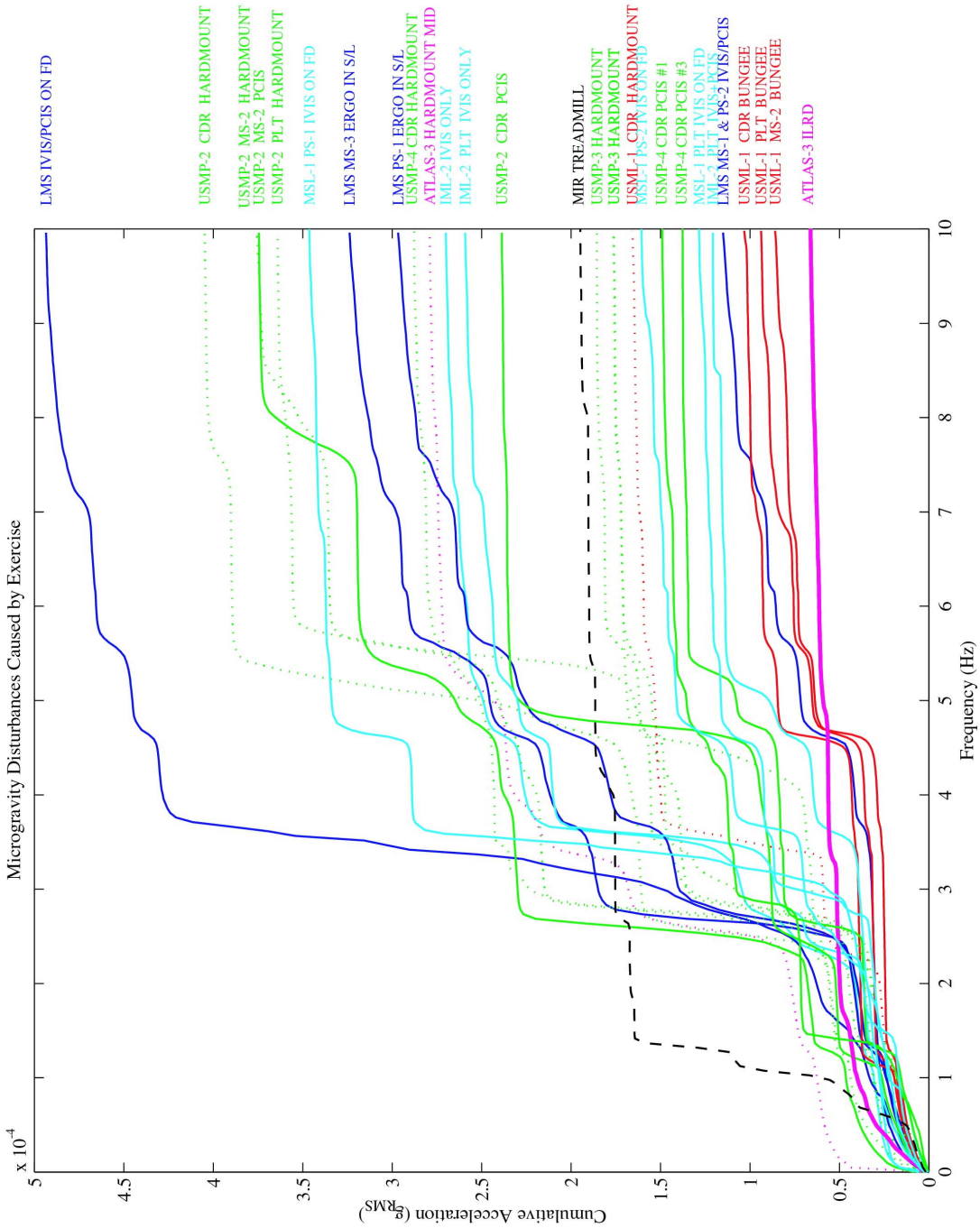

Figure 6-67 Cumulative RMS of Various Shuttle and Mir Exercise Periods (SAMS)

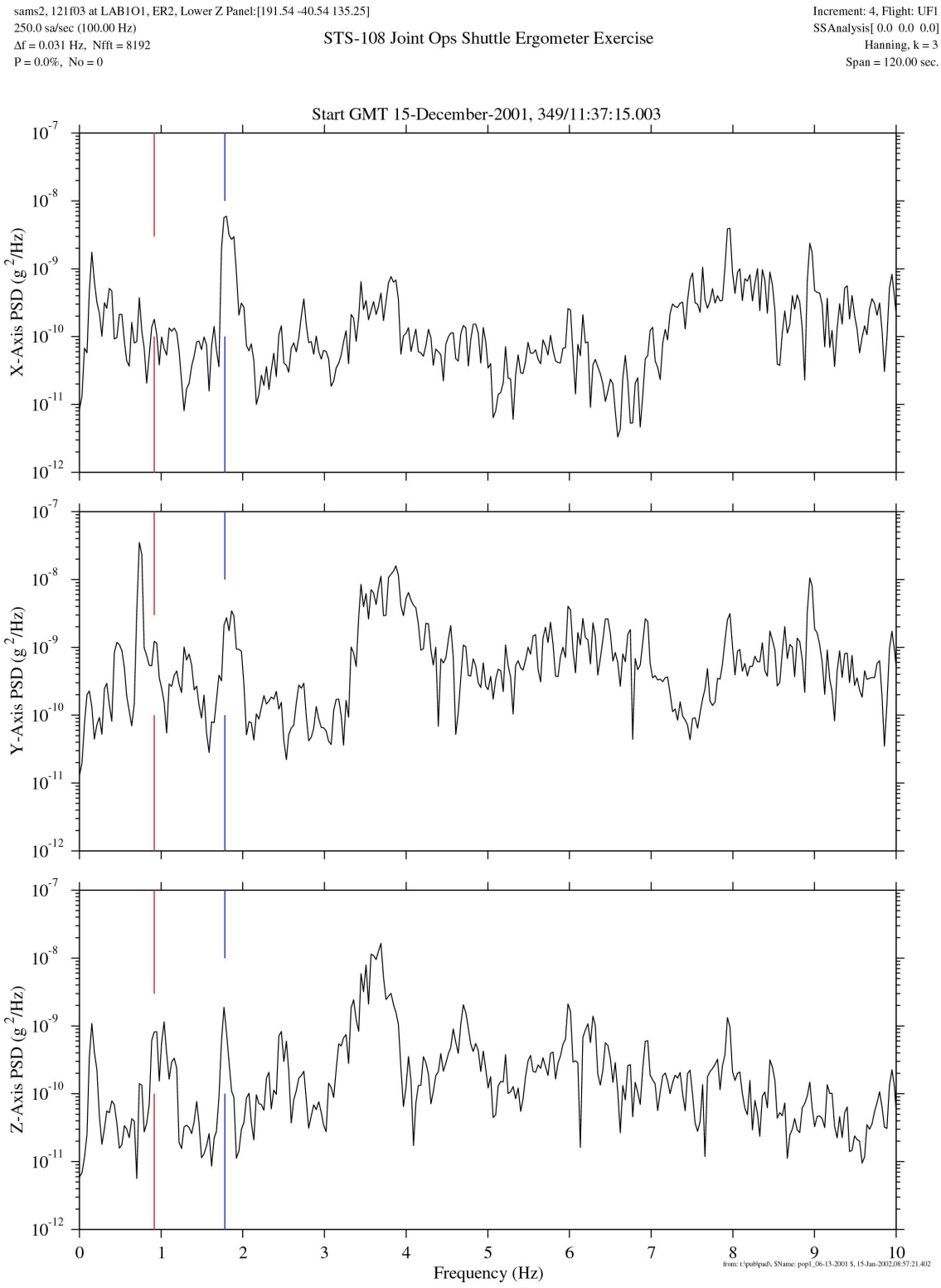

Figure 6-68 PSDs of STS-108 Shuttle Ergometer Exercise (121f03)

7 Principal Component Spectral Analysis

The PCSA histogram is computed from a large number of constituent PSDs. The resultant three-dimensional plot serves to summarize magnitude and frequency variations of significant or persistent spectral contributors and envelops all of the computed spectra over the time frame of interest. The two-dimensional histogram is comprised of frequency-magnitude bins in units of Hz and $\log_{10}(g^2/Hz)$. The third dimension, represented by a color scale, is the percentage of time that a spectral value was counted within a given frequency-magnitude bin.

TABLE 7-1 MAMS HIRAP (100 HZ) PCSA PARAMETERS

Roadmap Set #	Resolution		GMT	
	Frequency	Temporal		
	(Hz)	(seconds)	From	To
0055	0.1221	8.192	20-August-2001 16:00	30-August-2001 16:00
Total Number of PSDs: 102,694			*Total Number of Hours: 233.7*	

TABLE 7-2 SAMS 121F06 (25 HZ) PCSA PARAMETERS

Roadmap Set #	Resolution		GMT	
	Frequency	Temporal		
	(Hz)	(seconds)	From	To
0062	0.0305	32.768	08-September-2001 00:00	12-September-2001 00:00
Total Number of PSDs: 8,607			*Total Number of Hours: 78.3*	

TABLE 7-3 SAMS 121F05 (25 HZ) PCSA PARAMETERS

Roadmap Set #	Resolution		GMT	
	Frequency	Temporal		
	(Hz)	(seconds)	From	To
0063	0.0305	32.768	08-September-2001 00:00	12-September-2001 00:00
Total Number of PSDs: 6,161			*Total Number of Hours: 56.1*	

TABLE 7-4 SAMS 121F04 (25 HZ) PCSA PARAMETERS

Roadmap Set #	Resolution		GMT	
	Frequency	Temporal		
	(Hz)	(seconds)	From	To
0057	0.0305	32.768	28-August-2001 16:00	30-August-2001 14:00
Total Number of PSDs: 4,914			*Total Number of Hours: 44.7*	

TABLE 7-5 SAMS 121F03 (25 HZ) PCSA PARAMETERS

Roadmap Set #	Resolution		GMT	
	Frequency	Temporal		
	(Hz)	(seconds)	From	To
0057	0.0305	32.768	28-August-2001 16:00	30-August-2001 14:00
Total Number of PSDs: 4,919			*Total Number of Hours: 44.8*	

Note from these tables that the total number of hours in the last row is derived from temporal resolution and the number of PSDs used. If this number is smaller than the sum of the GMT spans shown for each subset, then the difference comes from data gaps in those spans. Figure 7-1 shows the resultant PCSA plot corresponding to Table 7-1, Figure 7-2 for Table 7-2, Figure 7-3 for Table 7-3, Figure 7-4 for Table 7-4, and Figure 7-5 for Table 7-5.

Examination of these PCSA figures yielded the following observations:

- The ADVASC disturbances discussed in Increment-2 report, which dominated the acceleration spectra near the HiRAP location are not evident; this experiment equipment was not active during the time these spectra were calculated.
- The SKV-1 disturbance at 23.5 Hz was much weaker in the 121f06 spectra than those of the HiRAP; the 121f06 sensor was mounted on the ARIS ER2. During the times these spectra were computed, this disturbance at the HiRAP location was weaker than at the Z-panel-mounted sensors 121f03 and 121f04.
- The spectra for 121f03 and 121f04 are similar below 25 Hz with a notable exception being the broadband 12-16 Hz disturbance centered at about 14.5 Hz. The source of this disturbance is unknown.

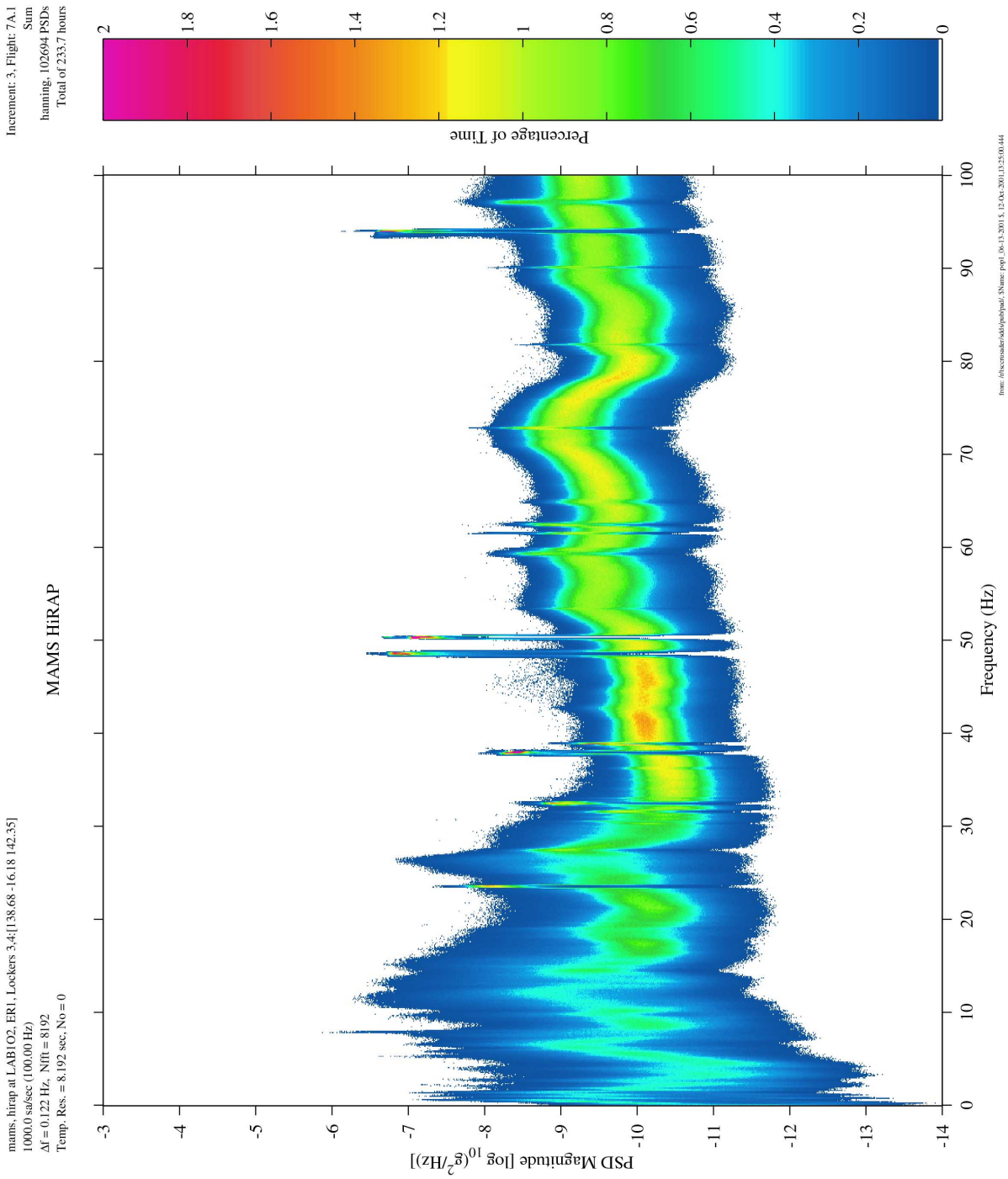

Figure 7-1 PCSA for MAMS HiRAP (HiRAP)

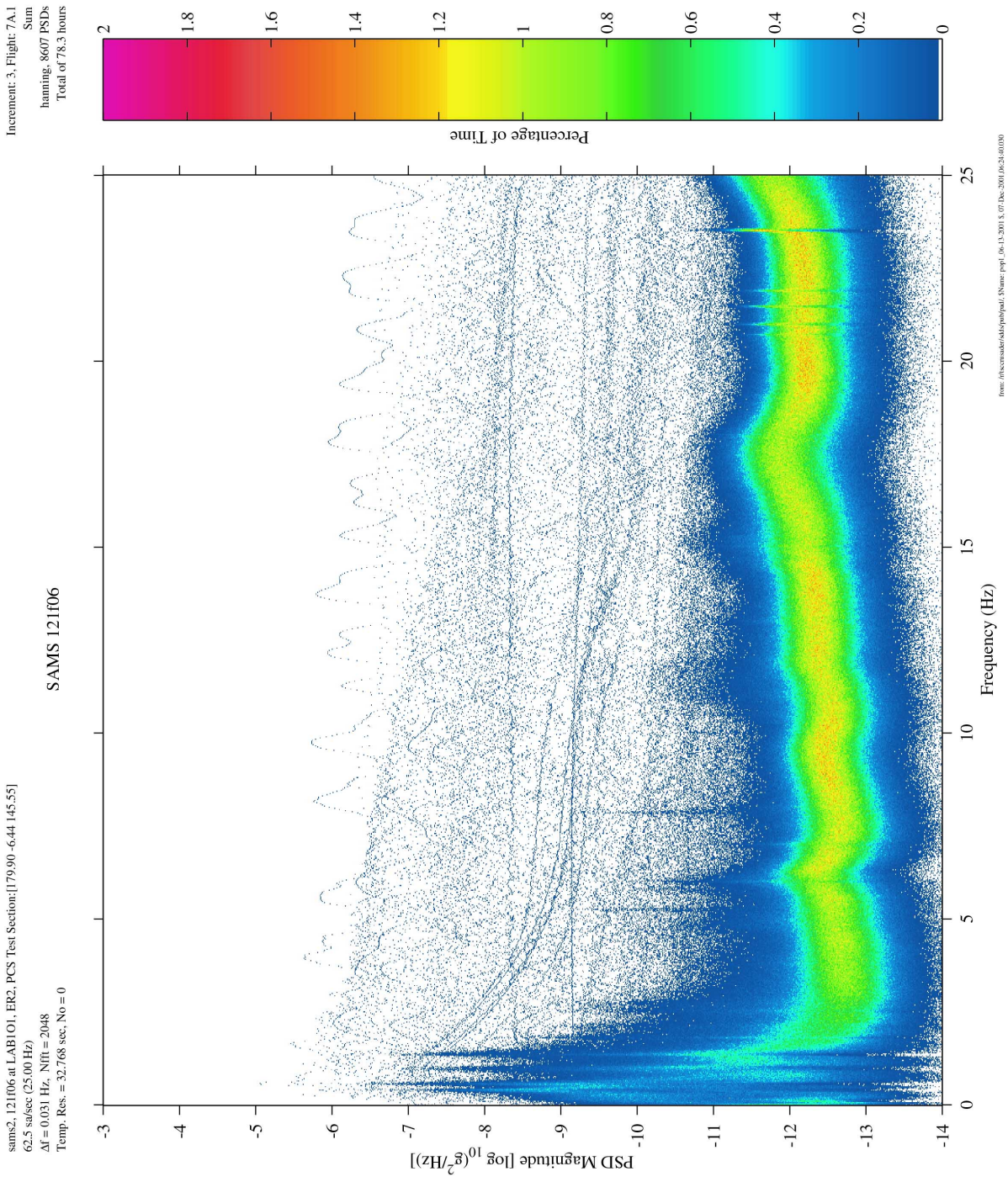

Figure 7-2 PCSA for SAMS 121f06 (121f06)

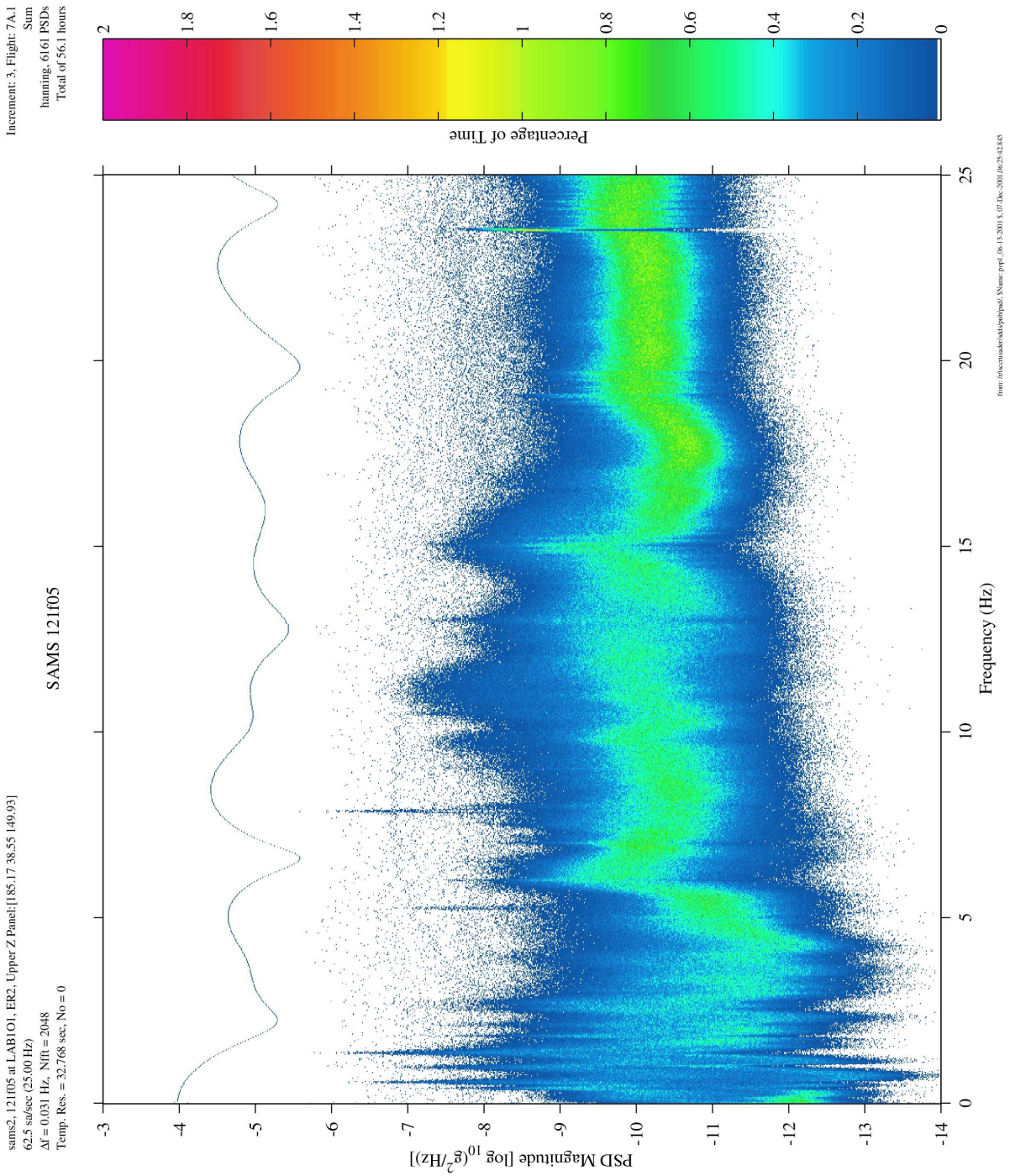

Figure 7-3 PCSA for SAMS 121f05 (121f05)

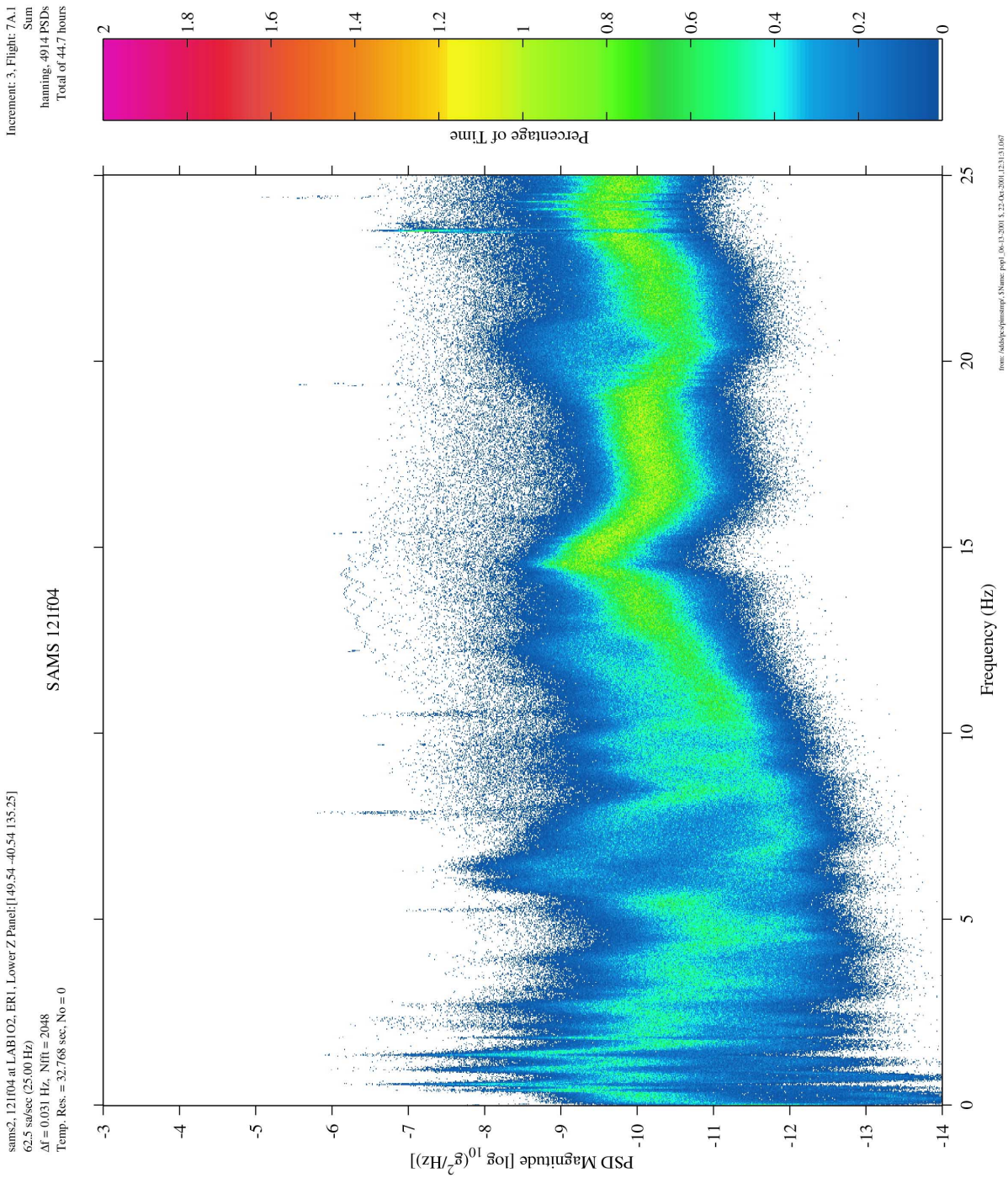

Figure 7-4 PCSA for SAMS 121f04 (121f04)

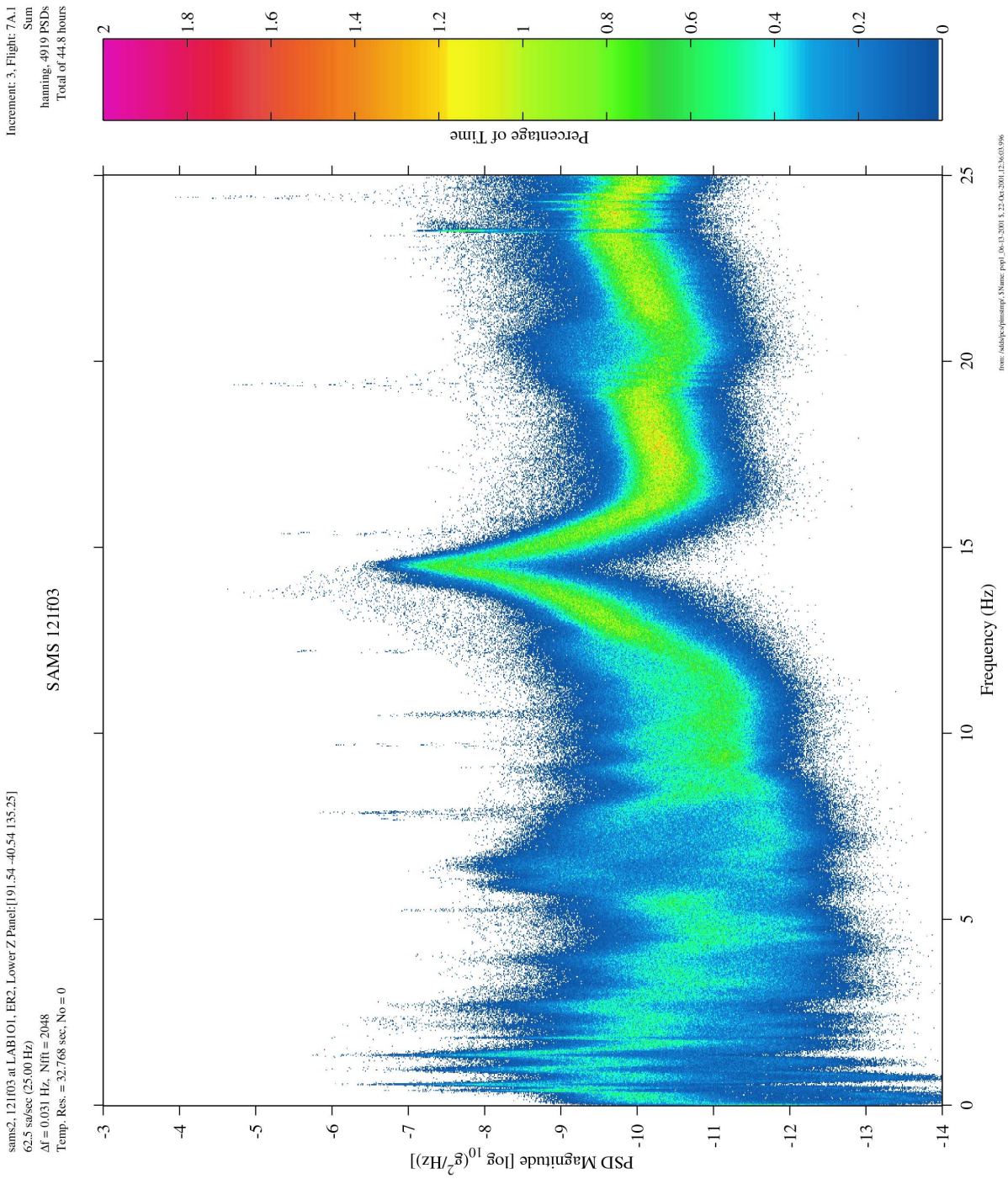

Figure 7-5 PCSA for SAMS 121f03 (121f03)

8 Vehicle Dynamics

Using the excitation environment provided by the transient and disturbance sources on the ISS, frequency responses were calculated to identify location specific versus global responses. Autospectra were used to calculate ratio response curves from pre-and post UF1 docking configurations denoting the end of Increment 3 operations. The two SAMS SE heads utilized where 121f03 and 121f04 both mounted on the Z-panel structure at the EXPRESS rack 1 and 2 locations, respectively. These triaxial sensors are slightly over 1 meter apart in the SSA X-axis direction.

A number of global bending modes are present in the XY and XZ plane within the ISS UF1 configuration. Numerous ISS system-bending modes have been calculated for a previous 4A-Flight configuration from 0.1 to 5 Hz [20]. The Increment 3 configuration will see shifts in these mode shapes dependent on the overall modal mass participation for these various mode shapes. The global XY and XZ bending modes are well represented within the frequency responses as seen in Figure 8-1 and Figure 8-2 for the times shown. Figure 8-1 shows the Y-axis, an ensemble average of a 15-minute window prior to undocking while Figure 8-2 is a 15-minute window after Endeavor undocked. As seen in these two sets of curves the sensors are registering global system responses from .1 to 3 Hz and then the levels become location dependent. The global bending modes all show a shift up in frequency once the shuttle has undocked. Figure 8-3 and Figure 8-4 give a ratio of the averaged spectra for the Y-axis for sensors 121F03 and 121F04 demonstrating that the response of the accelerometers becomes location dependent after 1 Hz in the case of the shuttle docked and shuttle undocked. Within these PSD averaged curves and the ratio responses, it is evident that the structural response measured by the two sensors at the EXPRESS Rack 1 and 2 locations become location dependent at or near a few Hertz. The ISS structure is more rigid when the shuttle is undocked and the global response of the orbiter shifts up in frequency requiring more excitation for the structure to respond equivalently allowing location dependent accelerations to become more evident at lower frequencies.

The X-axis response is far more stiff and therefore global, or less location dependent, as seen in Figure 8-5 and Figure 8-6. These ratios of X-axis response for the two times shown in Figure 8-1 through Figure 8-4 demonstrate that the location response in the X-axis is very similar past 10 Hz.

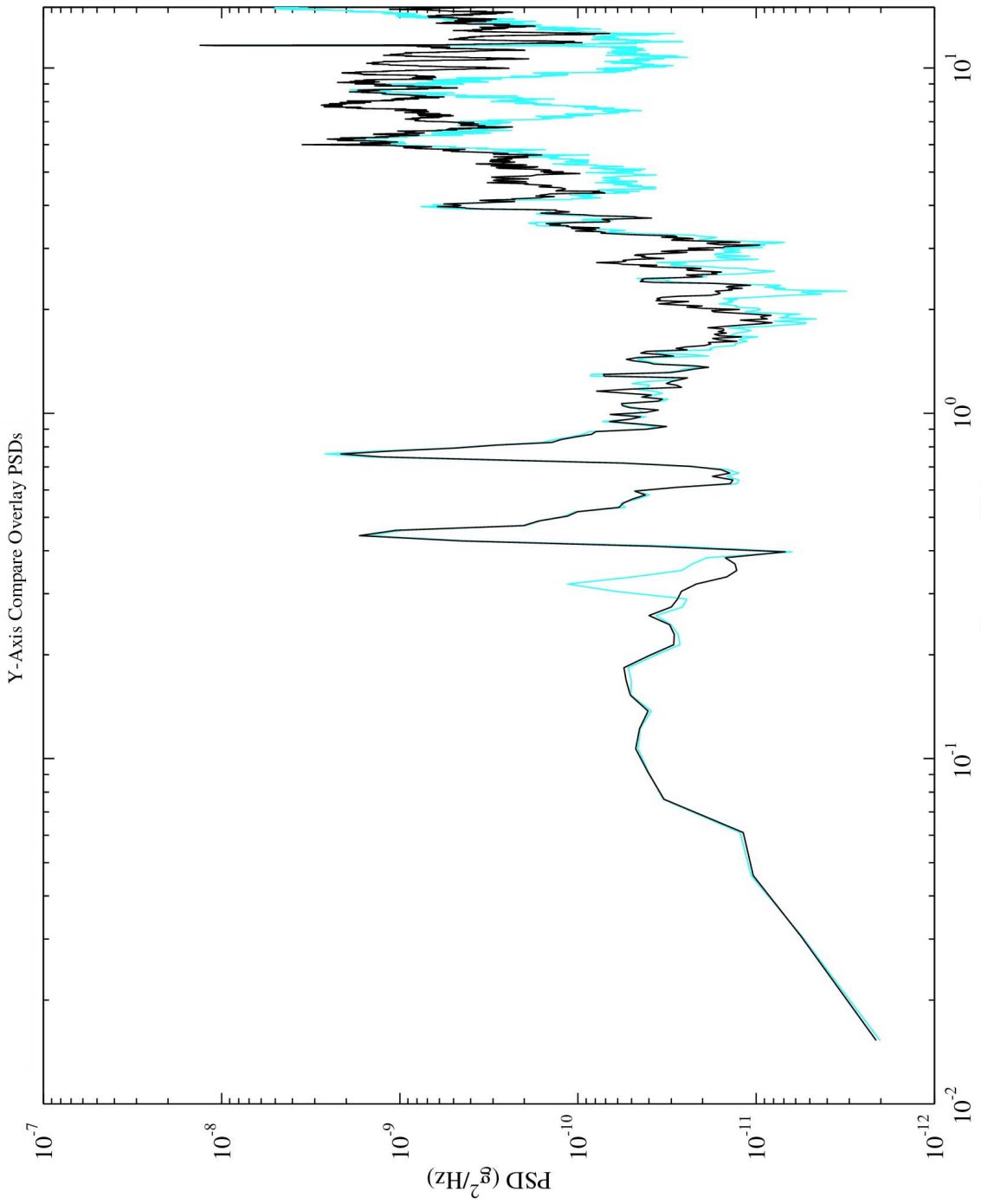

Figure 8-1 Y-Axis autospectra PSD Pre-Endeavor undocking

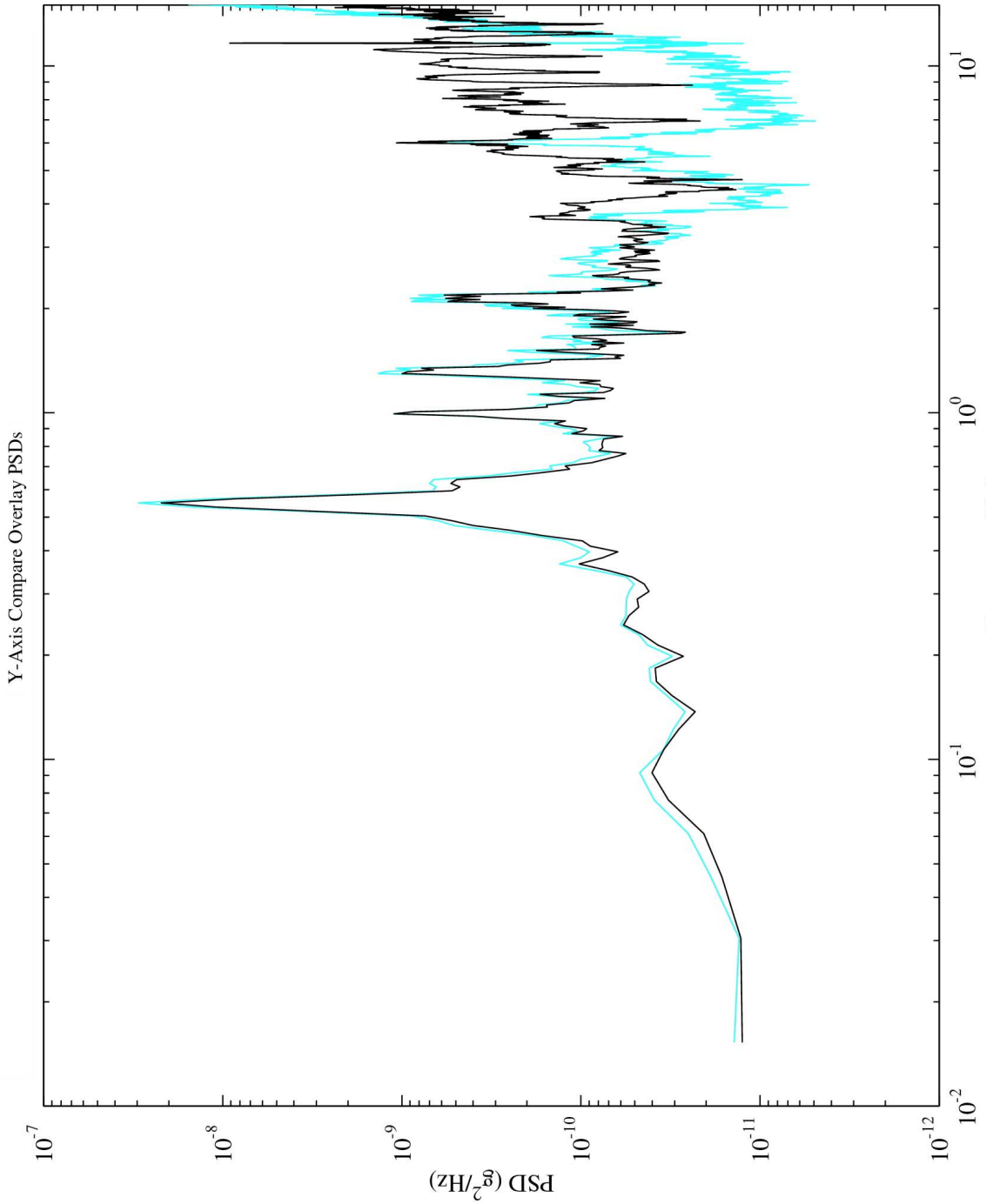

Figure 8-2 Y-Axis autospectra PSD post-Endeavor undocking

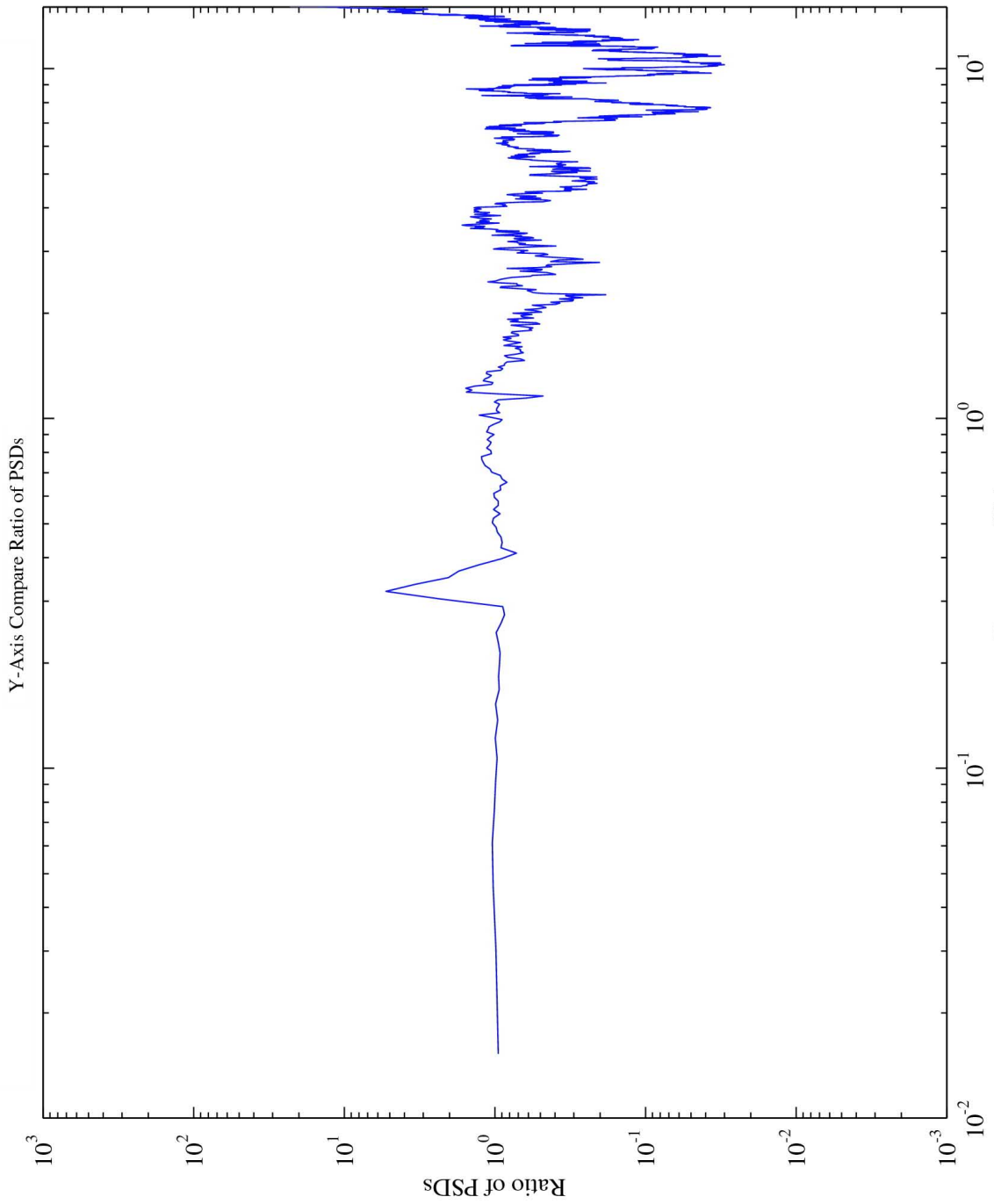

Figure 8-3 Y-Axis PSD ratio of SE 121F03 to 121F04 response for Pre-Endeavor undocking

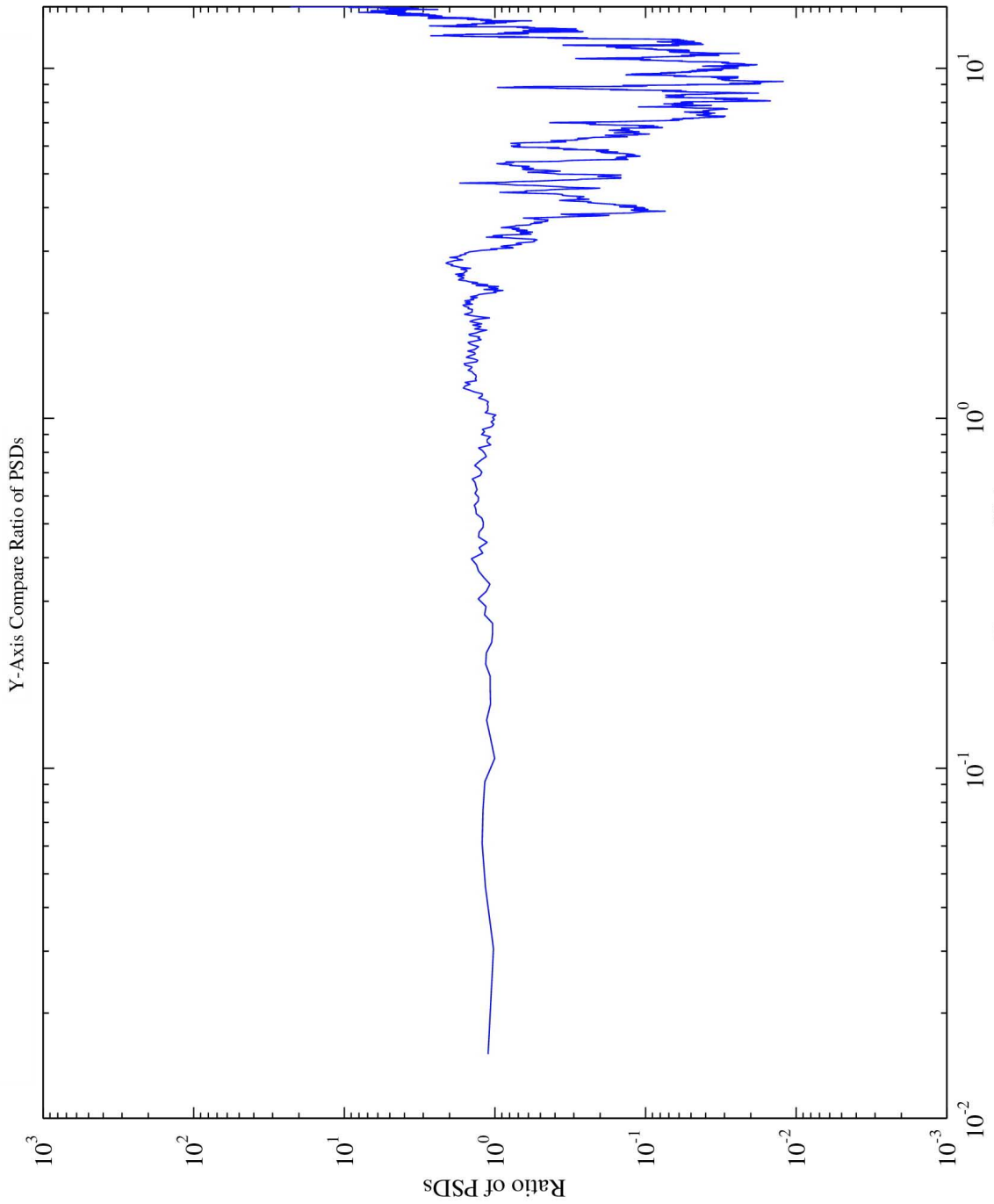

Figure 8-4 Y-Axis PSD ratio of SE 121F03 to 121F04 response for Post-Endeavor undocking

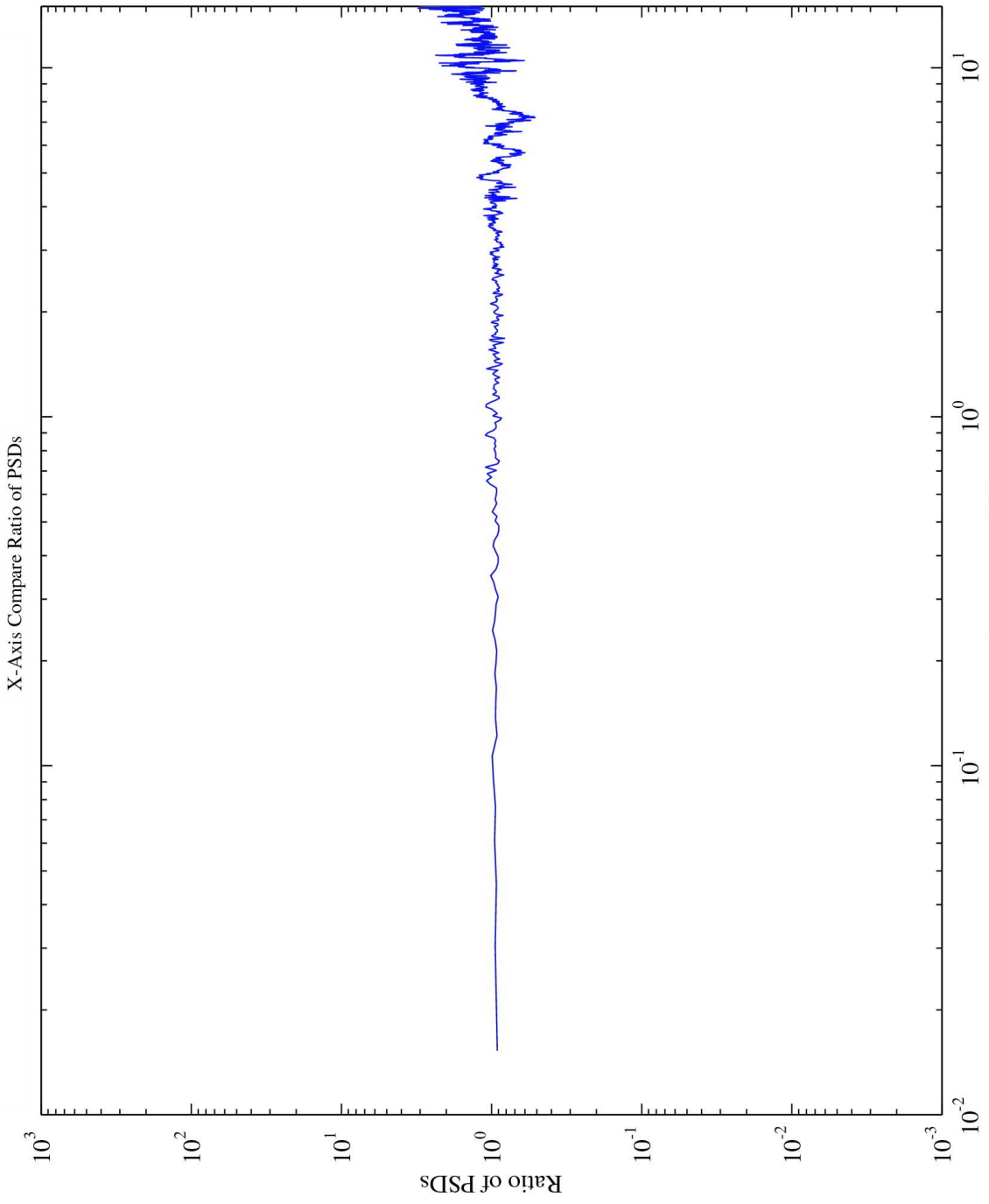

Figure 8-5 X-Axis PSD ratio of SE 121F03 to 121F04 response for Pre-Endeavor undocking

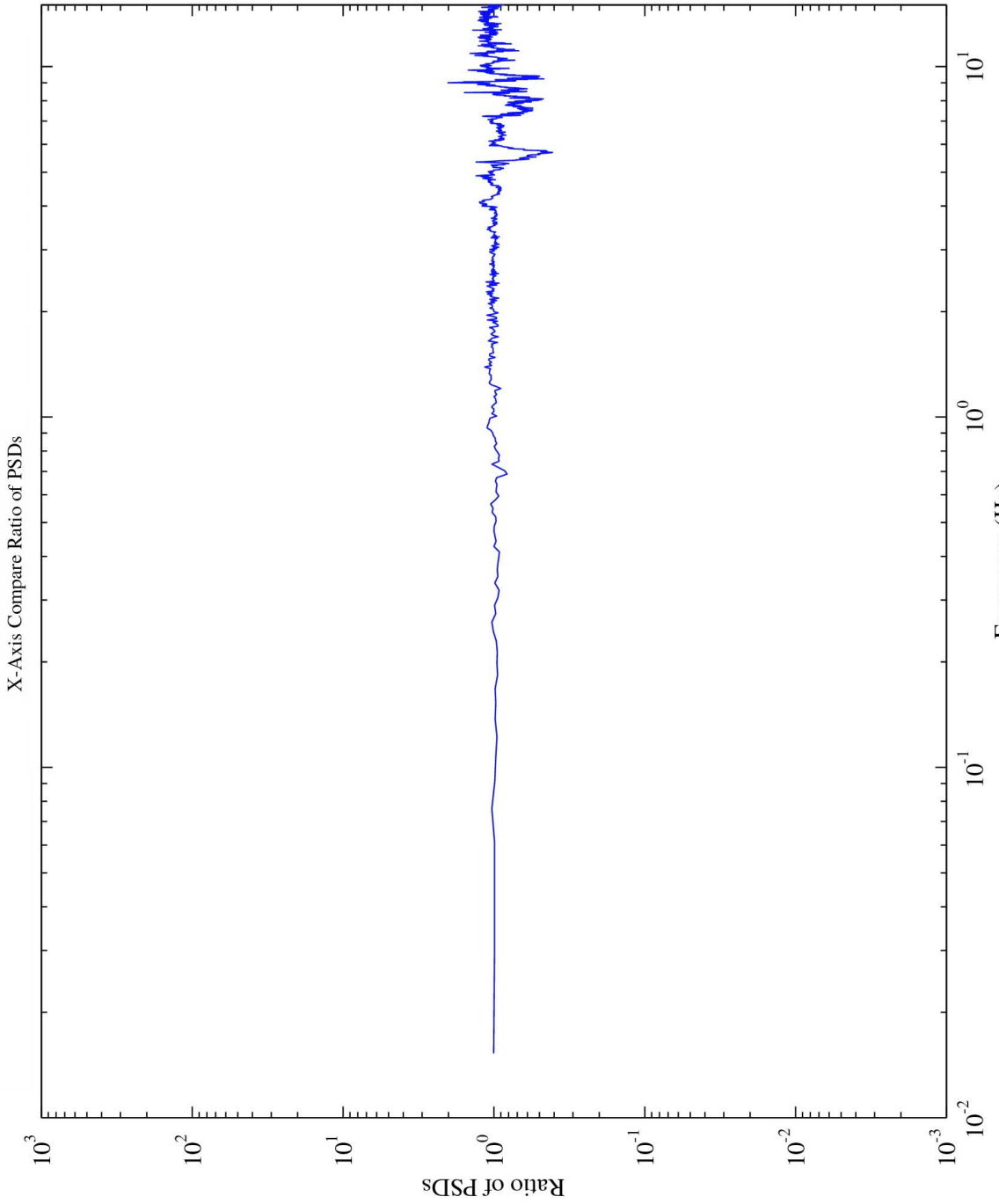

Figure 8-6 X-Axis PSD ratio of SE 121F03 to 121F04 response for Post-Endeavor undocking

9 Summary of Increment-3 Analysis

9.1 Quasi-steady Environment

This section aims to summarize results from the quasi-steady acceleration analysis for this report. As such, it does not completely characterize the event under consideration, but serves to highlight the key impacts on the quasi-steady regime.

For more detail, see the applicable technical narrative sections of this report. Also, and most importantly, if this report does not include specific analysis for a particular event that would aid in correlation with science or other data of interest, then please contact pimsops@grc.nasa.gov for further assistance.

TABLE 9-1 SUMMARY OF FINDINGS FOR INCREMENT-3 QUASI-STEADY ANALYSIS

Source	Effect	GMT
TEA Attitude	–0.80 µg mean in Z_A axis 0.94 µg mean magnitude	Various
XPOP Attitude	1.89 µg mean in X_A axis 2.05 µg mean magnitude	Various
Progress 4P Undocking	10-20 µg peak in - X_A direction	22-August-2001, 234/06:07:00
DC1 Docking	10-25 µg in - X_A direction	17-September-2001, 260/01:05:00
CMG 2 Testing	Increased variation on X_A, Y_A, and Z_A axes.	11-October-2001, 283/04:50:00
Soyuz 2 Relocation	8-10 µg peak in - X_A direction	19-October-2001, 291/07:58:00
EVA Activities	12-18 µg peak in -Y_A, and -Z_A directions.	08-October-2001, 281/14:23 12-November-2001, 316/21:41
SSRMBS Maneuvers	7-13 µg in the -X_A, and -Z_A directions.	08-October-2001, 281/14:23
DC1/PkhO Depressurization	4 µg peak in -X_A direction 1.5 peak in -Y_A direction	08-October-2001, 281/14:23 12-November-2001, 316/02:35
Thrusters Inhibited Recovery	10-20 µg in -X_A direction for extended period	03-December-2001, 337/13:20
Progress 5P Prop Purge	3.5 –5.7 µg in Y_A, and -Z_A directions.	20-November-2001, GMT 234/19:10

9.2 Vibratory Environment

This section aims to summarize results from the vibratory acceleration analysis for this report. As such, it does not completely characterize the event under consideration. The column labeled "Effect" in the table below is an attempt to encapsulate the impact of the corresponding "Source" acceleration event on the vibratory regime. The quantities referred to in the "Effect" column are one of the following:

- PEAK, the peak acceleration vector magnitude
- RMS, the acceleration root-mean-square value for the frequency range shown

For more detail, see the applicable technical narrative sections of this report. Also, and most importantly, if this report does not include specific analysis for a particular event that would aid in correlation with science or other data of interest, then please contact pimsops@grc.nasa.gov for further assistance.

TABLE 9-2 SUMMARY OF FINDINGS FOR INCREMENT-3 VIBRATORY ANALYSIS

Source	State	Effect	Frequency Range (Hz)	Sensor	GMT
EXPPCS	Activation	RMS: 0.12 mg	119.55 - 119.71	SAMS 121f03	21-August-2001, 233/16:11:46
Progress 4P Undocking		PEAK: 1.02 mg	0 - 25	SAMS 121f02	22-August-2001, 234/06:07:14
Progress 5P Thruster Test		PEAK: 1.93 mg	0 - 25	MAMS HiRAP	27-August-2001, 239/01:34:36
Progress 5P Thruster Test		PEAK: 3.03 mg	0 - 25	SAMS 121f05	27-August-2001, 239/01:34:00
Progress 5P Thruster Test		PEAK: 2.78 mg	0 - 25	SAMS 121f06	27-August-2001, 239/01:34:00
Progress 5P Docking		PEAK: 18.72 mg	0 - 100	MAMS HiRAP	23-August-2001, 235/09:52:19
Apparent STS-108 Joint Ops X_A Structural Modes		RMS: 13.0 µg RMS: 3.8 µg RMS: 4.3 µg RMS: 5.6 µg RMS: 2.6 µg RMS: 2.2 µg RMS: 3.3 µg	0.12 - 0.20 0.27 - 0.35 0.35 - 0.43 0.63 - 0.72 0.72 - 0.79 1.11 - 1.21 1.73 - 1.83	SAMS 121f04	15-December-2001, 349/16:30:00
Apparent STS-108 Joint Ops Y_A Structural Modes		RMS: 9.4 µg RMS: 11.9 µg	0.40 - 0.53 0.69 - 0.89		
Apparent STS-108 Joint Ops Z_A Structural Modes		RMS: 10.5 µg RMS: 1.9 µg RMS: 3.0 µg RMS: 5.8 µg RMS: 2.3 µg RMS: 2.4 µg	0.12 - 0.20 0.35 - 0.43 0.58 - 0.70 0.99 - 1.11 1.13 - 1.21 1.73 - 1.83		
Apparent X_A Structural Modes After STS-108 Undocking		RMS: 1.8 µg RMS: 2.0 µg RMS: 0.9 µg RMS: 1.5 µg RMS: 2.5 µg RMS: 1.5 µg RMS: 3.8 µg RMS: 6.6 µg RMS: 1.9 µg RMS: 3.1 µg RMS: 6.2 µg RMS: 4.0 µg	0.02 - 0.09 0.09 - 0.20 0.20 - 0.24 0.24 - 0.32 0.32 - 0.44 0.44 - 0.50 0.50 - 0.63 0.79 - 0.99 1.16 - 1.22 1.22 - 1.27 1.27 - 1.34 1.71 - 1.88	SAMS 121f03	15-December-2001, 349/18:30:00
Apparent Y_A Structural Modes After STS-108 Undocking		RMS: 22.6 µg RMS: 4.0 µg RMS: 6.2 µg	0.43 - 0.66 1.22 - 1.27 1.27 - 1.36		
Apparent Z_A Structural Modes After STS-108 Undocking		RMS: 11.3 µg RMS: 21.0 µg RMS: 8.0 µg RMS: 14.5 µg RMS: 24.2 µg RMS: 4.2 µg	0.35 - 0.47 0.73 - 0.99 1.16 - 1.22 1.22 - 1.27 1.27 - 1.34 1.74 - 1.82		
STS-108 Joint Ops Shuttle Ergometer Exercise (atypical)		RMS: 150 µg	0 - 25	SAMS 121f03	15-December-2001, 349/11:37:15
ARIS Environment Comparison	non-isolated	PEAK: 315 µg	0 - 25	SAMS 121f05	11-September-2001, 254/08:09:19
ARIS Environment Comparison	ARIS active	PEAK: 25 µg	0 - 25	SAMS 121f06	

10 References

1. Hamacher, H., Fluid Sciences and Materials Science in Space, Springer-Verlag, 1987.

2. International Space Station User's Guide Release 2.0, NASA.

3. Expedition Three Press Kit: Expanding Space Station Scientific Research, Boeing/NASA/United Space Alliance, July 25, 2001

4. The International Space Station Fact Book, NASA, October 2000.

5. International Space Station Coordinate Systems, SSP-30219, Revision F.

6. International Space Station Flight Attitudes, D-684-10198-06 DCN-002, December 1, 1999.

7. International Space Station Research Plan—Office of Biological and Physical Research, NASA, August 2000.

8. Steelman, April., "Flight 6A Microgravity Analysis", Microgravity AIT, August 1999.

9. Increment-3 As Flown ISS Attitude Timeline (ATL)

10. On-Orbit Vehicle Configuration Data Book for Mission 6A, Shuttle-ISS NSTS-37324-6A, Rev. 001, NASA, March 01.

11. Microgravity Environment Interpretation Tutorial (MEIT), NASA Glenn Research Center, March 2001.

12. Expedition Three Overview Fact Sheet, NASA, July 2001.

13. EXPRESS RACKS 1-2 /4-5 Fact Sheet, NASA, February and July 2001.

14. EXPRESS Rack, Flight 6A On-Orbit Configuration, Teledyne Brown Engineering DL 5221003, Nov. 99.

15. Expedition Three Fact Sheets: Expedition Three Payload Overview, NASA, July 2001.

16. Matisak, B.P.,Rogers, M.J.B & Alexander J.I.D., "Analysis of the Passive Accelrometer System (PAS) Measurements During USML-1", AIAA 94-0434, December 1994.

17. http://spaceflight.nasa.gov/station/reference/issug/ISSUG35-50.pdf

18. "Concept of Operation and Utilization, Revision C, Volume I: Principles", SSP 50011-01, April 26, 1996.

19. Simon, C., "Orbit Operations Checklist, STS-108 Flight Supplement", JSC-48036-108, June 4, 2001

20. "Flight-4A Post-Flight Analysis: Modal Analysis, Model Validation and Correlation", Prepared by ISS Loads and Dynamics Team, Houston, Texas, June 2001-A92-J332-STN-M-MK-2001-0080, Authors: Mo Kaouk, Ted Bartkowicz, Sydney Haley, Steve Scheer.

21. Software Requirements for Processing Microgravity Acceleration Data from the International Space Station, PIMS-ISS-001, May 2000.

22. Canopus Systems, Inc., OARE Technical Report 149, STS-78 (LMS-1) Final Report, CSI-9604, September 1996.

23. Canopus Systems, Inc., OARE Technical Report 151, STS-94 (MSL-1) Final Report, CSI-9704, August 1997.

24. Hogg, Robert V., "Adaptive Robust Procedures: A Partial Review and Some Suggestions for Future Applications and Theory", Journal of the American Statistical Association, Vol. 69, December 1974.

25. Canopus System, Inc., Microgravity Environment Interpretation Tutorial 2001 Presentation, Section 5, James Fox, March 2001.

26. Microgravity Analysis Integration Team, "Microgravity Control Plan (Revision B)", Report No: SSP-50036 B, the Boeing Company, Houston, TX, NASA Contract No. NAS15-1000 (DRIVE-16), February 1999.

Appendix A. On-line Access to PIMS Acceleration Data Archive

Acceleration data measured by the MAMS and the SAMS on the ISS are available over the Internet via FTP from a NASA GRC file server. The flow chart shown in Figure A - 1 diagrams a procedure that can be used to download data files of interest:

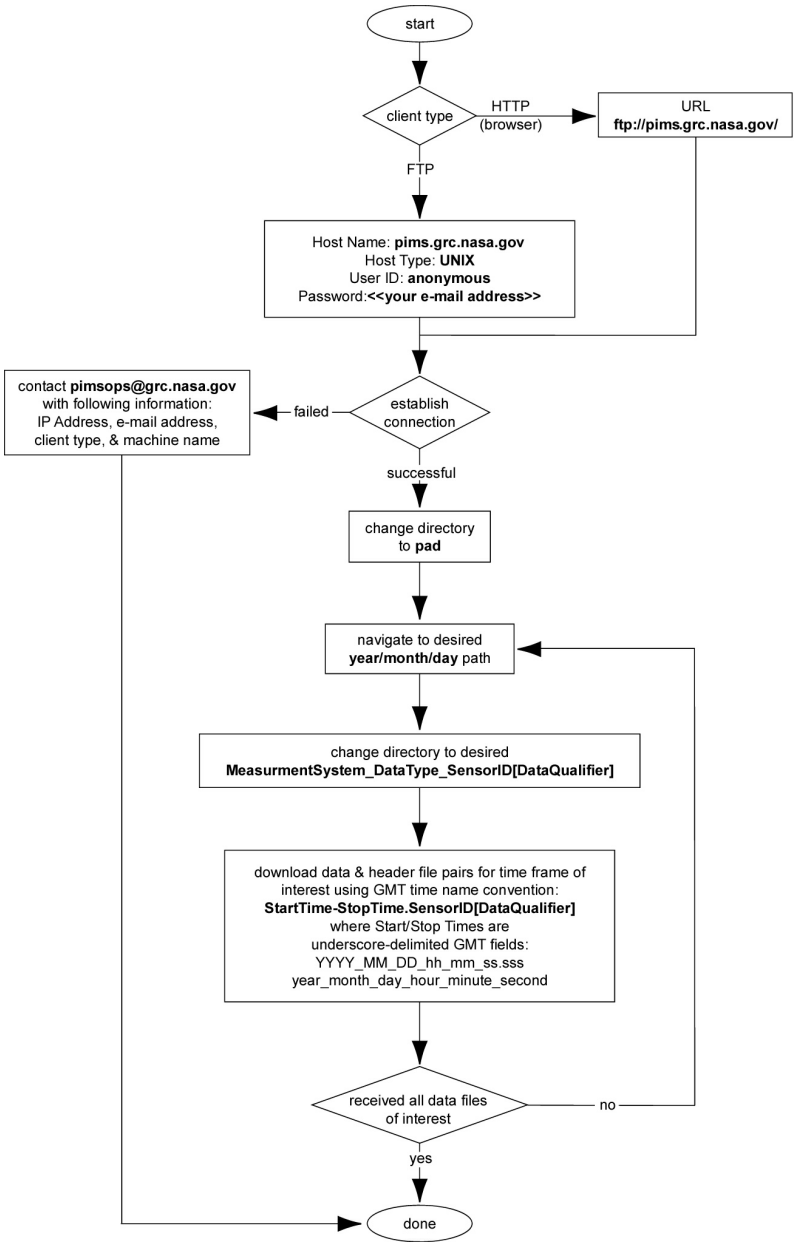

Figure A - 1 On-Line Data Access Flow Chart

A fictitious file listing is shown in Figure A - 2 depicting the PIMS Acceleration Data (PAD) file system hierarchy.

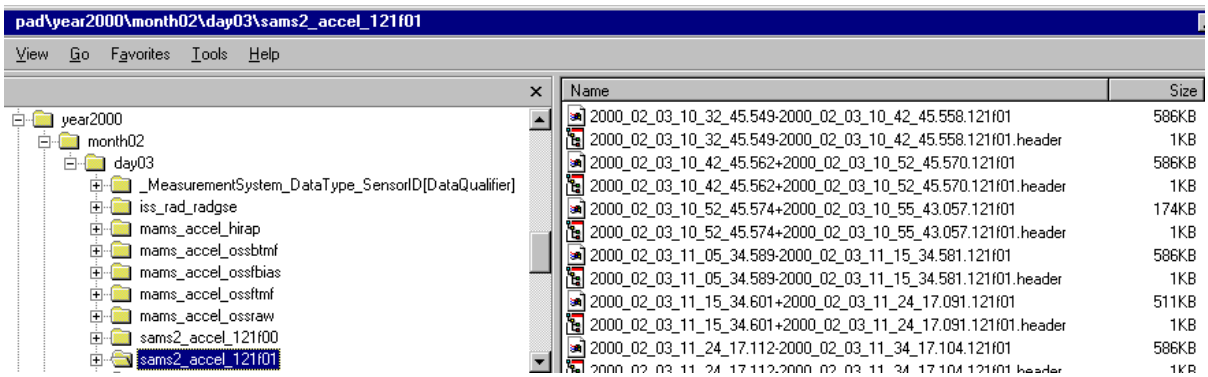

Figure A - 2 Screenshot of Sample PAD File Listing

For the directory highlighted on the left of this sample listing, the measurement system is "sams2" and the sensor identifier is "121f01". On the right, there is a partial listing of the acceleration header and data files available for this sensor collected on the day indicated (day 3). These files are named according to the PIMS-ISS-001 document [21].

If you encounter difficulty in accessing the data using this procedure, then send an electronic mail message to pimsops@grc.nasa.gov. Please describe the nature of the difficulty, and give a description of the hardware and software you are using to access the file server, including the domain name and/or IP address from which you are connecting.

Appendix B. Some Useful Acceleration Data and Microgravity Related URLs

Below is a list of some URLs that the microgravity scientific community might find very useful. They are all microgravity related. NASA does not endorse or cannot be held liable for the information contained on any site, which is not NASA's. The PIMS Project provides this listing only as a service to the microgravity community.

1. For more information on the EXPPCS experiment go to: http://microgravity.grc.nasa.gov/6712/PCS.htm

2. For more information on EXPRESS RACK go to: http://liftoff.msfc.nasa.gov/Shuttle/msl/science/express.html

3. For more information on ARIS-ICE go to: http://www.scipoc.msfc.nasa.gov

4. For more information on Expedition Three go to: http://www1.msfc.nasa.gov/NEWSROOM/background/facts/exp3fact.html

5. For more information on Microgravity Acceleration Measurement go to: http://microgravity.grc.nasa.gov/MSD/MSD_htmls/mmap.html

6. For more information on MAMS OSS, MAMS HiRAP and SAMS go to: http://pims.grc.nasa.gov

7. For information on MAMS, SAMS data request go to: http://pims.grc.nasa.gov/html/RequestDataPlots.html

8. For information on upcoming Microgravity Environment Interpretation Tutorial (MEIT) go to: http://www.grc.nasa.gov/WWW/MMAP/PIMS/MEIT/meitmain.html

9. For information on upcoming Microgravity Meeting Group (MGMG) go to: http://www.grc.nasa.gov/WWW/MMAP/PIMS/MGMG/MGMG_main.html

10. For information on SAMS go to: http://microgravity.grc.nasa.gov/MSD/MSD_htmls/sams.html

11. For information on MAMS/HiRAP go to: http://microgravity.grc.nasa.gov/MSD/MSD_htmls/mams.html

Appendix C. Acronym List and Definition

Acronyms used in this Summary Report are listed below. A more extensive list of NASA ISS-related acronyms can be found through the Internet at:

http://spaceflight.nasa.gov/station/reference/index.html

ACRONYM	DEFINITION
AAA	Avionics Air Assembly
ADCO	Attitude Determination and Control Officer
AOS	Acquisition of Signal
APCF	Advanced Protein Crystallisation Facility
ARIS	Active Rack Isolation System
ARIS-ICE	ARIS ISS Characterization Experiment
ATL	Attitude Timeline
BCTA	Bias Calibration Table Assembly
CAM	Centrifuge Accommodation Module
CBM	Common Berthing Mechanism
CEVIS	Cycle Ergometer with Vibration Isolation System
CMG	Control Moment Gyro
DC	Direct Current (electrical acronym generalized for mean value)
DC-1	Russian Docking Compartment
DTO	Detailed Test Objective
EE	Electronics Enclosure
ER 1/2	EXPRESS Rack 1 or 2
ESA	European Space Agency
EVA	Extravehicular Activity
EXPPCS	Experiment of Physics of Colloids in Space
EXPRESS	Expedite the Processing of Experiments to the Space Station
FGB	Functional Cargo Block (Russian translation: Functionalui Germatischeskii Block)
g	nominal gravitational acceleration at Earth's surface (9.81 m/s^2)
GMT	Greenwich Mean Time
GRC	NASA Glenn Research Center
GSE	Ground Support Equipment
HiRAP	High Resolution Accelerometer Package
HOSC	Huntsville Operation Support Center
Hz	Hertz
ICU	Interim Control Unit
ISS	International Space Station
ISPR	International Standard Payload Rack
JSC	NASA Johnson Space Center
kbps	kilobits per second
KSC	NASA Kennedy Space Center
LAB	U. S. Laboratory Module
LOS	Loss of Signal
LVLH	Local Vertical Local Horizontal
MAMS	Microgravity Acceleration Measurement System
MCC-H	Mission Control Center-Houston
MCOR	Medium-rate Communication Outage Recorder

MCS	Motion Control System
MEP	Microgravity Environment Program
MEWS	Mission Evaluation Workstation System
MPLM	Mini Pressurized Logistics Module or Multipurpose Logistics Module
MSFC	NASA Marshall Space Flight Center
NASA	National Aeronautics and Space Administration
NASDA	National Space Development Agency of Japan
OARE	Orbital Acceleration Research Experiment
ODRC	Operational Data Request Center
OSS	OARE Sensor Subsystem
OTO	One-Third Octave
PAD	PIMS Acceleration Data
PAO	Public Affairs Office
PCSA	Principal Component Spectral Analysis
PDSS	Payload Data Services System
PI	Principal Investigator
PIMS	Principal Investigator Microgravity Services
PMA	Pressurized Mating Adapter
PRO	Payload Rack Officer
PSD	Power Spectral Density
QTH	Quasi-steady Three-dimensional Histogram
RED	Resistive Exercise Device
RMS	Root-Mean-Square
RSS	Root-Sum-Square
SAMS	Space Acceleration Measurement System
SE	Sensor Enclosure
SO	Starboard Truss Segment 0
SSA	Space Station Analysis
SSPCM	Space Station Power Control Module
SSRMS	Space Station Remote Manipulator System
STS	Space Transportation System
TEA	Torque Equilibrium Attitude
THC	Temperature/Humidity Control System
TMF	Trimmed Mean Filtered
TSC	Telescience Support Center
TVIS	Treadmill Vibration Isolation System
XPOP	X Principal Axis Perpendicular to the Orbit Plane
XVV	X body axis toward the Velocity Vector
μg	micro-g, 1 x 10^{-6}g
WWW	World Wide Web

Appendix D. SAMS and MAMS Data Flow Descriptions

The MAMS hardware contains two acceleration measurement systems called MAMS OSS and MAMS HiRAP, each with a distinct measurement objective. The purpose of the MAMS OSS data is to measure the quasi-steady accelerations on the ISS. MAMS OSS data are obtained at a rate of 10 samples per second and are low-pass filtered with a cutoff frequency of 1 Hz. Each MAMS OSS data packet contains 16 seconds of MAMS OSS acceleration data and is transmitted in real-time at a rate of one data packet every 16 seconds. MAMS has the capability to store 25.6 hours of MAMS OSS data on board. Activated at MAMS power up or via ground command, this on board storage capability allows capturing of critical quasi-steady acceleration events for later downlink. These stored acceleration data can be transmitted to ground at a ground commanded rate between 20 and 200 kbps.

The MAMS HiRAP data are obtained at a fixed rate of 1000 samples per second and low pass filtered with a cutoff frequency of 100 Hz. The purpose of the MAMS HiRAP data is to measure the vibratory and transient accelerations on the ISS. Each MAMS HiRAP data packet contains 192 acceleration readings and is transmitted at a rate of one data packet every 0.192 seconds. MAMS does not have any capability to store MAMS HiRAP data on board.

Like MAMS HiRAP, the SAMS sensor heads are designed to measure the vibratory and transient accelerations on the ISS. Each SAMS sensor can be commanded to measure and downlink acceleration data at one of five sampling rates, with five corresponding cutoff frequencies. Since the SAMS sampling rate can be varied, the number of readings per packet and the number of packets per second varies as a function of the user selected sampling rate. Table D - 1 illustrates the relationship amongst sampling rate, cutoff frequency, acceleration readings per packet, and acceleration data packets per second for the SAMS sensors.

TABLE D - 1 SAMS DATA FLOW RATES

Sampling Rate (samples/sec)	Cutoff Frequency (Hz)	Readings Per Packet	Packets Per Second
62.5	25	31 or 32	2
125	50	62or 63	2
250	100	74 or 51	4
500	200	74 or 28	8
1000	400	74 or 56	14

Telemetry from the ISS is not continuous. A time interval where real time data downlink is available is referred to as an Acquisition of Signal (AOS) interval. Similarly, the lack of real time data downlink availability is referred to as a Loss of Signal (LOS) interval. Both SAMS and MAMS acceleration data must rely on ISS on board storage capabilities to eventually obtain acceleration data collected during LOS intervals. The Medium-rate Communication Outage Recorder (MCOR) provides this ISS on board storage capability. Consequently, real time acceleration data are available on the ground during AOS periods and acceleration data are stored on the MCOR during LOS periods for eventual downlink. Under normal circumstances, both SAMS and MAMS will measure and transmit acceleration data continuously throughout a given increment.

When acceleration data are transmitted to the ground, either real time data downlink or data transmitted from a dump of the MCOR memory, the resultant acceleration data packets are routed through the White Sands Facility, through Johnson Space Center (JSC), through the Marshall Space Flight Center (MSFC), Huntsville Operation Support Center (HOSC), and ultimately to PIMS Ground Support Equipment (GSE) located at the TSC. The PIMS GSE writes each received packet into a database table dedicated to each accelerometer supported by PIMS. Therefore, a separate database table exists for MAMS OSS, MAMS HiRAP, and for each of the five SAMS sensor heads.

The primary function of the database tables is to automatically merge AOS and LOS data packets for each accelerometer. As there exists overlap between the AOS and LOS acceleration data packets received, each sensor's dedicated database table discards any redundant data packets, resulting in a table containing a contiguous set of acceleration data packets.

Data are accessed from the database table to serve two separate purposes. The first purpose involves obtaining the most recent acceleration data from the table to generate real time plots of the acceleration data in a variety of plot formats supported by PIMS [21]. These real time plots are updated during AOS intervals and electronic snapshots of the data are routed to the PIMS ISS web page (http://pims.grc.nasa.gov).

The second purpose involves obtaining the oldest acceleration data from the “bottom” of the table. These acceleration data are used to generate the PIMS acceleration data archives used by the PIMS data analysts to generate the plots described in this report. Since the data are processed from the “bottom” of the table, MCOR dumps will have had time to be downlinked, received, and merged by the database table. PIMS currently waits 24 hours before generating any acceleration data archives. Like the electronic snapshots of the real time acceleration data plots, the acceleration data archives are available for download via the PIMS ISS web page.

Appendix E. Data Analysis Techniques and Processing

E. Data Analysis Techniques and Processing

This section briefly describes some assumptions, considerations, and procedures used to acquire and analyze the acceleration data measurements made by the two accelerometer systems: MAMS and SAMS.

E.1. Acceleration Data Coordinate Conversion

During the life of the Space Station, PIMS will frequently be asked to present acceleration data in a coordinate system other than that of the sensor. The purpose of this section is to provide the mathematical definitions and conventions PIMS will use when performing coordinate transformations.

PIMS maintains a coordinate system database for use in PIMS real-time and offline software that contains the information necessary to describe the location and orientation of various coordinate systems relative to the Space Station Analysis Coordinate System. Each entry for a coordinate system contains the location of the origin in SSA coordinates (x,y,z) and the Euler angles (Y, P, R) describing the orientation in a yaw-pitch-roll sequence of rotations with respect to the SSA frame. A positive rotation follows the right hand rule. So, an observer standing at positive infinity on the axis of rotation, looking towards the origin would see a counterclockwise rotation of the other two axes.

Transformation of acceleration data from the SSA coordinate system to a NEW coordinate system is accomplished by the formulation of a transformation matrix, M.

$$M_A^{NEW} = \begin{bmatrix} \cos P \cdot \cos Y & \cos P \cdot \sin Y & -\sin P \\ \sin R \cdot \sin P \cdot \cos Y - \cos R \cdot \sin Y & \sin R \cdot \sin P \cdot \sin Y + \cos R \cdot \cos Y & \sin R \cdot \cos P \\ \cos R \cdot \sin P \cdot \cos Y + \sin R \cdot \sin Y & \cos R \cdot \sin P \cdot \sin Y - \sin R \cdot \cos Y & \cos R \cdot \cos P \end{bmatrix}^{NEW}$$

Equation E.1-1

$$M_A^{NEW} = \begin{bmatrix} m_{11} & m_{12} & m_{13} \\ m_{21} & m_{22} & m_{23} \\ m_{31} & m_{32} & m_{33} \end{bmatrix}$$

Equation E.1-2

$$\begin{bmatrix} a_x \\ a_y \\ a_z \end{bmatrix}^{NEW} = M_A^{NEW} \cdot \begin{bmatrix} a_x \\ a_y \\ a_z \end{bmatrix}^{A}$$

Equation E.1-3

Transformation of acceleration data from the NEW coordinate system to the SSA coordinate system is accomplished by multiplying the vector by the transpose of matrix M[**]. The transpose of M, M^T, can be calculated by swapping the rows and columns as depicted in Equation E.1-4.

[**] For orthogonal matrices, $M^T = M^{-1}$.

$$M^T = M^A_{NEW} = \begin{bmatrix} m_{11} & m_{21} & m_{31} \\ m_{12} & m_{22} & m_{32} \\ m_{13} & m_{23} & m_{33} \end{bmatrix}$$

Equation E.1-4

$$\begin{bmatrix} a_x \\ a_y \\ a_z \end{bmatrix}^A = M^T \cdot \begin{bmatrix} a_x \\ a_y \\ a_z \end{bmatrix}^{NEW}$$

Equation E.1-5

In general, PIMS will transform data from SENSOR coordinate system to a NEW coordinate system. This is a four step process:

1. **The orientation of the SENSOR coordinate system is found $[YPR]_{SENSOR}$ from the coordinate system database and used to calculate the transformation matrix M,**

$$M^{SENSOR}_A = \begin{bmatrix} \cos P \cdot \cos Y & \cos P \cdot \sin Y & -\sin P \\ \sin R \cdot \sin P \cdot \cos Y - \cos R \cdot \sin Y & \sin R \cdot \sin P \cdot \sin Y + \cos R \cdot \cos Y & \sin R \cdot \cos P \\ \cos R \cdot \sin P \cdot \cos Y + \sin R \cdot \sin Y & \cos R \cdot \sin P \cdot \sin Y - \sin R \cdot \cos Y & \cos R \cdot \cos P \end{bmatrix}^{SENSOR}$$

Equation E.1-6

$$M^{SENSOR}_A = \begin{bmatrix} m_{11} & m_{12} & m_{13} \\ m_{21} & m_{22} & m_{23} \\ m_{31} & m_{32} & m_{33} \end{bmatrix}$$

Equation E.1-7

2. **Since the data is currently in SENSOR coordinates, the transpose of M is calculated.**

$$M^A_{SENSOR} = \begin{bmatrix} m_{11} & m_{21} & m_{31} \\ m_{12} & m_{22} & m_{32} \\ m_{13} & m_{23} & m_{33} \end{bmatrix}$$

Equation E.1-8

$$\begin{bmatrix} a_x \\ a_y \\ a_z \end{bmatrix}^A = M^A_{SENSOR} \cdot \begin{bmatrix} a_x \\ a_y \\ a_z \end{bmatrix}^{SENSOR}$$

Equation E.1-9

3. **The orientation of the NEW coordinate system is found $[YPR]_{NEW}$ from the coordinate system database and used to calculate the transformation matrix N,**

$$N^{NEW}_A = \begin{bmatrix} \cos P \cdot \cos Y & \cos P \cdot \sin Y & -\sin P \\ \sin R \cdot \sin P \cdot \cos Y - \cos R \cdot \sin Y & \sin R \cdot \sin P \cdot \sin Y + \cos R \cdot \cos Y & \sin R \cdot \cos P \\ \cos R \cdot \sin P \cdot \cos Y + \sin R \cdot \sin Y & \cos R \cdot \sin P \cdot \sin Y - \sin R \cdot \cos Y & \cos R \cdot \cos P \end{bmatrix}_{NEW}$$

Equation E.1-10

$$\begin{bmatrix} a_x \\ a_y \\ a_z \end{bmatrix}^{NEW} = N \cdot \begin{bmatrix} a_x \\ a_y \\ a_z \end{bmatrix}^{A}$$

Equation E.1-11

4. **The equivalent transformation matrix T is calculated by substitution of Equation E.1-9 into Equation E.1-11**

$$T_{SENSOR}^{NEW} = N_{A}^{NEW} \cdot M_{SENSOR}^{A}$$

Equation E.1-12

$$\begin{bmatrix} a_x \\ a_y \\ a_z \end{bmatrix}^{NEW} = T_{SENSOR}^{NEW} \cdot \begin{bmatrix} a_x \\ a_y \\ a_z \end{bmatrix}^{SENSOR}$$

Equation E.1-13

E.2. Quasi-steady Regime

MAMS OSS data is collected at 10 samples per second, low pass filtered with a cutoff frequency of 1 Hz and sent to GSE for further processing and storage. PIMS is currently storing the OSS data as raw acceleration files and also trimmed mean filtered data that are compensated for sensor bias.

E.2.1. Trimmed Mean Filter

The OSS data is processed with an adaptive trimmed mean filter (TMF) to provide an estimate of the quasi-steady acceleration signal by rejecting higher magnitude transients such as thruster firings, crew activity, etc. The trimmed mean filter algorithm used by the MAMS GSE operates on a sliding window of 480 samples, every 16 seconds. The filtering procedure, depicted in Figure E - 1, sorts the data by magnitude and calculates the deviation from a normal distribution using the Q parameter according to the equation:

$$Q = \frac{[Upper(20\%) - Lower(20\%)]}{[Upper(50\%) - Lower(50\%)]}$$

Equation E.2-1

Where the upper and lower percentage is determined from the sorted data set. Q is used in the following equation to calculate α, an adaptively determined amount of data to trim from the tails.

$$\alpha(Q) = \begin{cases} 0.05 & Q <= 1.75 \\ 0.05 + 0.35 * \dfrac{(Q - 1.75)}{0.25} & 1.75 < Q < 2.0 \\ 0.4 & Q >= 2.0 \end{cases}$$

Equation E.2-2

The quasi-steady acceleration level is computed to be the arithmetic mean of the trimmed set. Trimmed mean filtered data is stored in the PAD archive under "ossbtmf". Further information concerning the trimmed mean filter can be found in [22-24].

E.2.2. Mapping of Quasi-Steady Data

During the life of the station, PIMS is required to "map" quasi-steady data to locations other than that of MAMS OSS. Mapping is a prediction of what the quasi-steady environment would be at an alternate location, knowing the acceleration levels at MAMS.

E.2.2.1 Background and Assumptions

The methods used by PIMS in offline and real-time algorithms make the assumption that the ISS vehicle can be considered a rigid body in regards to the quasi-steady regime. The three main contributions to the quasi-steady acceleration environment are aerodynamic drag, rotational and gravity gradient effects. Drag effect is the same for any point attached to the vehicle and is considered to act opposite to the direction of flight. Rotational effects are the tangential and radial acceleration contributions due to the rotation of the vehicle. It is assumed that the accelerations in the tangential direction are negligible.

The gravity gradient effect refers to accelerations acting on any point in a rigid body away from the center of mass. An independent particle will tend to gravitate towards the ISS center of mass (CM) if it is in front or behind the CM along the x-axis of LVLH. This is a positive acceleration in the vehicle frame of reference. The particle will also gravitate towards the CM if it is to the left or right of the CM (aligned with the y-axis of LVLH). The gravity gradient will tend to gravitate a particle away from the CM if it is above or below the CM (along the z-axis of LVLH). [16]

E.2.2.2 Mapping Algorithm

The following is a list of required parameters that are necessary to map data to any given location onboard the ISS.

- Location of MAMS sensor in Space Station Analysis (A) Coordinates
- Alternate locations to be mapped to in Space Station Analysis Coordinates
- Location of ISS center of mass in Space Station Analysis Coordinates
- Position of ISS in J2000 coordinate system.
- Quaternion representations for a yaw-pitch-roll sequence describing the orientation of the LVLH coordinate system relative to the Space Station Analysis coordinate system.
- ISS body angular rates about the X_A, Y_A and Z_A-axes.

These are the steps PIMS uses to map MAMS OSS acceleration data from the measurement location (MAMS) to any other location (NEW). All distances are in meters, angles in radians, angular rates in radians/s, radius of the earth, $r_e = 6.3781 \times 10^6$ (meters), and $g_e = 9.81$ m/s^2. Definitions of the various coordinate systems can be found in [5].

1. **Calculate the position vectors of MAMS and NEW relative to the center of mass (CM).**

   The distance from the center of mass to the MAMS location:

$$\vec{r}_{MAMS}^{SSA} = \begin{bmatrix} x \\ y \\ z \end{bmatrix}_{MAMS}^{A} - \begin{bmatrix} x \\ y \\ z \end{bmatrix}_{CM}^{A} = \begin{bmatrix} rx \\ ry \\ rz \end{bmatrix}_{MAMS}^{A}$$

Equation E.2-3

   The distance from the center of mass to the NEW location:

$$\vec{r}_{NEW}^{SSA} = \begin{bmatrix} x \\ y \\ z \end{bmatrix}_{NEW}^{A} - \begin{bmatrix} x \\ y \\ z \end{bmatrix}_{CM}^{A} = \begin{bmatrix} rx \\ ry \\ rz \end{bmatrix}_{NEW}^{A}$$

Equation E.2-4

2. **Calculate transformation matrix from SSA to LVLH coordinate system using transformation matrix.**

$$T_{LVLH}^{A} = \begin{bmatrix} q_0^2 + q_1^2 - q_2^2 - q_3^2 & 2(q_1 \cdot q_2 + q_0 \cdot q_3) & 2(q_1 \cdot q_3 - q_0 \cdot q_2) \\ 2(q_1 \cdot q_2 - q_0 \cdot q_3) & q_0^2 - q_1^2 + q_2^2 - q_3^2 & 2(q_2 \cdot q_3 + q_0 \cdot q_1) \\ 2(q_1 \cdot q_3 + q_0 \cdot q_2) & 2(q_2 \cdot q_3 - q_0 \cdot q_1) & q_0^2 - q_1^2 - q_2^2 + q_3^2 \end{bmatrix} = \begin{bmatrix} m_{11} & m_{12} & m_{13} \\ m_{21} & m_{22} & m_{23} \\ m_{31} & m_{32} & m_{33} \end{bmatrix}$$

Equation E.2-5

   ISS GN&C uses a yaw-pitch-roll sequence from LVLH to SSA coordinates. PIMS uses a yaw-pitch-roll sequence from SSA to LVLH. For this reason, when calculating acceleration transformations, we must use the transpose of the resultant of Equation E.2-5.

$$T_{A}^{LVLH} = \left[T_{LVLH}^{A}\right]^T$$

Equation E.2-6

$$T_{A}^{LVLH} = \begin{bmatrix} m_{11} & m_{21} & m_{31} \\ m_{12} & m_{22} & m_{32} \\ m_{13} & m_{23} & m_{33} \end{bmatrix}$$

Equation E.2-7

3. **Convert position vectors to LVLH coordinate system by matrix multiplication.**
   Position vector of MAMS relative to center of mass in LVLH coordinate system:

$$\vec{r}_{MAMS}^{\,LVLH} = T_A^{LVLH} \cdot \vec{r}_{MAMS}^{\,A} = \begin{bmatrix} rx \\ ry \\ rz \end{bmatrix}_{MAMS}^{LVLH}$$

Equation E.2-8

Position vector of NEW relative to center of mass in LVLH coordinate system:

$$\vec{r}_{NEW}^{\,LVLH} = T_A^{LVLH} \cdot \vec{r}_{NEW}^{\,A} = \begin{bmatrix} rx \\ ry \\ rz \end{bmatrix}_{NEW}^{LVLH}$$

Equation E.2-9

4. **Calculate the radius to the vehicle.**

$$r_O = \sqrt{r_x^2 + r_y^2 + r_z^2}$$

Equation E.2-10

5. **Calculate the gravity gradient components in LVLH coordinates (in micro-g)**

Gravity gradient component at MAMS location:

$$gg_{MAMS}^{LVLH} = \left(\frac{g_e \cdot r_e^2}{r_O^2} \right) \begin{bmatrix} rx \\ ry \\ -2 \cdot rz \end{bmatrix}_{MAMS}^{LVLH} \cdot \left(\frac{1x10^6}{g_e} \right)$$

Equation E.2-11

Gravity gradient component at NEW location:

$$gg_{NEW}^{LVLH} = \left(\frac{g_e \cdot r_e^2}{r_O^2} \right) \begin{bmatrix} rx \\ ry \\ -2 \cdot rz \end{bmatrix}_{NEW}^{LVLH} \cdot \left(\frac{1x10^6}{g_e} \right)$$

Equation E.2-12

6. **Convert the gravity gradient components to SSA coordinates by matrix multiplication**

MAMS gravity gradient component in SSA coordinates:

$$gg_{MAMS}^{A} = T_{LVLH}^{A} \cdot gg_{MAMS}^{LVLH}$$

Equation E.2-13

NEW gravity gradient component in SSA coordinates:

$$gg_{NEW}^{A} = T_{LVLH}^{A} \cdot gg_{NEW}^{LVLH}$$

Equation E.2-14

7. **Calculate rotational acceleration matrix**

$$A = \begin{bmatrix} -(\omega_y^2 + \omega_z^2) & \omega_x\omega_y & \omega_x\omega_z \\ \omega_x\omega_y & -(\omega_x^2 + \omega_z^2) & \omega_y\omega_z \\ \omega_x\omega_z & \omega_y\omega_z & -(\omega_x^2 + \omega_y^2) \end{bmatrix}$$

Equation E.2-15

8. **Calculate rotational components in SSA coordinates (in micro-g):**
   Rotational component at MAMS location:

$$rot^A_{MAMS} = A \cdot \vec{r}^{\,A}_{MAMS} \cdot \left(\frac{1x10^6}{g_e} \right)$$

Equation E.2-16

   Rotational component at NEW location:

$$rot^A_{NEW} = A \cdot \vec{r}^{\,A}_{NEW} \cdot \left(\frac{1x10^6}{g_e} \right)$$

Equation E.2-17

9. **Complete acceleration mapping by subtracting MAMS components and adding NEW components:**

$$A^A_{NEW} = A^A_{MAMS} - gg^A_{MAMS} - rot^A_{MAMS} + gg^A_{NEW} + rot^A_{NEW}$$

Equation E.2-18

E.2.3. OSS Bias Measurements

MAMS OSS triaxial sensor bias is measured by a sequence of Bias Calibration Table Assembly (BCTA) rotations. A complete bias measurement for a given axis consists of 50 seconds of data recorded in a normal orientation and 50 seconds of data recorded when the axis has been rotated 180 degrees to its opposite orientation. The 50 seconds of data are processed by the MAMS GSE with TMF algorithm applied to the resulting 500 points. Four measurements are made, corresponding with normal X_{oss} and Y_{oss}, opposite X_{oss} and Y_{oss}, opposite X_{oss} and normal Z_{oss}, and normal X_{oss} opposite Z_{oss}. The outputs for each axis and its opposite are summed and divided by two to obtain the bias value. The value is evaluated in relation to the collection of past bias measurements for a given power cycle and is included in the new mean bias calculation or ignored if determined to be out of range. A disturbance in the microgravity environment is sufficient to cause an up ranging in the OSS sensor, which, in turn, will automatically cause the bias to fail. Failed bias calibrations are not repeated. One of the initial goals during Increment-3 operations for MAMS was the characterization of the OSS sensor bias. To accomplish this, bias measurements were initially performed once per hour, but has since been set to one every six hours.

In the past, MAMS predecessor, the Orbital Acceleration Research Experiment (OARE), showed a significant initial transient in the bias measurements that would take one to two days to settle out. This phenomenon was not observed in the MAMS OSS data suggesting that the transient was an effect of launch. However, there is a bias temperature dependency. Ground testing indicates a temperature bias coefficient of 0.05 μg / °C [25]. At power up, the MAMS instrument takes roughly 4-6 hours to reach the nominal operating temperature of 40 °C, at which point, the bias values can be considered constant. We have not verified the bias

coefficient on-orbit. For this reason, PIMS is recommending that users avoid OSS data within the first 6 hours after a MAMS power on event. When MAMS OSS support is requested, this 6-hour "settling" time must be taken into consideration.

E.2.4. Quasi-steady Plot Types

The two types of plots used in the analysis of quasi-steady data are acceleration versus time and the quasi-steady three-dimensional histogram (QTH). Unless otherwise noted, these plot types use trimmed mean filtered OSS data.

E.2.4.1 OSS Trimmed Mean Acceleration versus Time

These are single (X, Y, Z, or vector magnitude) or three axes (X, Y, and Z) plots of acceleration in units of μg versus time. These plots give the best accounting of the quasi-steady acceleration vector as a function of time.

E.2.4.2 Quasi-steady Three-dimensional Histogram (QTH)

This type of analysis results in three orthogonal views of the quasi-steady vector. The time series is analyzed using a two-dimensional histogram method where the percentage of time the acceleration vector falls within a two-dimensional bin is plotted as a color. Areas showing colors toward the red end of the spectrum indicate a higher number of occurrences. Conversely, areas showing colors towards the blue end are indicative of a lower percentage, with no occurrences being shown as white. This plot provides a summary of the quasi-steady vector during the total time period considered. Exact timing of an acceleration event is lost in this type of plot.

E.3. Vibratory Regime

The frequency response of the accelerometer systems used to collect vibratory data may extend below 0.01 Hz down to DC, but those instruments are not optimized for making quasi-steady or DC measurements. The MAMS OSS instrument is specialized for this purpose. Therefore, unless otherwise noted, it is assumed that the vibratory data have been demeaned for plots and analyses of vibratory data. Access to data availability plots for a given calendar month can be obtained via ftp at,

ftp://pims.grc.nasa.gov/pad/yearXXXX/monthYY/XXXX_YY_padprofile.pdf

where XXXX=the year of interest and YY=the month of interest. For example,

ftp://pims.grc.nasa.gov/pad/year2001/month10/2001_10_padprofile.pdf

provides access to data availability for October, 2001 for the five SAMS SEs and the MAMS sensors. Availability for a given month is listed across the x-axis and cutoff frequencies for the sensor heads are listed at the top. Notice that the figures are color-coded. Each color is associated with a cutoff frequency. The white vertical lines in-between the color bars are the gaps in the acceleration data collected by that specific sensor. This means that data is not

available for that time span. These figures should be used as a starting point to determine whether certain sets of data are available before filling out and submitting a data request form at:

http://pims.grc.nasa.gov/html/RequestDataPlots.html.

E.3.1. Demeaned Vibratory Acceleration Data

In the analysis of the vibratory regime, it is understood that a certain amount of bias intrinsic to the measurement process does exist. This bias is manifest as a DC shift of the acceleration measurements away from the true mean value. Similar bias considerations also exist for measurements collected with the intent of analyzing the quasi-steady regime. However, much effort is expended to account for and remove bias from quasi-steady acceleration measurements, whereas in the vibratory regime, the mean value is effectively ignored in the process of demeaning. That is, for vibratory acceleration data, the mean value of the acceleration (on a per-axis basis) is subtracted over the time frame under consideration leaving effectively zero mean acceleration.

E.3.2. Interval Statistics

A plot of acceleration interval statistics in units of g versus time gives some measure of acceleration fluctuations as a function of time. This display type allows relatively long periods to be displayed on a single plot. There are three such interval statistic plots that are employed for this and other reasons as described below: (1) interval average, (2) interval root-mean-square and (3) interval minimum/maximum.

E.3.3. Interval Average

Interval average plots show net accelerations, which last for a number of seconds equal to or greater than the interval parameter, used. Short duration, high amplitude accelerations can also be detected with this type of plot; however, the exact timing and magnitude of specific acceleration events cannot be extracted. This type of display is useful for identifying overall effects of extended thruster firings and other activities that tend to cause the mean acceleration levels to shift. This display type is rarely used for vibratory data.

E.3.4. Interval Root-Mean-Square

Interval root-mean-square (RMS) plots show oscillatory content in the acceleration data. For the period of time considered, this quantity gives a measure of the variance of the acceleration signal. This data representation is useful for identifying gross changes in acceleration levels usually caused by the initiation or cessation of activities such as crew exercise or equipment operations.

E.3.5. Interval Minimum/Maximum

An interval minimum/maximum plot shows the peak-to-peak variations of the acceleration data. For each interval, this plot type shows both the minimum and maximum values, and thereby

shows the acceleration data envelope. This type of display is another way to track gross changes in acceleration.

E.3.6. Power Spectral Density

The power spectral density (PSD) is computed from the Fourier transform of an acceleration time series and gives an estimate of the distribution of power with respect to frequency in the acceleration signal. It is expressed in units of g^2/Hz. The method used for computation of the PSD is consistent with Parseval's theorem, which states that the RMS value of a time series signal is equal to the square root of the integral of the PSD across the frequency band represented by the original signal.

E.3.7. Power Spectral Density Versus Time (Spectrogram)

Spectrograms provide a road map of how acceleration signals vary with respect to both time and frequency. To produce a spectrogram, PSDs are computed for successive intervals of time. The PSDs are oriented vertically on a page such that frequency increases from bottom to top. PSDs from successive time slices are aligned horizontally across the page such that time increases from left to right. Each time-frequency bin is imaged as a color corresponding to the base 10 logarithm of the PSD magnitude at that time and frequency. Spectrograms are particularly useful for identifying structure and boundaries in time and frequency over relatively long periods of time.

E.3.8. RMS Acceleration Versus One-Third Octave Frequency Bands

This type of plot quantifies the spectral content in proportional bandwidth frequency bands for a given time interval of interest (nominally 100 seconds). The (nearly) one-third octave bands are those defined by the ISS microgravity requirements; see Table 4 [26]. The results of this analysis are typically plotted along with a bold stair step curve representing the ISS combined vibratory limits in order to compare the acceleration environment to these prescribed limits. These plots are not particularly useful for identifying the source of a disturbance for a band that exceeds the desired limits.

E.3.9. Cumulative RMS Acceleration Versus Frequency

A plot of cumulative RMS acceleration versus frequency quantifies, in cumulative fashion, the contributions of spectral components to the overall measured RMS acceleration level for the time frame of interest. This plot is also derived from the PSD using Parseval's theorem. It quantitatively highlights key spectral regions - steep slopes indicate strong narrowband disturbances that contribute significantly to the acceleration environment, while shallow slopes indicate relatively quiet portions of the spectrum.

E.3.10. Principal Component Spectral Analysis (PCSA)

The PCSA histogram is computed from a large number of constituent PSDs. The resultant three-dimensional plot serves to summarize magnitude and frequency variations of significant or persistent spectral contributors and envelops all of the computed spectra over the time frame of

interest. The two-dimensional histogram is comprised of frequency bins in units of Hz and PSD magnitude bins in units of $\log_{10}(g^2/Hz)$. The third dimension, represented by a color scale, is the percentage of time that a spectral value was counted within a given frequency-magnitude bin.

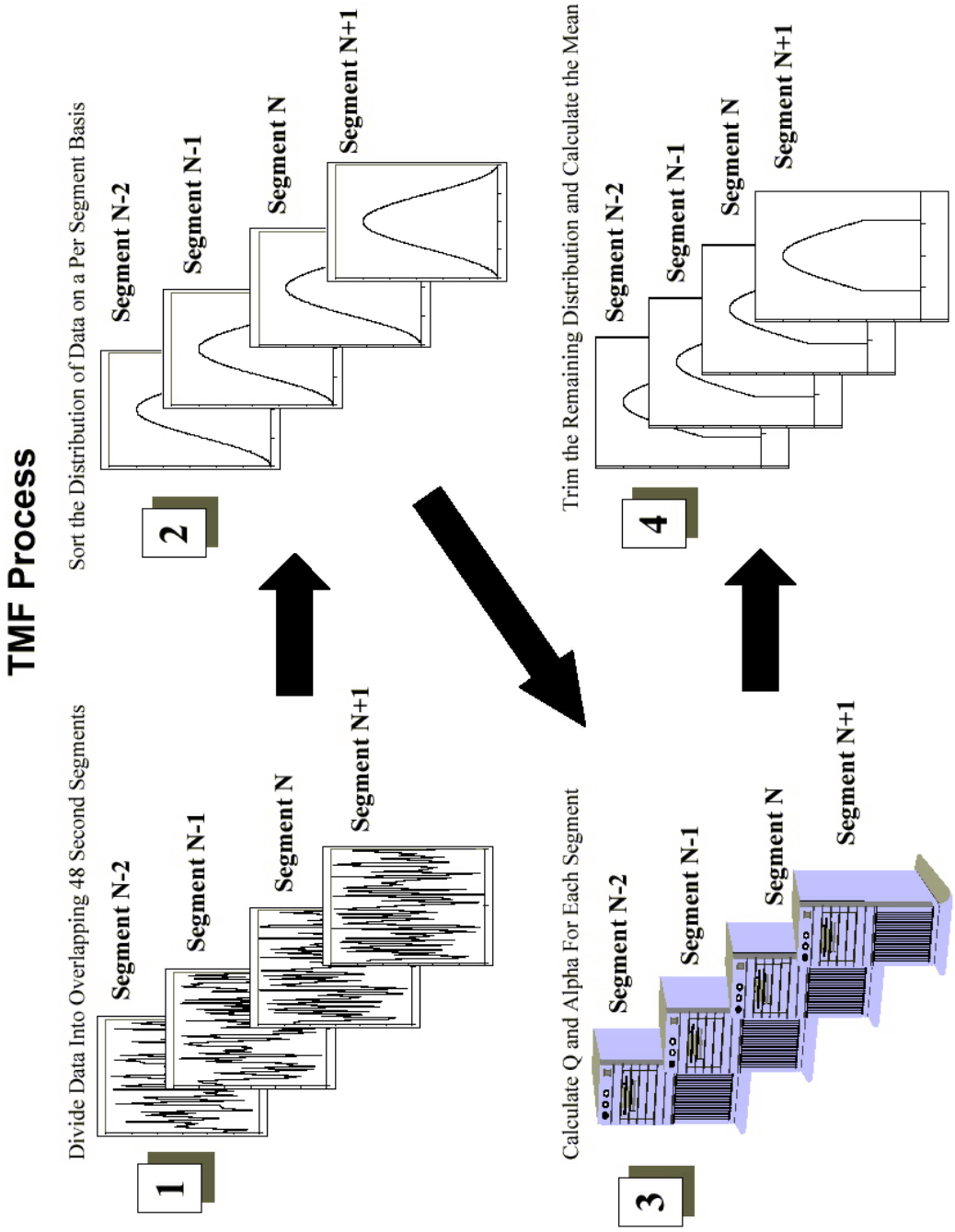

Figure E-1 Trimmed Mean Filter Process

REPORT DOCUMENTATION PAGE

Form Approved
OMB No. 0704-0188

Public reporting burden for this collection of information is estimated to average 1 hour per response, including the time for reviewing instructions, searching existing data sources, gathering and maintaining the data needed, and completing and reviewing the collection of information. Send comments regarding this burden estimate or any other aspect of this collection of information, including suggestions for reducing this burden, to Washington Headquarters Services, Directorate for Information Operations and Reports, 1215 Jefferson Davis Highway, Suite 1204, Arlington, VA 22202-4302, and to the Office of Management and Budget, Paperwork Reduction Project (0704-0188), Washington, DC 20503.

1. AGENCY USE ONLY (*Leave blank*)	2. REPORT DATE	3. REPORT TYPE AND DATES COVERED
	June 2002	Technical Memorandum

4. TITLE AND SUBTITLE

International Space Station Increment-3 Microgravity Environment Summary Report

5. FUNDING NUMBERS

WU–400–35–40–00

6. AUTHOR(S)

Kenol Jules, Kenneth Hrovat, Eric Kelly, Kevin McPherson, Timothy Reckart, and Carlos Grodsinksy

7. PERFORMING ORGANIZATION NAME(S) AND ADDRESS(ES)

National Aeronautics and Space Administration
John H. Glenn Research Center at Lewis Field
Cleveland, Ohio 44135–3191

8. PERFORMING ORGANIZATION REPORT NUMBER

E–13424

9. SPONSORING/MONITORING AGENCY NAME(S) AND ADDRESS(ES)

National Aeronautics and Space Administration
Washington, DC 20546–0001

10. SPONSORING/MONITORING AGENCY REPORT NUMBER

NASA TM—2002-211693

11. SUPPLEMENTARY NOTES

Kenol Jules and Kevin McPherson, NASA Glenn Research Center; Kenneth Hrovat, Eric Kelly, Timothy Reckart, and Carlos Grodsinksy, ZIN Technologies, Inc., Brook Park, Ohio 44142. Responsible person, Kenol Jules, organization code 6727, 216–977–7016.

12a. DISTRIBUTION/AVAILABILITY STATEMENT

Unclassified - Unlimited
Subject Categories: 19 and 35 Distribution: Nonstandard

Available electronically at http://gltrs.grc.nasa.gov/GLTRS

This publication is available from the NASA Center for AeroSpace Information, 301–621–0390.

12b. DISTRIBUTION CODE

13. ABSTRACT ***(Maximum 200 words)***

This summary report presents the results of some of the processed acceleration data measured aboard the International Space Station during the period of August to December 2001. Two accelerometer systems were used to measure the acceleration levels for the activities that took place during Increment-3. However, not all of the activities were analyzed for this report due to time constraint and lack of precise timeline information regarding some payload operations and station activities. The National Aeronautics and Space Administration sponsors the Microgravity Acceleration Measurement System and the Space Acceleration Microgravity System to support microgravity science experiments which require microgravity acceleration measurements. On April 19, 2001, both the Microgravity Acceleration Measurement System and the Space Acceleration Measurement System units were launched on STS-100 from the Kennedy Space Center for installation on the International Space Station. The Microgravity Acceleration Measurement System unit was flown to the station in support of science experiments requiring quasi-steady acceleration measurements, while the Space Acceleration Measurement System unit was flown to support experiments requiring vibratory acceleration measurement. Both acceleration systems are also used in support of the vehicle microgravity requirements verification. The International Space Station Increment-3 reduced gravity environment analysis presented in this report uses acceleration data collected by both sets of accelerometer systems: (1) The Microgravity Acceleration Measurement System, which consists of two sensors: the Orbital Acceleration Research Experiment Sensor Subsystem, a low frequency range sensor (up to 1 Hz), is used to characterize the quasi-steady environment for payloads and vehicle, and the High Resolution Accelerometer Package, which is used to characterize the vibratory environment up to 100 Hz. (2) The Space Acceleration Measurement System, which is a high frequency sensor, measures vibratory acceleration data in the range of 0.01 to 400 Hz. This summary report presents analysis of some selected quasi-steady and vibratory activities measured by these accelerometers during Increment-3 from August to December, 2001.

14. SUBJECT TERMS

SAMS; MAMS; Microgravity; International Space Station; Quasi-steady; Vibratory; Transient

15. NUMBER OF PAGES

157

16. PRICE CODE

17. SECURITY CLASSIFICATION OF REPORT	18. SECURITY CLASSIFICATION OF THIS PAGE	19. SECURITY CLASSIFICATION OF ABSTRACT	20. LIMITATION OF ABSTRACT
Unclassified	Unclassified	Unclassified	